Master's thesis

NTNU
Norwegian University of Science and Technology
Faculty of Engineering
Department of Civil and Environmental Engineering

Camilla Soland
Sebastian Qvist

A Parametric Study of Timber Network Arch Bridges with Timber Deck on Transversal Crossbeams

Master's thesis in Civil and Environmental Engineering
Supervisor: Kjell Arne Malo
Co-supervisor: Francesco Mirko Massaro
June 2023

NTNU
Norwegian University of
Science and Technology

Camilla Soland
Sebastian Qvist

A Parametric Study of Timber Network Arch Bridges with Timber Deck on Transversal Crossbeams

Master's thesis in Civil and Environmental Engineering
Supervisor: Kjell Arne Malo
Co-supervisor: Francesco Mirko Massaro
June 2023

Norwegian University of Science and Technology
Faculty of Engineering
Department of Civil and Environmental Engineering

NTNU
Norwegian University of
Science and Technology

Department of Structural Engineering
Faculty of Engineering
NTNU- Norwegian University of Science and Technology

ACCESSIBILITY

Open

MASTER THESIS 2023

SUBJECT AREA:	DATE:	NO. OF PAGES:
Structural Design Timber Structures	11.06.2023	69 + 120 (Appendices)

TITLE:

A Parametric Study of Timber Network Arch Bridges with Timber Deck on Transversal Crossbeams

En parametrisk studie av Nettverksbuebroer i tre med tredekke på tverrbærere

BY:

Camilla Soland and Sebastian Qvist

ABSTRACT:
Network arch bridges offer a structurally efficient solution for covering long spans and minimizing material usage due to the favorable bending moment distribution. Traditionally, network arch bridges have employed steel arches in combination with a concrete slab. These materials have a substantial carbon footprint as opposed to timber.

This master's thesis investigates and optimizes different concepts for network arch bridges with timber as the primary material. The objective is to enable long spans while minimizing the number of connections along the arches to enhance durability while maintaining structural integrity. The thesis also explores the structural impact of introducing splices in the arches. Additionally, new design approaches are proposed to regulate the distribution of moments along the arches and at the arch ends.

A fully parametric model is developed to explore various design configurations using Grasshopper and Karamba3D. A multi-objective optimization approach using Octopus is employed to optimize various design configurations. The investigations include different span lengths, sets of hangers, and designs incorporating splices, alternative corner designs, and leaned arches.

By leaning the arches toward each other, the out-of-plane stiffness increases. As a result, there is less need for wind bracing, reducing material cost and the number of exposed connections, consequently increasing the durability of the bridge. Similarly, the study showed that by merging designated hanger connections on the lower edge of the arch, the total number could be reduced by 1/3 without affecting structural performance. Simulations indicated an optimum hanger angle between 43 and 47 degrees. With skew loading, some hangers may be unloaded, meaning they are relaxed. This could lead to an unfavorable moment distribution. Relaxation of hangers may be a greater challenge with leaned arches due to lower optimum hanger angles.

For all the explored bridge configurations, out-of-plane buckling was the most critical design check. Consequently, the optimized width-to-height ratio ranged between 1.5 and 2. The number of splices in the arches had a noticeable effect on buckling, nonetheless negligible influence on other objectives. Implementing splices in the arch increased the design check values, while the number of splices exhibited an insignificant difference. Overall, the structural performance was satisfactory with the assumed splice design. Moreover, an increasing arch height toward the supports was implemented. An adjustment of the height would considerably change the bending moment distribution.

This study serves as a feasibility analysis of network arch bridges using timber, providing insights into design optimization and performance considerations.

SUPERVISOR(S): Kjell Arne Malo
Francesco Mirko Massaro
CARRIED OUT AT: Department for Structural Engineering, NTNU

"Any idiot can build a bridge that stands, but it takes an engineer to build a bridge that barely stands."
-Unknown

Abstract

Network arch bridges offer a structurally efficient solution for covering long spans and minimizing material usage due to the favorable bending moment distribution. Traditionally, network arch bridges have employed steel arches in combination with a concrete slab. These materials have a substantial carbon footprint as opposed to timber.

This master's thesis investigates and optimizes different concepts for network arch bridges with timber as the primary material. The objective is to enable long spans while minimizing the number of connections along the arches to enhance durability while maintaining structural integrity. The thesis also explores the structural impact of introducing splices in the arches. Additionally, new design approaches are proposed to regulate the distribution of moments along the arches and at the arch ends.

A fully parametric model is developed to explore various design configurations using Grasshopper and Karamba3D. A multi-objective optimization approach using Octopus is employed to optimize various design configurations. The investigations include different span lengths, sets of hangers, and designs incorporating splices, alternative corner designs, and leaned arches.

By leaning the arches toward each other, the out-of-plane stiffness increases. As a result, there is less need for wind bracing, reducing material cost and the number of exposed connections, consequently increasing the durability of the bridge. Similarly, the study showed that by merging designated hanger connections on the lower edge of the arch, the total number could be reduced by 1/3 without affecting structural performance. Simulations indicated an optimum hanger angle between 43 and 47 degrees. With skew loading, some hangers may be unloaded, meaning they are relaxed. This could lead to an unfavorable moment distribution. Relaxation of hangers may be a greater challenge with leaned arches due to lower optimum hanger angles.

For all the explored bridge configurations, out-of-plane buckling was the most critical design check. Consequently, the optimized width-to-height ratio ranged between 1.5 and 2. The number of splices in the arches had a noticeable effect on buckling, nonetheless negligible influence on other objectives. Implementing splices in the arch increased the design check values, while the number of splices exhibited an insignificant difference. Overall, the structural performance was satisfactory with the assumed splice design. Moreover, an increasing arch height toward the supports was implemented. An adjustment of the height would considerably change the bending moment distribution.

This study serves as a feasibility analysis of network arch bridges using timber, providing insights into design optimization and performance considerations.

Sammendrag

Nettverksbuebroer er en strukturelt effektiv løsning for lange spenn samtidig som materialbruken minimeres på grunn av den gunstige momentfordelingen. Tradisjonelt sett benyttes buer i stål i kombinasjon med et betongdekke i nettverksbuebroer. Disse materialene har et betydelig klima-avtrykk, i motsetning til tre.

Denne masteroppgaven undersøker og optimaliserer ulike konsepter for nettverksbuebroer med tre som hovedmateriale. Målet er å muliggjøre lange spenn, samtidig som antallet forbindelser langs buen minimeres for å øke bestandigheten mens den strukturelle integriteten opprettholdes. Oppgaven utforsker også den strukturelle påvirkningen av å innføre skjøter i buene. I tillegg foreslås nye design for å tilpasse fordelingen av bøyemoment langs buene og i enden av buene.

En fullstendig parametrisk modell er utviklet for å utforske ulike design ved hjelp av Grasshopper og Karamba3D. En flerobjektiv optimaliseringsmetode ved bruk av Octopus benyttes for å optimalisere ulike konfigurasjoner. Undersøkelsene inkluderer ulike spennlengder, sett med hengere og design som inkluderer skjøter, alternative hjørnedesign og skråstilte buer.

Ved å lene buene mot hverandre, øker stivheten mot utbøying. Som et resultat er det mindre behov for vindfagverk, noe som reduserer materialkostnader og antall eksponerte forbindelser, og dermed øker broens bestandighet. I tillegg viste studien at ved å slå sammen bestemte hengerforbindelser på undersiden av buen, kunne det totale antallet reduseres med 1/3 uten å påvirke det strukturelle. Simuleringene indikerte en optimal hengervinkel mellom 43 og 47 grader. Ved usymmetrisk belastning kan noen hengere bli ubelastet, noe som betyr at de blir avslappet. Dette kan føre til en ugunstig fordeling av bøyemoment. Avslapping av hengere kan være en større utfordring med skråstilte buer på grunn av lavere optimale hengervinkler.

For alle de utforskede brokonfigurasjonene, var knekking ut av planet den mest kritiske design-sjekken. Som et resultat av dette, varierte det optimaliserte bredde-til-høyde-forholdet til buene mellom 1,5 og 2. Innføring av skjøter i buene hadde en merkbar effekt på knekking, men liten påvirkning på andre objektiver. Implementering av skjøter i buene økte verdien av design-sjekkene, mens antallet skjøter viste en ubetydelig forskjell. Totalt sett var den strukturelle oppførselen tilfredsstillende. I tillegg ble det implementert en økende buehøyde mot opplagerne. En justering av høyden førte til betydelig endring i momentfordelingen.

Denne oppgaven fungerer som en mulighetsstudie av nettverksbuebroer i tre, og gir innsikt i designoptimalisering og vurderinger av strukturell oppførsel.

Preface

This master's thesis completes our 5-year study in Civil and Environmental Engineering at the Norwegian University of Science and Technology, NTNU.

We would like to extend our gratitude towards our supervisor Kjell Arne Malo for his guidance during our work, and for keeping an open-door policy. In addition, our gratitude is extended to Francesco Mirko Massaro for his valuable guidance during the final stages of our research. Finally, we would like to thank Marcin Luczkowski for his invaluable assistance in facilitating our initiation with Grasshopper and Karamba3D.

Their assistance has been deeply appreciated.

Table of Contents

1 Introduction

The network arch bridge, originally introduced by Per Tveit in 1955 [30], comprises a network hanger pattern that connects the bearing arches to the bridge deck. The bridge concept is highly effective due to the moment distribution along the arch, which reduces material. Although steel and concrete are commonly used materials for the arches and deck, the utilization of timber can be favored due to its environmental benefits and carbon-neutral properties. Therefore, in this thesis, the focus is on constructing the arches and the deck using glued laminated timber supplemented with transversal crossbeams and hangers in steel.

To enhance the stiffness of arches in the out-of-plane direction, wind trusses are installed when vertical arches are used. However, this necessitates a significant number of connections in the arches, which can compromise durability when exposed to moisture and affect structural performance in timber arches.

When using a stress-laminated timber deck in network arch bridges, the hangers may not be sufficiently prestressed because of the low weight of the deck compared to a concrete deck. This results in some hangers being subjected to compression; they relax, with skew loading, resulting in a loss of structural performance of the hangers. The moment may, as a result, increase closer to the arch ends, which is where the hangers tend to relax. Furthermore, the arches are typically hinged at the supports, and issues may arise if the hinges are not completely rotationally free, resulting in bending moments at the arch ends. If the supports have rotational stiffness in-plane, larger end moments arise.

One of the main objectives of network arch bridges is to achieve a uniform in-plane distribution of binding moments along the arches. Timber elements are of limited length due to transportation restrictions and need, therefore, to be spliced on-site to achieve longer spans. Introducing splices in the timber arches is necessary for longer spans and has a structural influence on the arches' behavior and moment distribution.

1.1 Purpose

The purpose of this master's thesis is to investigate and optimize different concepts for network arch bridges to enable long spans, using timber as the primary material. The optimization process aims to minimize the number of connections in timber elements to enhance durability while maintaining structural integrity. Additionally, new design approaches will be proposed to regulate the distribution of moments along the arches and at the arch ends. Furthermore, the study will investigate the structural impact of introducing splices in the arches.

The research topics addressed in this study are as follows:

- Can the number of connection points along the arches be reduced without compromising structural performance?
- How do the proposed designs for the arch ends affect the bending moments near the supports?
- How does the introduction of splices in the arches affect the structural performance of the bridge?

1.2 Method

To address these topics, a fully parametric model is developed in Grasshopper, utilizing Karamba3D to create a finite element model. The parametric model enables the investigation and optimization of various design configurations within the same framework. The behavior of network arch bridges with different lengths, heights, and designs are optimized using Octopus, a multi-objective optimization plug-in for Grasshopper. The optimization process consists of five simulations, for each specified bridge design, with different objectives optimized in each simulation. This approach allows for the comparison of designs with their respective optimal configurations.

The investigated bridge designs have introduced splices and alternative corner designs. Furthermore, leaned arches are implemented to reduce the number of connections. Alternative bridge designs will be incorporated by introducing additional design functions or removing existing ones. This comparative analysis will provide insights into the effectiveness of different design approaches.

1.3 Limitations

This thesis primarily investigates the global structural system of network arch bridges. The specific connections between elements are not further investigated, and a simplified load approach is employed. The structural investigation conducted in this thesis resembles a feasibility study, laying the foundation for further detailed analysis and exploration.

2 Theory

2.1 Timber as a construction material

Timber is a material of natural origin, which includes both pros and cons. As a construction material, timber has a high strength-to-weight ratio compared to other materials, such as steel and concrete. In many situations, it can be preferable with light materials to keep the weight of the construction low, for instance in situations with challenging ground conditions or for pedestrian bridges, where the self-weight of the construction often is a limiting factor. On the contrary, constructions with wood are more prone to dynamic problems due to its low self-weight.

In contrast to most building materials, timber is orthotropic with direction-dependent properties. There are three main directions, as shown in Figure 2.1, longitudinal, tangential, and radial. Along the grains of the material, the material strengths are greater. The two other directions are perpendicular to the grain and have considerably lower strength. Strength properties are given parallel or perpendicular to the grain.

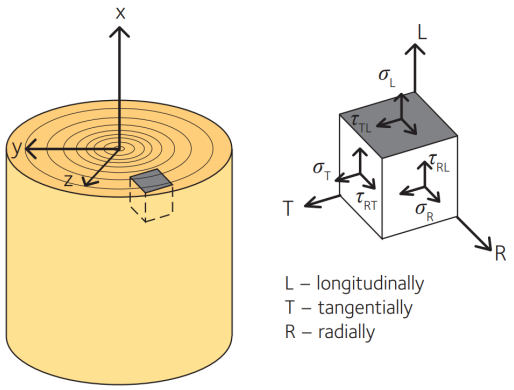

Figure 2.1: Definition of normal- (σ) and shear- (τ) stresses and directions of wood.

Source: [2]

Variation and uncertainties

When designing structures with timber, NS-EN 1995-1-1 (Eurocode 5) should be used to verify the construction. Timber is often called a "living" material since its appearance and material properties change with time and climate conditions. With long-lasting, constant loading, timber will creep, and the deformation increases. Moreover, the moisture level will have a significant impact since wood is hygroscopic. A lower moisture content will lead to greater strength. With this in mind, it is important to consider the climate at the building site, as well as to what extent the material is exposed. Regardless of this, measures for moisture protection, especially variations in moisture level, should always be implemented. Because of these influences, a number of safety factors are used to compensate for the uncertainties. For instance, through Table 3.1 in Eurocode 5, the safety factor k_{mod} is based on material, climate class, and load duration [28].

Material composition

Solid wood as a construction material has been used for ages. Multiple different compositions of timber have been tested to increase the usage of wood as a material for beams, plates, and

more. The relevant material for this thesis is glued laminated timber. Glued laminated timber, also called glulam, has lamellas consisting of multiple boards glued together with finger joints for increased surface and better adhesion. The lamellas are then glued on top of each other, with the grain direction parallel to the length, to the desired height. This practice will spread defects in the material, minimizing differences. Decreasing uncertainties in the material enables the possibility of using lower material safety factors. Indeed, this difference is displayed in Table NA.2.3 in the Norwegian National Annex in Eurocode 5, where the safety factor is 1.25 for solid timber and 1.15 for glulam. The span of a glulam beam can be considerably larger than for solid timber. This is due to both the strength properties and the limitations of tree sizes to make a solid timber beam. Often, transportation is the limiting factor for glulam beams. Transportation of the construction is often an important factor for the total economy of the project [13]. The design of a glulam beam has many possibilities for varying cross sections and curvatures, and the outer lamellas are often stronger to increase the beam's total strength.

Environmental aspect

Timber is a renewable material of natural occurrence. Through its lifetime, a tree will absorb large quantities of CO_2, which is released through decomposition or burning of the tree. The emissions connected to the use of timber as a construction material are mainly due to processing and transport. The availability of timber in Norway is good, especially in the eastern parts. Therefore a large number of constructions in these areas are built with timber. Compared to concrete and steel, timber constructions have considerably lower emissions. This is becoming more appealing in many building projects as sustainability plays a more important part, becoming a requirement for several companies. Timber constructions are durable for a long time with the right design and maintenance. As a reusable material, timber can, after the lifetime of the construction, be used in other constructions or as firewood.

Prefabrication

Timber has been prefabricated for several years in different forms. Previously, log houses were built in rural areas before being disassembled and transported to the building site for assembly. Today, this is done in different types of constructions, especially with timber, because of its low weight, making it suitable for transportation. At the same time, building in a controlled space, for instance, a workshop, give greater reliability and utilization of the material [36]. Prefabrication facilitates a fast construction assembly due to many elements already being fitted and produced.

2.2 The network arch

The concept of the network arch bridge was introduced by Per Tveit in 1955 [30]. A network arch features inclined hangers, crossing at least twice, connecting the bridge deck to the tied arch. The network arch, like other tied arches, can be compared to a beam with a compression and tension zone. By increasing the arch's rise, the axial forces in the chord will be reduced, subsequently lowering the structure's weight. The rise, however, is often limited by aesthetic reasons or transportation constraints. The hangers act like a light web, taking some of the variations in the shear force. The maximum longitudinal bending moments can be 10 times smaller than for conventional tied arch bridges, resulting in the need for less materials [24]. Network arches are most suitable for spans ranging from 80 m to 170 m [30].

The precursor for the network arch is the Nielsen bridge, as shown in Figure 2.2. One of the main differences is the crossing of hangers. The Nielsen concept had a limitation when subjected to dynamic loads, which could cause tension to decrease, resulting in compression in certain hangers. By increasing the distance between nodal points, the likelihood of compression is reduced. Nevertheless, this results in a reduced buckling capacity. This problem was approached by Tveit by incorporating multiple intersections of hangers to avoid compression [3]. This hanger configuration is shown in Figure 2.3.

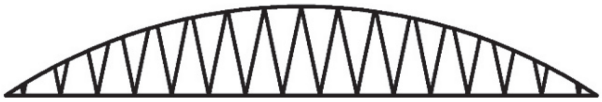

Figure 2.2: Nielsen hanger configuration.

Source: [21]

Figure 2.3: Network arch with radial hanger configuration.

Source: [21]

The ideal network bridge has all hangers in tension. In certain load cases, the hangers may be subjected to compression and lose their structural effect. These hangers are called relaxed. The hangers in a network arch bridge are only meant to take tension forces to distribute the bending moments along the arch. In the part of the arch connected to relaxed hangers, the moment distribution alters, which must be considered in calculations. To prevent excessive hanger relaxation, the angle between the hangers and the vertical axis cannot be too small. A large angle tends to increase the bending moments in the arches due to concentrated loads. A compromise should be found to minimize moments and hanger relaxation. All hangers can have the same cross-section and, ideally, nearly the same load. With no transverse beams, upper nodes are normally evenly distributed along the arch. The optimal network arch uses less material, making it environmentally friendly in a broader sense [31].

For load cases where hanger relaxation is of small scale, network arches act very much like many trusses on top of one another, where the bending in the tie and the arches is small. The tie of the network arch bridges is usually made of concrete to pre-stress the hangers with the self-weight of the deck. Relaxation of hangers may cause complications with calculations if the effect on the structure of the relaxed hangers cannot be taken fully into account [30]. Relaxed hangers can also be a problem in serviceability if they move too much out-of-plane. If hangers are made as rods, cyclic bending can lead to failure.

2.3 Timber in network arch bridges

For certain load combinations, the hangers in network arch bridges may relax. To prevent this, it is common practice to construct such bridges with a heavy concrete deck. The weight of the concrete deck provides sufficient pre-stressing to the hangers, minimizing relaxation. However, when replacing the concrete deck with a timber deck, the deck's density decreases from approximately 2500 kg/m^3 to around 430 kg/m^3. This decrease in total weight can pose challenges in pre-stressing the hangers and managing hanger relaxation.

Kolbein Bell conducted analyses on a network arch bridge with a stress-laminated timber deck to investigate the impact on hanger relaxation by a light timber deck [5]. He found that timber is too light to avoid relaxation of hangers in addition to generation of significant bending moments in the arch where the hangers are relaxed. One of the most problematic consequences observed was hangers buckling out-of-plane due to the decreased distance between fastening points [5].

Another significant effect of extensive hanger relaxation was the introduction of bending moments in the hangers, with the size dependent on the hanger's stiffness. Given the high likelihood of relaxation occurring in some of the hangers during movement of axle loads along the bridge deck, the relaxation phenomenon would frequently lead to unfavorable moments in the hangers. This issue becomes particularly problematic when considering the fatigue effects since the constant loading and unloading of the hangers with moments pose significant challenges. Additionally, the relaxation of such hangers would result in sudden sounds due to the outward bending of the material, which compromises the assurance of structural safety for bridge users. Halse investigated this challenge in a timber network arch bridge by introducing three-hinged hangers to implement controlled in-plane "buckling" [9].

Using a timber deck in a network arch bridge also implements transversal crossbeams. With crossbeams, the hanger arrangement is modified. The hanger connection points are distributed evenly on the crossbeams, as opposed to concrete decks, where the hangers are evenly distributed on the arch. This means the distribution along the arch depends on the number of crossbeams and hanger angle and may become unevenly spaced along the arches.

2.3.1 Hanger arrangement

The hanger arrangement in the network arch greatly influences the stress distribution. The hanger arrangement is decided by the number of hanger sets, the number of hangers in each set, the distance between hangers in one set, and the inclination of the hangers. A set of hangers corresponds to a group of hangers that are inclined towards the same direction or follow the same rate of change in inclination or pattern. The second set is usually symmetrical to the first set, mirrored about the bridge's midpoint. The third set can be positioned in the middle of the previous sets, creating a mirror line between them. A longer bridge with larger loads requires more hangers. A good hanger pattern distributes the bending moments well in the arches.

Some examples of pattern types are rhombic pattern, pattern with a constant inclination of hangers, pattern with a constant change of inclination of hangers, elliptical pattern, and radial pattern [20]. The radial pattern has a constant angle between the arch's radius line and the hangers. This pattern was developed by Schanack and Bruun for a 100 m network bridge [24]. In this pattern, the hangers can be distributed evenly along the deck or the arch.

The modified radial pattern, introduced by Anna Ostrycharczyk, implements focal points to create a radial ray to spread the angle [20]. The radial ray is a straight line from the focal point, through the crossbeams, toward the arch. This focal point is the center for radial rays. The angle is

constant between the radial rays and the hangers. The focal point lies in the plane of the arch and can be shifted horizontally and vertically relative to the center of the arch to optimize the pattern. For shifts in the horizontal direction, two or three focal points are created, depending on if the number of crossbeams is odd or even; see Figure 2.4. The angle, α, is measured from these radial rays, as shown in Figure 2.5. The modified radial pattern allows for control over the hanger distribution in the arch.

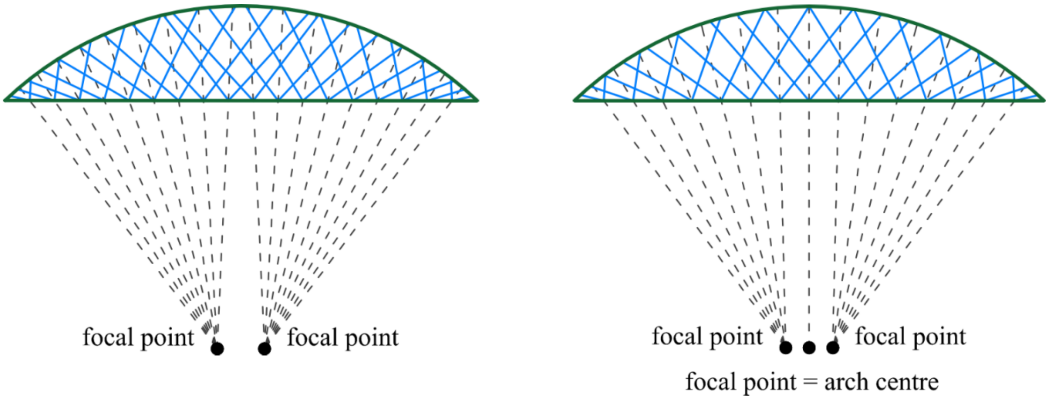

(a) Even number of crossbeams.

(b) Odd number of crossbeams.

Figure 2.4: Modified radial pattern.

Source: [20]

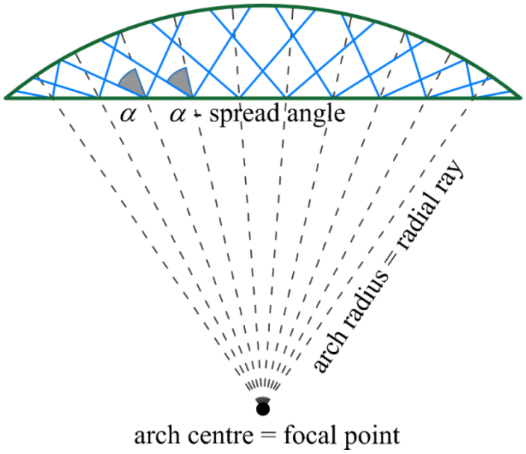

Figure 2.5: Radial pattern with classical xy-configuration.

Source: [20]

2.4 Finite Element Analysis

Finite Element Analysis (FEA) solves structural problems by breaking down a complex structure into smaller elements. FEA calculates with these elements rather than the entire structure, making the problem more manageable. The accuracy of FEA results depends on the level of discretization, i.e., the number of elements used. A finer mesh, with more elements, provides more accurate results but requires more computational time. However, a balance between accuracy and computational efficiency should be found to achieve reliable results within a reasonable timeframe. To ensure convergence, the structure must have a stiffness. FEA constructs a systems stiffness matrix, which relates to the structure's stiffness, using interpolation functions. The system stiffness matrix may become singular if zero energy modes are introduced or if rigid body modes are not restrained in the system. A singular stiffness matrix is not invertible and should be avoided. Careful consideration of discretization, convergence, and the presence of singularities is necessary to obtain meaningful and solvable results.

The choice of elements in a discretized model is crucial as different elements have varying capabilities to represent desired results. To accurately capture bending moments in structural analysis, elements with rotational Degrees of Freedom (DOFs) are necessary. The complexity of an element, including the available DOFs and the interpolation functions used to describe its behavior, affects the computational time required for convergence. Therefore, it is important to consider the desired results before selecting an element type.

Truss elements, on the other hand, only possess translational DOFs along their longitudinal axis. As a result, they can only model axial stresses and strains, making them improper for shear or bending moment problems. However, truss elements are useful when studying structures where axial strains are the main concern, such as hangers in a bridge.

Beam elements are relatively simple with translational and rotational DOFs. They can be used for both 2D and 3D problems and can represent axial forces, shear forces, and bending moments. Solving beam elements in computer-aided design (CAD) programs is generally efficient due to their simplicity.

The Timoshenko-Ehrenfest beam theory, formulated by Stephen Timoshenko and Paul Ehrenfest, is a beam model that incorporates both shear deformation and rotational bending effects. This model is particularly well-suited for analyzing the behavior of thick beams and sandwich composite beams. By considering these additional effects, the Timoshenko-Ehrenfest beam theory provides a more accurate representation of the mechanical response and deformation characteristics of beam structures [16].

Shell elements are employed to model 3D geometry when the thickness of the shell is significantly less than its length. These elements serve as approximations of solid elements in three dimensions, offering a balance between computational efficiency and accuracy, thus making them a desirable choice for various applications. Kirchhoff plate theory assumes that a vertical line remains straight and perpendicular to the neutral plane of the plate during bending. Consequently, thin plates are reliably described by Kirchhoff plate theory [10].

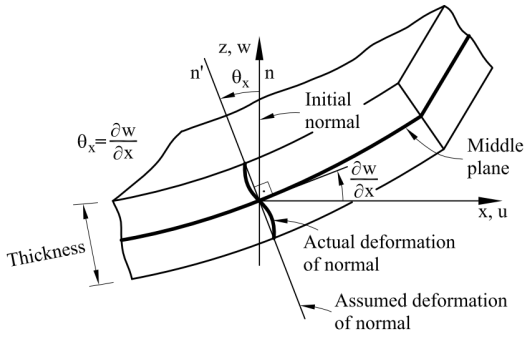

Figure 2.6: Deformation of the normal vector and in-plane displacement field in a thin plate.

Source: [19]

TRIangular Composite (TRIC) element is a triangular, simple, yet sophisticated, flat shell element capable of accurately analyzing thin and moderately thick isotropic plate and shell structures [12]. This method, introduced by Argyris, distinguishes the pure deformational modes from the rigid body movements of the element. Stiffness matrices are derived using straightforward algebraic expressions. It utilizes exact integrations and explicitly derives the stiffness, mass, and geometric matrices. The kinematics of the TRIC element is decomposed into six rigid-body modes and twelve straining modes of deformation.

A crucial aspect of the TRIC shell element formulation lies in adopting the natural coordinate system, where the three axes align with the sides of the triangle, as illustrated in Figure 2.7. Additionally, the local elemental coordinate system is positioned at the centroid of the triangle and the global Cartesian coordinate system governs global equilibrium. The TRIC elements can be layered, where each layer of the triangular structure defines a material coordinate system labeled as 1, 2, and 3, with axis 1 parallel to the direction of the fibers. These distinct coordinate systems enable the TRIC element to model multilayer anisotropic shell structures effectively. The TRIC element can also simulate sandwich or single-layer configurations when required [11].

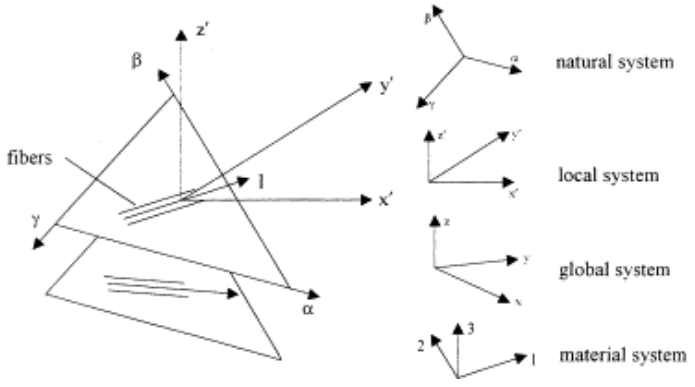

Figure 2.7: Coordinate systems of the multilayer triangular TRIC element.

Source: [11]

2.5 Multi-Objective Optimization

Multi-Objective Optimization (MOO) implements a simulation process that varies several parameters to optimize multiple objectives simultaneously. These objectives are often conflicting, thus making the relative individual importance governing in finding the optimum solution. Using the Strength Pareto Evolutionary Algorithm, SPEA, the various configuration of parameters are categorized depending on their Pareto efficiency. A Pareto optimal solution is a configuration that requires that none of the objective functions can be improved without degrading others [14]. The results are often illustrated using a Pareto front, including all configurations considered Pareto optimal.

When using genetic algorithms for multi-objective optimization, two important operators are crossover and mutation. Crossover involves combining pieces of multiple parent chromosomes to create offspring chromosomes. At the same time, mutation introduces random changes to the offspring chromosomes to increase genetic diversity and prevent the algorithm from getting stuck. It's important to balance exploration and exploitation when determining the crossover and mutation rates. A moderate rate between 0.6 to 1 is often recommended for crossover, depending on the problem and algorithm used. High crossover rates can lead to premature convergence, whereas a low rate might cause a lack of diversity. As for mutation, a rate between 0.01 to 0.1 is commonly suggested, but it depends on the optimization problem and algorithm. A suitable parameter selection is crucial for successful MOO using genetic algorithms [8, 14].

Strength Pareto Evolutionary Algorithm, SPEA, starts with an empty archive and an initial population. Thereafter it ranks each solution with a strength value based on the number of solutions the population it dominates. All non-dominated solutions, equivalent to Pareto optimal, are added to the archive whilst removing the dominated solutions [38]. If the predefined archive size is exceeded, further archive members are removed by a clustering technique that preserves the characteristics of the non-dominated solutions. To obtain a varied population, SPEA recombines the union between the population and the archive with mutation and crossover. The offspring from this process forms the new population. The simulation continues until the archive converges to a set of non-dominated solutions, which can form the Pareto front. SPEA2, the enhanced version of SPEA, incorporates a fine-grained fitness assignment strategy that includes density information. The archive size is fixed and adjusted by adding dominated solutions if the number of non-dominated solutions is less than the archive size. If the archive size is exceeded, SPEA2 incorporates a reduction method that does not lose boundary points [37]. A flowchart showing the SPEA2 framework is shown in Figure 2.8.

A different MOO algorithm is the Hypervolume Estimation algorithm, HypE. HypE utilizes a hypervolume indicator to evaluate the quality of a set of solutions [4]. The hypervolume indicator measures the volume of objective space dominated by the solution and ranks them thereafter. A higher level of dominated space corresponds to a superior solution. The algorithm starts with a random set of solutions and then tries to improve the hypervolume indicator by adding or removing solutions. It selects solutions based on their hypervolume ranking and diversity. This process continues until the hypervolume indicator converges to a set of non-dominated solutions, similar to SPEA2.

Regarding multi-objective optimization algorithms, it is beneficial to incorporate elitism. This involves holding onto the most successful solutions from each generation to ensure they aren't lost during selection. Keeping elitism moderately low can help avoid getting stuck in local optima and lead to improved convergence [25]. Achieving optimal parameters in MOO algorithms requires balancing exploration and exploitation, diversity, and convergence.

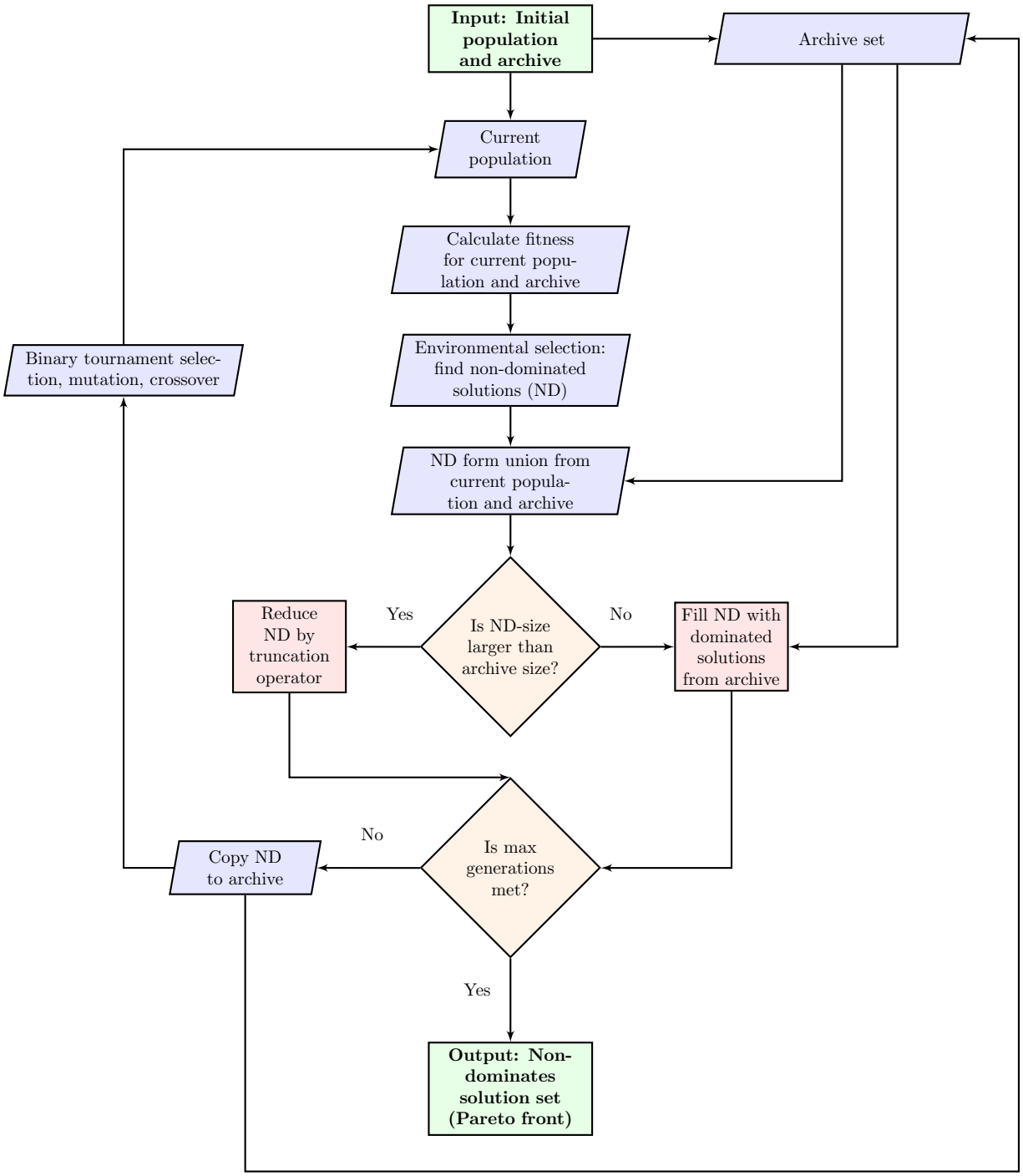

Figure 2.8: SPEA2 framework.

3 Modelling and applied methods

3.1 Model

3.1.1 Software

Rhinoceros and Grasshopper

Rhinoceros, a commercial 3D computer graphics and CAD software offers a comprehensive suite of tools for creating, editing, analyzing, and rendering various types of geometric entities. These entities include NURBS curves, surfaces, solids, point clouds, and polygon meshes. At the core of Rhino's geometry lies the Non-Uniform Rational B-Splines (NURBS) mathematical model, which enables the precise and flexible representation of 3D shapes. NURBS can accurately describe objects from simple 2D lines, circles, arcs, and curves to intricate 3D organic free-form surfaces or solids. Consequently, NURBS models find utility across a wide spectrum of applications, from illustration and animation to manufacturing processes [18].

Within Rhino, users can enhance their design workflow with *Grasshopper*, a visual scripting language and environment that functions as a powerful parametric modeling tool within Rhino. Grasshopper provides a graphical algorithm editor that enables the creation of programs by assembling components on a canvas [7]. Users can connect one component's outputs to subsequent inputs, forming a visual programming environment. This intuitive approach empowers designers and architects to efficiently explore and manipulate complex design systems.

Furthermore, Grasshopper offers a range of plug-ins that facilitate the integration of physical models created within the Grasshopper environment with programs for structural analysis or optimization. This capability enhances the utility of Grasshopper as a versatile tool for integrating design exploration and analysis. These plug-ins provide additional tools, functionalities, and integration, allowing users to incorporate advanced analysis, optimization, and simulation techniques into the design processes.

In Grasshopper, sliders and Boolean toggles play a significant role in enabling user interaction. Sliders allow users to vary numerical inputs by adjusting the component within a range, with a defined step size. When incorporated into a model, sliders introduce parametric behavior, enabling the geometry to adapt dynamically based on the slider values. Consequently, the entire model can be modified in a number of ways within the same file as the geometry responds to changes in the slider values. The Boolean toggles are "buttons" outputting True or False. This value can, for instance, be programmed to switch on and off different functions or conditions in the model. This parametric approach grants the flexibility to explore numerous design variations efficiently without reconstructing the entire model.

Karamba3D

Karamba3D is a parametric finite element plug-in in Grasshopper. It makes it easy to combine parametric design and structural analysis and optimization algorithms such as Octopus. It can perform linear, nonlinear, and dynamic analysis and includes various tools for visualizing and analyzing results, such as diagrams for stress and deformation. Karamba3D is highly flexible and allows users to customize the preferred analysis and workflow using Grasshopper.

It is important to note that Karamba3D is tailored for architects and engineers in the early design

stage, meaning more detailed calculations and design checks should be employed in other finite element programs. Karamba3D has Eurocode 1993-1-1 (Eurocode 3) implemented and does not include the function of exporting reports of results. If other Eurocodes are required, the design checks must be manually implemented. In the case of timber, Eurocode 5 should be used. Simple analyses have been made with Autodesk Robot to see if Karamba3D produces the same results for a simple timber network arch bridge in 2D. The results are identical, indicating Karamba3D gives sufficient results for the purpose of this thesis.

Octopus

Octopus is a plug-in for Grasshopper, initially developed for multi-objective evolutionary optimization. It employs the Pareto principle for multiple objectives, allowing the search for numerous results simultaneously and producing a range of optimized solutions between the extremes. This differs from the included Grasshopper plug-in, Galapagos, which performs single-objective optimization with multiple parameters. Octopus is based on the SPEA2 and HypE algorithm with a user interface that is customized yet derived from Galapagos.

Octopus is an advanced tool that offers a range of features to find desirable solutions. It can search for a single goal, provide various solutions, and locate the best trade-offs between multiple goals. Additionally, it can improve solutions based on similarity goals and change objectives during a search. Octopus provides visual feedback on solutions' 3D models in objective space, records history, and saves all data within the Grasshopper document, and exports them as .txt files. There are also various options for optimization customization, most relevant; SPEA2 reduction, HypE reduction, and costume mutation. SPEA2- and HypE reduction refers to the method of removing solutions from the archive. Octopus employs several optimization techniques, including elitism, mutation, and crossover. The user interface is shown in Figure 3.1.

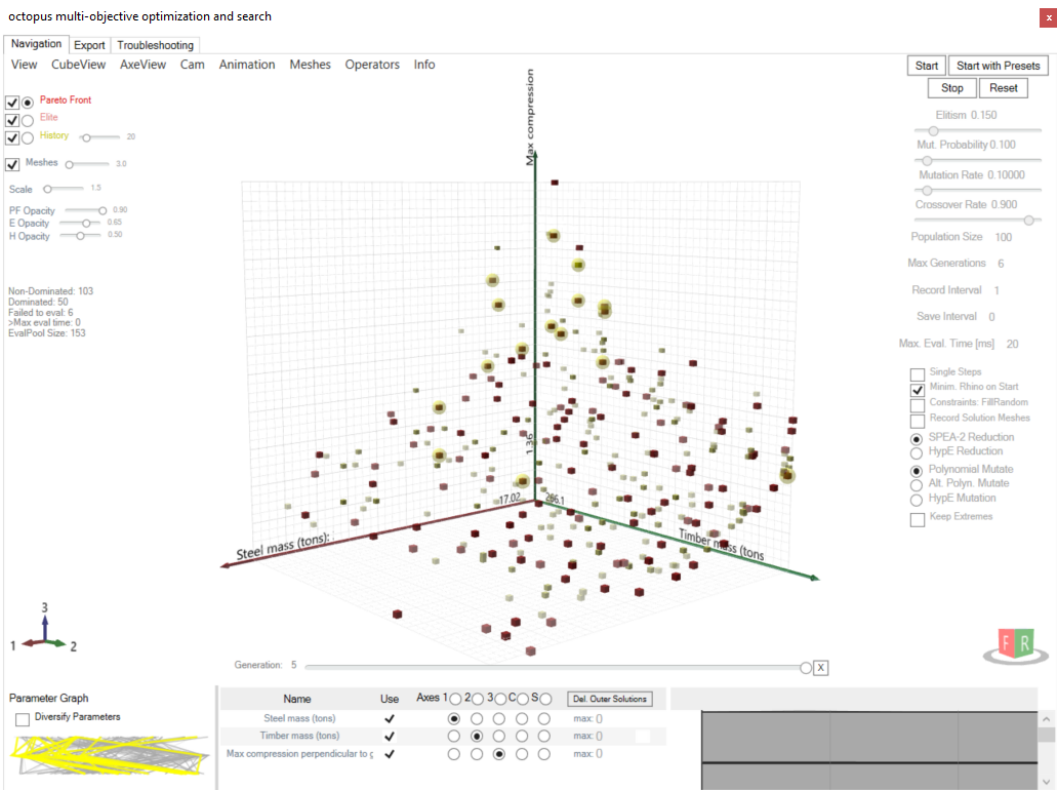

Figure 3.1: Octopus interface after a simulation.

In the case of optimizing the network arch bridge, a smaller population size and fewer generations may be sufficient to investigate the search space and finding suitable solutions. Compared to other computational problems, the possible range of configurations is limited. However, the mutation- and probability rate should be kept at reasonably low levels, depending on the size of the search space and the complexity of the problem. Elitism is set to 0.15 to preserve the best solutions while exploring new combinations in the next generations. The mutation rate and probability are initially set to 0.1. The crossover rate is set to 0.9 to allow for good recombination of non-dominated solutions. The population size is set to 100, while the number of generations is between 5 and 30 for all simulations. These numbers are thought to be high enough to cover the search space efficiently and find the optimal combinations without taking up too much computational time per simulation. For this problem, both SPEA2 and HypE reduction can be used as they are both suitable for MOO- problems. The chosen algorithm was SPEA2 since Hypervolume generally requires significant calculation time. As for mutation, the polynomial mutation is considered a good choice as it is efficient in exploring the search space. The chosen parameters for Octopus are fixed for all simulations and are listed in Table 3.1.

Elitism	0.15
Mutation probability	0.1
Mutation rate	0.1
Crossover rate	0.9
Population size	100
Number of generations	5 - 30

Table 3.1: Parameters in Octopus.

3.1.2 Geometry

The evaluated bridge concepts in this thesis are timber network arch bridges with a timber deck on transversal crossbeams. A configuration, referred to as "the standard configuration", includes two sets of hangers, leaned arches, increased arch heights near the supports, and top- and side beams. This configuration is illustrated in Figure 3.2.

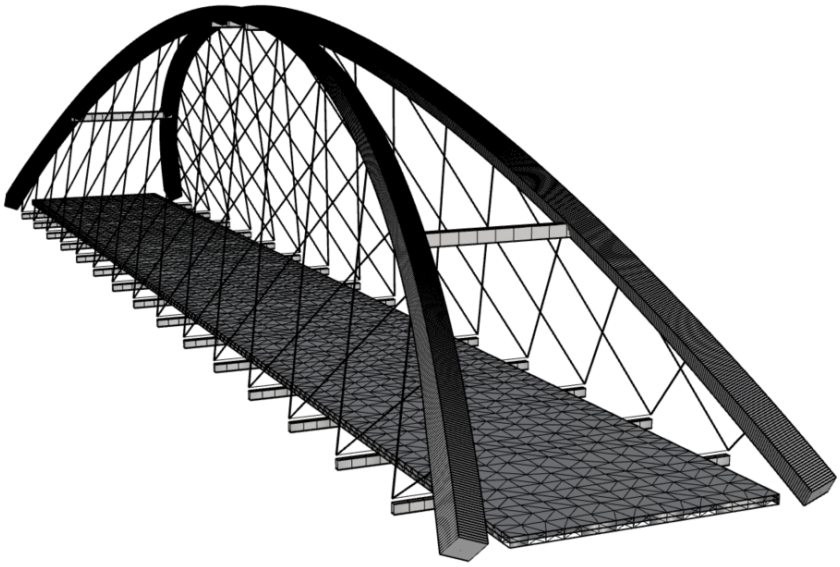

Figure 3.2: General geometry of the standard bridge configuration.

The bridge models optimized in this thesis were modeled in Grasshopper. The length of the bridge lies along the global x-direction, the width of the bridge along the global y-direction, and the arch rise is along the global z-direction. The bridge is double symmetric, mirrored about the xz- and yz-plane with origin in the mid-point of the bridge, which refers to the point at the bridge's mid-span. The elements' local x-direction lies along the element's length.

Material properties

Karamba3D has Eurocode 3 (EC3) implemented, as steel is the default material [27]. Consequently, the definition and calculation of timber members require manual implementation by the user [15]. In the material definition in Karamba3D, the orthotropic behavior of wood is incorporated by distinguishing between material properties parallel and perpendicular to grain. The implementation of orthotropic materials is limited to shell elements in Karamba3D. Only the material properties corresponding to the first direction are considered when using beam elements. This corresponds to the longitudinal direction. For shell elements, the first material direction aligns with the local x-axis of the element, meaning the longitudinal direction of the bridge. The other directions are perpendicular to the local x-axis [15].

The materials used in the model are glued laminated timber and steel. The glulam quality chosen for the arch beams is GL30h and GL30c for the deck. The steel grade of all steel elements is S355, with the default material properties from Karamba3D. The material properties are shown

for GL30h, GL30c, and S355 in Tables 3.2, 3.3, and 3.4, respectively.

$E_{0,g,mean}$ $\left[\frac{N}{mm^2}\right]$	$E_{0,g,05}$ $\left[\frac{N}{mm^2}\right]$	$E_{90,g,mean}$ $\left[\frac{N}{mm^2}\right]$	$E_{90,g,05}$ $\left[\frac{N}{mm^2}\right]$	$G_{g,mean}$ $\left[\frac{N}{mm^2}\right]$	$G_{g,05}$ $\left[\frac{N}{mm^2}\right]$	$G_{r,g,mean}$ $\left[\frac{N}{mm^2}\right]$	$G_{r,g,05}$ $\left[\frac{N}{mm^2}\right]$
13 600	11 300	300	250	650	540	65	54
$f_{t,0,g,k}$ $\left[\frac{N}{mm^2}\right]$	$f_{t,90,g,k}$ $\left[\frac{N}{mm^2}\right]$	$f_{c,0,g,k}$ $\left[\frac{N}{mm^2}\right]$	$f_{c,90,g,k}$ $\left[\frac{N}{mm^2}\right]$	$f_{v,g,k}$ $\left[\frac{N}{mm^2}\right]$	$\rho_{g,mean}$ $\left[\frac{kg}{m^3}\right]$	α_T $\left[\frac{1}{C^\circ}\right]$	ν_{12} $\left[-\right]$
24	0.5	30	2.5	3.5	480	5.0E-6	0.6

Table 3.2: Material properties of GL30h, from Table 5 in NS-EN 14080 [29]. Exception is α_T and ν_{12} which is from Karamba3D and [17], respectively.

$E_{0,g,mean}$ $\left[\frac{N}{mm^2}\right]$	$E_{0,g,05}$ $\left[\frac{N}{mm^2}\right]$	$E_{90,g,mean}$ $\left[\frac{N}{mm^2}\right]$	$E_{90,g,05}$ $\left[\frac{N}{mm^2}\right]$	$G_{g,mean}$ $\left[\frac{N}{mm^2}\right]$	$G_{g,05}$ $\left[\frac{N}{mm^2}\right]$	$G_{r,g,mean}$ $\left[\frac{N}{mm^2}\right]$	$G_{r,g,05}$ $\left[\frac{N}{mm^2}\right]$
13 000	10 800	300	250	650	540	65	54
$f_{t,0,g,k}$ $\left[\frac{N}{mm^2}\right]$	$f_{t,90,g,k}$ $\left[\frac{N}{mm^2}\right]$	$f_{c,0,g,k}$ $\left[\frac{N}{mm^2}\right]$	$f_{c,90,g,k}$ $\left[\frac{N}{mm^2}\right]$	$f_{v,g,k}$ $\left[\frac{N}{mm^2}\right]$	$\rho_{g,mean}$ $\left[\frac{kg}{m^3}\right]$	α_T $\left[\frac{1}{C^\circ}\right]$	ν_{12} $\left[-\right]$
19.5	0.5	24.5	2.5	3.5	430	5.0E-6	0.6

Table 3.3: Material properties of GL30c, from Table 4 in NS-EN 14080 [29]. Exception is α_T and ν_{12} which is from Karamba3D and [17], respectively.

E $\left[\frac{N}{mm^2}\right]$	G $\left[\frac{N}{mm^2}\right]$	f_y $\left[\frac{N}{mm^2}\right]$	ρ $\left[\frac{kg}{m^3}\right]$	α_T $\left[\frac{1}{C^\circ}\right]$	ν $\left[-\right]$
210 000	80 760	360	8000	1.2E-5	0.3

Table 3.4: Material properties of S355, as given in Karamba3D.

Spliced Arches

The arches are modeled as circular-shaped arches with an incline towards each other at the top. The arch curves are divided into elements and implemented in the mesh through the "Line to beam"-component in Karamba3D. With beam elements, each segment has a node at its start and end, with translational and rotational degrees of freedom. The beam elements in Karamba3D are shear deformable according to the Timoshenko beam theory. Lines meeting at the same point are automatically rigidly connected. Material and cross-sectional properties are assigned to each element. The material properties of timber are defined manually with properties are from NS-EN 14080 [29].

The general length limit for transportation is about 30 m. Splices are placed along the arches to ensure that each part of the arch does not exceed this limit. The splices are symmetrically placed about the mid-point, and the number of splices depends on the length of the bridge. An efficient and practical approach to model splices is by implementing a reduced E-modulus in the area of the arch where the splice is intended [1]. This is to implement the reduced stiffness in the splice into the model. The reduced E-modulus is equal to 50% of the original material's E-modulus and applied over a length of four times the arch height. The reduced E-modulus is based on what should be a conservative and simplified assumption with a splice combination, as seen in Figure 3.3. The width of the arch, at the spliced area, is halved for each part. Reducing the E-modulus by half is

[1] The practice of reducing the E-modulus to model connections is from a conversation in person with K.A. Malo

approximately equivalent to reducing the width of the cross-section by half in these areas in terms of displacement out-of-plane. This is verified by simple checks in Karamba3D. After comparing it with a splice of half the cross-sectional width and getting similar results, the splice configuration is not further investigated.

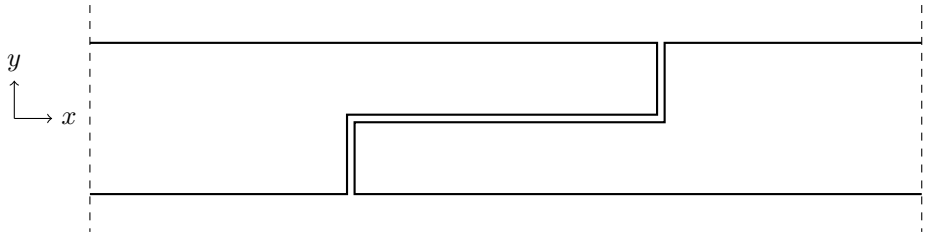

Figure 3.3: Simplified splice in the global xy-plane, seen from above.

The beam orientation can be modified with the "Line to Beam"-component. This is adapted to make the arches lean toward each other with the lower edge perpendicular to the hanger plane. By default, the system lines of the beams are in the center of the elements. The local eccentricities of the arches are set to half the arch height and moved in the local z-direction. This results in the system line of the arches being at the lower edge. This connects the hanger on the lower edge instead of in the middle of the arch cross-section. Limitations in Karamba3D make this the only option because the hanger nodes need to intersect with the arch nodes, located along the system line, to establish a connection. As a result, the arches will be subjected to bending moments induced by the eccentricities at the supports. The end supports must also coincide with the system line for computational purposes in Karamba3D. Initial investigation showed that by adjusting the eccentricity, only the in-plane bending moments near the end supports had a noticeable change. It is comparable to applying an initial imperfection at the supports. By changing the maximum arch height at the support, additionally described later, it is possible to modify the in-plane bending moment diagram for the arches and adapt it to suit multiple load cases.

Deck

The deck is defined as multiple surfaces meshed with the "Mesh Breps"-component. Loads and supports are attached to mesh nodes. When two meshes have common boundaries, they need identical vertices along the connecting border to be structurally connected. Support points at the deck end, and nodes on the crossbeams that coincide with the deck, are specifically included in the mesh to make the nodes in the shell elements coincide with the nodes on the crossbeam elements. The deck is meshed into triangular shell elements. The target mesh size is 1 m, meaning there will be two triangular shell elements per square meter in the deck mesh. The mesh is relatively coarse but consists of equal-sized elements, which gives better results from the mesh. Therefore, for a constant distributed load, this should represent the behavior sufficiently. Bending stiffness is included for the mesh. The shell element formulation used in Karamba3D is based on the TRIC element, as described in Section 2.4 [12]. Contrary to the standard TRIC element, the shell element in Karamba3D is based on Kirchoff's theory. There are three nodes per element with six degrees of freedom per node, and a constant strain state is assumed for each layer, illustrated in Figure 3.4. No in-plane rotational stiffness is added. Karamba3D neglects transverse shear deformation in the case of shell elements.

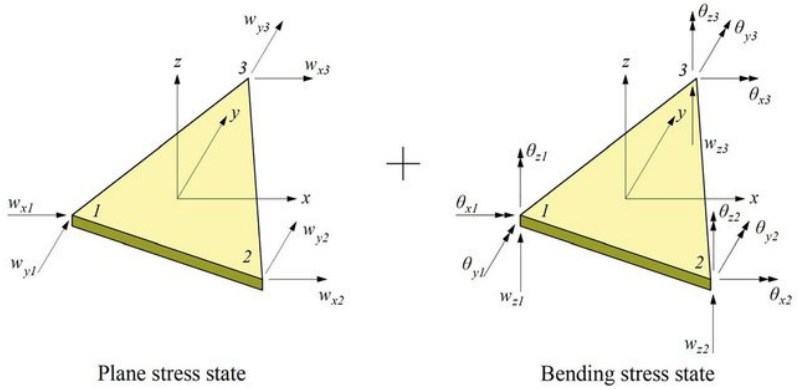

Figure 3.4: Three-node plane triangular shell element based on Kirchhoff- Love plate theory.

Source: [1]

Crossbeams

The crossbeams are made of steel and are evenly distributed along the length of the deck. They are defined as beam elements, where each crossbeam is divided into eight elements. HEB-sections were initially examined as crossbeams, but it was observed that the outer part of the crossbeams experienced substantial stresses and deformation due to torsional moments. They were subsequently replaced with rectangular hollow sections to enforce adequate torsion resistance. The "Eccentricity on cross-section"-component moves the crossbeams in the negative z-direction. They are moved at a distance equal to half the height of the crossbeams in addition to half the deck thickness so that the upper edge of the crossbeams coincides with the lower edge of the deck, making the system lines align. This simplified approach is assumed to have a negligible effect on the structural result.

Hangers

Steel hangers connect the arches to the rest of the structure. The hangers are connected from the ends of the crossbeams to the lower edge of the arches. They lie within the same plane as the arches, creating a "stiff plane". A simple check is performed by moving the hangers out of the arch's plane, making the configuration asymmetric about the arch's local xz-plane. This results in significantly larger stresses and displacements. The model is therefore scripted so that such configurations are avoided. The hanger configuration implemented in the model is inspired by Anna Ostrycharczyk's modified radial pattern, which is described in Section 2.3.1 and illustrated in Figure 2.5. Ostrycharczyk found that this modified radial pattern could improve the structural performance of the network arch [20].

The hangers are evenly distributed along the deck, while the hanger distribution along the arch depends on the hanger angle, focal point, and the number of crossbeams. To reduce the number of connection points in the arch, a Python script is implemented to merge connections for the two sets of hangers. Two connection points are merged if they are within a certain distance and from different sets. Only two hangers can be merged in the midpoint between the original pair of connection points. The effect is seen by comparing Figure 3.5 and Figure 3.6. The merging function can be utilized to distribute the connections evenly along the arch while keeping the pattern close to the original modified radial pattern if the merging distance is set right. Depending on the merging distance and the hanger pattern, the number of connection points can be reduced considerably. The effect of merging the hangers is visualized in Figures 3.5 and 3.6.

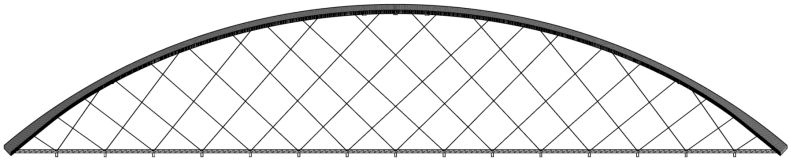

Figure 3.5: 100 m span with 3 splices with Ostrycharczyk's modified radial pattern [20].

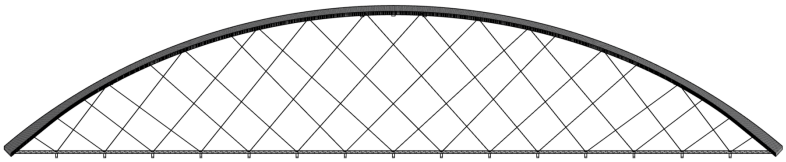

Figure 3.6: 100 m span with 3 splices with merged hanger connections.

The hangers are defined as beam elements with circular S355 steel cross-sections. Due to their desired function, dividing them into smaller elements is unnecessary. Each hanger consists of one element with a rotationally free node at each end. They are given the behavior of hangers, or chains, by eliminating the ability to withstand compression. This is done by introducing the "Tension/compression eliminator"-component in Karamba3D, which is applied after assembling the final model. This component calculates the axial forces and eliminates the compressed hangers. This is a simplified way of ensuring the hangers cannot take any compression forces by removing them if compressed. In this way, the effect of relaxed hangers on the arches' moment distribution is taken into consideration in the model. A simple check was performed by comparing the chain-element in Autodesk Robot to the hangers after the "Tension/compression eliminator"-component for a simple 2D timber network arch bridge. A skew load case was considered, resulting in the same hangers being relaxed and giving identical in-plane bending moments in the arch with relaxed hangers. This indicates that the "Tension/compression eliminator" provides the hangers with their desired function.

Top- and side- beams

Three top beams and two side beams connect the arches. The beams are made of rectangular hollow sections of steel S355. The side beams have a height of 650 mm, while the top beams are made up of sections with a height of 900 mm from Table 3.5. The beams consist of one beam element each, with a node at each end. A total of five beam elements.

The investigation of the arch connection was not the primary focus of this thesis. However, to simulate a scenario where the tops of the arches are connected over a certain length, a configuration consisting of three top beams rigidly connected to the arches was implemented. In practice, the connections would be somewhere between fixed and rotationally free. However, as this study serves as a preliminary investigation, the assumption was made that the connection at the top is fixed.

The cross-sections are set to ensure they do not buckle while supporting the arches. The top beams are modeled as large cross-sections to connect the top of the arches rigidly. The large cross sections are selected to guarantee that the top beams can withstand the load, making the arch design critical. The top beams are placed four meters apart, with the middle top beam positioned at the mid-point of the bridge. The end nodes of the side beams are rotationally free in the connection to the arch. Further investigation of the cross-sections was not performed. Different

cross-sectional properties may alter the moment distribution on the arch, leading to different results in the simulations.

Alternative designs

The cross-sectional height of the arches can be increased gradually towards the arch supports, with a gradient from a user-defined variation graph. The graph used in this thesis is illustrated in Figure 3.7. This feature allows for customized cross-sectional profiles along the ends of the arches. This design was implemented in the simulations.

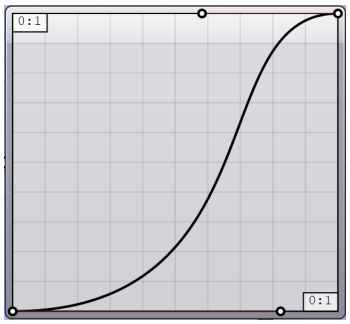

Figure 3.7: Graph defining the rate of increasing arch height. The right part of the graph being the end of the arch.

Stiffening, triangular corners were implemented as an alternative. These triangles consist of two beams, the first spanning from the arch's endpoints and connected to two consecutive crossbeams. The second beam connects the end of the first beam to the arch, following the same inclination as the hanger it replaces; see Figure 3.8. The two beams and the arch form a triangle. The presence of the triangles effectively replaces the hangers within the triangle. The horizontal beams are each made of two beam elements, from crossbeam to crossbeam, while the skew beam consists of a single beam element. The design is shown in Figure 3.8.

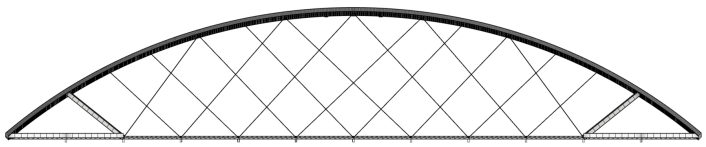

Figure 3.8: Bridge with triangular corners.

Only one of the two corner designs can be active simultaneously, meaning the triangular corners are deactivated while increasing cross-sectional height is activated, and vice versa. This is to see the effect of one design at a time.

A different design implemented includes vertical arches. This configuration includes K-trusses comprising three K's on each side of the bridge's midpoint. The truss beams have quadratic cross-sections with height and width equal to half the arches' cross-sectional height. It spans over 48 meters in the global x-direction. Straight beams from arch to arch are whole and consist of two elements each, while the diagonal beams consist of one element each, i.e., the wind truss consists

of 22 beam elements in total. The elements are connected rotationally free about their local y- and z-axis. The alternative is illustrated in Figure 3.9.

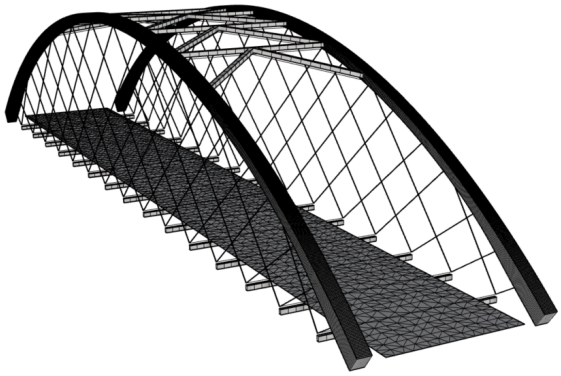

Figure 3.9: Bridge with vertical arches.

In addition, the model allows a third set of hangers. From each crossbeam, the additional hanger coincides with the radial rays. The hangers are modeled similarly to the other two hanger sets, and the configuration is illustrated in Figure 3.10.

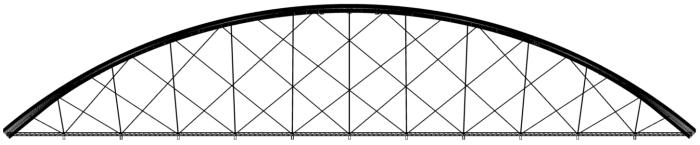

Figure 3.10: Bridge with three sets of hangers.

The standard bridge configuration can be evaluated without the two side beams. This configuration is displayed in Figure 3.11.

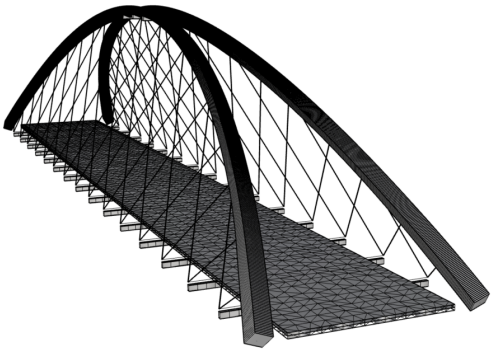

Figure 3.11: Bridge with no side beams.

Supports and joints

By default, element nodes are rigidly connected at their intersections. To modify the connections, it is necessary to define specific joint or support conditions. However, it is important to note that the focus of this thesis was not a detailed investigation of connections. As a result, the stiffness of all connections was simplified rather than accurately determined. The simplification assumes that the connections can either be fully released or fixed in translation or rotation along different directions, disregarding that real connections have some sort of stiffness. The intention is to attempt to conservatively define joint and support conditions to capture the structural behavior of the model.

The ends of the arches are defined as supports using the "Support"-component. They are fixed for translation in all directions while rotationally released in local y- and z-direction to simulate the structures' behavior without large dependency on the support conditions. In this thesis, the aim is that the supports should not need to be a crucial part of the structural performance. The elements are rigidly fixed from rotating in the local x-direction, preventing them from torsional or twisting movements. Five supports are distributed evenly along each deck end. Here, only the rotation in the local y-direction is released.

Load application

The "Loads"-component in Karamba3D lets the user choose between load types, such as gravity-, point-, or mesh load. These three load types are the ones used in the model. The gravity load uses the self-weight of all elements in the structure, where the user assigns the load vector. Gravity applies to all active elements in the structural model. The gravity load uses a gravitational force of 9.81 m/s^2 in the global z-direction. The wind load was applied on the arches, with point loads along the arch in the global y-direction and distributed along the length of both arches, where all the points in the arch mesh are included, mimicking a constant line load. The wind load was also applied on the deck with a constant mesh load distributed over the bridge deck in the global y-direction. The constant mesh load type creates point- and line loads to distribute the input surface load in kN/m^2. The traffic load is also defined as a constant load applied on the deck mesh in the negative z-direction.

Mesh adaption

Ensuring compatibility for finite element analysis requires the nodes of the connecting elements to coincide. The model utilizes the "Closest point"-component in Grasshopper to achieve this. This component takes a point or a list of points and identifies the closest corresponding points in a specified point cloud. This connects different structural elements, ensuring every connection has intersecting nodes. For instance, in the case of the hanger connections to the arch, the point cloud consists of the points in the arch mesh, while the input points are the endpoints of the hangers. The "Closest point"-component finds the points closest to the desired hanger connection points in the arch mesh. The hanger connections are then moved to coincide with these points. As a result, the geometry undergoes slight modifications. This procedure is employed for all other relevant connections between elements. By employing a fine mesh, the resulting alterations in geometry are considered negligible.

Analysis

The component "AnalyzeThII" in Karamba3D analyzes the model, including normal forces from second-order effects, N_{II}, in addition to the cross-section forces N. In Karamba3D, there is a distinction between normal force N, which cause stresses in members, and N_{II}, which results in second-order effects. The "AnalyzeThII"-component calculates the normal forces N_{II} from the cross-section forces, N_x. N_{II} influences the structure's stiffness, subsequently impacting the distribution of cross-section forces. Hence, an iterative procedure is applied with repeated updates of N_{II}- forces.

The "Optimize Cross-Section" component automatically selects the most suitable cross-sections for beams and shells. This component selects the optimum cross sections from Table 3.5 for each element in all crossbeams according to EC3 for steel structures. Since they are beams, Annex B in EC3 applies [27]. It considers the load-bearing capacity of the cross-sections and, if desired, restricts the maximum deflection of the structure. Initially, the beams have a specific height and width. In statically indeterminate structures, the section forces depend on the stiffness of the members, including the cross-section and materials used. Hence, an iterative procedure is necessary. The input for the component comprises a family of cross-sections. The component determines the appropriate cross-section for each element in the crossbeams through the following procedure:

1. Calculation of section forces at multiple points along all beams using the initial cross-section.
2. For each element or given set of elements, the first suitable entry from the corresponding cross-section family is selected.
3. If no changes were required in step two, or if the maximum number of design iterations has been reached, the algorithm stops. Otherwise, it returns to step one using the selected cross sections from step two.

Table 3.5: Possible cross-sections for the crossbeams. Rectangular hollow sections (RHS).

Height [mm]	250	350	450	550	650	750	900	1050	1200	1400
Width [mm]	150	200	250	300	350	400	500	600	700	850
Thickness [mm]	8	12	16	20	23	26	30	34	38	43

Starting with the first item of a cross-section family, the algorithm tests all members and stops when it finds a cross-section with utilization below a preset value set to 0.8, corresponding to 80%. The utilization is calculated as the maximum stress in a point divided by the material strength. In the case of steel, the Von Mises stress applies. Once structural failure safety is ensured, an optional second step follows, where Karamba3D attempts to achieve a user-defined maximum deflection. The number of design iterations should be appropriately chosen, with five usually being sufficient. If the given loads exceed the load-bearing capacity of the largest available cross-section in the cross-section family, Karamba3D issues a warning.

The "Buckling modes"-component performs a linear elastic buckling analysis on the structure by solving the general eigenvalue problem involving elastic geometric stiffness matrices. The geometric stiffness depends on the second-order normal forces, N_{II}. The "Buckling modes"-component checks the global buckling of the chosen structural parts.

To determine the buckling length of the arches using Karamba3D, a series of steps is followed. Initially, the original geometry of the arches was analyzed using the "AnalyzeThII"-component

and then analyzed with the "Buckling modes"-component to identify the critical buckling mode. This buckling mode can be visualized using "Model view", which allows for extracting both the original model geometry and the deformed model after buckling.

The model's geometry is modified using the "Model View"-component to introduce initial imperfections to the structure. The distances between corresponding points in the original and buckled model geometries are calculated and scaled, ensuring that the maximum distance between any two points in the arches is equal to 0.0025 times half the arch length, as specified in EC5, Eq. (5.2) [28]. By examining the first buckling shape obtained from the "Buckling modes"-component, an estimation is made that the length l is approximately half the total length of the arch. The first buckling mode is shown in Figure 3.12. Consequently, the points in the original model are adjusted by these scaled distances, effectively deforming the original geometry towards the buckling shape while maintaining the largest initial deformation at $0.0025 \cdot l$.

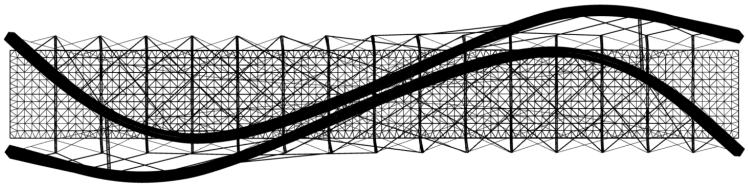

Figure 3.12: First buckling mode, significantly up-scaled.

A new model was created using the scaled deformed geometry and analyzed using "AnalyzeThII" and the "Buckling modes"-component. This process ensures that the model is modified with the appropriate scale and shape to introduce an initial imperfection in the geometry unfavorable for buckling. This new model requires only one analysis using "AnalyzeThII," as the initial analysis is primarily needed to adapt the geometry. The resulting "Buckling modes"-component provides a buckling load factor, k, which can be utilized in Euler's buckling formula for further analysis. When multiplied with the buckling load factors, the current normal forces N_{II} would lead to an unstable structure [15]. The initial deformation is inspired by Figure 3.13 from EC5 [28].

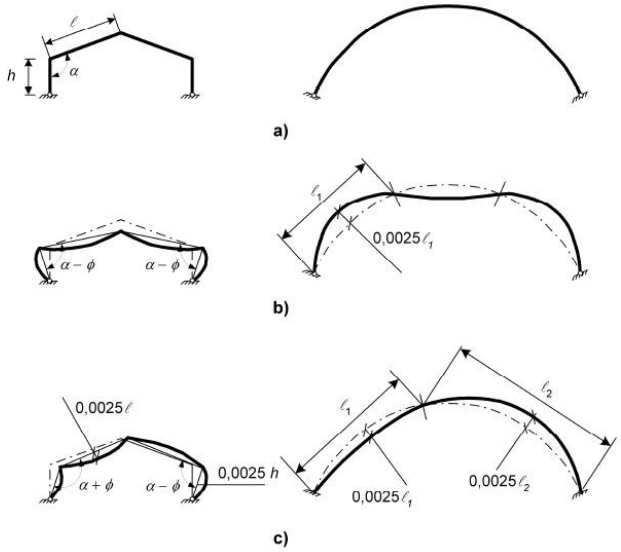

Figure 3.13: Expected initial deformation of frames.

Source: Figure 5.3 from EC5 [28]

3.1.3 Basis for design

Geometric requirements

The arch rise and deck width of the bridge are determined by the geometric demand of the road. The width of the deck should be able to fit two notional lanes, a sidewalk, and railing. The notional lanes should be either 3 m with 0.75 m for the hard shoulder or 3.25 m with 1 m hard shoulder, depending on whether the road is in dimension class Hø1 or H1. The sidewalk is 2 m wide plus an added section for the curb of 0.5 m, according to Table 3.3-3 and Clause 2.3.1-3 in N100 [32]. The height for an 80 m bridge is set to 18% of the span length in the simulations due to the height requirement of 4.9 m over the notional lanes and the sidewalk according to Clause 5.4.1 in N400 [34]. The added safety distance of a minimum of 4 m free space measured vertically from the road surface, and 1 m horizontal distance from this free room to a bearing element, according to Clause 4.3.2-8 in N101 [33]. All the requirements are satisfied with a 12 m wide deck and a two-meter crossbeam extension on each deck side for a rise of 14.4 m. The type of road depends on the annual average daily traffic. This was not decided, though the requirements for road class Hø1 are satisfied. The configurations with longer spans of 100 and 120 m also satisfy the H1 requirements.

Loads

Clause 5.6.1-1 in N400 determines the bridge's wind class. To fall within wind class I, the structure's natural period, T, must be less than 2 seconds [34]. Since T is the inverse of the natural frequency, f, this corresponds to a f larger than 0.5 Hz. According to Clause 5.6.2-1 in N400 [34], the wind load in this class should be calculated with Clause NA.4.5 from Eurocode 1991-1-4 (EC1-4) [26]. However, as this is a preliminary study, simplifications are made. The peak velocity pressure is estimated with Eq. (8.2) in EC1-4 [26], where a simplified force from wind in the x-direction is used. The reference area depends on the length and thickness of the deck and is simplified for the deck, as the arches will be the most affected by the wind load in the global y-direction in the model, corresponding to the x-direction in EC4-1. This means the reference area for the deck is simply the length times the height of the deck. For the arches, the reference area is the total height of the arch beams times the length of the arch curves. This is conservative since the wind load is applied equally on both arches even though one of the arches, in reality, will be somewhat sheltered from the wind by the other arch. The basic wind speed is calculated with the directional factor, c_{dir}, and seasonal factor, c_{season}, set to 1.0. The basic wind speed, $v_{\text{b},0}$ is estimated as 30 m/s, as a conservative assumption. The wind load factor is from Table 8.2. The reference height is simplified to be smaller than 20 m, even though the bridge's rise ranges from 14.4 m to 21.6 m, depending on the span length. Wind load in the z-direction is not considered. The wind load is distributed along the arches and the deck. Along the arch, the load in kN/m^2 is multiplied by the height of the beam and then distributed equally in each arch mesh point in the positive y-direction. The deck load is multiplied by the deck thickness, then divided over the width of the deck before it is distributed on the deck mesh in the global y-direction. The calculated wind load can be found in Appendix A.1. The gravity load applied to the bridge is simply the self-weight of the structure. The weight of elements such as railings and asphalt are not included in the calculations, as the load situation is simplified.

The two load cases used in the simulations create symmetric and asymmetric loading about the bridge's mid-span. The load cases are to be used for traffic load. The gravity load and wind load are the same for both load cases. The first load case distributes equal loading over the entire deck. The second load case is skew loading, where the distributed load is applied over the whole deck width but only on a part of the length, starting from the deck support. Per Tveit has previously

used a loading length of 54% for the skew load case to make the effects unfavorable [31]. To investigate if this is the most unfavorable loading length for the model, a simple testing procedure was performed on a 100 m span bridge with 20 crossbeams. The most unfavorable load situation in terms of in-plane bending moment stresses in the arch was observed for a loaded length of 52% - 57%. This loading length is estimated by loading the bridge from the deck support to the closest crossbeam past the mid-span. This makes the loaded length for skew loading equal to 52% - 58% for 10 - 25 crossbeams, depending on the number of crossbeams. The loading length cannot end between two crossbeams due to the lack of connectivity with the mesh. Applying load from crossbeam to crossbeam allows for the load boundary nodes to coincide with the crossbeam nodes.

The traffic load is based on Section 3.2 in V412 [35], using class Bk10/50, with a lorry load model where one lorry equals 480 kN. Two such lorries are applied. The load of the lorries is combined with a constant distributed load, an average load for a selection of light, empty, heavy, and loaded vehicles. This load equals 3 kN/m^2. The total traffic load is combined, and the resultant of the lorry- weight and the distributed load is uniformly distributed, as a simplification. The full load case involves a distributed load of 3 kN/m^2 over the full length in addition to 960 kN distributed evenly over the full length. In contrast, the skew load case involves a distributed load of 3 kN/m^2 over the skew loading length deck in addition to 960 kN distributed evenly over the skew loading length. In both cases, the load is distributed over the whole deck width. The calculated traffic load can be found in Appendix A.2. The traffic load was applied for the two different load cases. The first load case is shown in Figure 3.14a, while the other load case with skew loading is shown in Figure 3.14b.

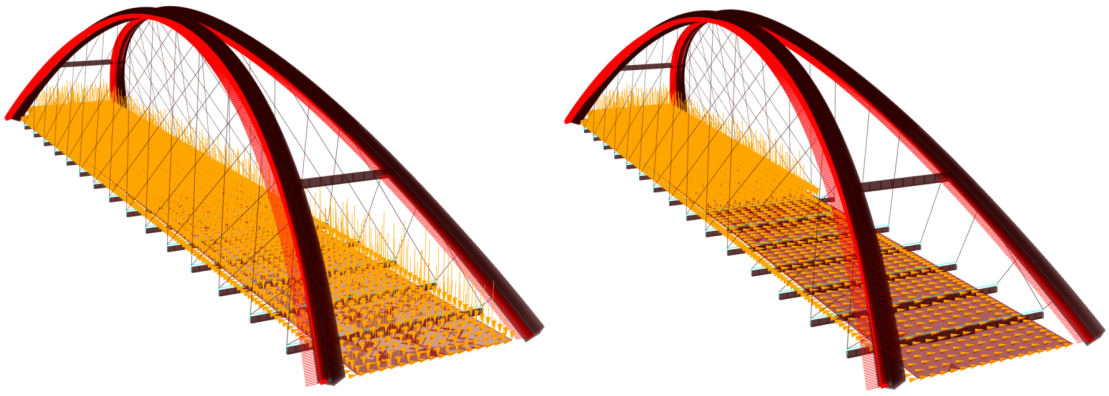

(a) Full load (b) Skew load

Figure 3.14: Load cases including wind and traffic load, where the red arrows represent point load and yellow arrows represent mesh load.

Design checks

The strength values and coefficients for the design checks are based on Chapters 2 and 3 in EC5. The modification factor, k_{mod}, is from Table 3.1. In this thesis, service class II was selected, as it is assumed that the timber elements will be protected by cladding and asphalt when built. The load duration class was selected as short-term action, as the traffic load falls within this category and is the dominating load. The wind load is classified as instantaneous action, but it would not be conservative to increase the strength parameters for this load action, as the wind may not be present. This results in a k_{mod} equal to 0.9 for glulam.

The design checks for the arches are derived from EC5, Chapter 6 [28]. The out-of-plane buckling length is found for each element, i, as each element has its properties and load. This buckling

length is found using Euler's formula and the buckling load factor f_1 from Karamba3D.

$$P_{cr} = \frac{\pi^2 \cdot E \cdot I}{L^2} = N_{x,i} \cdot f_1 = \frac{\pi^2 \cdot E_i \cdot I_{z,i}}{(k \cdot L_i)^2} \tag{3.1}$$

Equation 1: Euler's buckling formula [6].

In this case, P_{cr} is the critical buckling load, equal to the critical buckling load factor, f_1, times the axial compressive force in the element, $N_{x,i}$. E_i is the E-modulus of the element, $I_{z,i}$ is the second moment of inertia about the local z-axis of the element, and L_i is the length of the element. f_1 is kept constant for all elements, which is a conservative assumption, as using the same buckling load factor for all elements indicates buckling in all elements simultaneously. k is the buckling length factor obtained using Equation 3.1. k times L gives the buckling length out-of-plane of each element. The in-plane buckling length is more complex, as the hangers restrain the arches from buckling. Since all the first buckling modes are out-of-plane, it is assumed that in-plane buckling is significantly restrained by the hangers. The buckling in-plane length is set to the maximum distance between two hanger connections in each arch, as it is assumed that each hanger restrains the arch at that point.

The arch is checked for the combined action of axial compression and bending according to EC5, Chapter 6.2.4 with Eq. (6.19) and Eq. (6.18), using the factor considering re-distribution of bending stresses in the cross-section, k_{m}, equal to 0.7 from EC5, Clause 6.1.6(2). Shear failure is evaluated using Eq. (6.13) from EC5, using a crack factor, k_{cr}, equal to 0.8 [13]. The stability of the arches is analyzed with EC5, Chapter 6.3, using characteristic material properties. In-plane, out-of-plane, and lateral torsional buckling are checked, as well as shear. For the simulations, including stability checks, a Boolean toggle switches from mean values to characteristic values for the material properties. For all design checks, every single element in the arches is controlled individually, being able to include the element's specific buckling length, second moment of area, and E-modulus. The equations for all design checks are in Appendix A.4. The checks are manually introduced into Grasshopper using the Karamba3D forces and moments. The main output is the arches' most critical design check value for the most critical element. The aim is to keep this number below the value one for all bridge configurations.

The evaluated failure criteria for the deck is the Tsai-Wu failure criteria, as it best describes the behavior of an anisotropic material such as timber. The Tsai-Wu criteria is also introduced manually to obtain good accuracy for the results. The Tsai-Wu failure criterion consists of only one scalar equation with independent interaction terms. It is valid for all coordinate systems and distinguishes between tension and compression. This check uses the material properties and principal stresses in every element in the deck and performs the check. Manually defining the Tsai-Wu criterion in Karamba3D allows for explicitly defining the interaction coefficient. The interaction parameter is based on Tsai-Hahn's expression from 1980 [22].

3.2 Parameters

Table 3.6: Parameters with slider values.

Parameters	Range (Step size)	Change..
Bridge length [m]	80 / 100 /120	.. the bridge length
Bridge rise [m]	14.4 / 18 / 21.6	.. the bridge rise
Arch base relative to deck [m]	0	.. the vertical distance between the arch support points and the deck
Deck width [m]	12	.. the deck width
Crossbeam extension [m]	2	.. the extension of the crossbeams beyond the sides of the deck
Number of crossbeams	10 - 25 (1)	.. the number of crossbeams
Arch lean	0.04 / 1 (0.01)	.. from straight arches (1) to arches intersecting at the top point (0)
Hanger angle [degrees]	35 - 60 (1)	.. angle between hangers and the radial rays for two sets of hangers
Hanger angle with three sets of hangers[degrees]	45 - 70 (1)	.. angle between hangers and the radial rays for three sets of hangers
Focal point vertical [m]	100	.. the focal point a distance below the arch center in vertical direction
Focal point horizontal [m]	10	.. the focal point a distance from the arch center in horizontal direction
Crossbeam displacement limit [mm]	250	.. the maximum allowed displacement of crossbeams
Deck thickness [mm]	300 - 750 (50)	.. the deck thickness
Arch height [mm]	500 - 2000 (50)	..the height of the cross-section of the arch
Arch width [mm]	500 - 2000 (50)	.. the width of the cross-section of the arch
Hanger diameter [mm]	40 / 50 / 60	.. the diameter of the cross-section of the hangers
Splice placement (1)	0 - 1 (0.1)	..splice 1 position from closest to supports (0) to closest to the middle of the bridge (1)
Splice placement (2)	0 - 0.5 (0.1)	.. splice position 2 from closest to supports (0) to closest to the middle of the bridge (1)
Arch elements	1000	.. the number of elements each arch consists of
Deck support points	5	.. the number of support points along the deck ends
Hanger connection merging distance [m]	6	.. the maximum distance between hanger connections for merging in the arch
Distance between top beams [m]	4	.. the horizontal distance between the top beams
Length of arch with increasing cross-section [%]	20	.. the % of the arch that is augmented from each arch endpoint
Max arch height at arch supports [mm]	1000 - 2000	.. the maximum height of the arch at the supports
Triangle beam height [mm]	= Arch height	.. the height of the beams in the triangular corners
Triangle beam width [mm]	= Arch height	.. the width of the beams in the triangular corners

The bridge model is fully parametric, implying the same model is used for all design alternatives, varying parameters in Grasshopper. The parameters varied with sliders are listed in Table 3.6. The sliders defining a quantity, for instance, the number of crossbeams, can have step sizes as integers. Geometrical parameters, such as dimensions and angles, can have an infinitesimally small step size. However, some ranges, step sizes, and parameters are fixed in the simulations. These fixed values are presented in Table 3.6.

Bridge length can be changed by a single slider value which simultaneously moves the position of the arch support points and the deck length. This thesis investigates the lengths 80, 100, and 120 m. The length influences the number of splices in the arches, and simulations are performed individually. *Bridge rise* can be adjusted with a slider, moving the top point of the arches in the global z-direction. In the simulations, the rise is fixed, corresponding to 18% of the span length. *Arch base relative to deck* can move the arch support points in the global z-direction while the deck position remains unchanged. This value was set to zero in the simulations. *Deck width* can be changed by a slider, simultaneously moving the arch support points and keeping the exact distance between the deck and the arches. The deck width is set to 12 m for all simulations. *Crossbeam extension* can be adjusted with a slider, where a value of 0 implies crossbeams of equal length to the deck width. A non-zero crossbeam extension value moves the arch support points simultaneously to keep the hanger connection points on the ends of the crossbeams in the arch plane. This extension was fixed at two meters for all simulations.

Number of crossbeams is varied in the simulations but remains evenly distributed along the length, keeping an equal distance between them. *Arch lean* can be changed with a slider ranging from 0 to 1, 0 corresponding to the top points of the arches intersecting, and 1 corresponding to vertical arches. The slider moves the top points in the global y-direction, meaning the z-coordinates of the points remain the same for a leaned and vertical arch. I.e., the arch length for a leaned arch is larger than for a vertical. An arch lean of 0.04 corresponds to the arch beams almost touching at the top. The arch lean was fixed at 0.04 for all simulations except for the bridge configuration with vertical arches.

Hanger angle corresponds to the angle of the hangers, α, measured from each side of the radial rays. *Hanger angle with three sets of hangers* is the angle between the radial rays and two of the hanger sets. The last hanger set remains aligned with the radial rays. The angle is selected through two separate sliders corresponding to two or three sets of hangers, with a value given in degrees. If the hanger angle is very large, the hangers will point downward from the horizontal line of the deck. In the model, these hangers will automatically be removed before the analysis.

Focal point vertical is the vertical shift of the focal point. The shift is decided by a slider, where a value of zero corresponds to the focal point being a vertical distance equal to the arch radius from the top of the arch. The radius for the 80, 100, and 120 m span bridges are 62.8, 78.4, and 94.1 m, respectively. A vertical shift larger than zero moves the focal point in the negative, global z-direction. The focal point vertical was fixed at 100 m for all simulations. *Focal point horizontal* is the horizontal shift of the focal point. A slider controls the shift, where 0 corresponds to one focal point at the bridge's mid-point. A horizontal shift larger than 0 results in two or three focal points, depending on the number of crossbeams, as shown in Figure 2.5. The horizontal shift moves the focal points away from the mid-point of the bridge in the global x-direction. The shift is symmetrical about the mid-point. This shift was set at 10 m for the simulations. Different values for the focal points are investigated for the bridge configurations in this thesis. The results were relatively similar within the range where the chosen positions produced good results. The explored position range for the focal points were derived from Ostrycharczyk's Ph.D. [20].

Hanger connection merging distance sets the limit for the maximum distance between two hanger connections at the lower edge of the arch that will merge. The two first hanger sets are merged

when this function is active. For the simulations, this distance was set to 6 meters. This distance distributes the connections along the arch while keeping the pattern close to the original modified radial pattern.

Deck thickness defines the thickness of the deck. The thickness is expanded symmetrically about the base surface. *Arch height* defines the arch beams' cross-sectional height. This height corresponds to the central part of the arch, where there is no gradual increase in cross-sectional height. *Arch width* defines the width of the arch beams' cross-section. The cross-section of the arch is tilted at the same angle as the arch plane. *Hanger diameter* is the diameter of the circular steel elements which form the hangers. In the simulations, the hanger diameter has a fixed value for the three-span lengths of 80, 100, and 120 m. The diameters are 40, 50 mm, and 60mm, respectively.

Crossbeam displacement limit sets the displacement limit for the crossbeams to be used in the "Optimize cross-section"-component in Karamba3D. This value is set by a slider value, given in millimeters. The range was initially set to 30 - 250 mm before the limit was fixed at 250 mm.

Splice placement (1) is the position of splices in each arch. Splice (1) corresponds to the splices closest to each arch support. The position of the splices is symmetric about the mid-point of the bridge and is positioned using a slider. This implies that for an 80 m span bridge with two splices, the slider is the only parameter for placing both splices. In comparison, for a 100 m span bridge with four splices, this parameter controls only the placement of the two splices closest to the arch supports. The parameter *splice placement (2)* positions the other two splices. This slider parameter controls the splice placement of the splices closer to the top of the arch. In a bridge with three splices, the middle splice is at the top of the arches for symmetry. The length limitation of each arch part restricts the splice placements. The length of each splice is set to four times the arch height. This means that each piece, including the splice, cannot exceed 30 m. This also implies that the splice placement is more limited for a 100 m span bridge with three splices than a 100 m span bridge with four splices. A splice placement of 0 makes the splice as close to the support as possible, this goes for both placements (1) and (2). For splice placement (1), the maximum value is 1, placing the splices as close to the top as possible, while for splice placement (2), the maximum value is 0.5. Splice placement (1) is always active, considering all bridge configurations have incorporated at least two splices. Splice placement (2) is activated automatically when the bridge configuration contains four splices in each arch. The 80 m span bridge can have two or three splices. The 100 m span bridge can have three or four splices, and the 120 m span bridge can only have four splices, as it needs at least four to fulfill the arch part length requirement.

Arch elements is the number of elements each arch is divided into. The arches were divided into several segments that comprised the elements in the mesh for the FEA. The number of elements was set by a slider, fixed at 1000 for the simulations.

Deck support points is the number of points along the ends of the bridge that are defined as supports. The points are evenly distributed along each end. The number of supports is set by a slider where the minimum value is 2, giving supports only at the corners of the deck. 5 support points were used in the simulations.

Distance between top beams is the distance between the middle top beam and the two outer top beams. It was set by a slider, fixed at 4 meters in the simulations.

Length of arch with increasing cross-section indicates the proportion of the arch length where an increasing cross-section is assigned. For instance, when set to 20%, the arch height increases from a point at a length equal to 0.2 times the total arch length from the support. The increase is gradual towards the arch support. This is symmetric about the mid-point of the bridge, meaning 40% of each arch's total length is assigned an increasing cross-section. A slider sets the proportion of the

arch length, given as a percentage. 20% was used in the simulations. *Max arch height at arch supports* defines the cross-section height at the arch support. This is the largest cross-sectional height in the arches.

Triangle beam height and *Triangle beam width* are the cross-sectional height and width of the beams forming the triangular corners. The values can be adjusted with sliders but was set equal to the arch height for the simulations.

Table 3.7: Parameters with Boolean toggles

Boolean toggles	True / False	Influence
Loaded length	Full / Skew	Traffic load applied to the full length or to part of the length of the bridge.
Loaded width	Full / Half	Traffic load applied to the full width or half the width of the deck.
Wind load	On / Off	Wind load activated or deactivated.
Side beam position	$\frac{1}{4}$ length / $\frac{1}{2}$ height	Side beams placed 1/4 arch length from the supports or at a height equal to half the bridge rise.
80 m span splices	2 / 3	2 or 3 splices are incorporated in each arch for an 80 m span bridge, splice placement (1) is active.
100 m span splices	3 / 4	3 or 4 splices are incorporated in each arch for a 100 m span bridge. If 3 splices are incorporated, splice placements (1) is active. If 4 splices are incorporated, splice placement (1) and (2) are active.
Triangular corners	On / Off	Activates or deactivates triangular corners. If active, increasing cross-section is inactive, and vice versa.
Sets of hangers	2 / 3	2 or 3 sets of hangers, the hanger angle corresponding to the chosen number of sets of hangers is activated.

Wind load can be activated or deactivated by a Boolean toggle. True was fixed in the simulations, thus active wind load, as calculated in Appendix A.1.

Loaded length is the parameter referring to the loaded length of the bridge. This component creates either one or two surfaces in the longitudinal direction to distribute the traffic load on either the entire span of the bridge or a part of the span. The surfaces represent the loaded length of the desired load case. True refers to the whole span being loaded, i.e., full load case, while False represents the skew load case.

Loaded width refers to the loaded width of the bridge. This component creates one or two surfaces over the width for the traffic load to be distributed on. One surface covers the full width, while two surfaces split the width in two, loading only half the bridge's width. True was selected for the simulations, meaning the entire width is loaded.

Side beam position refers to the position of the side beams on the arches. True refers to placing them at a distance along the arch beam of 1/4 the arch's length from the arch support. False refers to placing the beams at the points on the arches where the z-coordinate equals half the bridge rise. The position of the beams was fixed at False during the simulations. *80 m span splices* refers to the number of splices in each arch for an 80 m span bridge. True equals two splices, while False equals three. This Boolean toggle only affects the model if the length of the bridge is defined as

80 m. *100 m span splices* refers to the number of splices in each arch for a 100 m span bridge. True equals three splices, while False equals four. This Boolean toggle only affects the model if the length of the bridge is defined as 100 m. *Triangular corners* can be activated or deactivated by a Boolean toggle. True activates the triangular corners. When active, the arches' cross-sections are constant along the arch length. *Sets of hangers* turns on or off a third set of hangers. True equals two sets of hangers, while False implements a third set. When two sets are present, the hanger angle corresponding to two hangers is active, while the hanger angle corresponding to three sets of hangers is inactive, and vice versa.

Bridges used in simulations

Based on the parametric model, multiple bridge designs can be investigated. For the purpose of this thesis, nine different configurations were optimized. The five standard bridge configurations differ in length and number of splices in the arches. They have two sets of hangers, leaned arches, top- and side beams, and increasing arch height toward the supports. The standard bridge configurations are listed below.

- 80 m span with two splices
- 80 m span with three splices
- 100 m span with three splices
- 100 m span with four splices
- 120 m span with four splices

The four latter configurations implement some form of alternative design. They are based on the original configuration of the 100 m span bridge with three splices from the standard bridge configurations. The first alternative configuration includes a third set of hangers, the second configuration includes triangular corners, the third configuration has vertical arches and K-trusses instead of top- and side beams, and the last configuration excludes side- beams. The alternative bridge configurations are listed below.

- 100 m span with three splices and three sets of hangers
- 100 m span with three splices and triangular corners
- 100 m span with three splices and vertical arches
- 100 m span with three splices and no side beams

3.3 Simulation procedure

With multi-objective optimization, there are extensive possibilities to optimize a structure. Several different values can be minimized or maximized simultaneously while varying almost unlimited parameters. There are, however, some limitations. When comparing several different objectives at the same time, it can be challenging to evaluate how the results compare to each other to obtain the best solution. In some cases, it is necessary to compare several values at the same time, because optimization of one parameter may result in the compromise of another. In this situation, an evaluation of the different results in a 2D or 3D plot gives a better picture of the interaction between the results.

When evaluating more than three objectives, the optimization process is more clear if it is divided into several simulations. It is easier to evaluate two 2D plots than it is with one 4D plot. In this thesis, five different simulations were performed for each bridge. The simulations consisted mostly of two objectives minimized simultaneously, while one simulation included three objectives. The simulations were carried out in order to optimize the same objective against multiple objectives with different parameters. On the basis of multiple simulations often resulting in different values, a configuration was selected, trying to satisfy all objectives.

Each bridge configuration was equipped with reasonable values for the parameters before the simulation process begins. A qualified guess was carried out, considering the arch cross-section and deck thickness based on the span length of the bridge. This created a good base for the first simulations to adapt suitable values for the objectives. The splice placement was initially put in the middle of the possible range, and the rest of the starting values can be seen in Table 3.8.

Table 3.8: Starting values, in [mm], for the multi-objective optimization process for each bridge length.

	80 m	100 m	120 m
Arch height	700	800	1000
Arch width	1000	1200	1400
Deck thickness	400	400	400

Table 3.9: Parameters and objectives for the simulations.

	Parameters	Objectives
Simulation 1	Number of crossbeams Hanger angle	Peak M_y stress Steel mass
Simulation 2	Number of crossbeams Deck thickness C.B displacement limit	Stress 90°to grain Timber mass Steel mass
Simulation 3	Arch height Arch width	Critical design check Timber mass
Simulation 4	Splice placement (1) Splice placement (2) Hanger angle	Max moment in splices Peak M_y stress Number of relaxed hangers
Simulation 5	Number of crossbeams Hanger angle	Peak M_y stress Steel mass

In simulations 1 and 2, steel mass was a limiting objective. The steel mass used in these optimization processes corresponds to the weight of half the crossbeams. The reasoning behind this is the use of the Karamba3D component "Optimize cross-section". This component will find the smallest cross-section possible, to reduce steel mass, while still being within the design limits of Eurocode

3. Each crossbeam consists of 8 elements which are individually analyzed to find the optimum cross-section. For the skew-load case, as opposed to the full, the design of the crossbeams is not symmetrical about the mid-point due to only about half of the bridge being loaded. This leads to larger cross-sections at the loaded part than at the unloaded part. Therefore, when comparing the steel mass, only crossbeams from the loaded part were included in the weight calculations. At least half of the crossbeams were loaded in the skew load case. To obtain comparable results, only half the total number of crossbeams' weight was considered in the simulations for comparison of the load cases.

The bridge configuration with vertical arches was considered simply to illustrate the effect of the arches leaning toward each other. Therefore, this configuration was only optimized through simulations 1 and 3. Before these simulations, the crossbeams were fixed with identical geometry as obtained for the bridge with a span length of 100 m and 3 splices after all simulations. Similarly, the geometry of the bridge with no side beams wass equal to the final geometry of the 100 m bridge with 3 splices. However, no simulations were performed on this configuration. It represents the exact model as the 100 m span with 3 splices, except for the removal of the two side beams.

It is assumed that Octopus found the optimal solutions, or at least the area of the optimal solutions in the simulations. After each simulation, a sensitivity analysis between the results from the two load cases was performed to find the optimum configurations.

Simulation 1

The first simulation had the target of minimizing two objectives: peak in-plane bending stress (peak M_y stress) and steel mass. To obtain values for the objectives, multiple different scenarios were examined with a varying number of crossbeams and hanger angles. The hanger angle is known to be one of the most important factors in impacting the distribution of bending moments in the arch [31]. A higher hanger angle will distribute the concentrated forces from the deck loads to a greater area of the arch. Nevertheless, this could lead to a less favorable moment distribution for an evenly distributed load case. This results in various optimum solutions for different load cases. A larger number of crossbeams introduces more hangers and a more evenly distribution of forces. This is a preferred solution, though an increased number of crossbeams leads to more construction work as well as an increase in steel mass, which leads to a higher cost and environmental footprint. To find the optimum number, the favorable effects were contained by the limitation of steel mass.

Simulation 2

This simulation focused on the design of the deck. The deck stress resulting from compression perpendicular to grain (stress 90° to grain) was found to be the most critical design factor for the deck. Initial simulations found the deck deflection between crossbeams to be well below the design limit of Clause 3.5-2 in N400 [34]. To evaluate the deck capacity, each shell element was evaluated individually according to the Tsai-Wu criterion, which can be found in Appendix A.12. The design of the deck aimed to reduce the effects of stress perpendicular to the grain. High stress levels, exceeding the designated limit, pose a significant threat, resulting in damage to the deck on a localized and widespread scale. An alternative approach was considered, which involved minimizing the number of elements surpassing the Tsai-Wu criterion. However, initial investigations revealed that the majority of these elements only exceed the limit marginally. Consequently, placing excessive emphasis on reducing stress in these specific areas would yield minimal overall stress reduction for the deck. Therefore, the objective was chosen to be the maximum stress from compression perpendicular to grain.

Two of the most important factors for the resulting deck stress were the composition of crossbeams and the deck itself. The deck width and material have been fixed, leaving the option for changing the deck thickness. A greater thickness will reduce stresses in the deck, but this parameter was restricted by the objective of minimizing timber mass. Furthermore, the objective of minimizing steel mass would limit the configuration of crossbeams. The number of crossbeams was a variable parameter in this simulation. A reduced span length between crossbeams would subsequently reduce stresses in the deck. During the first simulations, the displacement limit for the crossbeams in "Optimize cross-section" was included as a parameter. For the different span lengths of the bridge, the crossbeams' maximum displacement was between 160 and 210 mm. The displacement limit varied between 30 and 250 mm, though it quickly became clear that a strict limit would greatly increase the steel mass due to the needed cross-sections of crossbeams without reducing the deck stresses significantly. Due to this rationale, the optimum configurations all included a displacement limit above the set maximum displacement of the crossbeams. Therefore, in the rest of the simulations, this parameter was fixed to 250 mm.

Simulation 3

In the third simulation, the aim was to design an effective arch cross-section. To obtain this, one of the objectives was to minimize the timber mass. This was done while trying to achieve a configuration close to, yet less than, the value 1 for the most critical design check. The design checks performed were from Eurocode 5-1 and were carried out on all 1000 elements in each arch. Two parameters, arch height and width, were modified in this simulation to acquire the arch cross-section, which was the ideal balance between the different design checks. After choosing a suitable configuration, the maximum arch height at the end supports was adjusted manually to fine-tune the moment distribution whilst decreasing the timber mass at the ends.

There is one important difference that separates simulation 3 from the rest. Since this simulation performed a buckling analysis of the arch, the characteristic values from EN 14080 were used, as opposed to the mean values, in the design [29]. All results obtained for the critical design check, as well as the buckling-load factor, were calculated using these values.

Simulation 4

The objective of simulation 4 was finding the most suitable placements of the splices. The placements are limited by a maximum length of each arch part. Each splice has a range to move within, where the aim was to find the placement with the smallest in-plane bending moments in the arches. The objectives to be minimized in this simulation were the maximum moment in the splices, the peak in-plane bending stress in the arch, as well as the number of relaxed hangers. The number of relaxed hangers was not included in the Octopus optimization process but was manually compared along with the other results. In each simulation, the splice placement and hanger angle were the parameters to be varied. For the bridge configurations with four splices, both splice placement (1) and (2) were parameters in the optimization in order to obtain all possible solutions. For configurations with three splices, one splice is fixed at the top of the arch to be symmetrical. The initial placement provided a rough estimate of the optimal position. In the event that the simulations indicated that the predefined step-size was too coarse, finer adjustments were made to refine the placement of the splices.

Simulation 5

The fifth and final simulation was identical to simulation 1. The simulation was repeated using the values for all other parameters obtained during the previous simulations, to verify the results obtained from the first simulation with the starting values in Table 3.8. After this simulation, the parameters were fixed. This also included fixing the cross-sections of the crossbeams, which were found by the "Optimize cross-section" component from Karamba3D. The cross-sections suggested by Karamba3D were investigated before a set configuration for all crossbeams was chosen. All objectives and other results for the bridge configuration were then investigated.

4 Results

In this section, a selection of results is presented as figures or tables. The full collection of results can be found in Appendix B.

The results are presented as figures with corresponding tables. In the figures, each dot represents the objective values of a unique configuration of the varied parameters. The aim was to find a configuration with a corresponding dot close to the bottom left of each figure. The non-dominated solutions from the simulation form the Pareto front, which is drawn as a red line. This is further elaborated in Section 2.5. The tables include a selection of the investigated configurations for each simulation. This includes the objective values, displayed as dots in the figures, and the corresponding values of the parameters.

4.1 80 m span with two splices

The detailed results in the form of figures and tables, for this bridge configuration, can be found in Appendix B.1.

Simulation 1

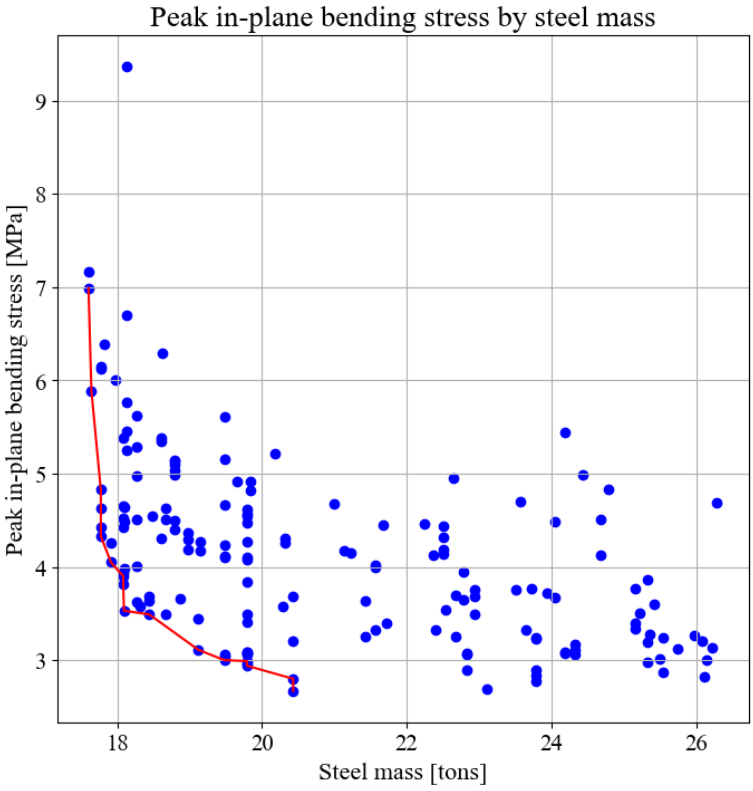

Figure 4.1: 80 m span with two splices: Simulation 1, Full load.

Figure 4.1 illustrates the peak in-plane bending stresses vs. steel mass, which were the objectives to be minimized in simulation 1. The desirable solutions for the full load case included between 12 and 16 crossbeams. A higher number of crossbeams resulted in a larger steel mass without

decreasing the stresses. On the other hand, a smaller number of crossbeams than 12 resulted in a significant increase in stresses, including roughly the same steel mass. The smallest stresses appeared with a hanger angle of around 35 and 16 crossbeams but slowly rose when increased to 43 degrees and 13 crossbeams. In most cases, a hanger angle of around 40 degrees resulted in low stresses, as presented in Table 4.1.

Table 4.1: 80 m span with two splices: Simulation 1, Full load.

Objective values		Parameter values	
Peak in-plane bending stress [MPa]	Steel mass [tons]	Number of crossbeams	Hanger angle [degrees]
2.7 - 3.2	20	16	35 - 40
2.9 - 3.5	20	15	36 - 45
3.5	18	13	41 - 44
3.5 - 4.3	18	12	35 - 52

Skew loading had similar tendencies to full loading, with some important differences. The preferred hanger angles were larger, spanning from 40 to 52 degrees. The parameters resulting in the smallest stress were 13 crossbeams and a hanger angle of 49 degrees. Increasing the number of crossbeams above 13 did not decrease the stresses further, though a number of 14 and 15 gave decent results. Fewer than 13 crossbeams also gave good results, though some increase in stresses.

Simulation 2

The total steel mass in this simulation was quite sensitive to changes in the crossbeam displacement limit. By reducing the displacement limit for the crossbeams by 1 cm, the total steel mass of the crossbeams increased by more than 8 tons, which is a 21% increase. Consequently, solutions including higher displacement limits were primarily focused on.

There was a clear correlation between the maximum stress perpendicular to grain in the deck, and the deck thickness. An increased thickness corresponded to lower stresses, with some exceptions. For instance, for the full load case with 13 crossbeams, a deck thickness of 300, 350, and 400 mm resulted in stresses of 4.57, 3.99, and 4.28 MPa, respectively. A thickness of 350 mm was chosen, though timber mass increased with 20 tons from a thickness of 300 mm. For all deck thicknesses, 13 crossbeams resulted in the lowest stresses perpendicular to grain in the deck.

The results from the skew load case were similar. The stresses perpendicular to grain for thicknesses 300, 350, and 400 mm were 4.33, 3.85, and 4.14 MPa, respectively. This is presented in Table B.4.

Simulation 3

For the full load case, several configurations had values within the range of 0.796 to 0.985 in terms of the critical design check. The width-to-height ratio varied from 1.125 to 2.09. The chosen dimensions for succeeding simulations were a height of 650 mm and a width of 1050 mm, resulting in the critical design check with a value of 0.881.

Subsequently, the maximum arch height at the supports was varied manually to adjust the moment distribution in the arch while minimizing the timber mass. The maximum arch height was reduced to 1000 mm, resulting in moments at the supports being larger than at the top while reducing timber mass by 8 tons. Subsequently, the critical design check resulted in a value of 0.956.

By investigating results from the simulation, it was clear that the dimensions obtained from the

full load case were critical regarding the design checks. The chosen configuration of height and width equal to 650 and 1050 mm resulted in the critical design check, Eq. A.24, equivalent to 0.852 for the half load case.

Simulation 4

The Pareto front for the full load case was dominated by a hanger angle of 43 degrees. At the highest point on the graph, the maximal moment in the splices was 137 kNm with a hanger angle of 35 degrees. This corresponded to the lowest stress for in-plane moments of 3.79 MPa. With this angle, as well as for the other alternatives, it was clear that a connection placement closer to zero, meaning closer to the ends of the arch, was preferable. With this splice placement, the maximal moments in the splices decreased significantly. The best result included a hanger angle of 43 degrees and a connection placement of 0, resulting in a maximal moment in the splices of 85 kNm and an in-plane stress of 4.22 MPa.

The stresses and moments obtained from skew loading of the bridge were higher than for full loading and were, therefore, design-critical. The most suitable connection placement was similar. Again, a hanger angle of 43 resulted in the smallest moments in the splices, with a value of 155 kNm, and an in-plane stress of 6.97 MPa. However, skew loading resulted in hangers losing tension. By increasing the hanger angle, the number of relaxed hangers decreased. Even with a hanger angle of 60 degrees, a hanger would relax, making the issue difficult to remove completely. The chosen solution was therefore based on attempting to minimize the number of relaxed hangers, though the focus was mainly on minimizing the stresses and moments. A hanger angle of 45 degrees stood out as the most suitable alternative, with a splice moment of 166 kNm and in-plane stress of 5.66 MPa, as well as 7 relaxed hangers. It should be noted that by increasing the hanger angle above 45 degrees, moments increased significantly. When applying these chosen parameters with full loading, the results were similar, though skew loading was design-critical.

Simulation 5

For both load cases, 13 crossbeams still gave good results after fixing parameters from the simulations. With full loading, the stresses could be reduced slightly with 14 or 15 crossbeams. Nevertheless, the stresses from the skew load case were greater, with 13 crossbeams resulting in the lowest stresses. The minimum value for in-plane bending stresses was 4.85 MPa, with a hanger angle of 48 degrees. Based on the previous simulation, a stress of 5.66 MPa and a hanger angle of 45 degrees remained a suitable solution.

4.2 80 m span with three splices

The detailed results in the form of figures and tables, for this bridge configuration, can be found in Appendix B.2.

Simulation 1

For the full load case, there was a large variation in the number of crossbeams for the solutions along the Pareto front, ranging from 11 crossbeams and an in-plane bending stress of 6.11 MPa, to 16 crossbeams with a stress of 2.68 MPa. More crossbeams resulted in an increase in both steel mass and stress. The steel mass increased slightly with the number of crossbeams. The best solutions were in the range of 13 to 16 crossbeams with a hanger angle from 35 to 44 degrees. No solution stood out as unambiguously best.

A more narrow range of solutions was present for the skew load case, ranging from 11 to 13 crossbeams with larger hanger angles along the Pareto front compared to full loading. 13 crossbeams stood out as the optimum number, with a hanger angle of 46 degrees. By comparing hanger angles ranging from 43 to 46 degrees for both load cases, an angle of 45 degrees was chosen due to the lowest peak stress equal to 4.26 MPa.

Simulation 2

In this simulation, there was no displacement limit for the crossbeams. Among all deck thicknesses, 13 crossbeams resulted in the lowest stresses perpendicular to grain in the deck. Therefore, the stresses compared to timber mass were the comparison criteria in this scenario. Deck thicknesses of 300, 350, and 400 mm resulted in the exact same stresses as for the bridge with two splices in both load cases.

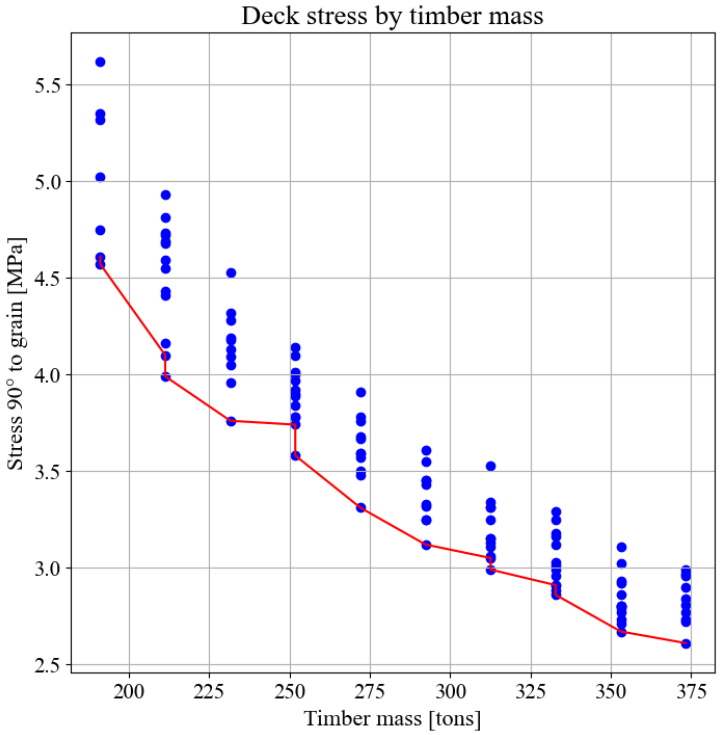

Figure 4.2: 80 m span with three splices: Simulation 2, Full load.

Simulation 3

With the same cross sections, the full load case resulted in the largest values in terms of the design checks. For the cases below the design limit, the configurations with the lowest timber mass mostly included cross sections with a width-to-height ratio of around 2. There was an instance of a cross-section with a larger height than width. However, both timber mass and design check value were larger than for the chosen configuration, which consisted of a height of 650 mm and a width of 1050 mm. The chosen configuration resulted in a value of 0.878 for the critical design check and a timber mass of 211 tons. By adjusting the maximum height of the arch to 1000 mm, the value of the design check increased to 0.953 whilst reducing the timber mass by 8 tons.

Simulation 4

To obtain as low bending moments in the splices as possible, both load cases required a hanger angle of 43 degrees. Then, the largest moment existed in the skew load scenario with a value of 155 kNm. An angle of 45 degrees increased the largest bending moment in the splices to 167, though it decreased the overall peak stress in-plane for the arch from 6.91 to 5.58 MPa. For all angles, the lowest moments in splices corresponded to a connection placement as close to the supports as possible. The moments increased slowly with the connection placements.

Simulation 5

Among the solutions around the Pareto front, the skew load case resulted in the largest in-plane bending stresses. The minimum peak stress resulted from a configuration of 13 crossbeams and a 49 degrees hanger angle. By comparing the stresses using 13 crossbeams for both load cases and different angles, the smallest stresses were obtained with 47 or 48 degrees. A hanger angle of 48 degrees resulted in 4 hangers in compression, while 47 degrees resulted in 3. Consequently, 48 degrees and 13 crossbeams were chosen.

4.3 100 m span with three splices

The detailed results in the form of figures and tables, for this bridge configuration, can be found in Appendix B.3.

Simulation 1

For the full load combination, an increased number of crossbeams decreased the peak in-plane bending stress. This trend was valid for 11 to 20 crossbeams. The lowest stress was obtained with 20 crossbeams, where more crossbeams resulted in a larger stress. The hanger angle mostly ranged between 35 to 39 degrees for the solutions around the Pareto front. Increasing the angle often increased the stress, though an angle of 39 degrees was the optimum for both 12 and 15 crossbeams.

A similar trend was observed when varying the number of crossbeams for skew loading. Here, the stresses decreased all the way down to 25 crossbeams. However, more than 16 crossbeams lead to a significant increase in steel mass compared to the decrease in stresses, making the solutions less profitable. The optimum number of crossbeams was 15 to 16, with hanger angles ranging from 41 to 49 degrees. Both load cases resulted in a chosen configuration of 15 crossbeams and a hanger angle of 40 degrees.

Simulation 2

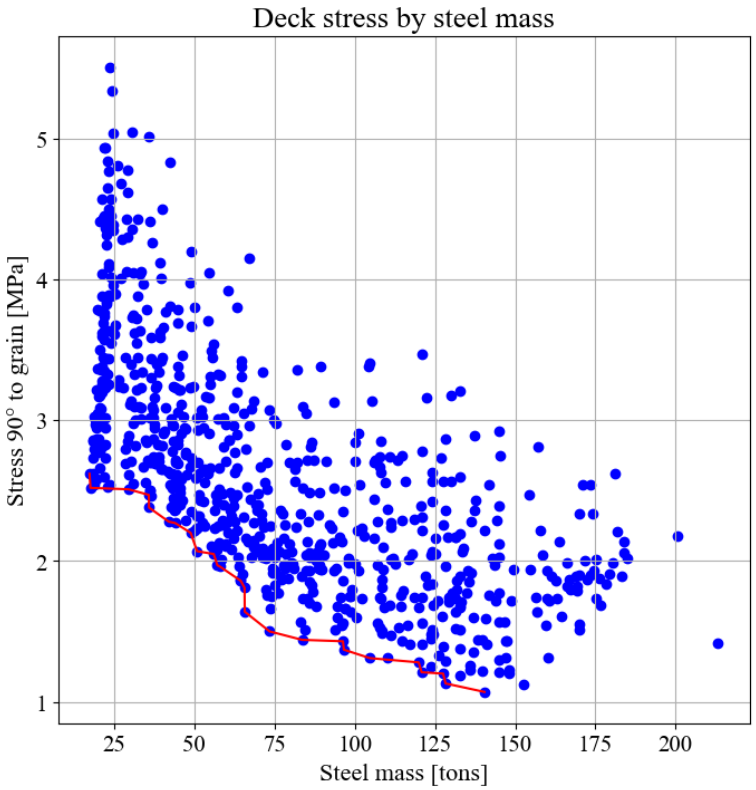

Figure 4.3: 100 m span with three splices: Simulation 2, Full load.

Solutions including higher displacement limits were primarily focused on. The simulations tend to prefer a small number of crossbeams to minimize steel mass. Furthermore, the stress perpendicular to grain in the deck was highly prone to changes in the displacement limit of the crossbeams. The areas in the deck which did not pass the Tsai-Wu criterion were in all cases positioned in the spans near the crossbeams closest to the bridge ends. This is a result of the "Optimize cross-section" component, which tends to minimize these cross-sections due to a lower global displacement at this proximity to the deck supports. However, the local displacement is large since there is zero transversal displacement at the supports. The rapid difference in curvature of the deck results in increased stresses.

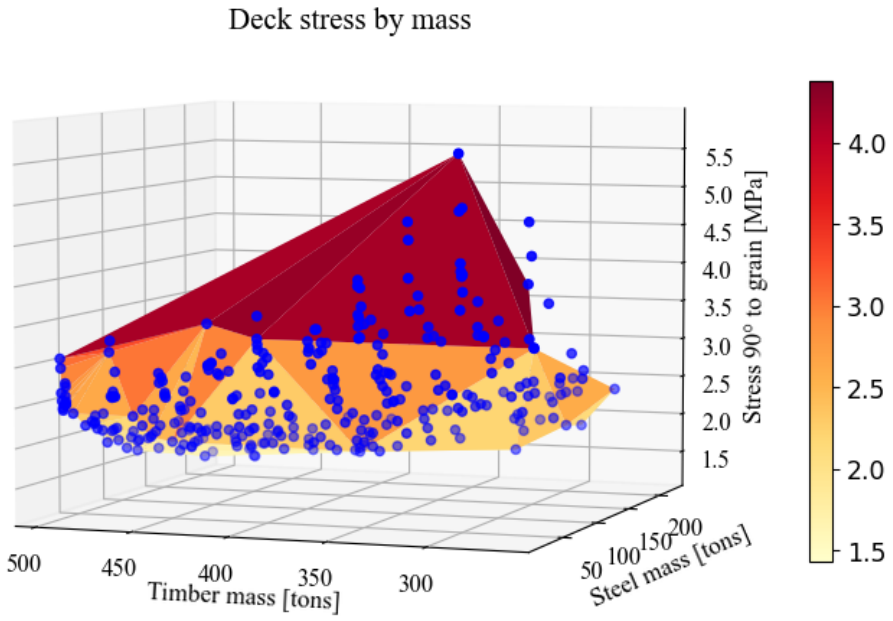

Figure 4.4: 100 m span with three splices: Simulation 2, Skew load.

Table 4.2: 100 m span with three splices: Simulation 2, Skew load.

Objective values			Parameter values	
Stress 90° to grain [MPa]	Steel mass [tons]	Timber mass [tons]	Number of crossbeams	Deck thickness [mm]
3.11	25.6	367.3	20	500
3.4	21.6	367.3	15	500
3.45	22.9	342	17	450
3.83	23.5	291.4	15	350

Simulation 3

All cross-sections resulting in high utilization and low timber mass had considerably larger widths than heights. The width-to-height ratio ranged between 2.4 and 1.4. For the skew loading load case, the cross sections were smaller, where some solutions had a ratio of 1. The full load case was

therefore critical for design, and a height of 800 and a width of 1250 mm was selected for further analysis. The maximum height of the arch was reduced to 1300 mm, increasing the critical design check from 0.872 to 0.904.

Simulation 4

For the full load case, the variation of in-plane bending stresses was small, ranging from 3.45 to 3.87 MPa. Therefore, the main objective was minimizing the bending moments in the splices. For each hanger angle, the optimum range for splice placement was different due to the variation of the bending moment diagrams in the arch when varying the hanger angle. The angles providing the best results were in the range of 40 to 43 degrees, where 43 degrees resulted in the lowest moment of 108 kNm. This was obtained within the range 0.3 to 1 for the connection placement. The bending moment diagram increased in both directions from the splice.

As for the full load case, 43 degrees resulted in relatively low moments in the splices for skew loading. The range in which the splice can be put was more narrow, as skew loading resulted in greater differences in the moment distribution. As visualized in Figure 4.5, a splice placement of 0.9 with a hanger angle of 43 degrees minimizes the moment in the splice. With this configuration, 7 hangers were relaxed.

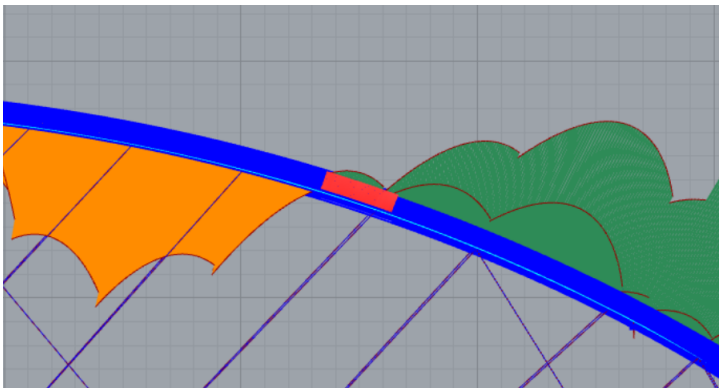

Figure 4.5: 100 m span with three splices: Simulation 5, Skew load. In-plane bending moment diagram with splice placement, marked in red.

Simulation 5

In the full load case, there was a clear trend that an increased number of crossbeams reduced the in-plane bending stresses in the arch. Increasing the number of crossbeams beyond 17 resulted in a significant increase in steel mass without reducing the stresses noteworthy. With both 16 and 17 crossbeams, the preferred hanger angle was 35 degrees, which resulted in large stresses for the skew load case. 15 crossbeams produced fairly good results in the range of 37 to 43 degrees, whilst 10 and 11 crossbeams preferred a hanger angle of 44 and 38 degrees, respectively.

Similar results were observed with skew loading, though including larger hanger angles along the Pareto front. Most configurations resulting in smaller stresses included hanger angles around 50 degrees. 15 crossbeams was the exception, providing similar results for the range of 40 to 55 degrees. 15 crossbeams and a hanger angle of 43 degrees was kept.

Tsai-Wu Criterion

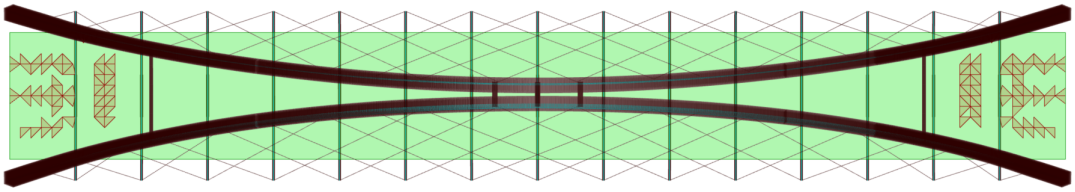

Figure 4.6: 100 m span with three splices: Full load. Elements exceeding the Tsai Wu criterion are marked in a darker shade.

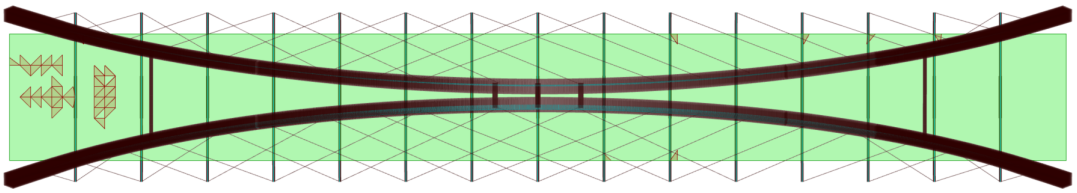

Figure 4.7: 100 m span with three splices: Skew load. Elements exceeding the Tsai Wu criterion are marked in a darker shade.

Figure 4.6 and 4.7 illustrate the elements in the top of the deck mesh that exceed the Tsai Wu criterion. For the full load case, the number of exceeding elements is 129, corresponding to 5.4 % of the deck. For skew load, the number is 46, corresponding to 1.9 % of the deck.

4.4 100 m span with four splices

The detailed results in the form of figures and tables, for this bridge configuration, can be found in Appendix B.4.

Simulation 1

The simulation with full load provided a variety of possible solutions. The lowest stress from the in-plane bending moment was 2.55 MPa, obtained with 17 crossbeams and a hanger angle of 35 degrees, whereas an angle of 40 degrees resulted in 3.05 MPa. For 15 and 19 crossbeams, the best results were obtained with a hanger angle of around 40 degrees. Increasing the number of crossbeams beyond 17 resulted in a greater steel mass without reducing the stress noticeably.

The range in the objective values differed for skew load, where steel mass varied significantly more than bending stress. The difference between the maximum and minimum values along the Pareto front was 0.83 MPa in bending stress, while it was 16 tons for steel mass. In contrast to the full loading case, skew loading resulted in lower stresses for larger hanger angles, ranging around 50 degrees. 15 crossbeams was the exception to this trend, with a preferred hanger angle in the range of 40 to 42 degrees. With 15 crossbeams and hanger angles in the range of 38 to 42 degrees, skew loading was the critical load case with the largest stresses. 40 degrees gave the smallest stress, corresponding to 4.2 MPa.

Simulation 2

In this simulation, there was no set displacement limit for the crossbeams. The combinations of number of crossbeams and deck thicknesses resulting in the lowest stresses perpendicular to grain in the deck while maintaining low timber mass, were in the range of 13 to 17 crossbeams with 350 to 500 mm deck. The stresses obtained are visualized in Table 4.3. An optimal solution was the combination of 17 crossbeams and a deck thickness of 400 mm. With this thickness, 17 crossbeams resulted in the lowest overall maximum stress in the two load cases. The number of crossbeams was set to 17, with a deck thickness of 400 mm and a hanger angle of 41 degrees to minimize in-plane bending stresses for the new simulation.

By changing from 15 to 17 crossbeams from the last simulation, the maximum stress obtained in the deck was reduced by 0.27 MPa for both load cases, while in-plane bending stress increased by 0.44 MPa. This was considered a good compromise, considering the bending stress still was well within the arch's capacity, while the stresses in the deck had exceeded the capacity of the deck.

Table 4.3: 100 m span with four splices: Simulation 2, Full load.

Objective values			Parameter values	
Stress 90° to grain [MPa]	Steel mass [tons]	Timber mass [tons]	Number of crossbeams	Deck thickness [mm]
3.64 - 4.1 - 4.7	22.9 - 23.5 - 23.3	342 - 317 - 291	17	450 - 400 - 350
3.88 - 4.37 - 4.85	21.4 - 22.1 - 23.2	342 - 317 - 291	15	450 - 400 - 350
3.75 - 3.84 - 4.25	22.1 - 23.8 - 22.6	342 - 291 - 317	16	450 - 350 - 400
4.01 - 4.07 - 4.42	23.7 - 22.4 - 22.4	291 - 342 - 317	14	350 - 450 - 400

Simulation 3

The solutions close to the critical design limit shared similar cross-sections with width-to-height ratios from 1.86 to 2.23 for the full load case. The full load case gave larger values of the design check than skew loading; hence it was critical. With a chosen cross-section with a width of 700 and height of 1400 mm, the design check resulted in 0.859 and a timber mass of 321 tons. Reducing the maximal arch height to 1400 mm resulted in a reduction of the maximal in-plane bending stress in the arches and an increase in the critical design check value to 0.878, while timber mass was reduced by 2 tons.

Simulation 4

The bending moment in-plane for the full load case was more evenly distributed than for skew loading. This makes the placement of the splices easier. Multiple different hanger angles in the range of 35 to 44 degrees resulted in small moments in the splices, as well as small in-plane bending stresses.

For the skew load case, one configuration stood out with both low moments in splices and bending stresses in the arch. This configuration has the two top splices placed right next to each other at the top, connecting one longer splice. The hanger angle was 52 degrees. Any other angles or splice placements resulted in significantly larger stresses. However, this configuration was similar to the three-spliced bridge, which had already been examined. Hence, this configuration was not used. For the rest of the configurations, with hanger angles of degrees 40 to 47, the resulting maximum moments in the splices were relatively similar. Changing the angle of 41 from the last simulation to 47 degrees decreased the peak in-plane bending stress, but decreased the maximum moment in the splices and reduces the number of relaxed hangers. Suitable splice placements for splice (1) and (2), were 0.8 and 0.15, respectively.

Simulation 5

The values of in-plane bending stresses along the Pareto front were larger in skew than in full loading. This was the critical load case. A configuration with 17 crossbeams minimized the peak stress, with the lowest value of 5.36 MPa for a hanger angle of 52 degrees. With 17 crossbeams, the stresses were compared for all possible angles and both load cases. The smallest maximum stress corresponded to a hanger angle of 50 degrees, though this increased the splice moments from 193 to 294 kNm. The configuration chosen in the previous simulations with 17 crossbeams and a 47-degree hanger angle, remains a suitable solution. A 47-degree hanger angle resulted in a peak in-plane bending stress of 5.89 MPa.

4.5 120 m span with four splices

The detailed results in the form of figures and tables, for this bridge configuration, can be found in Appendix B.5.

Simulation 1

For full loading, the optimal solutions tended to prefer a lower angle, typically ranging between 35 and 40 degrees. The favorable solutions encompassed a range of 10 to 25 crossbeams, with no discernible pattern or trend. In terms of moment stress, the variations were relatively modest, ranging from 2.2 MPa to 3.3 MPa, while the steel mass spanned approximately 22 to 32 tons. For skew loading, the optimal solutions tended to prefer a higher angle, typically within the range of 46 to 51 degrees. The number of crossbeams also displayed considerable variability, ranging from 10 to 20. The moment stresses from these solutions varied from 3.4 MPa to 4.5 MPa, while the steel mass ranged from 21.8 to 28.3 tons.

A higher and a configuration with an angle of 48 degrees and 19 crossbeams was selected, as it yields stresses and steel mass within the optimal ranges for both load scenarios. The moment stress was at 3.3 and 3.64 MPa for full and skew load, respectively. Steel mass was at 27.6 and 27.18 tons.

Simulation 2

Solutions including higher displacement limits for crossbeams were primarily focused on. Compression perpendicular to grain increased with decreasing steel and timber mass. With full load, the optimal solutions had 12 to 19 crossbeams and deck thickness from 300 to 500 mm. The steel mass varied from 23 to 56.7 tons, timber mass from 370.8 to 492.3 tons and compression in the deck perpendicular to grain from 2.9 to 4.4 MPa. With skew load, some of the same trends applied. Deck thickness varied from 300 to 400 mm and crossbeams from 10 to 19. Here, the steel mass varied from 22 to 48 tons, timber mass from 370.8 to 431.5 tons and compression in the deck perpendicular to grain from 3.4 to 5.3 MPa.

The selected number of crossbeams remained 19, as this was a result that worked well for both load situations. The deck thickness was selected as 400 mm, resulting in a compromise between timber mass and stress in the deck.

Simulation 3

For full loading the height of the arch varied from 750mm to 950mm, while the width ranged from 1450mm to 1750mm for critical design check values spanning from 0.823 to 0.935. For these dimensions, the corresponding timber mass varied between 430.7 tons and 439.5 tons, the most critical design check being buckling out-of-plane. Consequently, these results indicated that the width of the cross-section should be greater than its height. Similar trends were observed for the skew load. It is noteworthy that the required cross-sections for skew load were smaller than those for full load while maintaining the same critical design check factor. This made the full load case critical.

The selected cross-section had a height of 850mm and a width of 1600mm. It yielded a critical design check factor of 0.878 and a timber mass of 433.4 tons for full load. For skew load, the critical design check factor was 0.746. Additionally, the maximum height of the arch ends was adjusted to

1300, as it maintained the maximum stress in the beams at a low value while distributing the in-plane moment in the arch more evenly. This reduced the timber mass to 424.4 tons and increased the critical design check at 0.8 and 0.909 for full and skew load, respectively.

Simulation 4

For the full load, the selected solutions yielded a small range of moment stress in the beam, from 3.1 to 3.99 MPa. The range of maximum bending moments in the splices was larger, from 126 to 375 kNm. The corresponding hanger angles spanned from 36 to 41 degrees. Splice placement (1) ranged from 0.2 to 1.0, while splice placement (2) seemed insignificant.

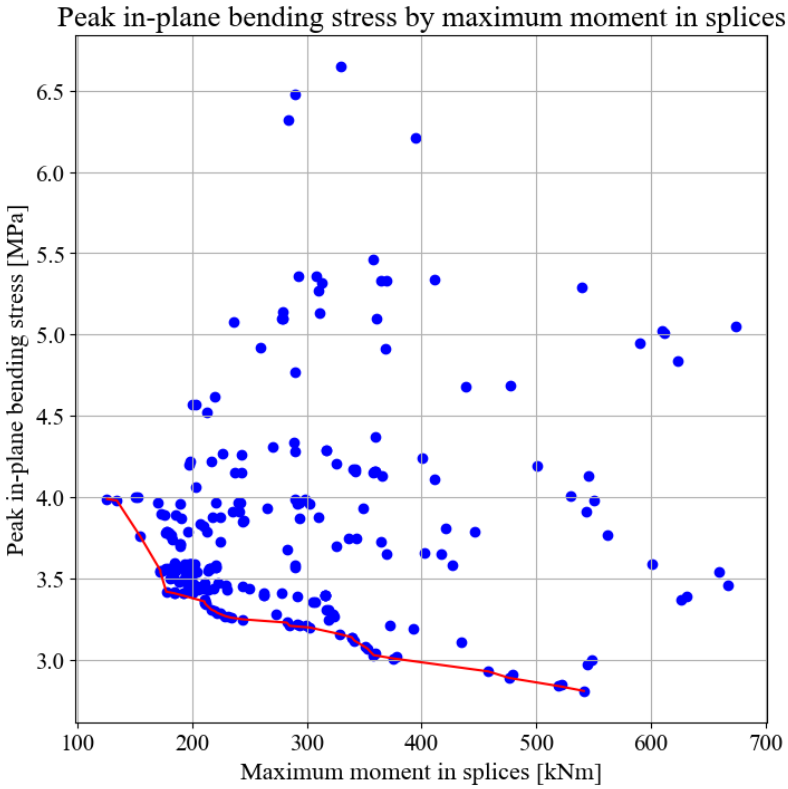

Figure 4.8: 120 m span with four splices: Simulation 4, Full load.

Table 4.4: 120 m span with four splices: Simulation 4, Full load.

Objective values		Parameter values		
Maximum moment in splices [kNm]	Peak in-plane bending stress [MPa]	Connection 1 placement [0, 1]	Connection 2 placement [0, 0.5]	Hanger angle [degrees]
125.7 - 134.3	3.99 - 3.98	0.4 - 0.6	0.3	40
154.7	3.76	0.2	0.3	41
172.3	3.54 - 3.55	0.8 - 0.9	0.2	36
375.1	3.01	0.4	0.5	38

Considering the skew load, the preferred solutions exhibited moment stresses between 4.96 and 5.88 MPa. The maximum bending moment in the splices ranged from 320 to 456 kNm. Consequently, the corresponding range for splice placement (1) was between 0 and 1, while splice placement (2) ranged from 0.1 to 0.3. The number of hangers in compression varied from 3 to 8.

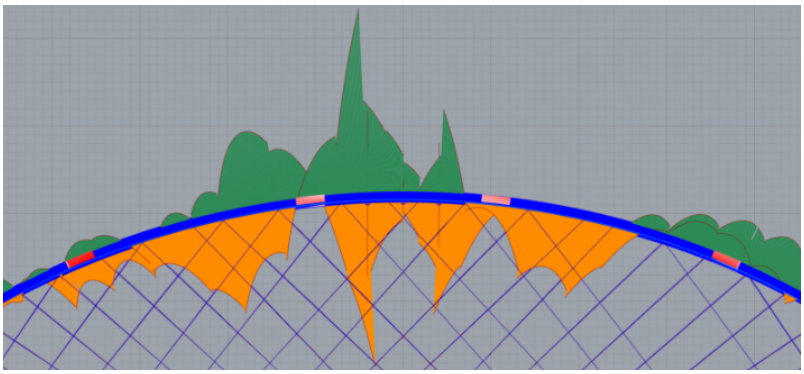

Figure 4.9: 120 m span with four splices: Simulation 5, Skew load. In-plane bending moment diagram with splice placements, marked in red.

The solution was found by placing the splices between peaks in the moment diagram, as depicted in Figure 4.9. Specifically, splice (1) and (2) were placed at 0 and 0.3, respectively. This configuration proved to be beneficial for both load situations. A hanger angle of 45 degrees minimized the moment in the splices for the skew load scenario and performs well under full load. The moment stress was 4 MPa for full load, with bending moment in the splices at 159 kNm. In the case of skew load, the moment stress was 5.66 MPa, and the maximum bending moment reached 313 kNm. 7 hangers were in compression.

Simulation 5

For the full load situation, the number of crossbeams varied between 10 and 11 or between 17 and 22. The hanger angle tended to be small, ranging from 35 to 39 degrees. In terms of moment stresses, the corresponding values ranged from 2.88 MPa to 4.10 MPa, while the steel mass ranged from 21.56 to 29.56 tons.

For skew load, a wider range of number of crossbeam and angles was observed among the selected solutions. The hanger angle tended to be higher than the full load scenario. Most solutions had angles in the range of 45 to 49 degrees with corresponding moment stresses ranging from 5.11 to 6.94 MPa, while the steel mass varied between 22.13 and 32.47 tons.

The previously chosen combination of 19 crossbeams and a hanger angle of 45 degrees remained a good solution. Among the skew load solutions, 19 was the most frequently selected number of crossbeams and represented a local optimum for stress levels for both load situations. 45 degrees was chosen as it represented a local minimum for steel mass, while the moment stresses were deemed acceptable.

4.6 100 m span with three splices and three sets of hangers

Figures and tables from this bridge configuration can be found in Appendix B.6.

Simulation 1

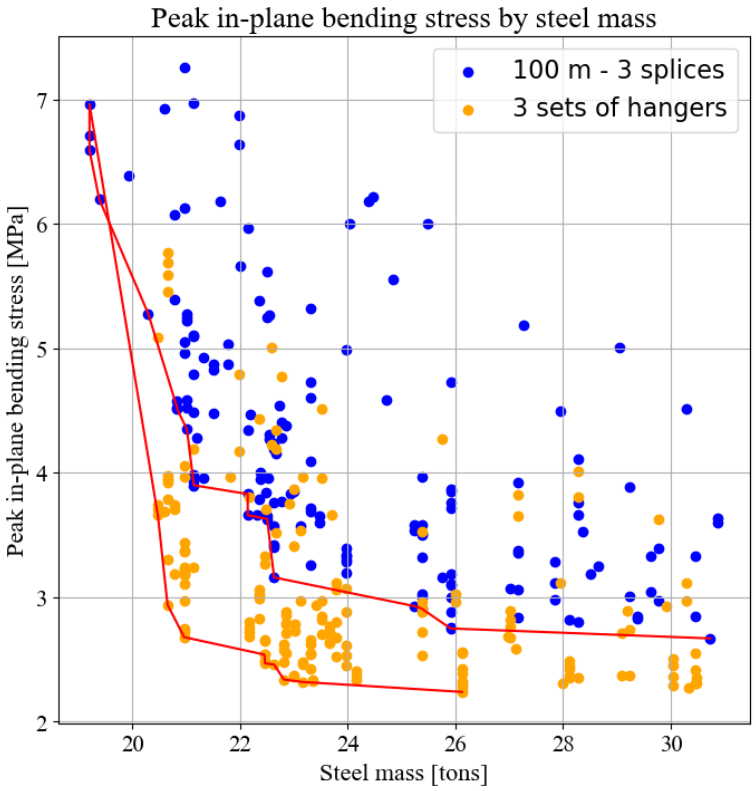

Figure 4.10: 100 m span with three splices vs. three sets of hangers: Simulation 1, Full load.

For the selected optimal solutions under full load, the number of crossbeams ranged from 10 to 16, with hanger angles varying from 43 to 52 degrees. The corresponding peak in-plane bending stress ranged from 2.3 to 3.66 MPa, and the steel mass from 20.46 to 23.16 tons.

In the case of skew load, the selected solutions had 10 to 16 crossbeams, with hanger angles ranging from 47 to 68 degrees. The corresponding moment stresses varied between 2.79 and 6.8 MPa, with steel mass ranging from 20.83 to 23 tons. It was observed that angles over 60 degrees resulted in the highest stresses.

The chosen configuration consisted of 16 crossbeams with a hanger angle of 50 degrees. This configuration lead to a moment stress of 2.46 and 3 MPa and a steel mass of 22.63 and 22.99 tons for full and half load, respectively. This configuration represented a local optimum for both number of crossbeams and angle for both load cases.

Simulation 2

In this simulation, there was no displacement limit for the crossbeams. Under full load, the selected solutions consisted of 10 to 15 crossbeams. The deck thickness ranged from 350 to 700

mm. The corresponding steel mass ranged from 17.57 to 23 tons, while the maximum compression perpendicular to the grain ranged from 2.5 to 3.76 MPa. The timber mass increased linearly with the deck thickness, ranging from 285.7 tons for a 35cm thickness to 488.2 tons for a 75cm thickness.

For skew load, the selected solutions had a number of crossbeams between 14 and 19, with a deck thickness ranging from 35 to 65cm. The corresponding steel mass ranged from 19.58 to 24.7 tons, and the compression perpendicular to the grain ranged from 2.59 to 3.76 MPa.

15 crossbeams and a deck thickness of 40cm provided compression perpendicular to the grain of 3.12 MPa and 3.67 MPa for full and skew load, respectively. These values fell within the ranges of the selected solutions for both load situations. The timber mass was 336.3 tons, while the steel mass was 22.74 tons for full load and 21.74 tons for skew load.

Simulation 3

The selected solutions had heights from 650 to 1000 mm in both load cases, more frequently in the middle of this range. The widths varied from 1100mm to 1450 mm. The corresponding critical design check factors varied from 0.823 to 0.928 and the timber mass varied from 338.1 to 346.9 tons for full load. For skew load, the critical design check factor was slightly lower for the same cross sections, varying between 0.716 and 0.987 with timber masses of 327.3 to 346.8 tons for the selected solutions. The combination chosen was with height of 750 mm and width of 1300 mm with growing arch size at 1300 mm. This combination gave critical design check factors of 0.896 and 0.756 for full and skew load, respectively. The timber mass was 339.7 tons.

Simulation 4

The full load case preferred an angle around 40 to 42 degrees. An angle higher than 45 degrees caused the maximum moment in the splices to increase significantly. The ideal splice placement changed from angle to angle, while 0.7 was a local minimum for the bending moment in splices for a few angles. There were 6 to 8 hangers in compression for all configurations. The optimal solutions gave maximum bending moment in splices below 100 kNm. The range of variation in moment stresses was small. For skew load, higher angles around 50 degrees were preferred. The splice placement followed the same trend as for full load. Here, 15 to 21 hangers were in compression, with lower angles giving the highest number of compressed hangers. The location of the compressed hangers relative to the load is illustrated in Figure 4.11.

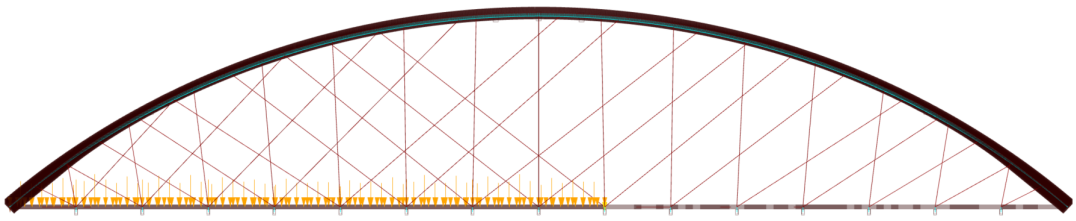

Figure 4.11: 100 m span with three splices and three sets of hangers: Simulation 4, Skew load.

Simulation 5

Moment stresses for full load were in the range 2.3 to 4.2 MPa for full load. The hanger angle was between 40 and 56, with the general trend that a higher angle gave higher stress. The exception to this within the selected solutions, was between 41 and 47 degrees for 15 crossbeams, where the moment stress decreased. The number of crossbeams was 10 to 25. Steel mass increased with increasing number of crossbeams, from 19.9 to 30.2 tons. For skew load, the same trend of angle/ stress follows, with a few exceptions for angles under 50 degrees. Hanger angles varied from 40 to 65, and crossbeams from 10 to 16. The moment stresses in-plane ranged from 2.9 to 6.35 MPa. Steel mass varied from 19.7 to 22.2, increasing with the number of crossbeams, similar to full load. The previously chosen configuration of 15 crossbeams and hanger angle of 52 degrees remained a good solution, with objective values within the optimal range.

In-plane bending moments

Figure B.105 shows the in-plane bending moment diagrams of the final configurations for the 100 m span bridge with three splices with two vs. three sets of hangers. The bridge with three hanger sets has a more distributed bending moment diagram, with more shallow peaks.

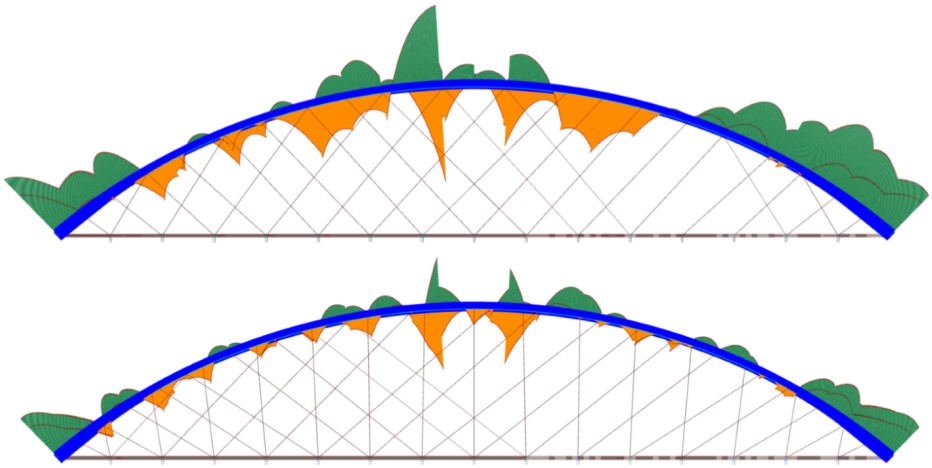

Figure 4.12: 100 m span with three splices vs. 100 m span with three splices and three sets of hangers: Skew load. Moment distribution in-plane with final configurations.

4.7 100 m span with three splices and triangular corners

The detailed results in the form of figures and tables, for this bridge configuration, can be found in Appendix B.7.

Simulation 1

For both load cases, the Pareto front included solutions with 10 to 12 crossbeams. An increase in the number of crossbeams from 10 to 12 decreased the peak in-plane bending stress. Among the configurations near the Pareto front, hanger angles were in the range of 54 to 58 degrees, with the exception of 46 to 47 degrees for 12 crossbeams. The parameters were set to 12 crossbeams with a 55-degree hanger angle, resulting in the lowest peak in-plane bending stress for both load cases.

Simulation 2

The second simulation resulted in significant stresses compared to previous bridge configurations. With a hanger angle of 55 degrees, most crossbeam configurations resulted in stresses from compression perpendicular to grain above 7 MPa. The high stresses posed the need for a new angle. The lowest stresses were obtained with 18 crossbeams. A new simulation was performed to find a hanger angle that satisfied both simulations 1 and 2. This optimization was performed using Galapagos, illustrated in Figure 4.13.

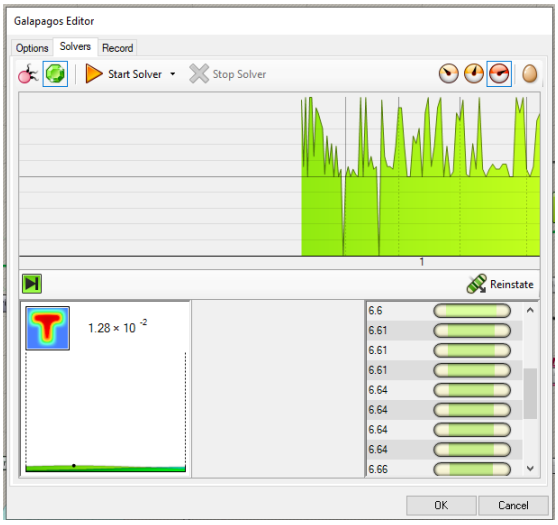

Figure 4.13: 100 m span with three splices and triangular corners: Simulation 5, Full load. Optimization with Galapagos, minimizing the peak in-plane bending stress with the hanger angle as the varying parameter. The green graph shows the different configurations tested, whilst the numbers in the bottom right gave the lowest obtained peak in-plane bending stresses.

The lowest possible peak in-plane bending stress with 18 crossbeams was 6.6 MPa for the full load case. This corresponded to hanger angles from 35 to 37 degrees. The deck stress was decreased to 3.57 MPa with a hanger angle of 40 degrees, while the peak in-plane bending stress increased to 6.66 MPa. This hanger angle was used for simulation 2.

The simulation was carried out and resulted in solutions near the Pareto front with 16 to 21 crossbeams for both load cases. Deck thicknesses varied from 300 to 550 mm, depending on the

number of crossbeams with resulting stresses. The chosen configuration was 18 crossbeams with a deck thickness of 400 mm.

Simulation 3

Along the Pareto front, all configurations which had a critical design value just below 1 had an arch height between 600 and 550 mm. The width was considerably larger, with values ranging from 1650 to 2000 mm, as seen in Figure 4.5. The full load case was the critical case with larger design check values for the same cross-sections compared to skew loading. The chosen cross-section was 600 mm x 1700 mm with a critical design check for the full load case of 0.934 and a timber mass of 320 tons.

Table 4.5: 100 m span with three splices and triangular corners: Simulation 3, Full load.

Objective values		Parameter values	
Critical design check [0, 1]	Timber mass [tons]	Arch height [mm]	Arch width [mm]
0.866 - 0.894	326 - 323	550	2000 - 1950
0.924	320	550	1900
0.934	320	600	1700
0.967	316	600	1650

Simulation 4

The variation in the peak in-plane bending stresses was small in both load cases, which lead to the differences mainly being the maximum bending moment in the splices. For the full load case, a hanger angle of 44 degrees and splice placement of 0.9 corresponded to the smallest moment in all splices. Similarly, the same configuration gave the smallest moments for skew loading. The bending moment obtained was 82 kNm. Other hanger angles resulted in larger moments with magnitudes near or beyond 100 kNm.

Simulation 5

Similar to the first simulation, the peak in-plane bending moment decreased when increasing the hanger angle. The configuration resulting in the smallest moment stresses for the full load case was 12 crossbeams and a 53-degree hanger angle, resulting in a stress of 6.58 MPa. However, this resulted in stress from compression perpendicular to grain in the deck of 6.16 MPa. By changing the configuration to 18 crossbeams with a 44-degree hanger angle, the peak in-plane bending stress for both load cases was 7.18 MPa and a maximum deck stress of 4.44 MPa.

4.8 100 m span with three splices and vertical arches

The detailed results in the form of figures and tables, for this bridge configuration, can be found in Appendix B.8.

Simulation 1

The full load case generally favored lower angles within the range of 36 to 42 degrees. Increasing the angles beyond this range tended to increase moment stresses in the arches. The moment stress also increased with a higher number of crossbeams, due to a greater steel weight. Higher angles between 48 and 53 degrees were preferred for skew load. Decreasing or increasing the angle resulted in greater moment stresses. The moment stresses were higher compared to the full load case, making the skew load case the critical case. The configuration with 15 crossbeams and an angle of 51 degrees yielded moment stresses of 2.3 MPa for full load and 2.81 MPa for skew load. The corresponding steel mass was 23.7 tons, and this was the configuration chosen for the next generation.

Simulation 3

The full load case consistently resulted in a higher critical design check factor compared to the skew load case, considering the same cross sections. The general trend was that the width was larger than the height. This trend was generally observed across a range of critical design check factors between 0.7 and 1.0, with a few exceptions where the width and height of the cross sections were identical. Notably, when the height was 850 mm and the width was 1200 mm, the cross-section yielded a critical design check factor of 0.879 for the full load case and 0.826 for the skew load case. This particular cross-section was positioned on the Pareto front for both load cases, highlighting its optimal performance in terms of meeting the design requirements. The growing arch size was decreased to 1550 mm, resulting in the critical design check factor of 0.886 for full load and 0.873 for skew load. The total timber mass for this bridge, including the wind truss, was 338.1 tons.

4.9 Comparison

4.9.1 Merging hanger connections

The hanger connections in the arch were merged using a merging distance of six meters. This resulted in the number of hanger connections being reduced from 60 to 40 for the 100 m span bridge with three splices. The structural effect of the merge can be seen in Table 4.6. The most noticeable effects appeared for the skew load case, where peak in-plane bending stress increased by 4%, while maximum bending moment in splices increased by 5%. It is observed that the structural effect of connecting two hangers in the same point is minor. The number of relaxed hangers increased by one, as a result of the marginal alteration of the hanger inclination. The calculated utilization and critical design checks were barely altered and still meet the necessary conditions.

Overall, the changes in the investigated structural properties were considered negligible compared to the effect of reducing the number of hanger connections by 1/3.

Table 4.6: 100 m span with three splices vs. 100 m span with three splices without merged hanger connections: Results with the final configuration for the 100 m span with three splices from Table 4.7. Both bridges with the same configurations except hanger connections.

	Merged Full load	Non-merged Full load	Merged Skew load	Non-merged Skew load
Peak in-plane bending stress [MPa]	3.91	3.87	4.53	4.35
Critical design check Eq. (6.24)	0.935	0.933	0.747	0.742
Buckling load factor	2.29	2.30	2.64	2.66
Natural frequency [Hz]	0.763	0.762	0.716	0.717
Max stress 90°to grain [MPa]	3.08	3.08	2.88	2.88
% of deck exceeding Tsai-Wu criterion	5.4	5.5	1.9	1.9
Max moment in splices [kNm]	106	108	130	123
Number of relaxed hangers	0	0	7	6
Maximum displacement [mm]	239	239	262	260
Crossbeam utilization [%]	79.4	79.3	87.5	85.1
Hanger utilization [%]	30.9	30.7	38.0	37.6

4.9.2 Final configurations

The values in Table 4.7 are obtained after all five simulations, with the exception of the bridge with vertical arches and with no side beams. All parameters have been changed during the simulations to satisfy multiple objectives. Arch height and width describe the cross-section of the arches, while the max arch height is the cross-sectional height at the arch supports. The different cross-sections for the crossbeams are referred to by the heights of the corresponding cross-section alternatives listed in Table 3.5. In the cases where the cross-section varies along its length, the two largest heights correspond to the two middle elements of the crossbeams. Furthermore, the total steel mass refers to the total mass of all crossbeams and hangers. The mass from the top- and side beams are excluded but corresponds to 10-12 tons depending on the configuration. The total timber mass includes all timber in the structure.

Table 4.7: Final configurations for all bridges.

	80 m 2	80 m 3	100 m 3	100 m 4	120 m 4	3 sets hangers	Tri. corner	Vertical arches	No side beams
Arch height [mm]	650	650	800	700	850	750	600	850	800
Arch width [mm]	1050	1050	1250	1400	1600	1300	1700	1200	1250
Max arch height [mm]	1000	1000	1300	1400	1300	1300	-	1550	1300
Deck thickness [mm]	350	350	400	400	400	450	400	400	400
Number of crossbeams	13	13	15	17	19	15	18	15	15
Crossbeam cross -section [mm]	450x6 550x2	450x6 550x2	450x6 550x2	450	450	450x6 550x2	450	450x6 550x2	450x6 550x2
Hanger angle [degree]	45	45	43	47	45	52	44	51	43
Splice placement	0 -	0 -	0.9 -	0.8 0.15	0 0.3	1 -	0.9 -	0.5 -	0.9
Total steel mass [tons]	48.7	48.7	63.5	66.6	88.3	72.0	68.7	64.8	63.5
Total timber mass [tons]	203	203	316	319	425	340	320	338	316

4.9.3 Final results

The final results, shown in Table 4.8, are the values for all objectives in the simulations, along with other interesting findings. They are the results of the configuration in Table 4.7. The values displayed are the most critical results, considering both load cases. Results from both load cases can be seen in the Appendix.

Table 4.8: Results with the final configuration from Table 4.7.

	80 m 2	80 m 3	100 m 3	100 m 4	120 m 4	3 sets hangers	Tri. corner	Vertical arches	No side beams
Peak in-plane bending stress [MPa]	5.21	5.12	4.53	5.53	5.27	3.15	6.50	2.59	5.32
Critical design check EC5: Eq.(6.24)	0.958	0.956	0.935	0.993	0.931	0.877	0.943	0.886	1.044
Buckling load factor	2.41	2.41	2.29	2.30	2.32	2.55	3.58	2.81	2.28
Natural frequency [Hz]	1.02	1.02	0.716	0.729	0.518	0.781	0.816	0.278	0.733
Max stress 90°to grain [MPa]	3.71	3.71	3.08	3.45	3.47	3.37	5.21	3.18	3.25
% of deck exceeding Tsai-Wu criterion	11.6	11.6	5.4	8.8	7.2	1.7	7.4	5.3	5.5
Max moment in splices [kNm]	147	146	130	161	257	127	91	246	268
Number of relaxed hangers	7	7	7	5	6	15	7	1	7
Maximum displacement [mm]	217	217	262	262	319	241	230	1301	323
Crossbeam utilization [%]	82.4	82.5	87.5	77.8	80.5	82.0	77.9	79.5	89.6
Hanger utilization [%]	55.5	55.7	38.0	34.4	25.3	28.8	34.4	34.7	38.9

5 Discussion

5.1 Results

The equations provided by Eurocode 5 were employed to determine the most critical design check for each bridge configuration; see Section A.4 in the Appendix. All of the relevant design checks were calculated for every single element in the arches. The critical design check value corresponds to the most critical element in the design check with the largest value. The largest value for the design checks corresponded to Eq. (6.24) in EC5, A.24, for all bridge configurations. This design check asses out-of-plane buckling and includes compression and bending moment in- and out-of-plane. As a result, the final configurations ended up with width-to-height ratios between 1.41 and 2.83, mostly between 1.5 and 2. Even with these dimensions, out-of-plane buckling was the most critical design check. The buckling load factors give a greater margin of safety than the design check values because it only considers normal forces and Euler buckling [2]. A buckling load factor of around 2.5 is often desirable, representing a safety margin for imperfection and error. [3] The arches in the bridge configuration with triangular corners have a shorter buckling length due to the triangles, in addition to an arch width of 1700 mm, the widest cross-section among the bridge configurations. Hence, the buckling load factor for the configuration with triangular corners is larger than for other configurations.

For the standard bridge configurations, the maximum deflection and natural frequencies are relative to the bridge spans, and it seems like an additional splice in the arches does not affect this noticeably. Among the alternative bridge designs, except for the vertical arches, the max deflections are moderate compared to the proposed designs. The bridges with an extra set of hangers and the triangular corners would seem to have a stiffer structure compared to the 100 m span bridge with three splices. This can be seen in the results, as the natural frequencies are larger, and the displacements are smaller for these alternatives. On the other hand, the bridge configuration with no side beams also has a larger natural frequency than the standard configuration, even though the stiffness is reduced. This could be due to the weight reduction from the steel side beams at a high point in the structure, which makes the overall structure more imbalanced. The maximum displacement is larger, however, with values similar to the 120 m span bridge. It is reasonable that the displacement increases when the out-of-plane stiffness is reduced since the maximum displacement of the structure is in the arches.

The bridge configuration with vertical arches has a noticeably lower natural frequency than the other configurations. This is because it is the only configuration where the arches do not create the triangular shape that stiffens the structure out-of-plane. With the triangular shape at the bridge entry, created by the arch lean, the necessity of fixing the arch supports against rotation out-of-plane lowers. As seen in Table 5.1, the bridge configuration with vertical arches is more sensitive to the boundary conditions and requires a rotational stiffness out-of-plane.

[2] The definition of the buckling load factor in Karamba3D is from correspondence with Clemens Preisinger, parametric engineer in Karamba3D

[3] The safety margin is sourced from a conversation in person with K.A. Malo.

Table 5.1: 100 m span with three splices vs. 100 m span with three splices and vertical arches: Full load. Comparing the difference in natural frequency, maximum deflection, and critical design check for pinned and fixed arch supports, out-of-plane.

	Pinned			Fixed		
	Nat. freq. [Hz]	Max def. [mm]	Cr. design check	Nat. freq. [Hz]	Max def. [mm]	Cr. design check
Vertical arches	0.278	1301	0.886	0.764	180	0.499
100 m - 3 splices	0.763	239	0.935	1.147	152	0.621

Throughout the simulations, the side beams have been rotationally free about their local y- and z-axis, while the top beams have been fixed to the arch. This led to a stable structure; however, the peak in-plane bending moment is typically located where the arch is connected to the two outer top beams due to a stress concentration around the fixed connections. In all the bending moment diagrams, there is a noticeable peak at these points. A sensitivity analysis was performed to see what effect the rotational stiffness has on the structure, as seen in Section B.6. By adjusting the rotational stiffness in both y- and z-direction for top- and side beams to 280 kNm/rad whilst setting the max arch height to double the rest of the arch, the maximum peak in-plane bending stress is 1.94 MPa, a significant reduction of 38.4% compared to fixed connections. Meanwhile, other objectives remain approximately unaffected. This shows the possibilities for further analysis of different parts of these bridge configurations.

Relaxed hangers pose an issue that should be avoided if possible and is one of the main differences between the Nielsen- and network arch bridges. The number of relaxed hangers directly corresponds to the hanger angle. This can be seen through the simulations, and in a specific instance where the 100 m bridge with three splices and a 43-degree hanger angle has 7 relaxed hangers, while the four-spliced alternative with a 47-degree hanger angle has 5 relaxed hangers. This result unveils when evaluating the different configurations, especially during simulation 4. The effect is not due to the arches leaning toward each other. For the vertical arch bridge, the number of relaxed hangers for the chosen configuration is only 1 due to a hanger angle of 51 degrees. However, by reducing the angle to 43 degrees, as for the 100 m three-spliced bridge, the number of relaxed hangers increases to 6. The solutions providing the best structural performance for the vertical arches include larger hanger angles, subsequently reducing the number of relaxed hangers. It could be that by leaning the arches towards each other, the configuration prefers smaller hanger angles to optimize structural performance. Only two simulations were carried out for the bridge with vertical arches, making it difficult to conclude the optimal hanger angle for this configuration. Considering the results, relaxed hangers could pose a greater challenge for the leaned arch configuration than for vertical arches.

The bridge alternative with three sets of hangers has a considerably larger number of relaxed hangers than other configurations. It is reasonable that the number of relaxed hangers increases when the total number of hangers increases. However, the number of relaxed hangers is doubled while the number of hangers only increases by 50%. This is the only bridge configuration with relaxed hangers with symmetric traffic loading; see Table B.69. During skew load, the hangers in the set inclined toward the opposite side of the bridge, located at the unloaded part, are compressed; see Figure 4.11. This could result from the “vertical” hanger set taking up tension forces previously covered by the, now relaxed, hanger set.

A larger hanger angle will decrease the number of relaxed hangers in a skew load case for all bridge configurations. On the other hand, by increasing the hanger angle above a certain angle, other negative effects will arise in the structure. The simulations showed that objectives such as peak in-plane bending stress, as well as stresses from compression perpendicular to grain in the deck,

will increase. A solution to the relaxed hangers is proposed by Halse [9], with the possibility of controlling the hanger "buckling" using three-hinged hangers. This seems like a possible solution, as the simulations in this thesis show that the challenge of relaxed hangers is not avoided without structural comprises.

The largest value for the peak in-plane bending stress was obtained with the skew load case for all the standard bridge configurations. Moreover, the two bridge alternatives with the largest and smallest peak in-plane bending stresses are the configurations with triangular corners and vertical arches, respectively. For the configuration with triangular corners, the peak stress, of 6.50 MPa, appears near the end supports of the arch. Unlike the other bridge configurations, there is no increase in arch height towards the ends. This results in larger in-plane bending moments, hence greater stresses from these moments. An implementation of the increasing arch height would reduce the stresses near the supports, making the largest stress from in-plane bending be at the position of the outer top beams, like the other configurations. This would result in a stress of 4.25 MPa, given the moment distribution from the final configuration for the triangular corners in Figure B.122, and full loading. By adjusting the maximum height of the arch, it is possible to manipulate the bending moment distribution to reduce peak in-plane bending stresses. Furthermore, the bridge configuration producing the smallest in-plane bending moments in the arch is the configuration with vertical arches. This differs greatly from the other alternatives, and there are probably two main reasons for the low bending stresses. The first reason is the constraints between the K-trusses and the arches. The connections between them are modeled as rotationally free, as opposed to the top beams used in the other configurations, which are fixed. As mentioned, fixing the top beams results in larger in-plane bending moments. Additionally, there are more K-trusses connected to the arches than top beams, which results in a more even moment distribution.

Regarding the configuration with three sets of hangers, it results in a significantly lower peak in-plane bending stress compared to the standard bridge configurations. This is due to the increase in the number, and spread, of hangers which distribute the forces more evenly along the arch. Compared to the 100 m with three splices, which have the lowest peak stress of the standard configurations, the three-set hanger bridge has a reduction of 30.5% in the peak stress. In addition, the even distribution makes it easier to place splices.

When designing a beam, or in this case, an arch, the optimum would be to produce it in one piece. There has not been developed a flawless splice that can act as an implemented part of the structure without compromising the structural performance. Therefore, it is important to place the splices in an area with a small impact on the structure. Existing splice types are not especially good at transferring moments, so it is preferable to minimize the bending moments at the location of the splices. For the standard bridge configurations, the largest bending moment appearing in any splice is 257 kNm, appearing in the 120 m span bridge. With a total arch length of 131 m, the splice placements are quite limited when each arch part can have a maximum length of 30 m. The restricted range of options may prevent the splices from being positioned optimally. Despite the limitations, the possible position appears to be the optimal choice, as seen in Figure 4.9. By comparing this situation to the 100 m span bridge with four splices, some interesting comparisons appear. The 100 m span, with an arch length of 109.6 m, has a considerably greater range of possible positions for the splices, which results in a maximum splice bending moment of 161 kNm, ref Table B.45. The maximum bending moment is substantially lower than for the 120 m span. As mentioned in Section 3.1.2, the splices are modeled as an area having half the E-modulus. By calculating the stresses corresponding to the maximum in-plane moment in the splice, the difference between the two configurations is small. The maximum splice stress in the 120 m span bridge is 2.67 MPa, compared to 2.82 MPa for the 100 m bridge with four splices, assuming a stress distribution in only half the width. The maximum moment in the splice is not necessarily the best measurement, but it gives a good indication of the impact on the splices.

The splice placement in this thesis is based on the in-plane bending moment distribution for full and skew loading. This is only one of several possible objectives to minimize in this optimization. Other possible objectives could have been out-of-plane bending moments or shear forces. For the arch cross-sections in the final configurations, Table 4.7, the widths are much greater than the heights, making the out-of-plane bending less influential in local problems. However, if the size of these out-of-plane bending moments is large enough, they could have an impact as well. Furthermore, the maximum shear force both in- and out-of-plane is 230 kN for the 100 m span with three splices, making the impact small compared to the bending moments. This is because the hangers act like a light web, taking some of the variations in the shear force. This is, for instance, illustrated by the bridge configuration with three sets of hangers. The maximum shear force is reduced to 209 kN in this case, due to more hangers being able to distribute the shear forces. However, the most desirable effect of an extra hanger set is the even bending moment distribution it causes. The in-plane bending moment diagrams for this configuration compared to the 100 m span bridge with three splices are illustrated in Figure 4.12. The even distribution of bending moment with small peaks makes the splice placement easier by having several possible positions. As mentioned, only the moment distribution for full and skew loading has been evaluated for the splice placement. Other load combinations could potentially cause larger bending moments at the selected placements. A bridge configuration with three sets of hangers would minimize the differences between the alternative load cases, making it a suitable solution.

Considering the same configurations with a different number of splices, the similarities are many. To see the full effect of the number of splices, identical geometries can be compared with different numbers of splices. The two 80 m span configurations have the same parameter values, with the only difference being two or three splices; see Table 4.7. When comparing the final results from Table 4.8 for the two configurations, it is clear that the differences are minimal. An extra splice for the 80 m span has almost no structural effects on the objectives compared in this thesis, with the splice definition used. Similar results can be seen for the 100 m span configurations. In Table B.46 in the Appendix, the 100 m span bridge with three splices is compared to the same configuration with an extra splice or no splice. The results, in this case, are also very similar for most objectives. Except for the maximum moment in splices, the only result with a considerable change is the value for the critical design check for skew loading, which increases from 0.747 to 0.857 from three to four splices. Compared to the spliced configurations, the design with no splices performs similarly in most investigated objectives, except for the critical design value, which is significantly reduced to 0.427. The reason for this difference could be that a varied number of splices will result in different bending moment distributions, and the corresponding values for in- and out-of-plane moments will vary, illustrated in Section B.4 in the Appendix. For the three-spliced and no spliced bridge, the most critical element in the arch is the element connected to the top beam furthest from the loaded part of the deck, whilst the element connected to the opposite top beam is the most critical for the four-spliced configuration. In the four-spliced configuration, the in-plane bending moments are considerably larger in the critical element, hence possibly the difference in the critical design check for skew loading; see Table B.47.

The design check used to control the timber deck is the Tsai-Wu criterion. For most final configurations, the maximum deck stress from compression perpendicular to grain ranges between 3 and 3.5 MPa, which is above the limit of 2.5 MPa, ref. Table 3.3. The largest values were obtained from the full load case for all standard bridge configurations. However, the maximum stresses occur in few of the shell elements in the deck. The percentage of elements exceeding the Tsai-Wu criterion indicates to what extent the stresses are too high. Investigation shows that most elements exceeding the criterion are just above the limit, indicating that minor changes to the bridge configurations could reduce the problem. It was observed that the areas in the deck exceeding the Tsai-Wu criterion were mainly concentrated around the crossbeam closest to the support. This

could be because the crossbeams will deform, inducing stresses in the deck. These stresses are not remarkably large in the middle of the bridge, but with a deformation at the supports equal to zero, a rapid difference in curvature is created in the deck close to the supports, inducing higher local stresses. By increasing the cross-section for the crossbeams closest to the supports, the deformation of these beams will be reduced, consequently acting as a middle step and a smoother transition toward crossbeam number two. As a result of this, the rapid difference is avoided, making the number of elements exceeding the Tsai-Wu criterion reduced significantly as seen in Table 5.2, and Figure B.49 to B.52 in the Appendix.

Table 5.2: 100 m span with three splices configuration from Table 4.7. The crossbeams closest to the end supports are varied to see the effect of the deck stresses.

		Full load		Skew load	
End crossbeam cross-sec [mm]	Steel mass [tons]	Exceed Tsai-Wu [%]	Max deck stress [MPa]	Exceed Tsai-Wu [%]	Max deck stress [MPa]
450x6 550x2	63.5	5.43	3.08	1.91	2.88
550	79.7	1.85	3.05	0.50	2.83
650	102.2	0.08	2.58	0	2.45

"Optimize cross-section" proved to be a good component to minimize the size of the crossbeams. It gave a good indication of the needed cross-section for all configurations before a final cross-section was chosen for all crossbeams to make them similar and easier to construct. The crossbeam utilization, calculated by Karamba3D using EC3, was in the range from 77.8% to 89.6% with the final configurations, from 4.7. The hanger diameters were not focused on in this thesis. The dimensions were initially decided and adapted to the bridge spans. A sensitivity analysis showed that by decreasing the hanger diameter for the bridge with a 100 m span and three splices from 50 to 30 mm, the hanger utilization increased to about 85%. The additional deformation, due to the smaller cross-section, increases the peak in-plane bending stress in the arch, critical design check, and deck stress. However, these increases are of insignificant magnitude.

The production of crossbeams with varying cross-sections is more challenging than uniform beams. It is done, however, to optimize the utilization and keep steel mass to a minimum. In an example with 15 crossbeams, using the varying cross-section with a height of 450 mm x 6 and 550mm x 2 in the two middle elements of each crossbeam, the total steel mass saved is 16.3 tons compared to using 550 for the whole beam. It could be possible to use 500 mm instead, but this was not investigated as an alternative cross-section in this thesis. Note that by choosing a configuration with a larger number of crossbeams, the required cross-sections are smaller, increasing the possibility of them being in the standard assortment at the manufacturer. Since the cross-sections are reduced for an increased number of crossbeams, the total steel mass is relatively similar.

A similar challenge occurs for the production of the arch. The production of an arch element with varying cross-section is more expensive and could be more difficult to perform. One could argue that the advantages of the increased arch height could compensate for the extra cost.

In contrast to this, the implementation of the merged hanger connections will reduce cost, assembly time, and complexity. For the standard configuration of a 100 m span with three splices, the number of hanger connections at the lower end of the arches is reduced from 60 to 40. This is a significant decrease in the number of connections, contributing to better durability due to fewer exposed areas.

5.2 Simulations

The order of the simulations can have a noticeable effect on the final configurations. The first simulation results in a selected hanger angle. In the next simulation, the objectives are optimized by varying the parameters to obtain the optimum configurations for this exact hanger angle. Thereafter, the following simulation originates in the configurations from the previous simulations, and so on. Several of the same parameters are varied for different objectives to make sure the chosen configuration suits multiple aspects. Moreover, the final simulation is the same as the first to ensure the values obtained are still optimum for the new bridge configuration. The effect of the simulation order could have been greater if the initial starting values, ref 3.8, were far off the final configuration.

Furthermore, it is atypical for there to exist a single desirable solution for each simulation. There are often multiple different configurations resulting in suitable values for the objectives. In these cases, a sensitivity analysis was performed to find the parameter values that also satisfy other objectives. Since multiple configurations are sufficient, a choice needs to be made, which opens the possibility for biased decision-making. Decisions have been attempted to be kept objective throughout the simulation process, though some bias is impossible to remove completely.

6 Conclusion

The implementation of arches leaning toward each other provided promising results. By creating a triangle between the arch supports and the top, the structure's natural frequency increased significantly compared to a configuration with vertical arches. The lack of this stiffening effect in configurations with vertical arches causes a greater dependency on the out-of-plane rotational stiffness of the supports. Furthermore, there is no need for multiple K-trusses connecting the two arches, reducing material cost and the number of exposed connections, consequently increasing the durability of the bridge. A similar effect is achieved by implementing merging of hanger connections. The number of connections could be reduced by 1/3 without compromising structural performance. Simulations indicated that a bridge configuration with leaned arches preferred hanger angles in the range of 43 to 47 degrees, which might be lower than for vertical arches. Thus relaxation of hangers could pose a greater challenge for leaned arches.

The hanger angle directly affects the number of relaxed hangers in the structure. The study showed that an increased hanger angle would reduce the number of relaxed hangers, though not without compromising structural performance. Similarly, the in-plane bending moment distribution is mostly influenced by the hanger arrangement. By introducing a third set of hangers, the structural performance is improved; however, increasing the number of relaxed hangers.

The most critical design check was out-of-plane buckling for all bridge configurations. This resulted in large width-to-height ratios for the arch cross-section, in the range of 1.5 to 2. The number of splices in the arches had a noticeable effect on buckling. Implementing splices in the arch increased the design check values, while the number of splices exhibited a negligible impact. Overall the structural performance was satisfactory with the assumed splice design.

Two alternatives were proposed to handle the moments near the arch ends induced by skew loading and relaxation of hangers. The configuration with an increasing arch height toward the end supports produced positive results. By adjusting the maximum height at the supports, the in-plane bending moment diagram could be manipulated. Additionally, an increased arch height reduces the stresses at the arch ends. Triangular corners proved to be less efficient.

The bridge deck was analyzed using the Tsai-Wu criterion. The deck elements exceeding the criterion were mainly concentrated around the crossbeam closest to the support. By increasing the size of only the end crossbeams, the stresses were reduced significantly.

6.1 Recommendations for further work

The parametric model created in this thesis offers a wide range of possible optimizations. A selection of potential objectives has been studied, analyzed, and optimized by varying multiple parameters. The main focus has been the global behavior of timber network arch bridges, as well as investigating how different parameters influence specific objectives. It should be noted that the current thesis does not fully exploit the model's capabilities, as several parameters remained constant or were limited in the calculations. Moving forward, the model script has the potential to further investigate the bridge design by addressing the following aspects, among many others:

- Connection design between the two arches: This includes exploring different joint configurations for the top or side beams, as well as developing new designs that better align with the intended function of the arches.
- Implementation of a splice with a more realistic and calculated rotational and translational stiffness corresponding to an actual splice.

In addition to the scope of this thesis, several other aspects warrant investigation for a comprehensive understanding of the bridge's behavior. These include:

- Detailed calculations of connections, boundary points, and local stresses.
- Methods for handling relaxed hangers e.g., by implementing controlled buckling.

Bibliography

[1] B. San et. al. 'Constrained shape optimization of free-form shells considering material creep'. In: *Engineering Optimization* 54.10 (2022), pp. 1787–1800. DOI: 10.1080/0305215X.2022.2061478.

[2] R. Cliger et al. *Design of Timber structures, Volume 1*. Swedish Forest Industries Federation, 2022.

[3] A. Asati. *Network Tied Arch Bridges*. Sept. 2021.

[4] J. Bader and E. Zitzler. *HypE: An Algorithm for Fast Hypervolume-Based Many-Objective Optimization*. Swiss Federal Institute of Technology (ETH) Zurich, 2011.

[5] K. Bell and E. Karlsrud. *Large Glulam Arch Bridges - A Feasibility Study*. URL: https://folk.ntnu.no/bell/Projects/Network_arch.pdf.

[6] Wikipedia contributors. *Euler's critical load*. Feb. 2023. URL: https://en.wikipedia.org/wiki/Euler%27s_critical_load (visited on 19th Feb. 2023).

[7] Wikipedia contributors. *Grasshopper 3D*. Feb. 2023. URL: https://en.wikipedia.org/wiki/Grasshopper_3D (visited on 19th Feb. 2023).

[8] S. Datta. *Genetic Algorithms: Crossover Probability and Mutation Probability*. URL: https://www.baeldung.com/cs/genetic-algorithms-crossover-probability-and-mutation-probability (visited on 8th May 2023).

[9] A. Halse. *Conceptual Study of Using Three-Hinged Hangers in a 2D-Timber Network Arch Bridge*. Norwegian University of Science and Technology, 2019.

[10] T. Haukaas. *Kirchhoff and Mindlin Plates*. 2019. URL: https://civil-terje.sites.olt.ubc.ca/files/2019/06/Kirchhoff-and-Mindlin-Plates.pdf.

[11] C. Apostolopoulou J.H. Argyris M. Papadrakakis and S.Koutsourelakis. 'The TRIC shell element: theoretical and numerical investigation'. In: *Computer Methods in Applied Mechanics and Engineering* 182.1 (2000), pp. 217–245. DOI: https://doi.org/10.1016/S0045-7825(99)00094-8.

[12] L. Tenek J.H. Argyris and L. Olofsson. 'TRIC: a simple but sophisticated 3-node triangular element based on 6 rigid-body and 12 straining modes for fast computational simulations of arbitrary isotropic and laminated composite shells'. In: *Computer Methods in Applied Mechanics and Engineering* 145.1 (1997), pp. 11–85. DOI: https://doi.org/10.1016/S0045-7825(96)01233-9.

[13] H. Liven K. Bell. *Limtreboka*. John Grieg Norske limtreprodusenters forening, 2015.

[14] S. Agarwal K. Deb A. Pratap and T. Meyarivan. 'A fast and elitist multiobjective genetic algorithm: NSGA-II'. In: *IEEE Transactions on Evolutionary Computation* 6.2 (2002), pp. 182–197.

[15] Karamba3D. *Karamba3D Manual*. URL: https://manual.karamba3d.com/ (visited on 11th May 2023).

[16] H. Li. *Timoshenko-Ehrenfest Beam Theory*. 2022. URL: https://encyclopedia.pub/entry/30338.

[17] K. A. Malo. *Anisotropy in Wooden Materials*. Aug. 2021.

[18] R. McNeel and Associates. *What are NURBS?* 2023. URL: https://www.rhino3d.com/features/nurbs/ (visited on 19th Feb. 2023).

[19] E. Oñate. *Structural analysis with the finite element method. Linear statics. Volume 2: Beams, plates and shells*. International Center for Numerical Methods in Engineering (CIMNE), 2013.

[20] A. Ostrycharczyk. 'Network arch timber bridges with light timber deck on transverse cross-beams'. PhD thesis. Norwegian University of Science and Technology, 2017.

[21] A. Pipinato. 'Structural Optimization of Network Arch Bridges with Hollow Tubular Arches and Chords'. In: *Modern Applied Science* 12 (Jan. 2018), p. 36. DOI: 10.5539/mas.v12n2p36.

[22] H. T. Hahn S. W. Tsai. *Introduction to Composite Materials*. Technomic Publishing Company, 1980.

[23] J.M. Gere S.P. Timoshenko. *Theory of Elastic Stability*. McGraw-Hill International Book Company, 1985.

[24] F. Schanack and B. Brunn. 'Analysis of the structural performance of network arch bridges'. In: *Indian Concrete Journal* 83 (Jan. 2009), pp. 7–13.

[25] N. Srinivas and K. Deb. 'Multiobjective Optimization Using Nondominated Sorting in Genetic Algorithms'. In: *Evolutionary Computation* 2.3 (1994), pp. 221–248.

[26] European Committee for Standardization. *Eurocode 1: Actions on structures - Part 1-4: General actions - Wind actions*. European Standard NS-EN 1991-1-4:2005+NA:2009. European Committee for Standardization, 2009.

[27] European Committee for Standardization. *Eurocode 1: Design of steel structures - Part 1-1: General rules and rules for buildings*. European Standard NS-EN 1993-1-1:2005+A1:2014+NA:2015. European Committee for Standardization, 2015.

[28] European Committee for Standardization. *Eurocode 5: Design of timber structures - Part 1-1: General - Common rules and rules for buildings*. European Standard EN 1995-1-1:2004+A1:2018+NA2010. European Committee for Standardization, 2010.

[29] European Committee for Standardization. *Timber structures - Glued laminated timber and glued solid timber - Requirements*. European standard NS-EN 14080:2013+NA:2016. European Committee for Standardization, 2016.

[30] P. Tveit. *An Introduction to the Network Arch*. Aug. 2006.

[31] P. Tveit. *The Network Arch.* Mar. 2014.

[32] Vegdirektoratet. *N100 Veg-og gateutforming*. 2022. URL: https://viewers.vegnorm.vegvesen.no/product/859962/nb.

[33] Vegdirektoratet. *N101 Trafikksikkert sideterreng og vegsikringsutstyr*. 2022. URL: https://viewers.vegnorm.vegvesen.no/product/859965/nb.

[34] Vegdirektoratet. *N400 Bruprosjektering*. 2023. URL: https://viewers.vegnorm.vegvesen.no/product/859957/nb.

[35] Vegdirektoratet. *V412 Bæreevneklassifisering av bruer, laster*. 2023. URL: https://viewers.vegnorm.vegvesen.no/product/859962/nb.

[36] Think Wood. *Designing sustainable, prefabricated wood buildings*. URL: https://www.thinkwood.com/wp-content/uploads/2018/07/Designing-Sustainable-Prefabricated-Wood-Buildings_Think-Wood-CEU.pdf (visited on 19th Feb. 2023).

[37] E. Zitzler, M. Laumanns and L. Thiele. *SPEA2: Improving the Strength Pareto Evolutionary Algorithm*. Swiss Federal Institute of Technology (ETH) Zurich, 2001.

[38] E. Zitzler and L. Thiele. 'Multiobjective Evolutionary Algorithms: A Comparative Case Study and the Strength Pareto Approach'. In: *IEEE Transactions on Evolutionary Computation* 3.4 (1999), pp. 257–271.

Appendices

Table of contents

A Calculations and equations

A.1 Wind force - Simplified method

$$F_w = \frac{1}{2} \cdot \rho \cdot v_b^2 \cdot C \cdot A_{ref,x} \tag{A.1}$$

Equation 1: Wind force: EC1-1-4, Eq. (8.2).

$$A_{ref,deck,x} = L_{bridge} \cdot D_{bridge} \tag{A.2}$$

Equation 2: Reference area deck: EC1-1-4, Clause 8.3.1 (simplified).

$$A_{ref,arch,x} = L_{arch} \cdot H_{arch} \tag{A.3}$$

Equation 3: Reference area arch.

$$v_b = c_{dir} \cdot c_{season} \cdot v_{b,0} \tag{A.4}$$

Equation 4: Basic wind speed: EC1-1-4, Eq. (4.1).

$$v_b = 1 \cdot 1 \cdot 30 = 30\frac{m}{s} \tag{A.5}$$

$$\rho = 2.5\frac{kg}{m^3} \tag{A.6}$$

Equation 6: Density of air: EC1-1-4, NA.4.5.

$$C = 3.6 \tag{A.7}$$

Equation 7: Wind load factor: EC1-1-4, Table 8.2.

$$F_w = \frac{1}{2} \cdot 1.25\frac{kg}{m^3} \cdot (30\frac{m}{s})^2 \cdot 3.6 \cdot A_{ref,x} \tag{A.8}$$

$$q_w = \frac{F_w}{A_{ref,x}} \approx 2\frac{kN}{m^2} \tag{A.9}$$

Equation 9: Distributed wind load.

A.2 Traffic load

$$q_{traffic} = \frac{3\frac{kN}{m^2} \cdot 12m \cdot L_{bridge} + 2 \cdot 480kN}{L_{bridge}} \tag{A.10}$$

Equation 10: V412, Table 3-1

A.3 Tsai-Wu failure criterion

$$F_i \cdot \sigma_i + F_{ij} \cdot \sigma_i \cdot \sigma_j = 1 \tag{A.11}$$

Equation 11: General expression

$$F_1 \cdot \sigma_1 + F_2 \cdot \sigma_2 + F_{22} \cdot \sigma_2^2 + F_{11} \cdot \sigma_1^2 + 2 \cdot F_{12} \cdot \sigma_1 \cdot \sigma_2 < 1 \tag{A.12}$$

Equation 12: Criterion for an orthotropic material with plane stress.

$$F_{12} = -\frac{1}{2} \cdot \sqrt{F_{11} \cdot F_{22}} \tag{A.13}$$

Equation 13: Interaction parameter.

$$F_1 = \frac{1}{f_{t,L}} - \frac{1}{f_{c,L}} \tag{A.14}$$

$$F_2 = \frac{1}{f_{t,R}} - \frac{1}{f_{c,R}} \tag{A.15}$$

$$F_{11} = \frac{1}{f_{t,L} \cdot f_{c,L}} \tag{A.16}$$

$$F_{22} = \frac{1}{f_{t,R} \cdot f_{c,R}} \tag{A.17}$$

A.4 Arch design checks

Ultimate limit state design checks derived from Eurocode 5 [28].

A.4.1 Shear and combined bending and axial compression checks

$$\frac{\tau_d}{f_{v,d}} = \frac{3}{2} \cdot \frac{V}{k_{cr} \cdot b \cdot h} \cdot \frac{1}{f_{v,d}} \leq 1 \tag{A.18}$$

Equation 18: Design check shear, EC5 Eq. (6.13).

$$\left[\frac{\sigma_{c,0,d}}{f_{c,0,d}}\right]^2 + \frac{\sigma_{m,y,d}}{f_{m,y,d}} + k_m \cdot \frac{\sigma_{m,z,d}}{f_{m,z,d}} \leq 1 \tag{A.19}$$

Equation 19: Design check combined bending and axial compression, EC5 Eq. (6.19).

$$\left[\frac{\sigma_{c,0,d}}{f_{c,0,d}}\right]^2 + k_m \cdot \frac{\sigma_{m,y,d}}{f_{m,y,d}} + \frac{\sigma_{m,z,d}}{f_{m,z,d}} \leq 1 \tag{A.20}$$

Equation 20: Design check combined bending and axial compression, EC5 Eq. (6.20).

A.4.2 Stability checks

$$\lambda_{rel,y} = \frac{\lambda_y}{\pi} \sqrt{\frac{f_{c,0,k}}{E_{0,05}}} \tag{A.21}$$

Equation 21: EC5 Eq. (6.21).

$$\lambda_{rel,z} = \frac{\lambda_z}{\pi} \sqrt{\frac{f_{c,0,k}}{E_{0,05}}} \tag{A.22}$$

Equation 22: EC5 Eq. (6.22).

$$\frac{\sigma_{c,0,d}}{k_{c,y} \cdot f_{c,0,d}} + \frac{\sigma_{m,y,d}}{f_{m,y,d}} + k_m \cdot \frac{\sigma_{m,z,d}}{f_{m,z,d}} \leq 1 \tag{A.23}$$

Equation 23: In-plane buckling: Design check members subjected to either compression or combined compression and bending, EC5 Eq. (6.23).

$$\frac{\sigma_{c,0,d}}{k_{c,z} \cdot f_{c,0,d}} + k_m \cdot \frac{\sigma_{m,y,d}}{f_{m,y,d}} + \frac{\sigma_{m,z,d}}{f_{m,z,d}} \leq 1 \tag{A.24}$$

Equation 24: Out-of-plane buckling: Design check members subjected to either compression or combined compression and bending, EC5 Eq. (6.24).

$$k_{c,y} = \frac{1}{k_y + \sqrt{{k_y}^2 - {\lambda_{rel,y}}^2}} \tag{A.25}$$

Equation 25: EC5 Eq. (6.25).

$$k_{c,z} = \frac{1}{k_z + \sqrt{{k_z}^2 - {\lambda_{rel,z}}^2}} \tag{A.26}$$

Equation 26: EC5 Eq. (6.26).

$$k_y = 0.5\big[1 + \beta_c\big[\lambda_{rel,y} - 0.3\big] + \lambda_{rel,y}^2\big] \tag{A.27}$$

Equation 27: EC5 Eq. (6.27).

$$k_z = 0.5\big[1 + \beta_c\big[\lambda_{rel,z} - 0.3\big] + \lambda_{rel,z}^2\big] \tag{A.28}$$

Equation 28: EC5 Eq. (6.28).

$$\beta_c = \begin{cases} 0.2 & \text{for solid timber} \\ 0.1 & \text{for glued laminated timber as LVL} \end{cases} \tag{A.29}$$

Equation 29: EC5 Eq. (6.29).

$$\lambda_{rel,m} = \sqrt{\frac{f_{m,k}}{\sigma_{m,crit}}} \tag{A.30}$$

Equation 30: EC5 Eq. (6.30).

$$\sigma_{m,crit} = \frac{M_{y,crit}}{W_y} \tag{A.31}$$

Equation 31: EC5 Eq. (6.31).

$$M_{y,crit} = \frac{\pi}{s_0}\sqrt{E_{0,05} \cdot I_z \cdot G_{0,05} \cdot I_{tor}} - \frac{E_{0.05} \cdot I_z + G_{0.05} \cdot I_{tor}}{2 \cdot r} \tag{A.32}$$

Equation 32: Critical moment, [23].

$$\frac{\sigma_m}{k_{cr} \cdot f_{md}} \leq 1 \tag{A.33}$$

Equation 33: Design check moment about strong axis, EC5 Eq. (6.33).

$$k_{crit} = \begin{cases} 1 & \text{for } \lambda_{rel,m} \leq 0.75 \\ 1.56 - 0.75 \cdot \lambda_{rel,m} & \text{for } 0.75 < \lambda_{rel,m} \leq 1.4 \\ \frac{1}{\lambda^2_{rel,m}} & \text{for } 1.4 < \lambda_{rel,m} \end{cases} \tag{A.34}$$

Equation 34: EC5 Eq. (6.34).

$$\left[\frac{\sigma_{m,d}}{k_{crit} \cdot f_{m,d}}\right]^2 + \frac{\sigma_{c,d}}{k_{c,z} \cdot f_{c,0,d}} \leq 1 \tag{A.35}$$

Equation 35: Lateral torsional buckling: Design check for members subjected to bending or combined bending and compression, EC5, Eq. (6.35).

B Results

The results are presented as figures with corresponding tables. For the figures, each dot represents an analysis of a unique configuration, meaning values for the varying parameters. This configuration results in values for the objectives optimized in the simulation. The aim is to find a configuration close to the bottom left of each figure. The non-dominated solutions from the simulation form the Pareto front, which is drawn as the red line. This is further elaborated in 2.5. The tables include a selection of the investigated configurations for each simulation. This includes the objective values, displayed as dots in the figures, and the corresponding values for the parameters.

B.1 80 m span with two splices

Simulation 1

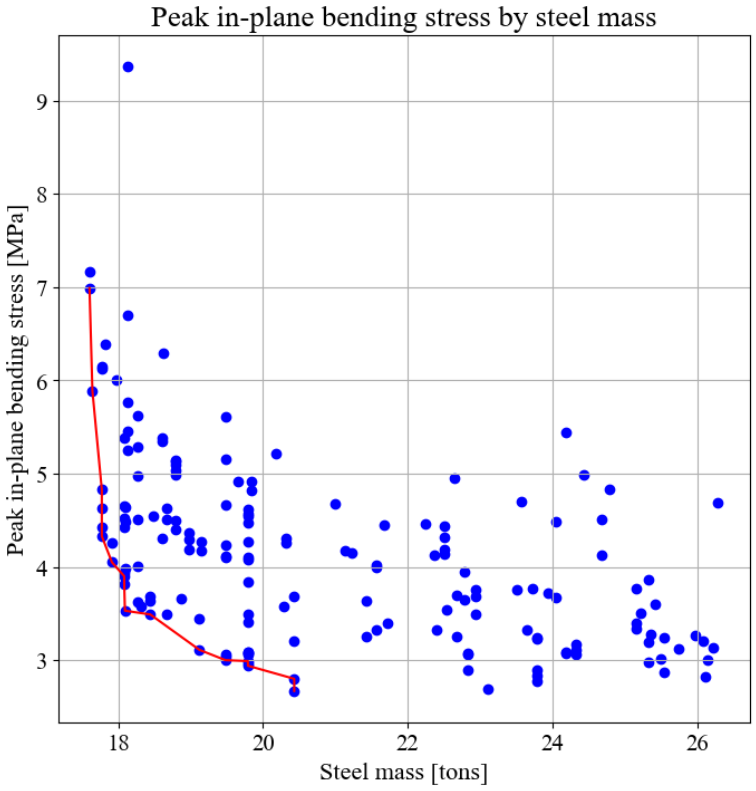

Figure B.1: 80 m span with two splices: Simulation 1, Full load

Table B.1: 80 m span with two splices: Simulation 1, Full load

Objective values		Parameter values	
Peak in-plane bending stress [MPa]	Steel mass [tons]	Number of crossbeams	Hanger angle [degrees]
2.7 - 3.2	20	16	35 - 40
2.9 - 3.1 - 3.5	20	15	36 - 40 - 45
3.5	18	13	41 - 43 - 44
3.5 - 4.3	18	12	35 - 52

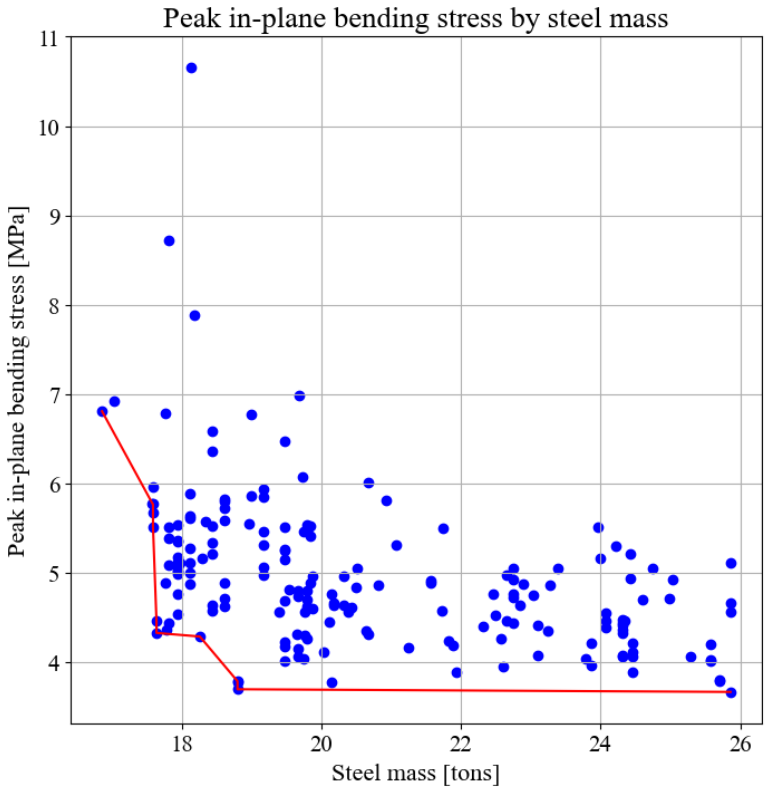

Figure B.2: 80 m span with two splices: Simulation 1, Skew load

Table B.2: 80 m span with two splices: Simulation 1, Skew load

Objective values		Parameter values	
Peak in-plane bending stress [MPa]	Steel mass [tons]	Number of crossbeams	Hanger angle [degrees]
3.7 - 4.3 - 4.6	19 - 18 - 18	13	49 - 45 - 41
3.8	20	15	45
4.2	19	14	46 - 52
4.5 - 4.9	18	12	51 - 40

Simulation 2

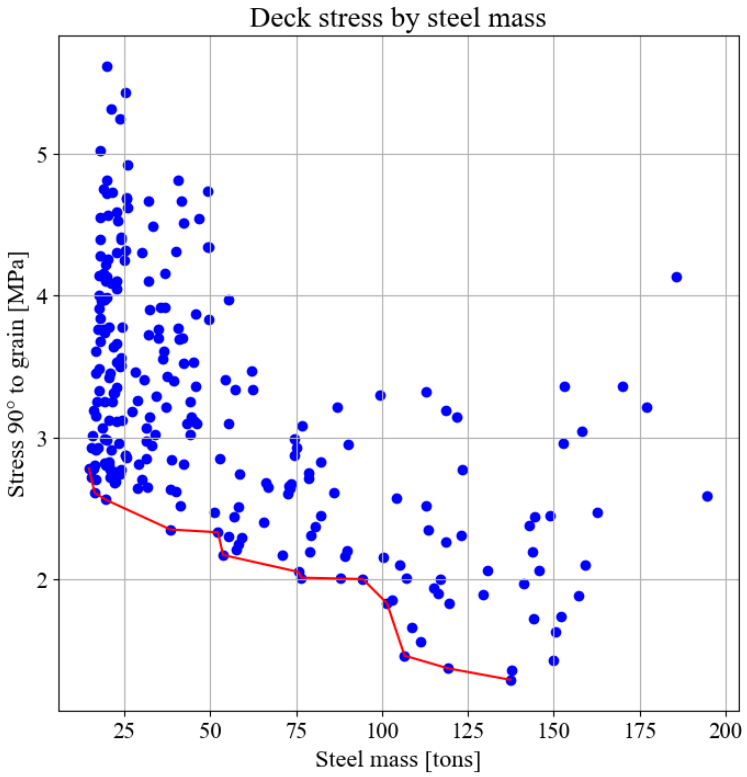

Figure B.3: 80 m span with two splices: Simulation 2, Full load

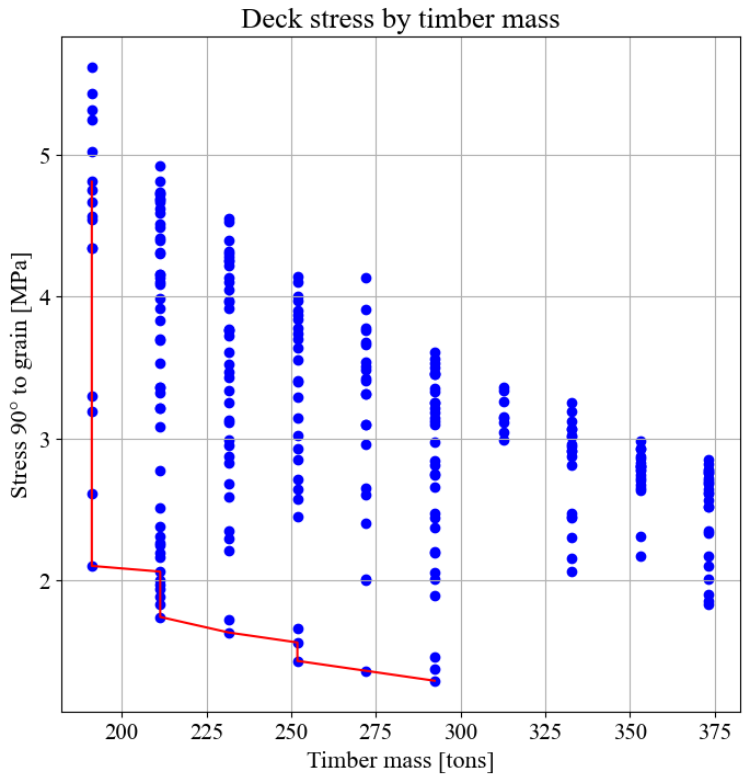

Figure B.4: 80 m span with two splices: Simulation 2, Full load

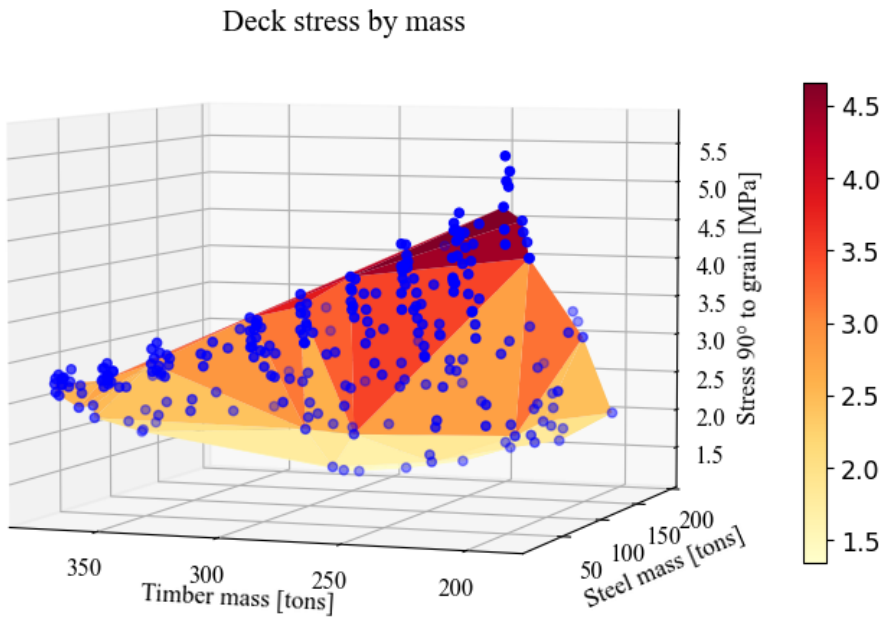

Figure B.5: 80 m span with two splices: Simulation 2, Full load

Table B.3: 80 m span with two splices: Simulation 2, Full load

Objective values			Parameter values	
Stress 90° to grain [MPa]	Steel mass [tons]	Timber mass [tons]	Number of crossbeams	Deck thickness [mm]
3.8	19	232	11	400
3.89	20	211	13	350
4.28	18	232	13	400
4.57	20	191	13	300

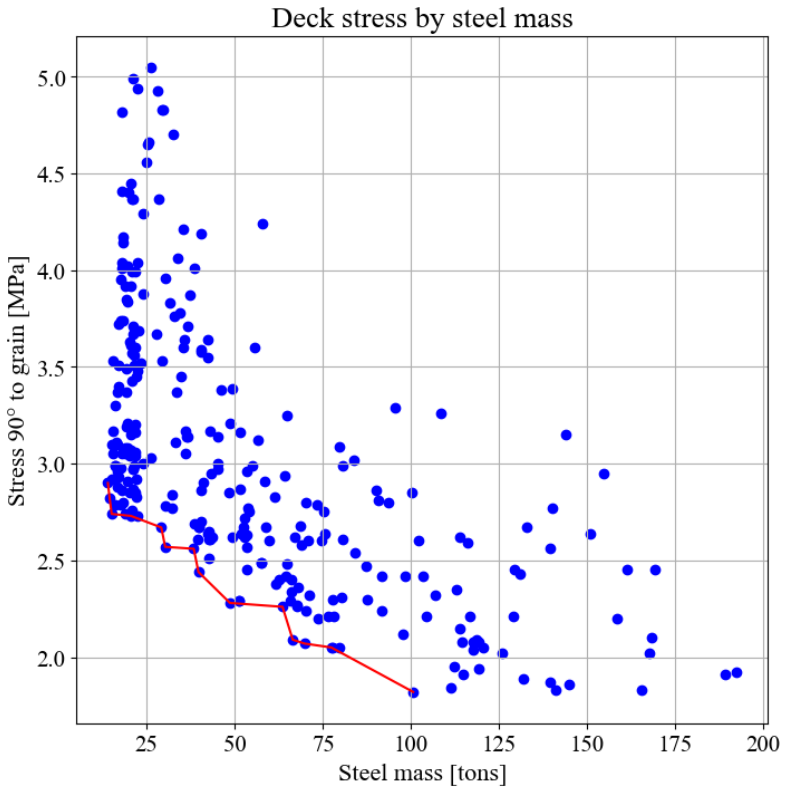

Figure B.6: 80 m span with two splices: Simulation 2, Skew load

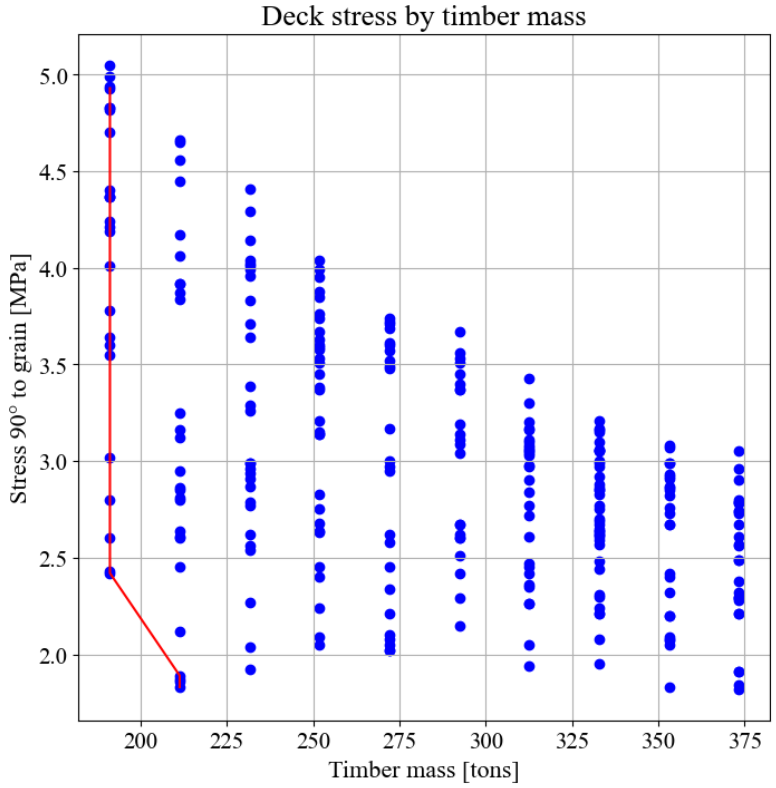

Figure B.7: 80 m span with two splices: Simulation 2, Skew load

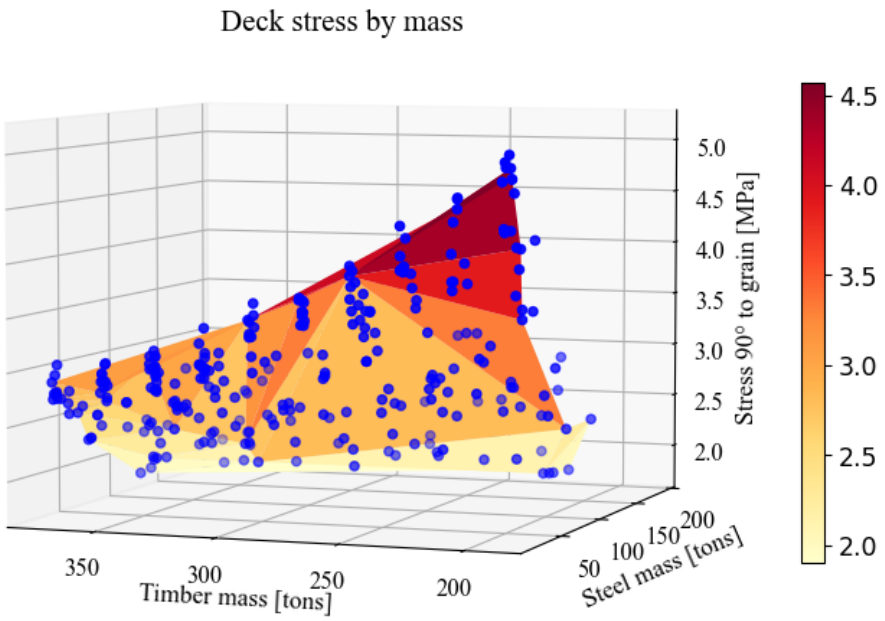

Figure B.8: 80 m span with two splices: Simulation 2, Skew load

Table B.4: 80 m span with two splices: Simulation 2, Skew load

Objective values			Parameter values	
Stress 90° to grain [MPa]	Steel mass [tons]	Timber mass [tons]	Number of crossbeams	Deck thickness [mm]
3.6	20	252	16	450
3.84 - 4.14	20 - 18	211 - 232	13	350 - 400
3.9 - 4.4	20 - 18	191 - 232	12	350 - 300
4.33	20	191	13	300

Simulation 3

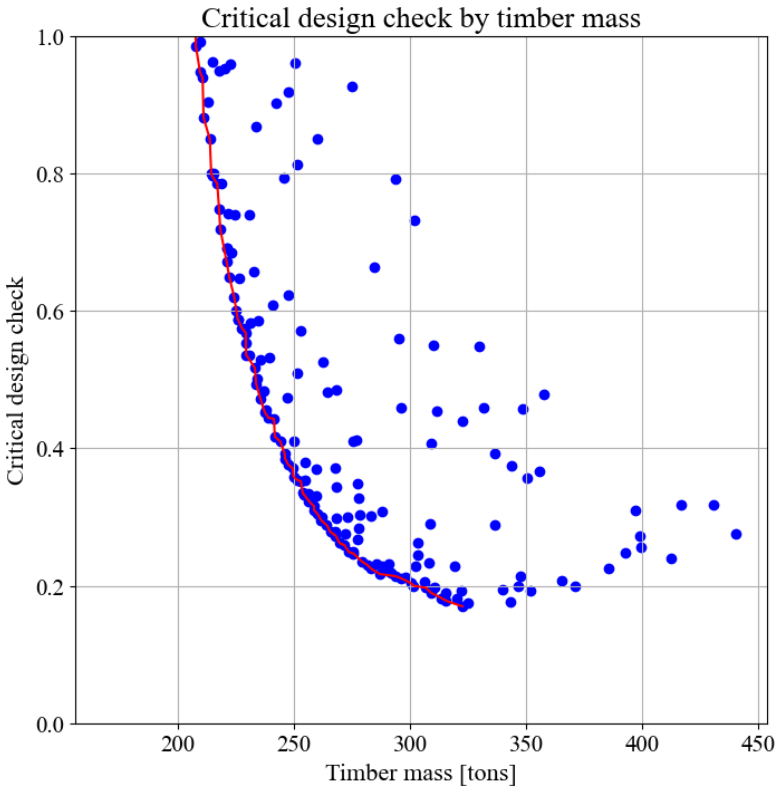

Figure B.9: 80 m span with two splices: Simulation 3, Full load

Table B.5: 80 m span with two splices: Simulation 3, Full load

Objective values		Parameter values	
Critical design check [0, 1]	Timber mass [tons]	Arch height [mm]	Arch width [mm]
0.85	214	850	950
0.881	211	650	1050
0.939	211	800	900
0.947	210	550	1150

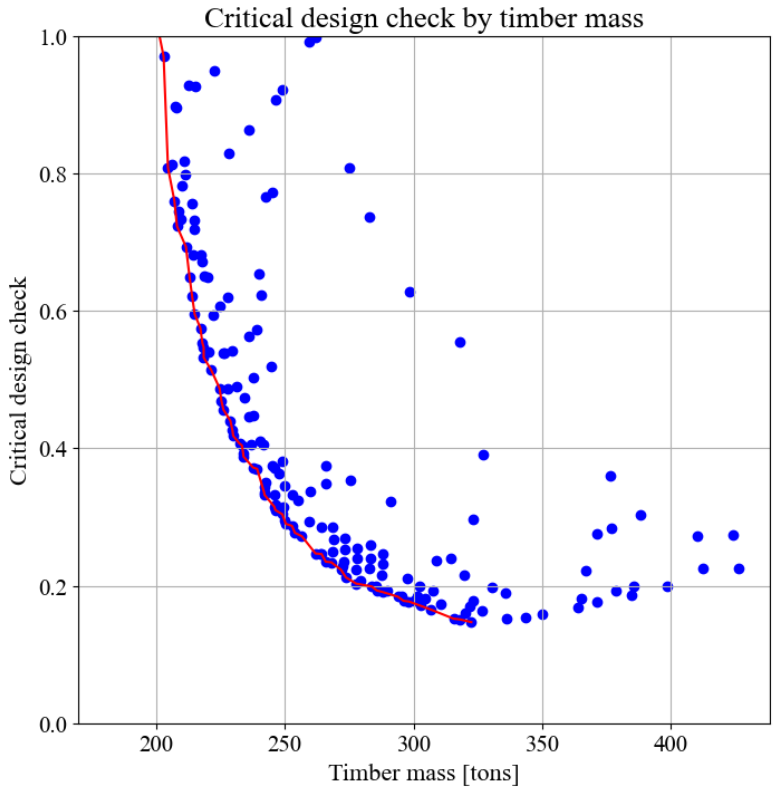

Figure B.10: 80 m span with two splices: Simulation 3, Skew load

Table B.6: 80 m span with two splices: Simulation 3, Skew load

Objective values		Parameter values	
Critical design check [0, 1]	Timber mass [tons]	Arch height [mm]	Arch width [mm]
0.723	208	700	950
0.802	211	650	1050
0.808	204	700	900
0.97	203	950	700

Simulation 4

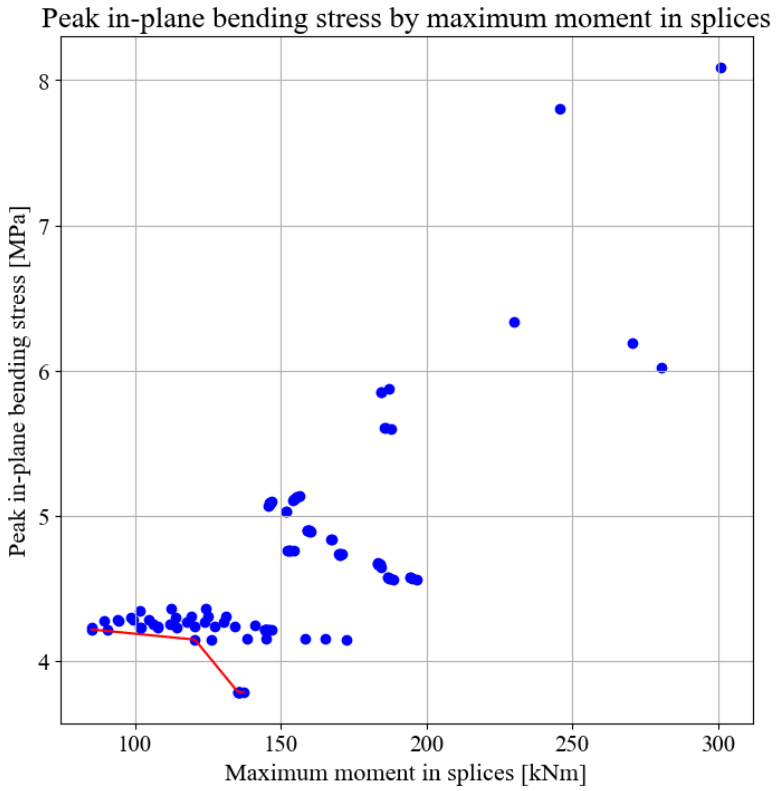

Figure B.11: 80 m span with two splices: Simulation 4, Full load

Table B.7: 80 m span with two splices: Simulation 4, Full load

Objective values		Parameter values	
Maximum moment in splices [kNm]	Peak in-plane bending stress [MPa]	Connection placement [0, 1]	Hanger angle [degrees]
85 - 91	4.22	0 - 0.1	43
102 - 114	4.24	0.3 - 0.5	43
121 - 126	4.15	0 - 0.1	44
137	3.79	0.1 - 0.9	35

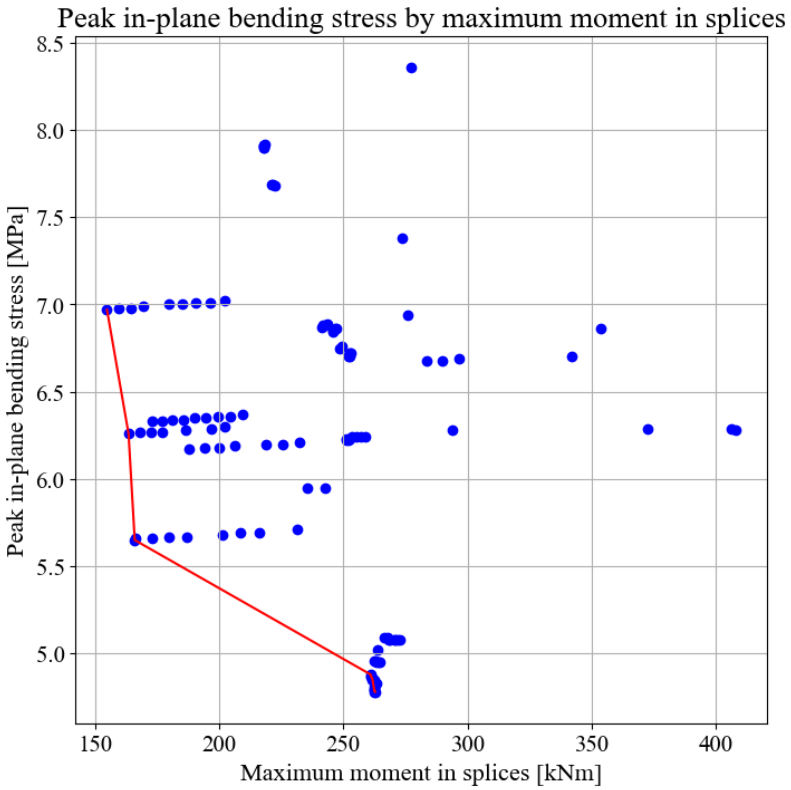

Figure B.12: 80 m span with two splices: Simulation 4, Skew load

Table B.8: 80 m span with two splices: Simulation 4, Skew load

Objective values			Parameter values	
Maximum moment in splices [kNm]	Peak in-plane bending stress [MPa]	Hangers in compression	Connection placement [0, 1]	Hanger angle [degrees]
155	6.97	9	0	43
166	5.66	7	0	45
231	5.71	7	1	45
262	4.85	4	0 - 0.8	48

Simulation 5

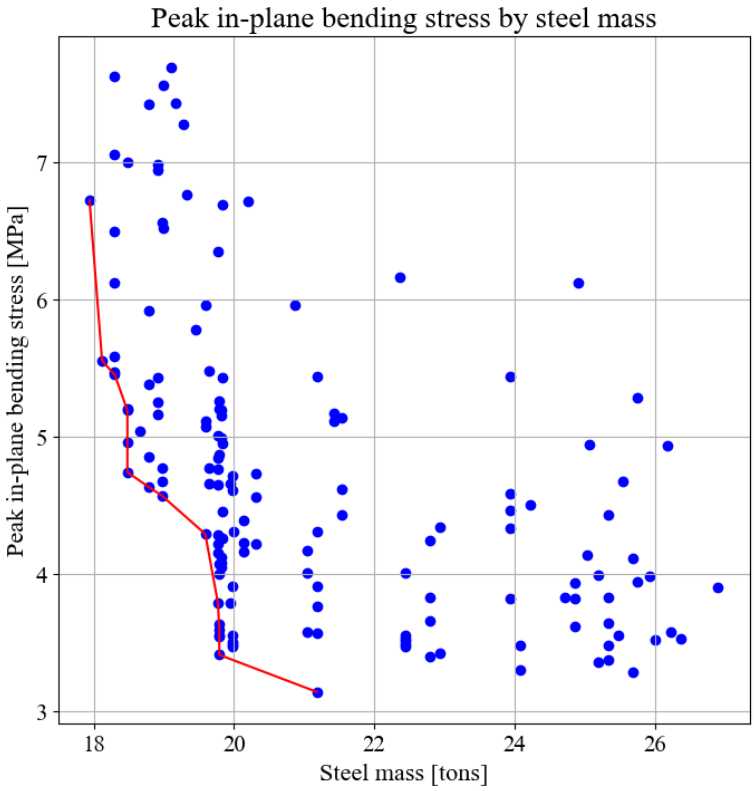

Figure B.13: 80 m span with two splices: Simulation 5, Full load

Table B.9: 80 m span with two splices: Simulation 5, Full load

Objective values		Parameter values	
Peak in-plane bending stress [MPa]	Steel mass [tons]	Number of crossbeams	Hanger angle [degrees]
3.47	20	14	38
3.39 - 3.63	20	14	37 - 43
4.15 - 4.3	19.6	13	44 - 41
4.6	18	10	43

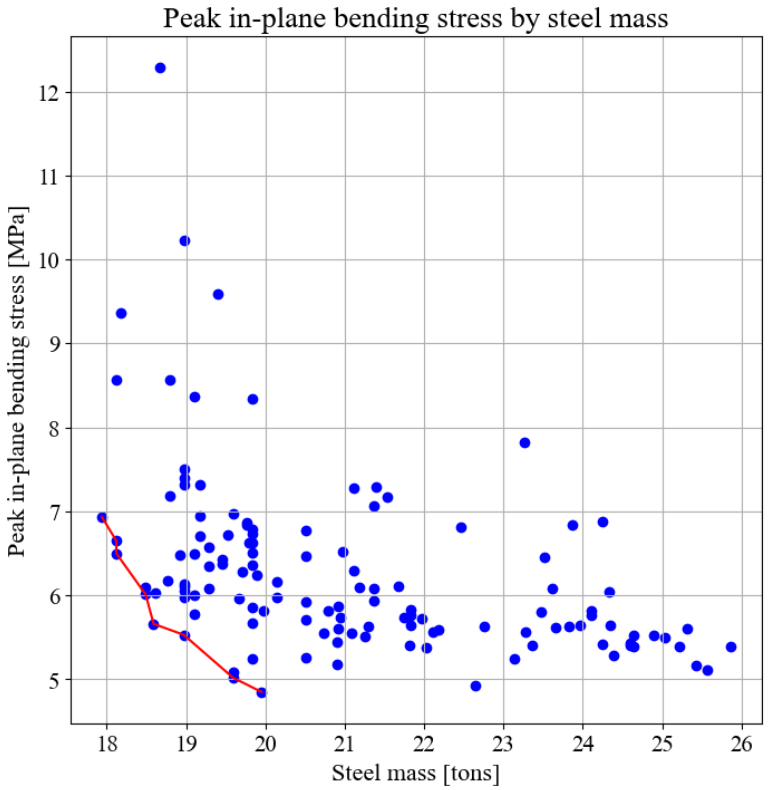

Figure B.14: 80 m span with two splices: Simulation 5, Skew load

Table B.10: 80 m span with two splices: Simulation 5, Skew load

Objective values		Parameter values	
Peak in-plane bending stress [MPa]	Steel mass [tons]	Number of crossbeams	Hanger angle [degrees]
4.85 - 5.02	20 - 19.6	13	48 - 47
5.66	18.6	13	45
6	18.5	12	53 - 54
6.5 - 6.93	18	10	45 - 51

Final results

Table B.11: 80 m span with two splices: Results with the final configuration from Table 4.7.

	Full load	Skew load	Governing load
Peak in-plane bending stress [MPa]	4.70	5.21	5.21
Critical design check Eq. (6.24)	0.958	0.857	0.958
Buckling load factor	2.41	2.98	2.41
Natural frequency [Hz]	1.05	1.02	1.02
Max stress 90°to grain [MPa]	3.71	3.47	3.71
% of deck exceeding Tsai-Wu criterion	11.6	5.3	11.6
Max moment in splices [kNm]	147	135	147
Number of relaxed hangers	0	7	7
Maximum displacement [mm]	209	217	217
Crossbeam utilization [%]	79.5	82.4	82.4
Hanger utilization [%]	48.2	55.5	55.5

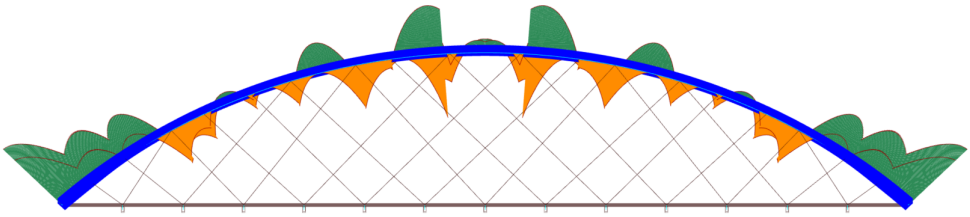

Figure B.15: 80 m span with two splices: Full load. Moment distribution in-plane with final configuration.

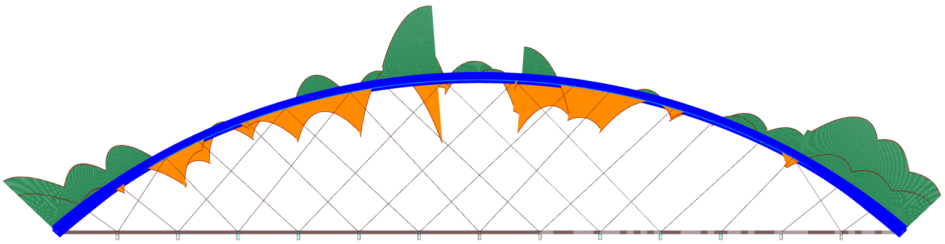

Figure B.16: 80 m span with two splices: Skew load. Moment distribution in-plane with final configuration.

B.2 80 m span with three splices

Simulation 1

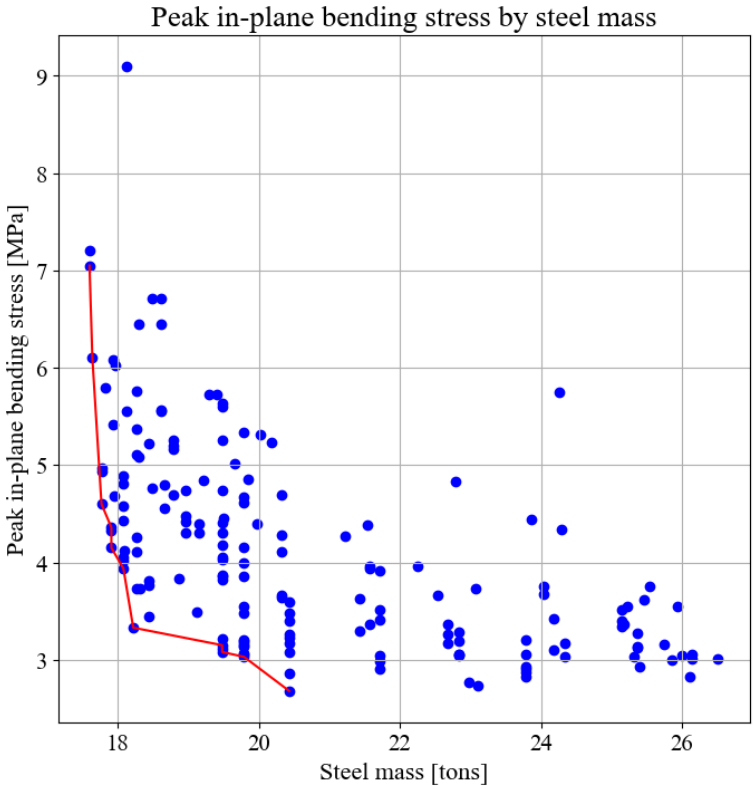

Figure B.17: 80 m span with three splices: Simulation 1, Full load

Table B.12: 80 m span with three splices: Simulation 1, Full load

Objective values		Parameter values	
Peak in-plane bending stress [MPa]	Steel mass [tons]	Number of crossbeams	Hanger angle [degrees]
2.68 - 3.59	20.4	16	35 - 44
3.03 - 3.2	19.8	15	38 - 43
3.33 - 3.44 - 4.02	18.4 - 18.1 - 18.4	13	35 - 43 - 38
6.11	17.6	11	58

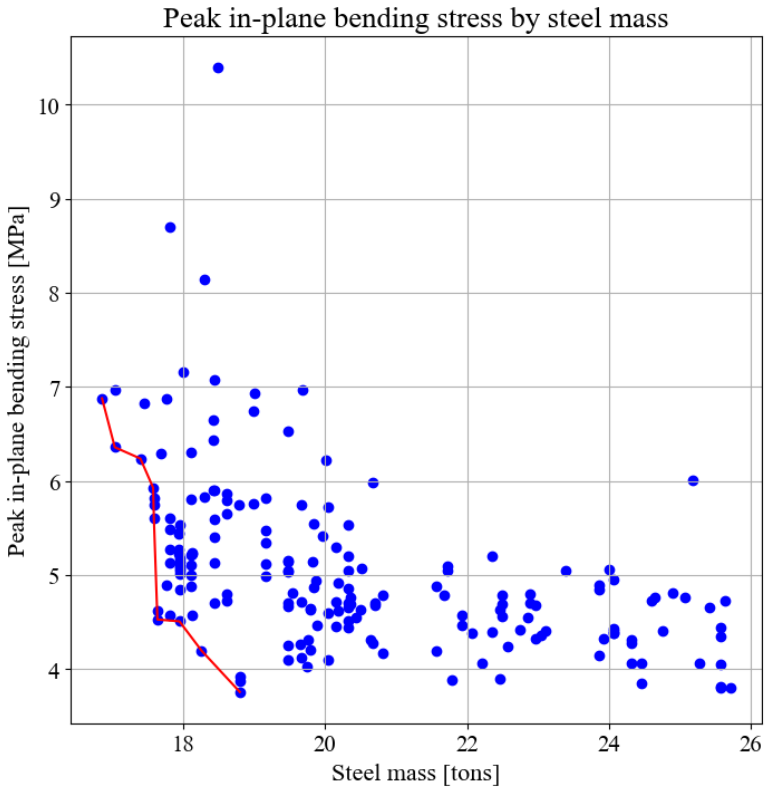

Figure B.18: 80 m span with three splices: Simulation 1, Skew load

Table B.13: 80 m span with three splices: Simulation 1, Skew load

Objective values		Parameter values	
Peak in-plane bending stress [MPa]	Steel mass [tons]	Number of crossbeams	Hanger angle [degrees]
3.76	18.8	13	46
4.2	18.3	13	45
3.51	18	12	52
4.53	17.6	11	50

Simulation 2

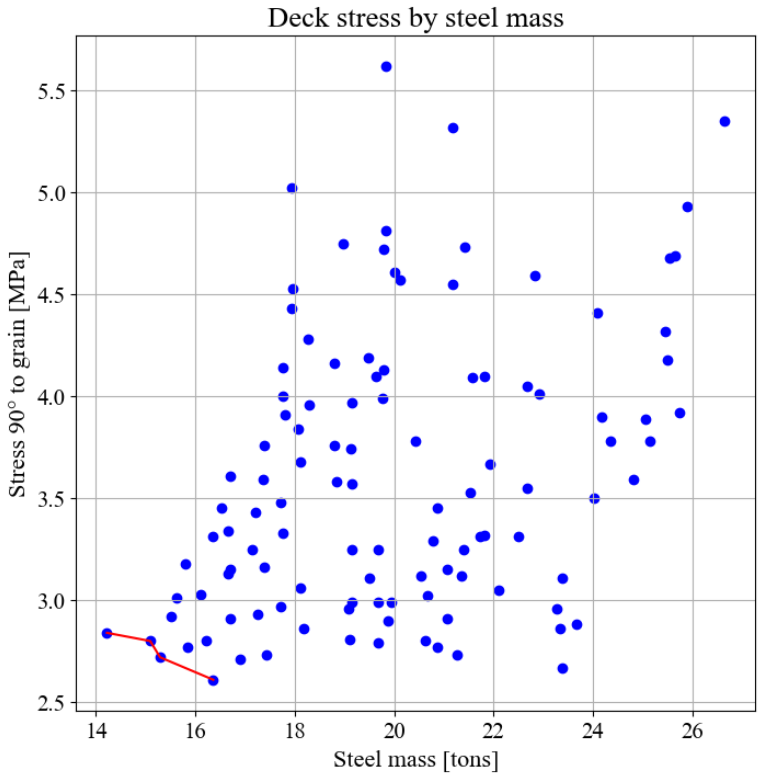

Figure B.19: 80 m span with three splices: Simulation 2, Full load

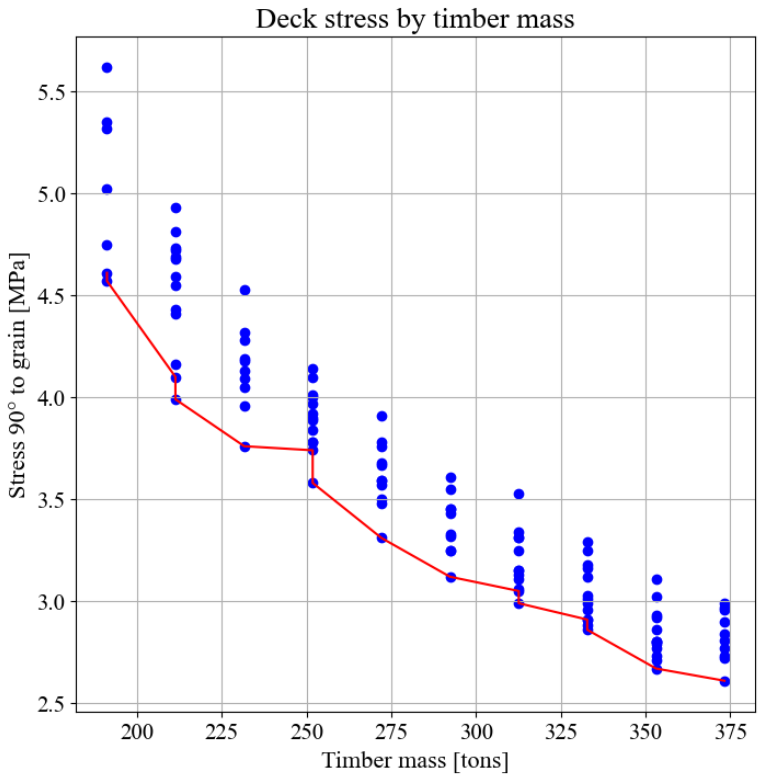

Figure B.20: 80 m span with three splices: Simulation 2, Full load

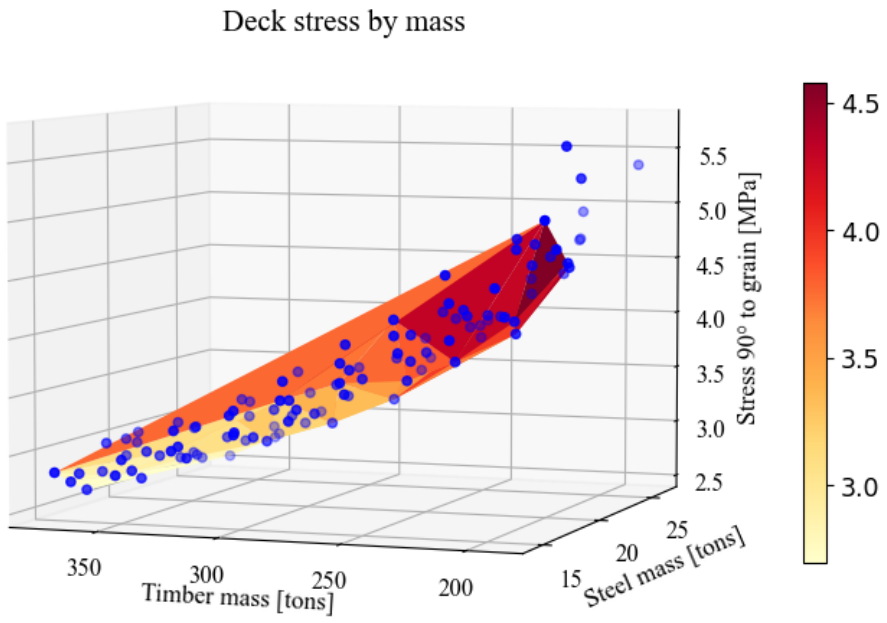

Figure B.21: 80 m span with three splices: Simulation 2, Full load

Table B.14: 80 m span with three splices: Simulation 2, Full load

Objective values			Parameter values	
Stress 90° to grain [MPa]	Steel mass [tons]	Timber mass [tons]	Number of crossbeams	Deck thickness [mm]
3.76 - 4.16	18.8	232	11	400 - 350
3.99	19.8	211	13	350
4.1	19.6	211	12	350
4.43	18	211	10	350

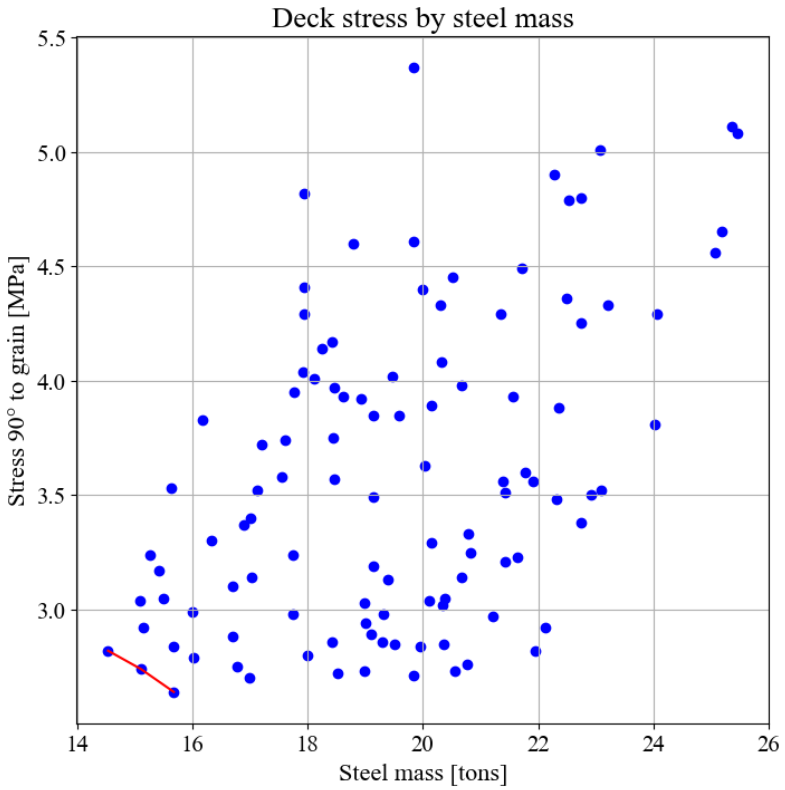

Figure B.22: 80 m span with three splices: Simulation 2, Skew load

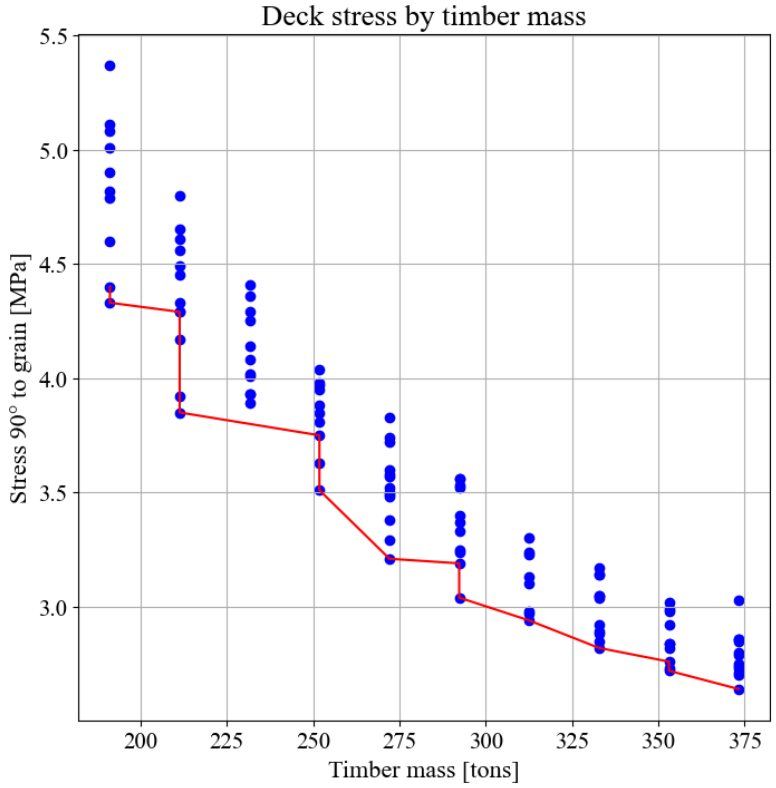

Figure B.23: 80 m span with three splices: Simulation 2, Skew load

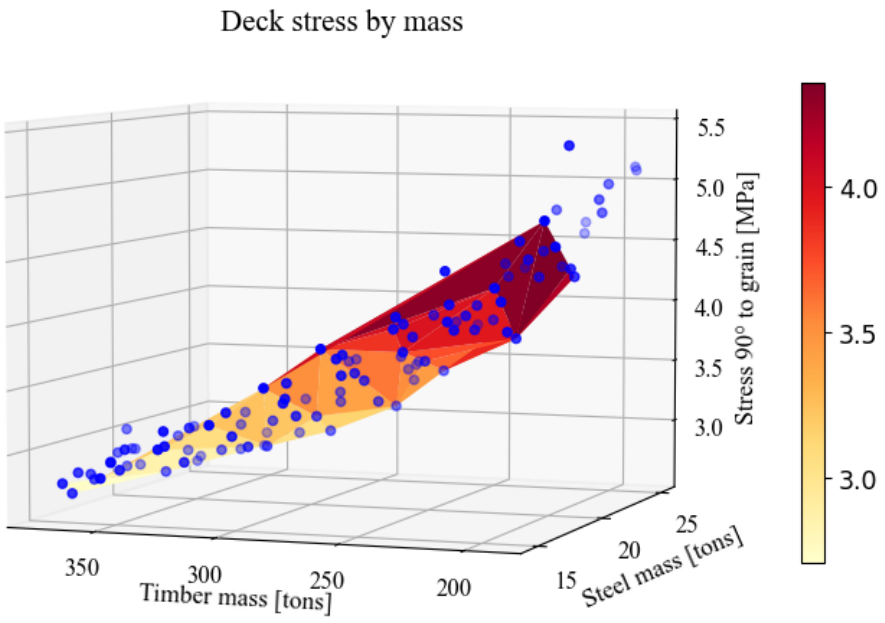

Figure B.24: 80 m span with three splices: Simulation 2, Skew load

Table B.15: 80 m span with three splices: Simulation 2, Skew load

Objective values			Parameter values	
Stress 90° to grain [MPa]	Steel mass [tons]	Timber mass [tons]	Number of crossbeams	Deck thickness [mm]
3.6	20	252	16	450
3.84 - 4.14	20 - 18	211 - 232	13	350 - 400
3.9 - 4.4	20 - 18	191 - 232	12	350 - 300
4.33	20	191	13	300

Simulation 3

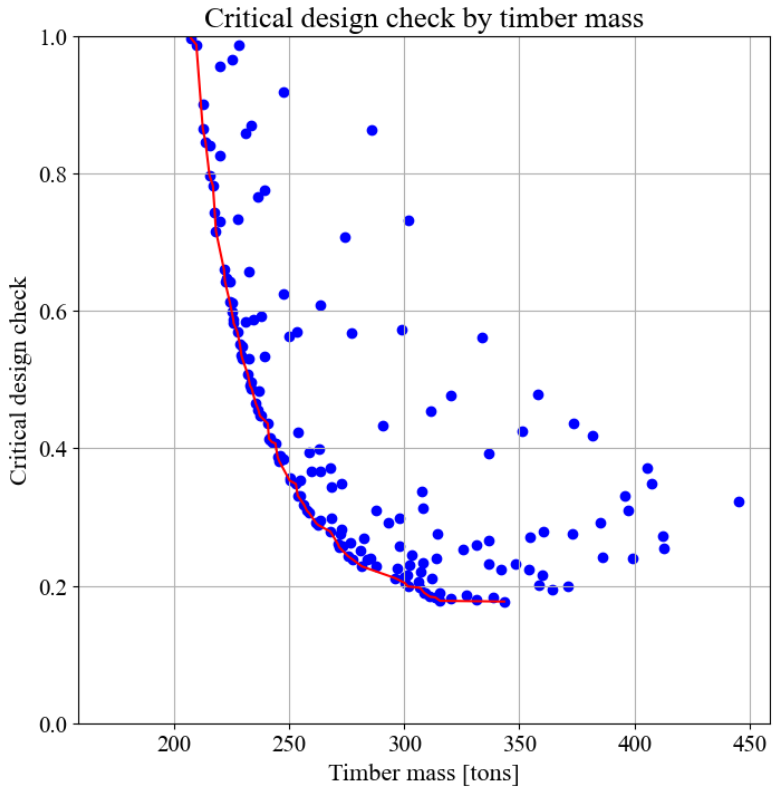

Figure B.25: 80 m span with three splices: Simulation 3, Full load

Table B.16: 80 m span with three splices: Simulation 3, Full load

Objective values		Parameter values	
Critical design check [0, 1]	Timber mass [tons]	Arch height [mm]	Arch width [mm]
0.865	217	550	1200
0.878	211	650	1050
0.901	213	900	850
0.987	210	850	850

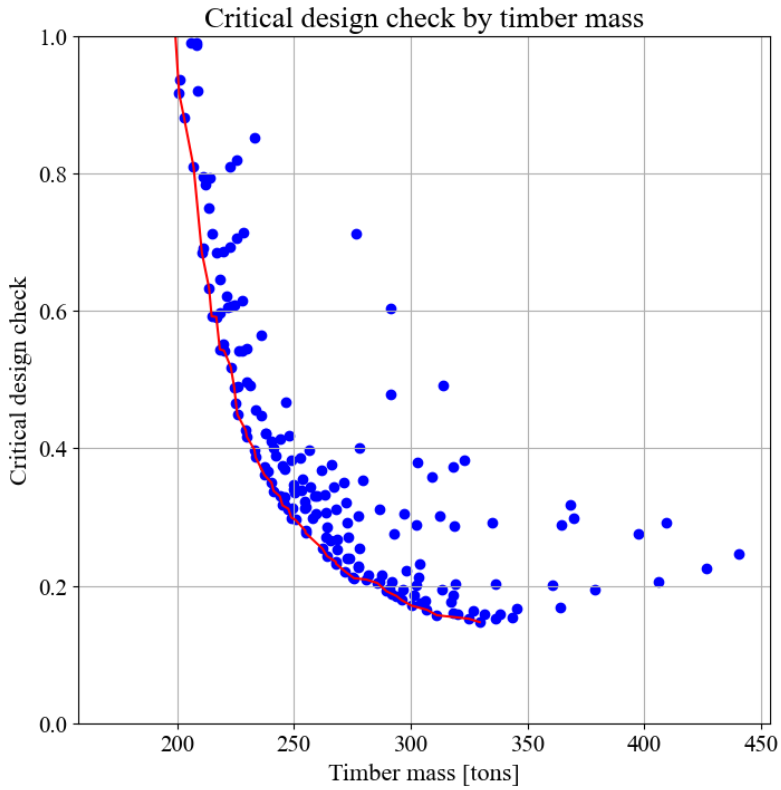

Figure B.26: 80 m span with three splices: Simulation 3, Skew load

Table B.17: 80 m span with three splices: Simulation 3, Skew load

Objective values		Parameter values	
Critical design check [0, 1]	Timber mass [tons]	Arch height [mm]	Arch width [mm]
0.685	211	600	1100
0.809	207	950	750
0.881	203	800	800
0.916	201	700	850

Simulation 4

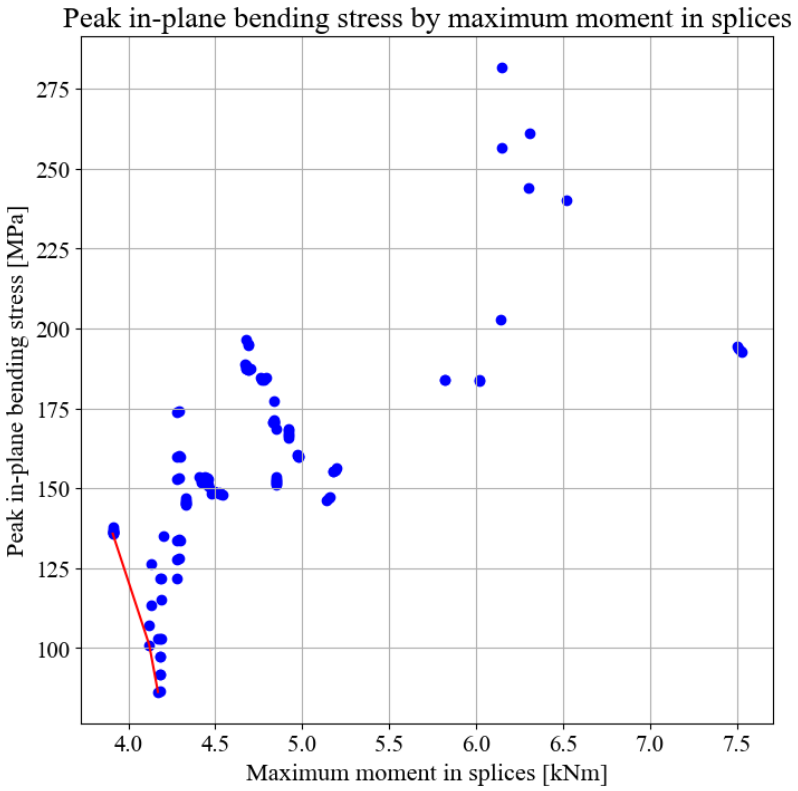

Figure B.27: 80 m span with three splices: Simulation 4, Full load

Table B.18: 80 m span with three splices: Simulation 4, Full load

Objective values		Parameter values	
Maximum moment in splices [kNm]	Peak in-plane bending stress [MPa]	Connection placement [0, 1]	Hanger angle [degrees]
86	4.17	0	43
92	4.18	0.1	43
122	4.28	0	44
151	4.85	0	45

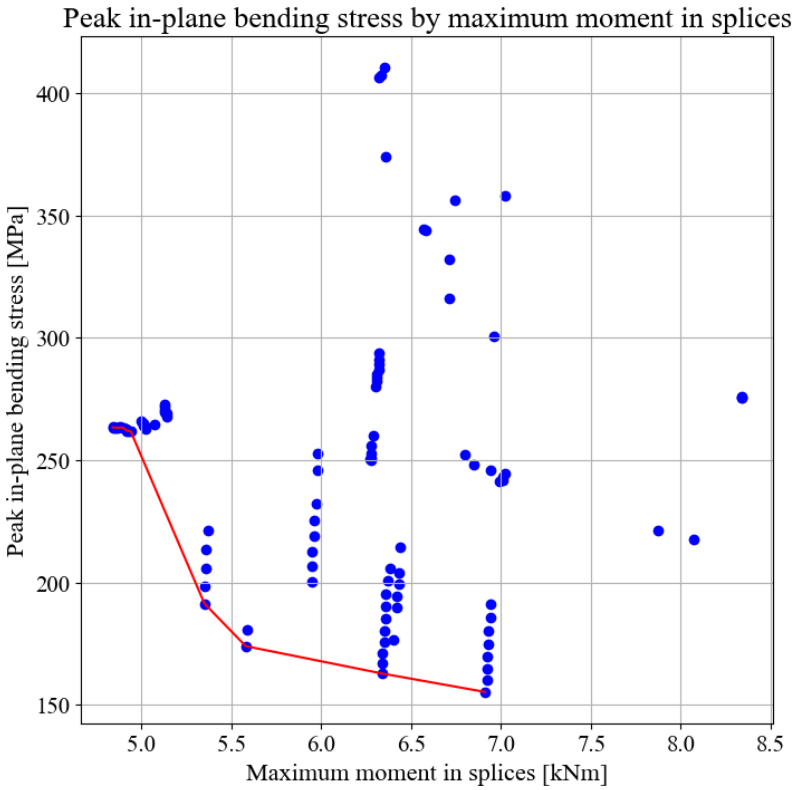

Figure B.28: 80 m span with three splices: Simulation 4, Skew load

Table B.19: 80 m span with three splices: Simulation 4, Skew load

Objective values			Parameter values	
Maximum moment in splices [kNm]	Peak in-plane bending stress [MPa]	Hangers in compression	Connection placement [0, 1]	Hanger angle [degrees]
155	6.91	9	0	43
163	6.34	9	0	42
167	5.58	7	0	45
200	5.95	8	0	44

Simulation 5

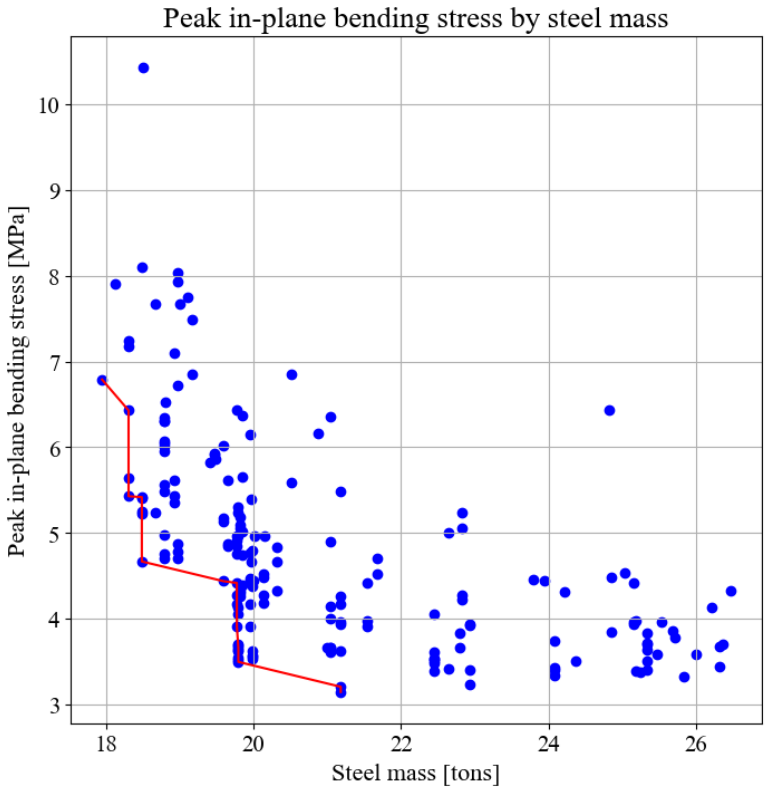

Figure B.29: 80 m span with three splices: Simulation 5, Full load

Table B.20: 80 m span with three splices: Simulation 5, Full load

Objective values		Parameter values	
Peak in-plane bending stress [MPa]	Steel mass [tons]	Number of crossbeams	Hanger angle [degrees]
3.15	21	16	35
3.5 - 3.71	20	15	38 - 43
4.44	20	13	41
4.67	18	10	43

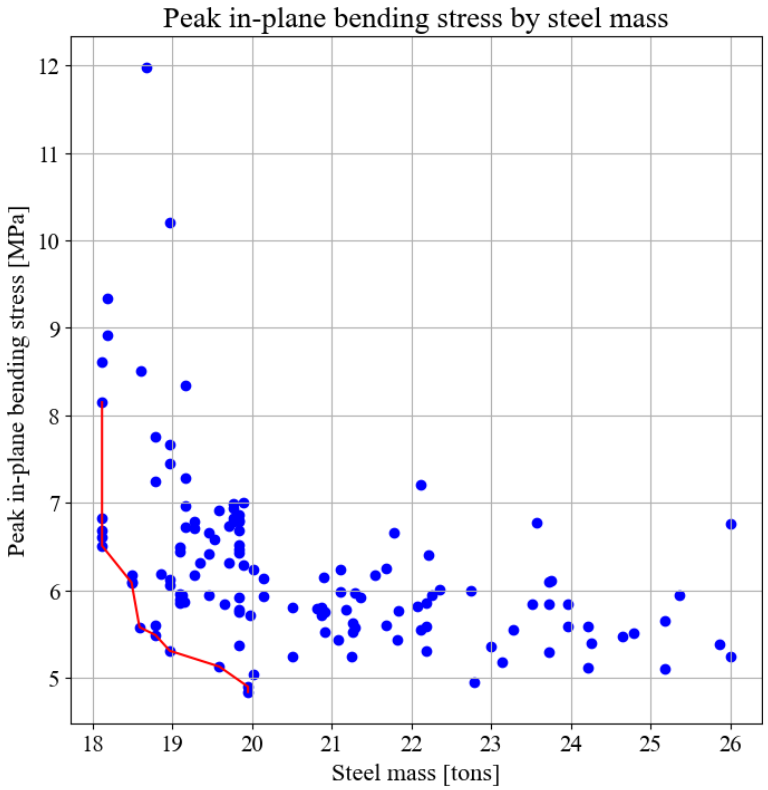

Figure B.30: 80 m span with three splices: Simulation 5, Skew load

Table B.21: 80 m span with three splices: Simulation 5, Skew load

Objective values		Parameter values	
Peak in-plane bending stress [MPa]	Steel mass [tons]	Number of crossbeams	Hanger angle [degrees]
4.84	20	13	49
5.13	19.6	13	46
5.49	18.8	11	50
5.58	20	13	45

Final results

Table B.22: 80 m span with three splices: Results with the final configuration from Table 4.7.

	Full load	Skew load	Governing load
Peak in-plane bending stress [MPa]	4.80	5.12	5.12
Critical design check Eq. (6.24)	0.956	0.706	0.956
Buckling load factor	2.41	2.91	2.41
Natural frequency [Hz]	1.05	1.02	1.02
Max stress 90°to grain [MPa]	3.71	3.46	3.71
% of deck exceeding Tsai-Wu criterion	11.6	5.3	11.6
Max moment in splices [kNm]	146	137	146
Number of relaxed hangers	0	7	7
Maximum displacement [mm]	210	217	217
Crossbeam utilization [%]	79.5	82.5	82.5
Hanger utilization [%]	48.2	55.7	55.7

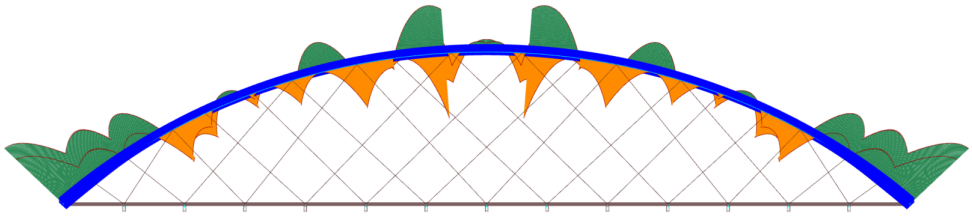

Figure B.31: 80 m span with three splices: Full load. Moment distribution in-plane with final configuration.

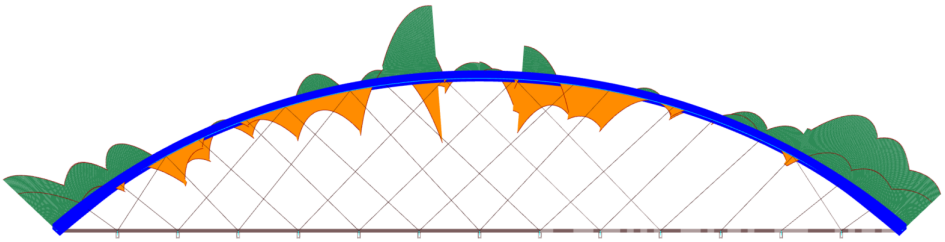

Figure B.32: 80 m span with three splices: Skew load. Moment distribution in-plane with final configuration.

B.3 100 m span with three splices

Simulation 1

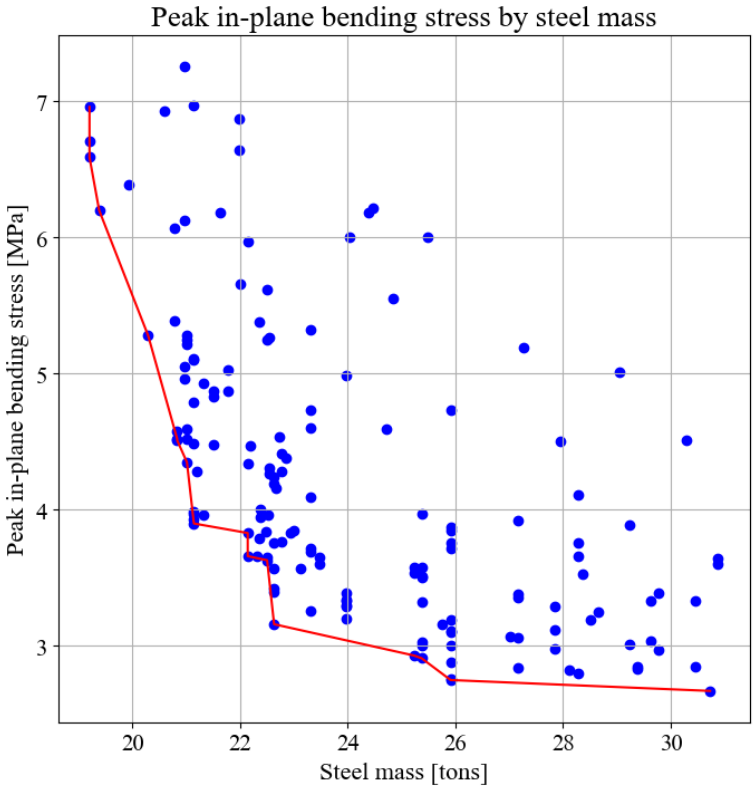

Figure B.33: 100 m span with three splices: Simulation 1, Full load

Table B.23: 100 m span with three splices: Simulation 1, Full load

Objective values		Parameter values	
Peak in-plane bending stress [MPa]	Steel mass [tons]	Number of crossbeams	Hanger angle [degrees]
2.75	26	20	36
3.66	22.1	15	35
3.83	22	15	40
3.9 - 3.97	21	11	38 - 36

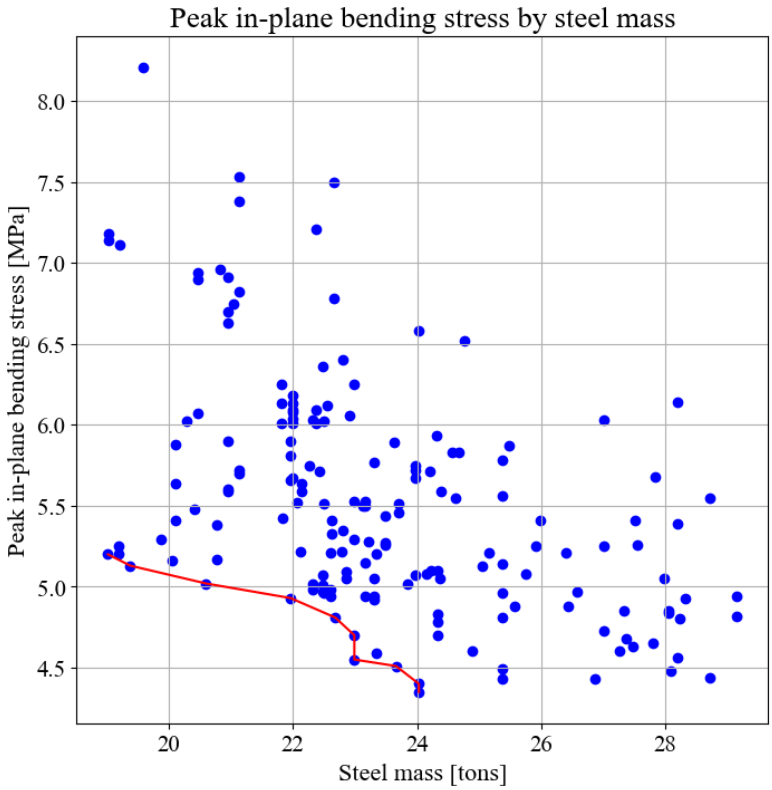

Figure B.34: 100 m span with three splices: Simulation 1, Skew load

Table B.24: 100 m span with three splices: Simulation 1, Skew load

Objective values		Parameter values	
Peak in-plane bending stress [MPa]	Steel mass [tons]	Number of crossbeams	Hanger angle [degrees]
4.55	23	16	48
4.81 - 4.96	23	15	55 - 53
4.93	22	15	40
5.02	21	11	50

Simulation 2

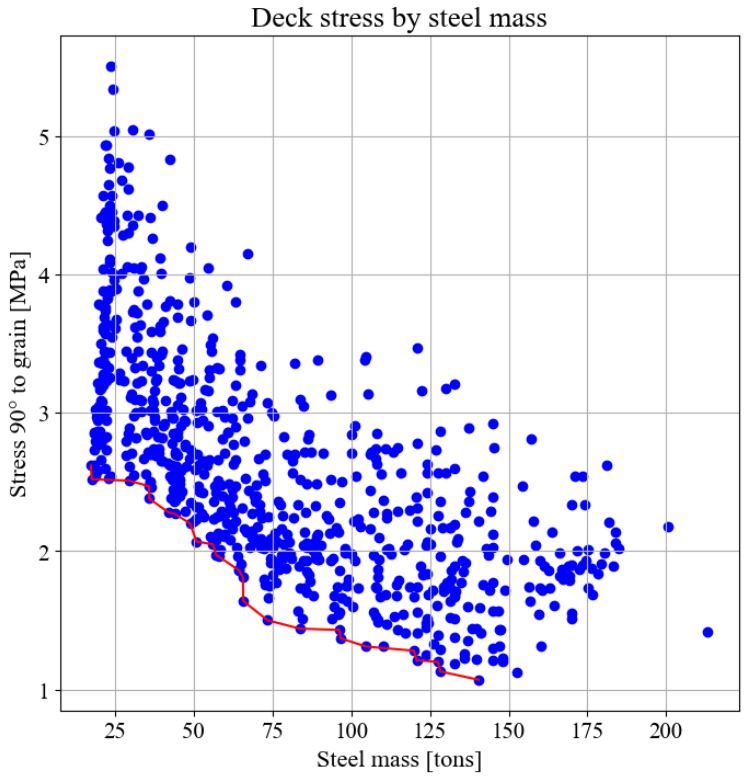

Figure B.35: 100 m span with three splices: Simulation 2, Full load

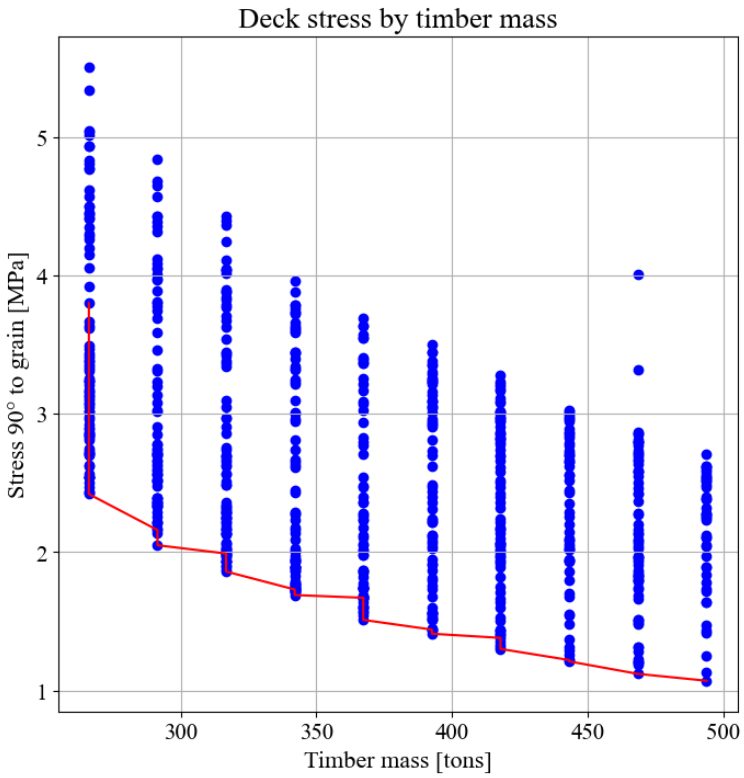

Figure B.36: 100 m span with three splices: Simulation 2, Full load

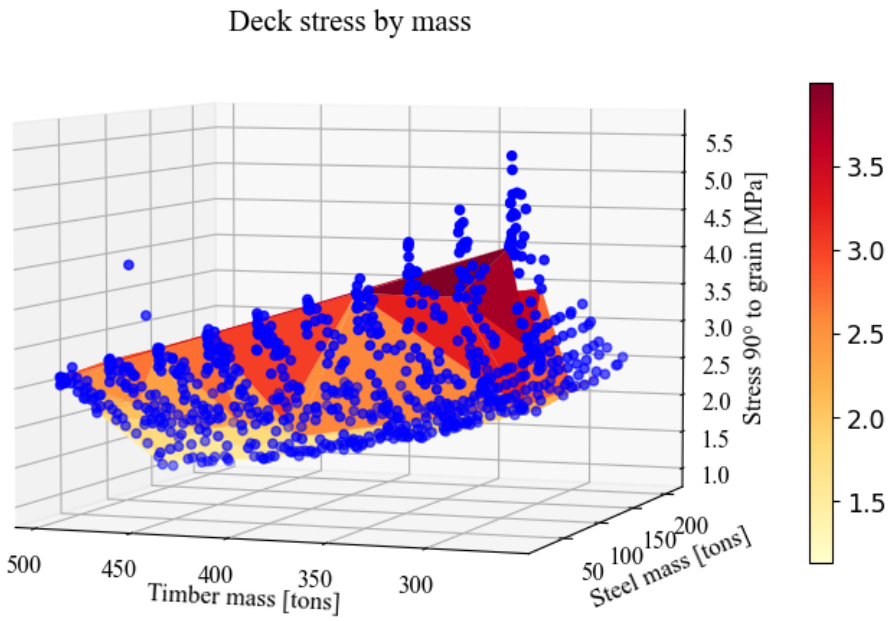

Figure B.37: 100 m span with three splices: Simulation 2, Full load

Table B.25: 100 m span with three splices: Simulation 2, Full load

Objective values			Parameter values	
Stress 90° to grain [MPa]	Steel mass [tons]	Timber mass [tons]	Number of crossbeams	Deck thickness [mm]
2.73	22.5	443	17	650
3.33	22.9	342	13	450
3.44	23.3	317	10	400
3.84	22.5	317	12	400

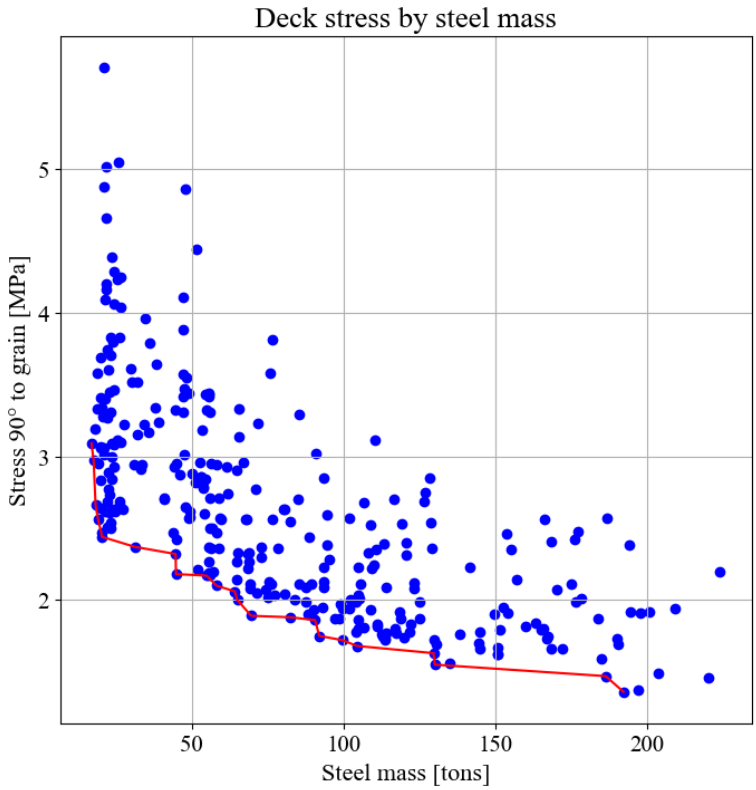

Figure B.38: 100 m span with three splices: Simulation 2, Skew load

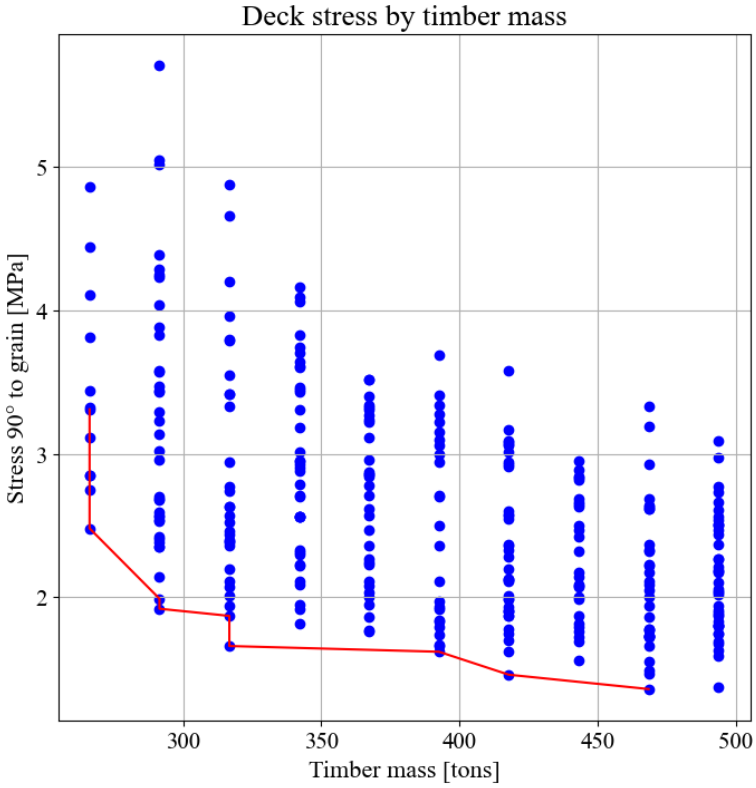

Figure B.39: 100 m span with three splices: Simulation 2, Skew load

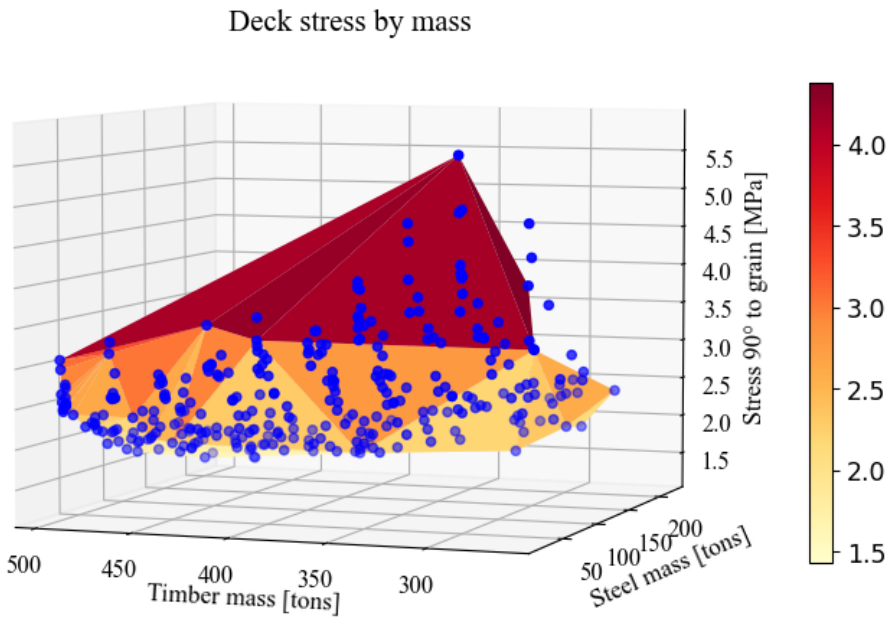

Figure B.40: 100 m span with three splices: Simulation 2, Skew load

Table B.26: 100 m span with three splices: Simulation 2, Skew load

Objective values			Parameter values	
Stress 90° to grain [MPa]	Steel mass [tons]	Timber mass [tons]	Number of crossbeams	Deck thickness [mm]
3.11	25.6	367	20	500
3.4	21.6	367	15	500
3.45	22.9	342	17	450
3.83	23.5	291	15	350

Simulation 3

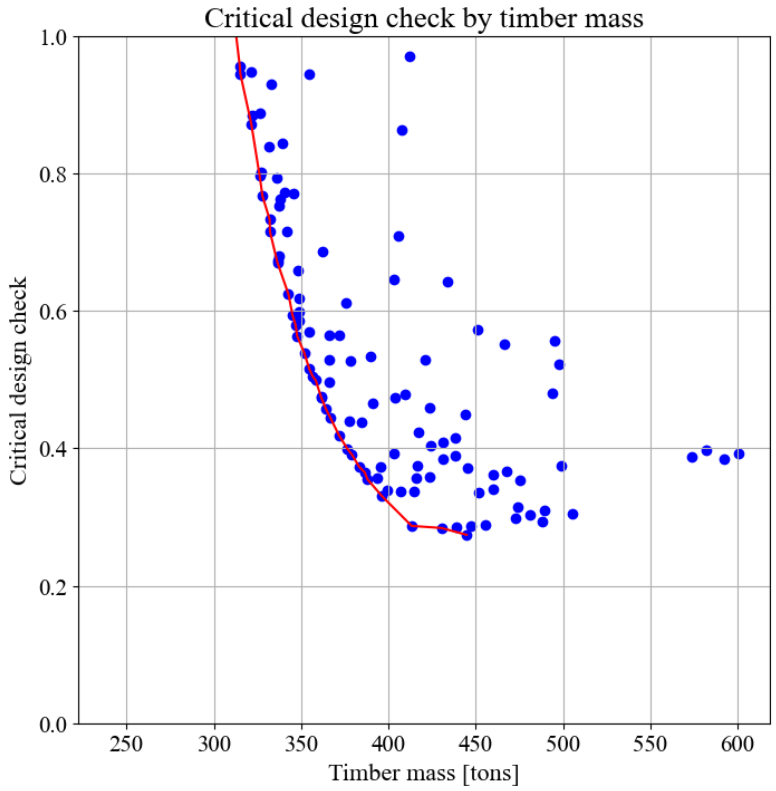

Figure B.41: 100 m span with three splices: Simulation 3, Full load

Table B.27: 100 m span with three splices: Simulation 3, Full load

Objective values		Parameter values	
Critical design check [0, 1]	Timber mass [tons]	Arch height [mm]	Arch width [mm]
0.796	326	800	1300
0.872	321	800	1250
0.884	322	850	1200
0.945	315	600	1450

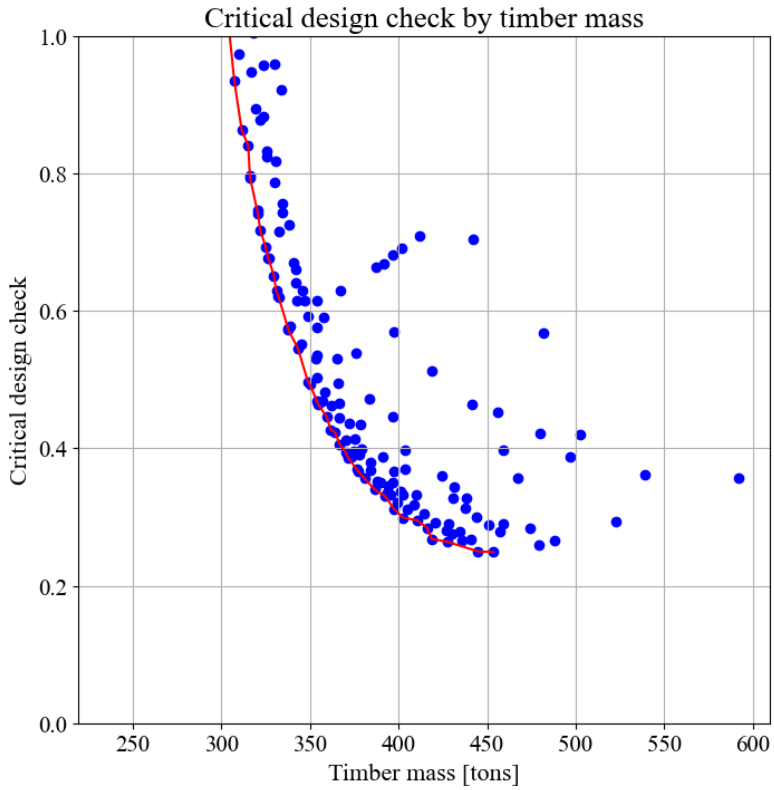

Figure B.42: 100 m span with three splices: Simulation 3, Skew load

Table B.28: 100 m span with three splices: Simulation 3, Skew load

Objective values		Parameter values	
Critical design check [0, 1]	Timber mass [tons]	Arch height [mm]	Arch width [mm]
0.797	316	750	1250
0.84	315	1000	1000
0.863	311	750	1100
0.935	307	800	1100

Simulation 4

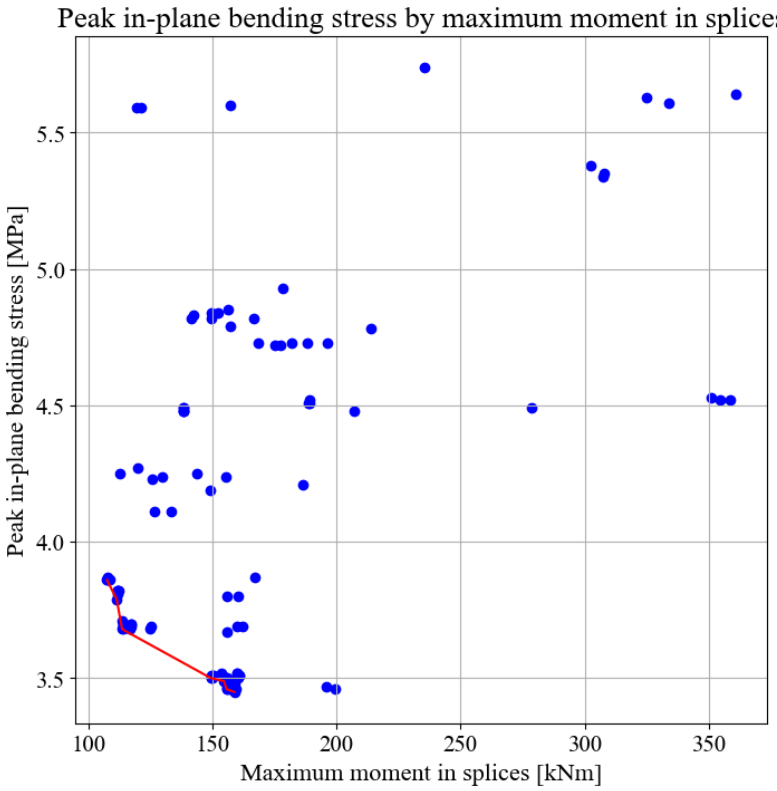

Figure B.43: 100 m span with three splices: Simulation 4, Full load

Table B.29: 100 m span with three splices: Simulation 4, Full load

Objective values		Parameter values	
Maximum moment in splices [kNm]	Peak in-plane bending stress [MPa]	Connection placement [0, 1]	Hanger angle [degrees]
108	3.87	0.3 - 1	43
111	3.79	0.3	42
114	3.68	0.3	40
159	3.45	0.7	39

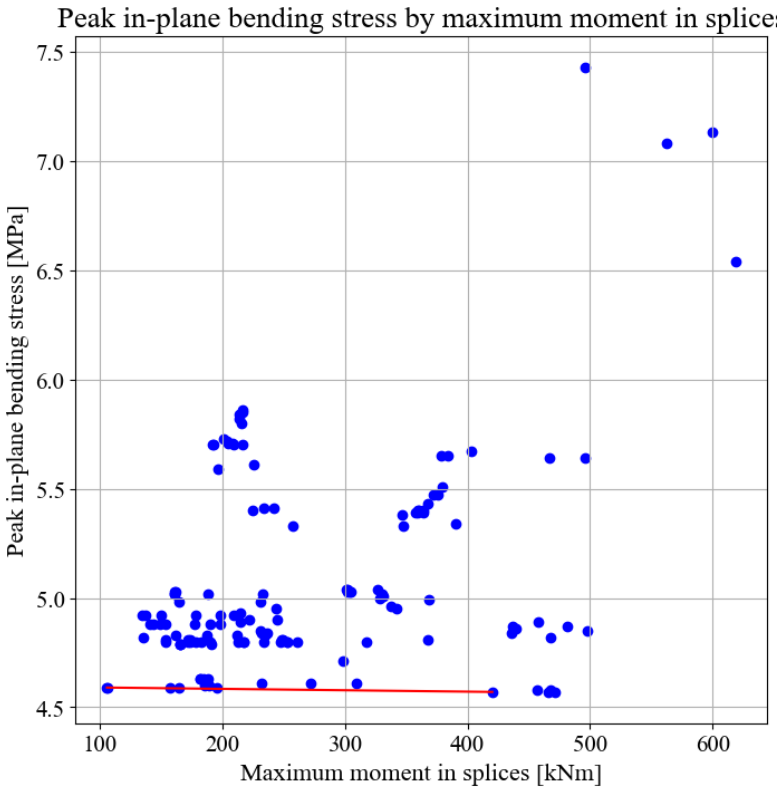

Figure B.44: 100 m span with three splices: Simulation 4, Skew load

Table B.30: 100 m span with three splices: Simulation 4, Skew load

Objective values			Parameter values	
Maximum moment in splices [kNm]	Peak in-plane bending stress [MPa]	Hangers in compression	Connection placement [0, 1]	Hanger angle [degrees]
106	4.59	6	1	46
134	4.92	7	0.9	42
135	4.82	8	1	41
141 - 154	4.88	7	1 - 0.7	43

Simulation 5

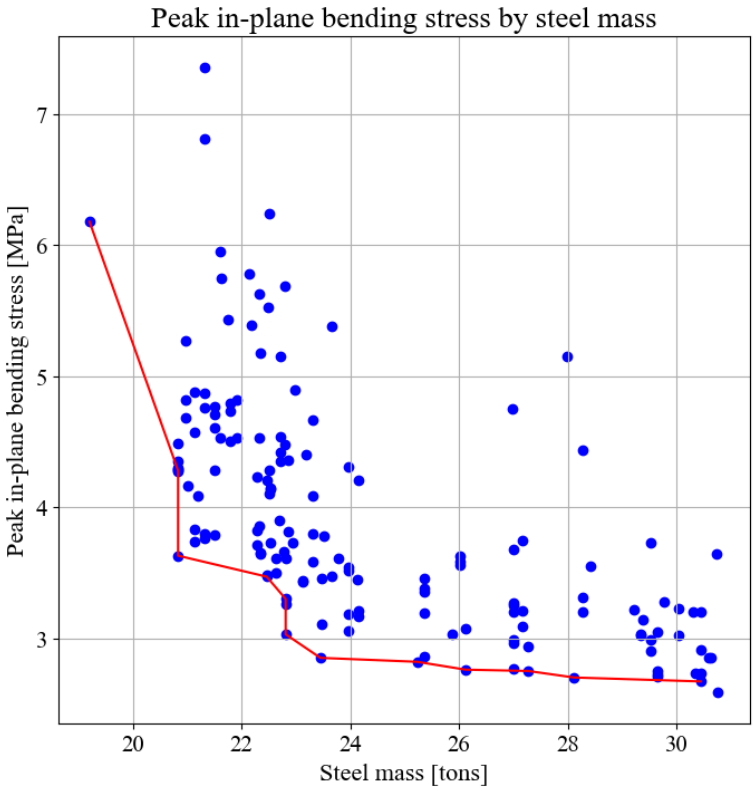

Figure B.45: 100 m span with three splices: Simulation 5, Full load

Table B.31: 100 m span with three splices: Simulation 5, Full load

Objective values		Parameter values	
Peak in-plane bending stress [MPa]	Steel mass [tons]	Number of crossbeams	Hanger angle [degrees]
2.85 - 3.03	23	17 - 16	35
3.47 - 3.71 - 3.86	22	15	38 - 40 - 43
3.63	21	10	44
3.74	21	11	38

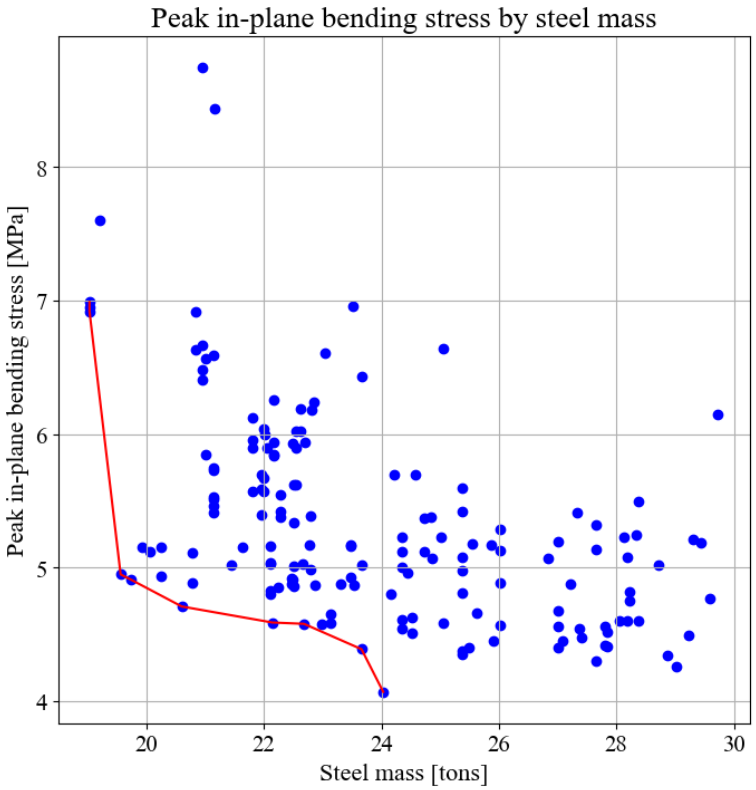

Figure B.46: 100 m span with three splices: Simulation 5, Skew load

Table B.32: 100 m span with three splices: Simulation 5, Skew load

Objective values		Parameter values	
Peak in-plane bending stress [MPa]	Steel mass [tons]	Number of crossbeams	Hanger angle [degrees]
4.07	24	17	52
4.59 - 4.8 - 4.88	22	15	46 - 40 - 43
4.71	21	11	50
4.95	20	10	50 - 51

Final results

Table B.33: 100 m span with three splices: Results with the final configuration from Table 4.7.

	Full load	Skew load	Governing load
Peak in-plane bending stress [MPa]	3.91	4.53	4.53
Critical design check Eq. (6.24)	0.935	0.747	0.935
Buckling load factor	2.29	2.64	2.29
Natural frequency [Hz]	0.763	0.716	0.716
Max stress 90°to grain [MPa]	3.08	2.88	3.08
% of deck exceeding Tsai-Wu criterion	5.4	1.9	5.4
Max moment in splices [kNm]	106	130	130
Number of relaxed hangers	0	7	7
Maximum displacement [mm]	239	262	262
Crossbeam utilization [%]	79.4	87.5	87.5
Hanger utilization [%]	30.9	38.0	38.0

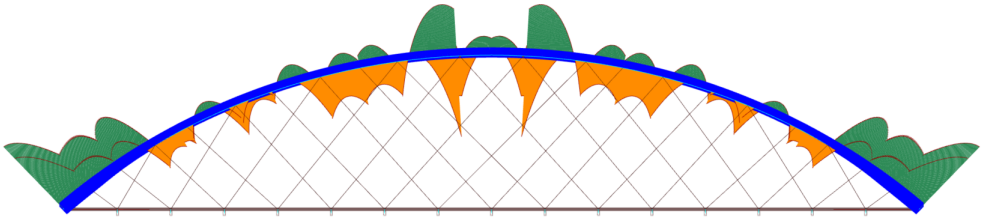

Figure B.47: 100 m span with three splices: Full load. Moment distribution in-plane with final configuration.

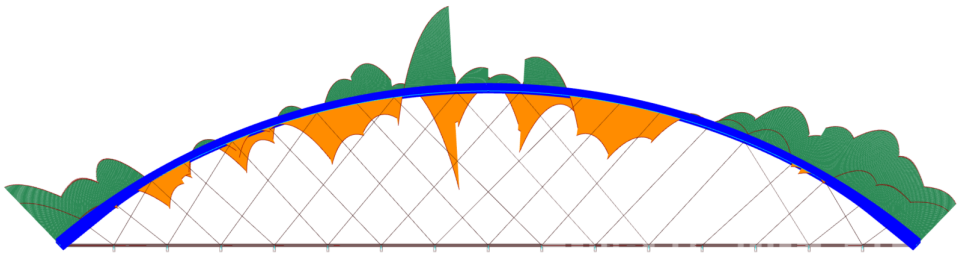

Figure B.48: 100 m span with three splices: Skew load. Moment distribution in-plane with final configuration.

Tsai Wu Criterion

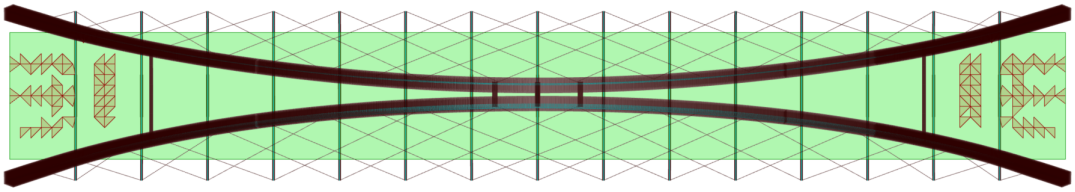

Figure B.49: 100 m span with three splices: Full load. Elements exceeding the Tsai Wu criterion are marked in a darker shade.

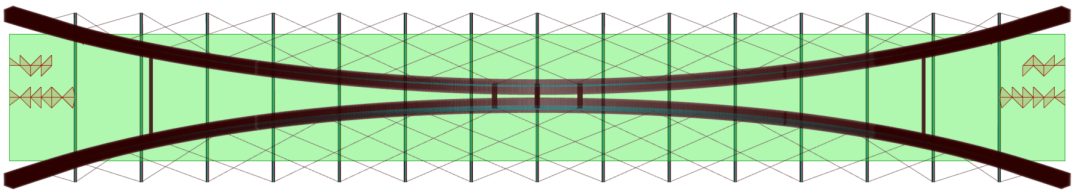

Figure B.50: 100 m span with three splices: Full load. The crossbeams closest to the deck supports are of constant height 550 mm. Elements exceeding the Tsai Wu criterion are marked in a darker shade.

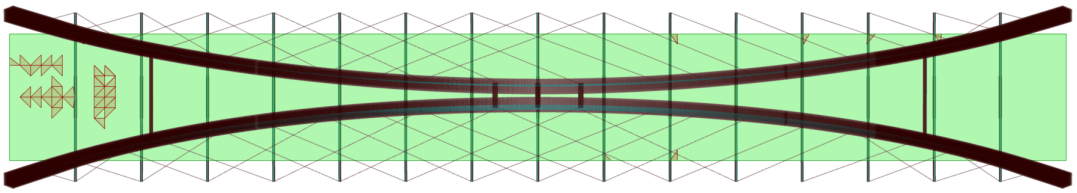

Figure B.51: 100 m span with three splices: Skew load. Elements exceeding the Tsai Wu criterion are marked in a darker shade.

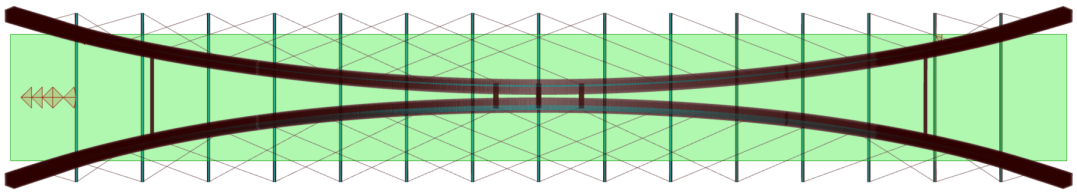

Figure B.52: 100 m span with three splices: Skew load. The crossbeams closest to the deck supports are of constant height 550 mm. Elements exceeding the Tsai Wu criterion are marked in a darker shade.

Table B.34: 100 m span with three splices configuration from Table 4.7. The crossbeams closest to the end supports are varied to see the effect of the deck stresses.

		Full load		Skew load	
End crossbeam cross-sec [mm]	Steel mass [tons]	Exceed Tsai-Wu [%]	Max deck stress [MPa]	Exceed Tsai-Wu [%]	Max deck stress [MPa]
450x6 550x2	63.5	5.43	3.08	1.91	2.88
550	79.7	1.85	3.05	0.50	2.83
650	102.2	0.08	2.58	0	2.45

B.4 100 m span with four splices

Simulation 1

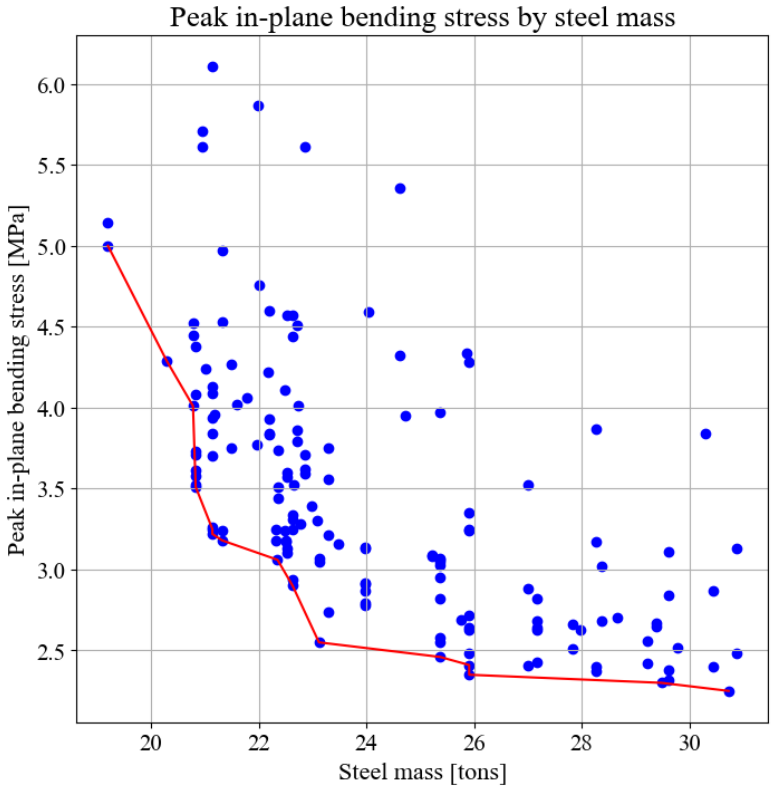

Figure B.53: 100 m span with four splices: Simulation 1, Full load

Table B.35: 100 m span with four splices: Simulation 1, Full load

Objective values		Parameter values	
Peak in-plane bending stress [MPa]	Steel mass [tons]	Number of crossbeams	Hanger angle [degrees]
2.46 - 3.07	23.4	19	36 - 42
2.55 - 3.05	23	17	35 - 40
3.06	22.3	12	36
3.17	22.5	15	39

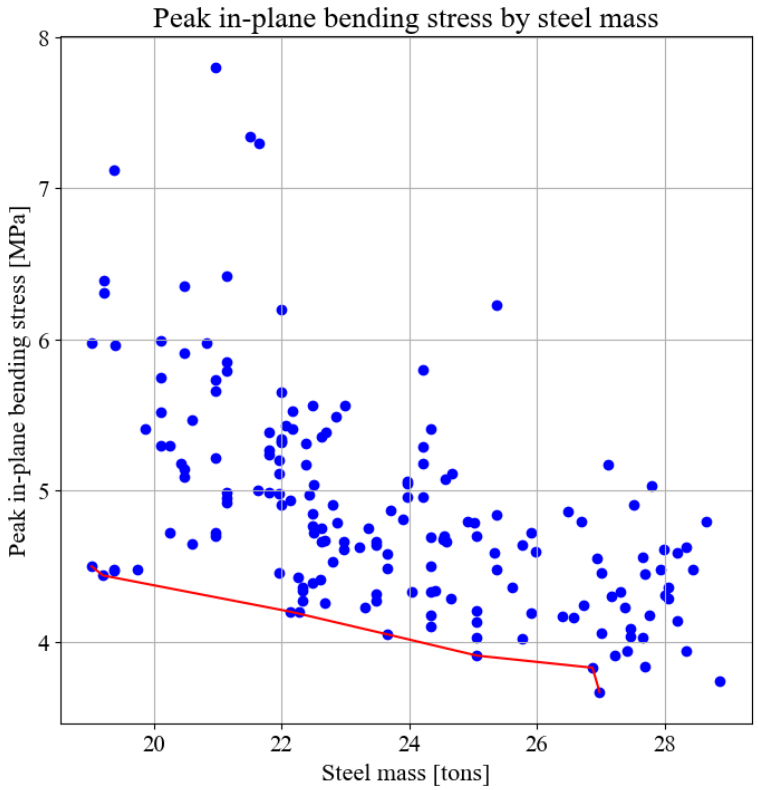

Figure B.54: 100 m span with four splices: Simulation 1, Skew load

Table B.36: 100 m span with four splices: Simulation 1, Skew load

Objective values		Parameter values	
Peak in-plane bending stress [MPa]	Steel mass [tons]	Number of crossbeams	Hanger angle [degrees]
3.67	27	22	52
4.2	22	15	40
4.36	22	15	42
4.5	19	10	49 - 52

Simulation 2

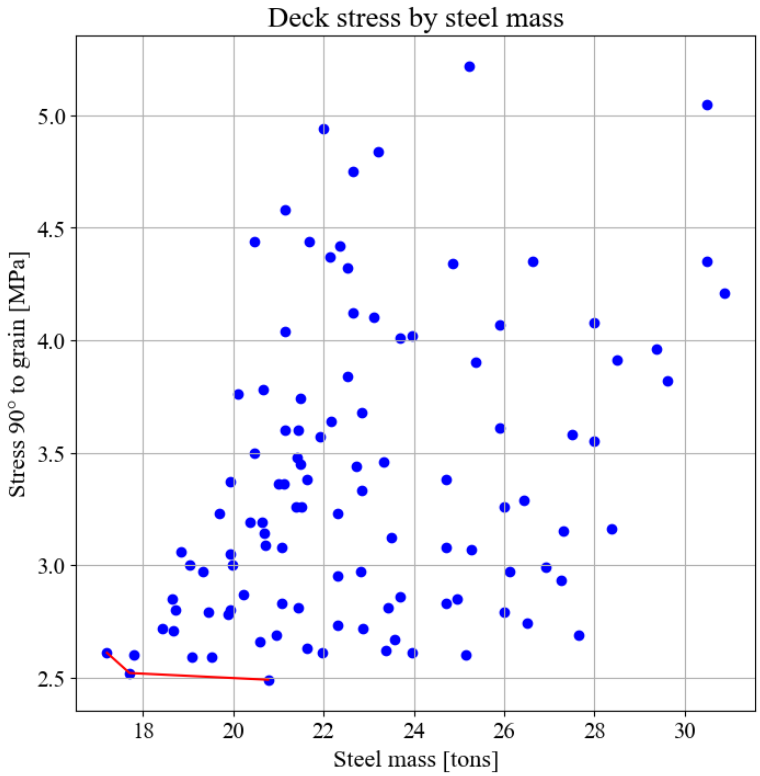

Figure B.55: 100 m span with four splices: Simulation 2, Full load

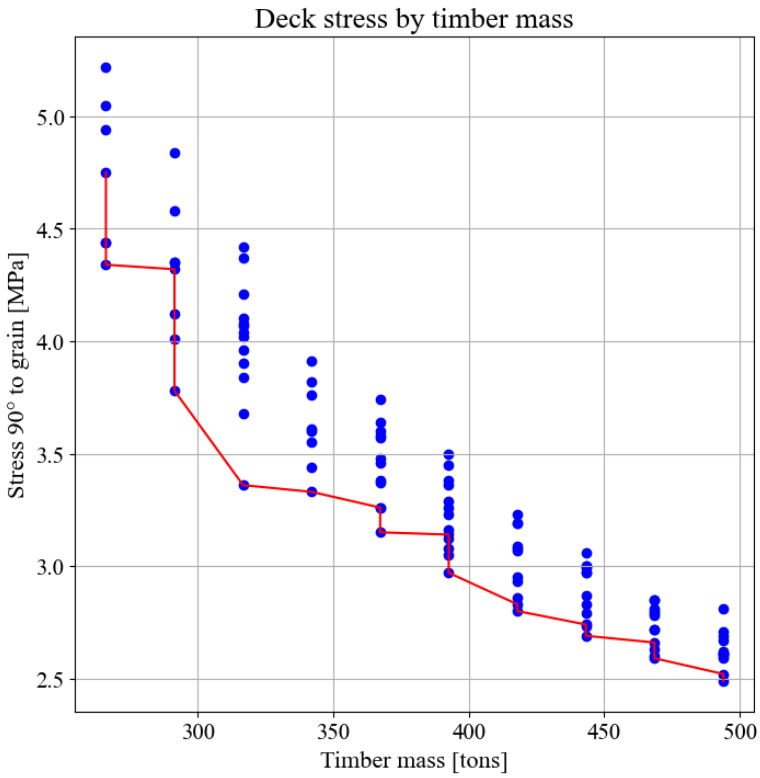

Figure B.56: 100 m span with four splices: Simulation 2, Full load

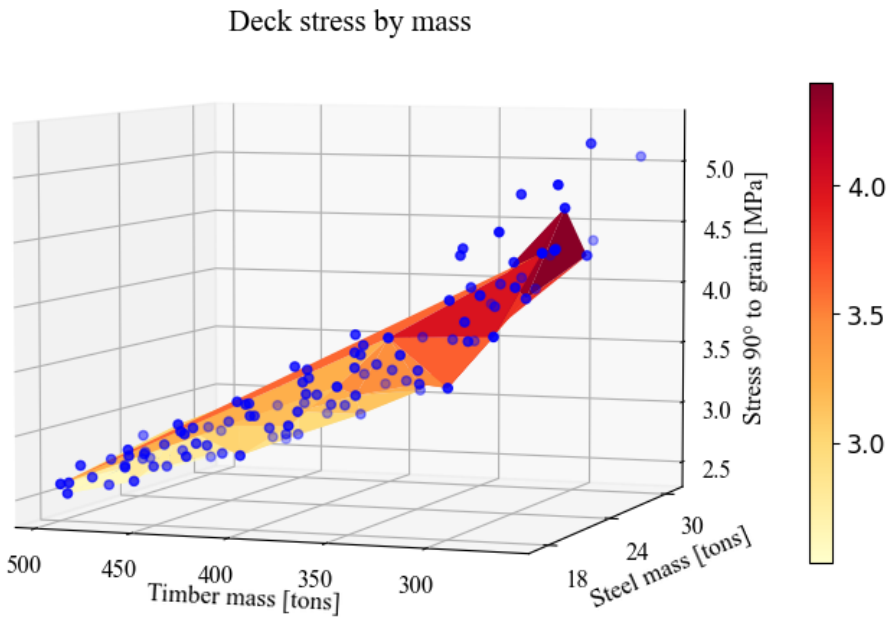

Figure B.57: 100 m span with four splices: Simulation 2, Full load

Table B.37: 100 m span with four splices: Simulation 2, Full load

Objective values			Parameter values	
Stress 90° to grain [MPa]	Steel mass [tons]	Timber mass [tons]	Number of crossbeams	Deck thickness [mm]
3.64 - 4.1 - 4.7	22.9 - 23.5 - 23.3	342 - 317 - 291	17	450 - 400 - 350
3.88 - 4.37 - 4.85	21.4 - 22.1 - 23.2	342 - 317 - 291	15	450 - 400 - 350
3.75 - 3.84 - 4.25	22.1 - 23.8 - 22.6	342 - 291 - 317	16	450 - 350 - 400
4.01 - 4.07 - 4.42	23.7 - 22.4 - 22.4	291 - 342 - 317	14	350 - 450 - 400

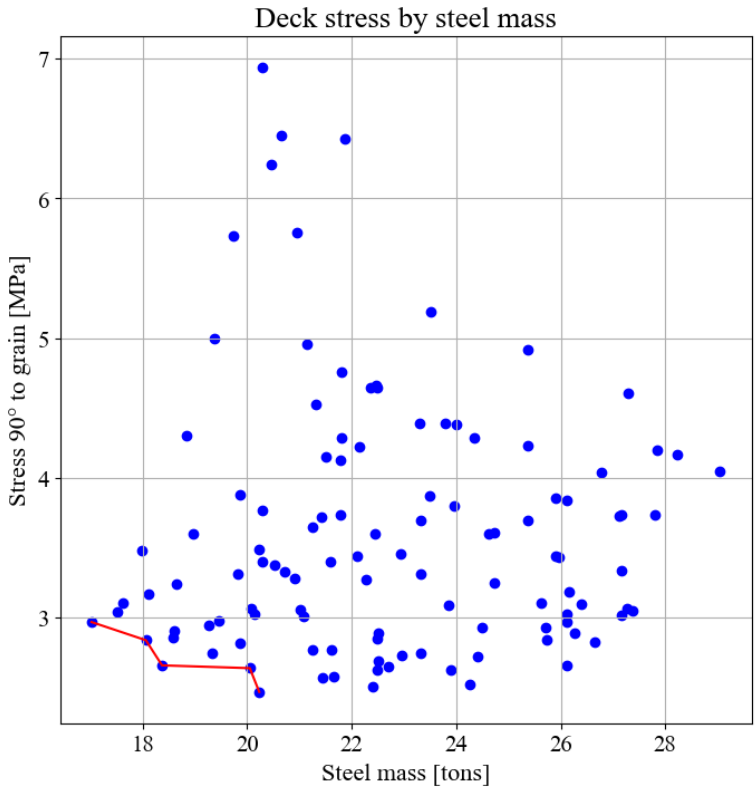

Figure B.58: 100 m span with four splices: Simulation 2, Skew load

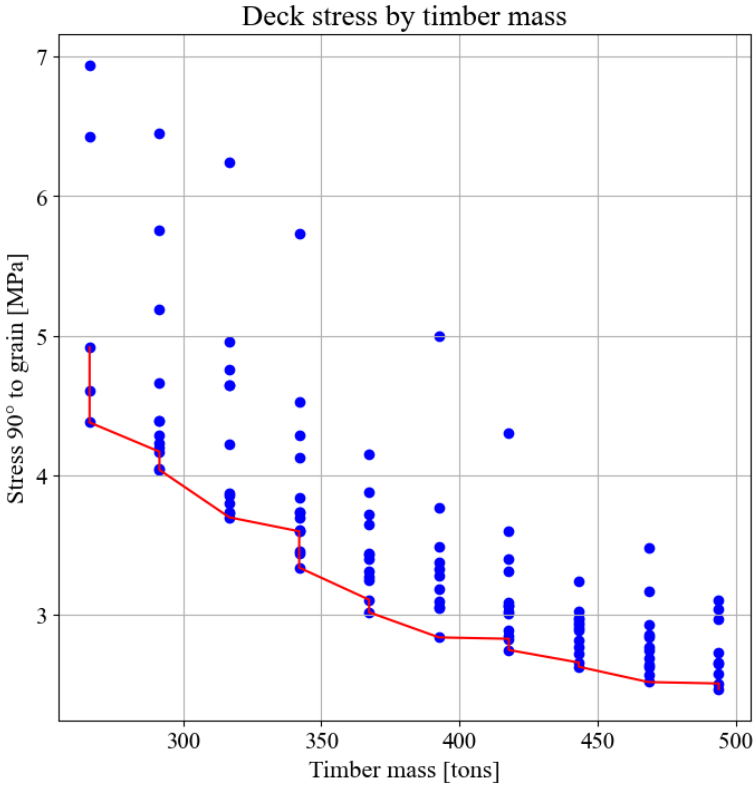

Figure B.59: 100 m span with four splices: Simulation 2, Skew load

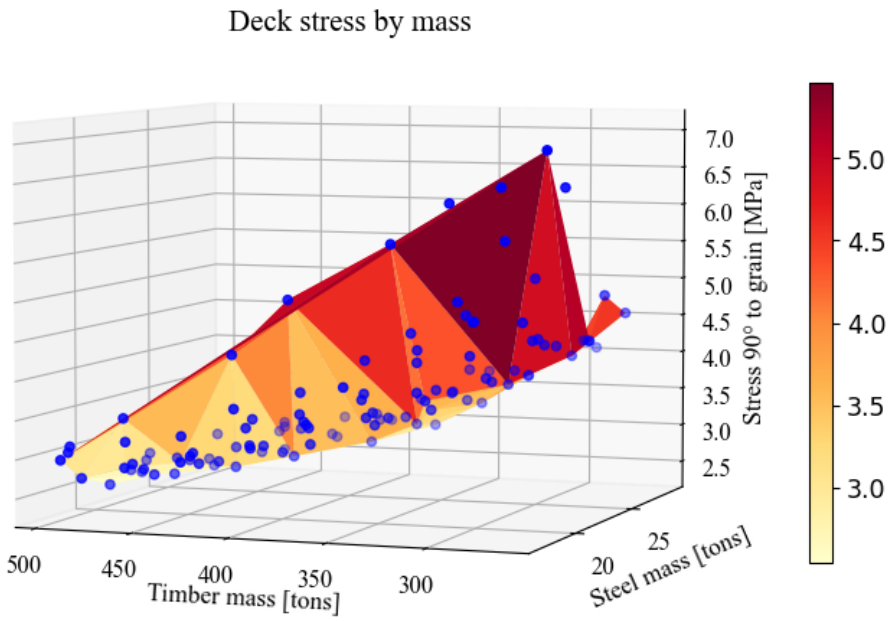

Figure B.60: 100 m span with four splices: Simulation 2, Skew load

Table B.38: 100 m span with four splices: Simulation 2, Skew load

Objective values			Parameter values	
Stress 90° to grain [MPa]	Steel mass [tons]	Timber mass [tons]	Number of crossbeams	Deck thickness [mm]
3.46 - 3.87 - 4.39	22.9 - 23.5 - 23.3	342 - 317 - 291	17	450 - 400 - 350
3.74 - 4.22 - 4.66	21.4 - 22.1 - 23.2	342 - 317 - 291	15	450 - 400 - 350
3.6 - 4.07 - 4.39	22.1 - 22.6 - 23.8	342 - 317 - 291	16	450 - 400 - 350
4.13 - 4.65 - 5.19	22.4 - 22.4 - 23.7	342 - 317 - 291	14	450 - 400 - 350

Simulation 3

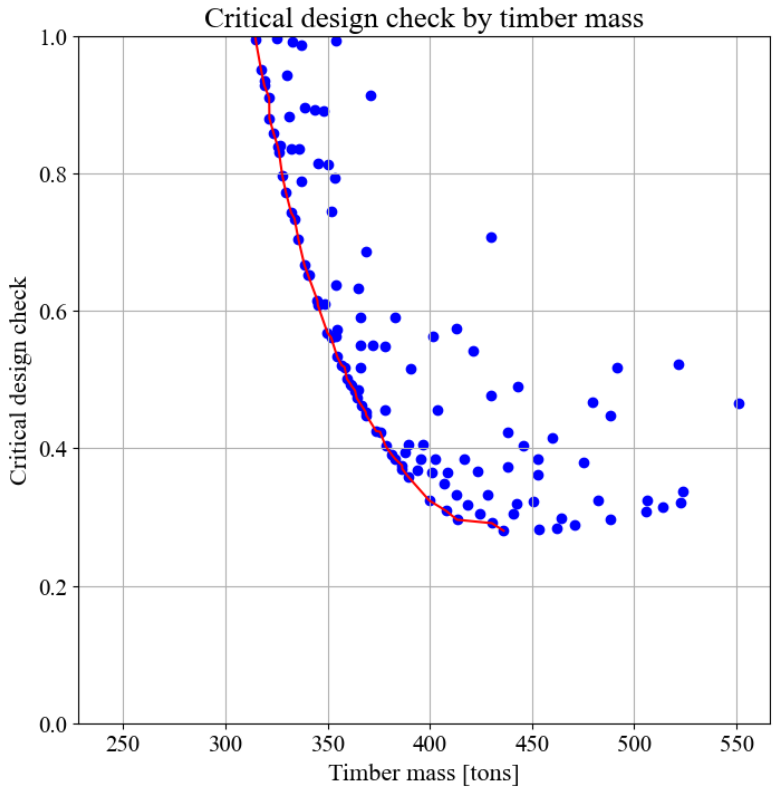

Figure B.61: 100 m span with four splices: Simulation 3, Full load

Table B.39: 100 m span with four splices: Simulation 3, Full load

Objective values		Parameter values	
Critical design check [0, 1]	Timber mass [tons]	Arch height [mm]	Arch width [mm]
0.859	323	700	1400
0.935	319	700	1350
0.951	317	650	1400
0.994	315	700	1300

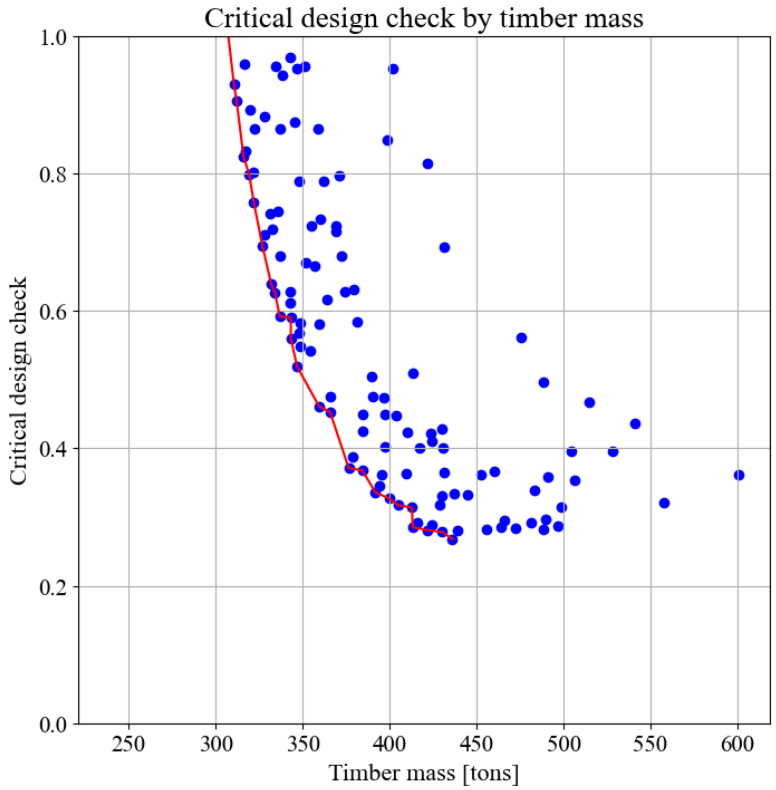

Figure B.62: 100 m span with four splices: Simulation 3, Skew load

Table B.40: 100 m span with four splices: Simulation 3, Skew load

Objective values		Parameter values	
Critical design check [0, 1]	Timber mass [tons]	Arch height [mm]	Arch width [mm]
0.694	327	850	1250
0.758	322	850	1200
0.824	316	750	1250
0.929	311	700	1250

Simulation 4

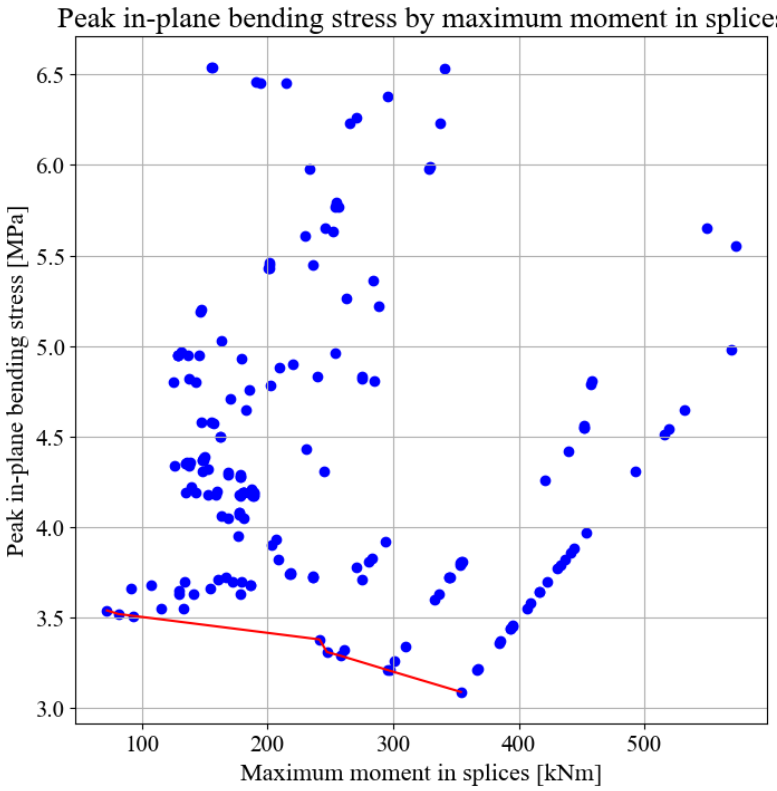

Figure B.63: 100 m span with four splices: Simulation 4, Full load

Table B.41: 100 m span with four splices: Simulation 4, Full load

Objective values		Parameter values		
Maximum moment in splices [kNm]	Peak in-plane bending stress [MPa]	Connection 1 placement [0, 1]	Connection 2 placement [0, 0.5]	Hanger angle [degrees]
72	3.54	0.1	0.2	35
93	3.54	0.3	0.2	35
125	4.34	0.6	0.1	40
125	4.8	0.6	0.2	44

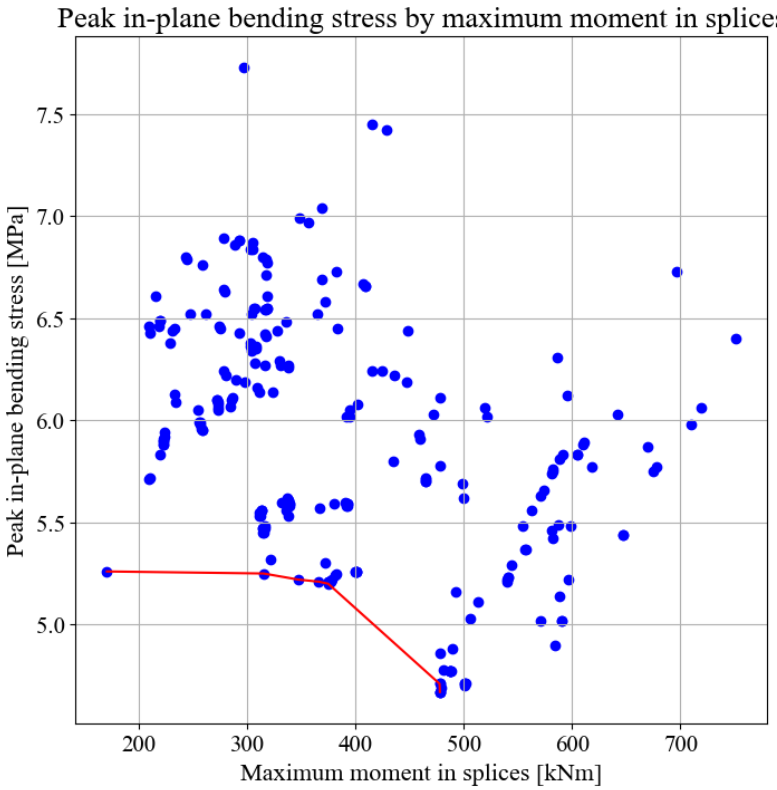

Figure B.64: 100 m span with four splices: Simulation 4, Skew load

Table B.42: 100 m span with four splices: Simulation 4, Skew load

Objective values			Parameter values		
Maximum moment in splices [kNm]	Peak in-plane bending stress [MPa]	Hangers in compression	Connection 1 placement [0, 1]	Connection 2 placement [0, 0.5]	Hanger angle [degrees]
171	5.26	3	0	0.5	52
209	6.43	9	0.3 - 0.4 - 0.7	0.1	41
210	5.71	6	0.7 - 0.8	0.2	47
223	5.88	6	0.5 - 0.7	0.2	46

Simulation 5

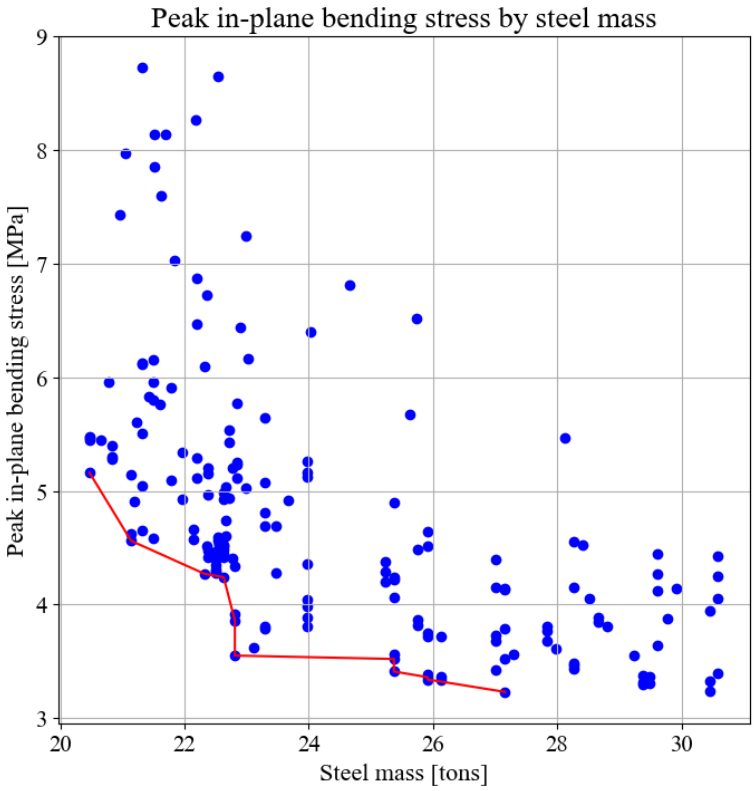

Figure B.65: 100 m span with four splices: Simulation 5, Full load

Table B.43: 100 m span with four splices: Simulation 5, Full load

Objective values		Parameter values	
Peak in-plane bending stress [MPa]	Steel mass [tons]	Number of crossbeams	Hanger angle [degrees]
3.34 - 3.41	26 - 25	20 - 19	36
3.55 - 4.24	23	16	35 - 41
4.27	22	15	40
4.65	21	11	39

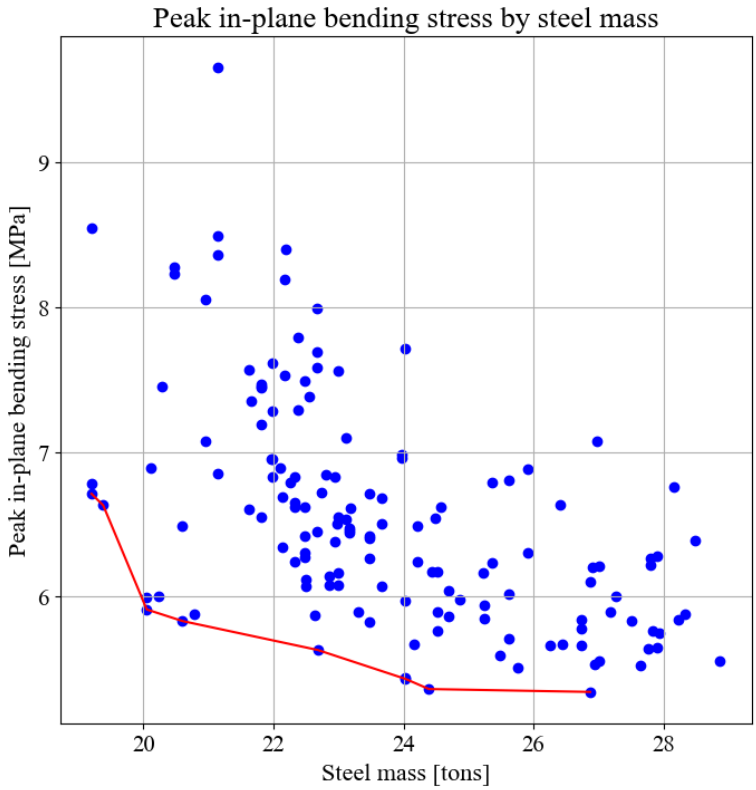

Figure B.66: 100 m span with four splices: Simulation 5, Skew load

Table B.44: 100 m span with four splices: Simulation 5, Skew load

Objective values		Parameter values	
Peak in-plane bending stress [MPa]	Steel mass [tons]	Number of crossbeams	Hanger angle [degrees]
5.36	24	17	52
5.36	24	17	50 - 51
5.63	23	15	53
6.63	19	10	50

Final results

Table B.45: 100 m span with four splices: Results with the final configuration from Table 4.7.

	Full load	Skew load	Governing load
Peak in-plane bending stress [MPa]	4.86	5.53	5.53
Critical design check Eq. (6.24)	0.993	0.813	0.993
Buckling load factor	2.30	2.68	2.30
Natural frequency [Hz]	0.784	0.729	0.729
Max stress 90°to grain [MPa]	3.45	3.24	3.45
% of deck exceeding Tsai-Wu criterion	8.8	3.7	8.8
Max moment in splices [kNm]	123	161	161
Number of relaxed hangers	0	5	5
Maximum displacement [mm]	251	262	262
Crossbeam utilization [%]	72.4	77.8	77.8
Hanger utilization [%]	28.9	34.4	34.4

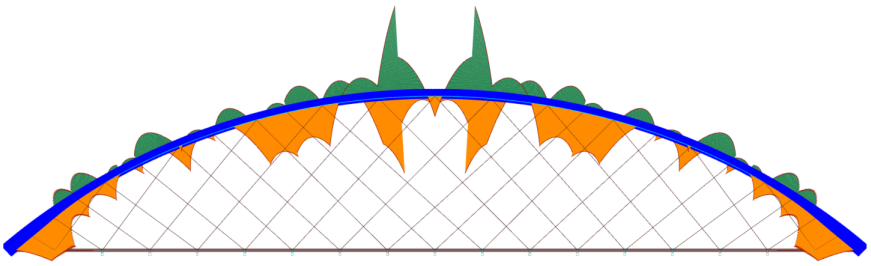

Figure B.67: 100 m span with four splices: Full load. Moment distribution in-plane with final configuration.

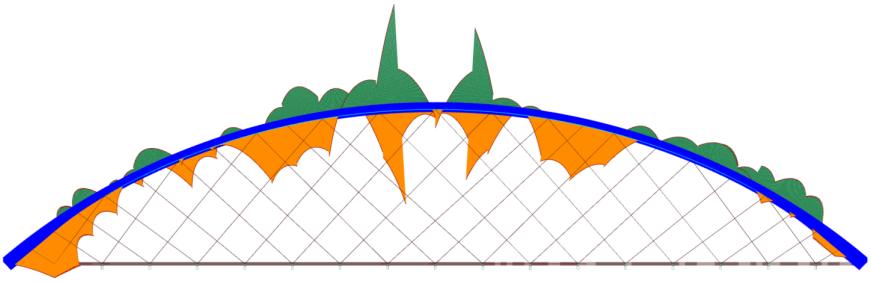

Figure B.68: 100 m span with four splices: Skew load. Moment distribution in-plane with final configuration.

Splice comparison

Table B.46: 100 m span with no splices vs. three splices vs. four splices: Results with the final configuration for the 100 m span with three splices from Table 4.7. All bridges with the same configurations.

	0 splices Full load	3 splices Full load	4 splices Full load	0 splices Skew load	3 splices Skew load	4 splices Skew load
Peak in-plane bending stress [MPa]	3.80	3.91	3.92	4.42	4.53	4.67
Critical design check Eq. (6.24)	0.559	0.935	0.953	0.427	0.747	0.857
Buckling load factor	2.43	2.29	2.28	2.81	2.64	2.66
Natural frequency [Hz]	0.789	0.763	0.760	0.739	0.716	0.713
Max stress 90°to grain [MPa]	3.08	3.08	3.08	2.88	2.88	2.88
% of deck exceeding Tsai-Wu criterion	5.4	5.4	5.4	1.9	1.9	1.9
Max moment in splices [kNm]	-	106	202	-	130	222
Number of relaxed hangers	0	0	0	7	7	7
Maximum displacement [mm]	217	239	240	241	262	264
Crossbeam utilization [%]	79.5	79.4	78.2	86.9	87.5	87.8
Hanger utilization [%]	30.8	30.9	30.9	37.8	38.0	38.1

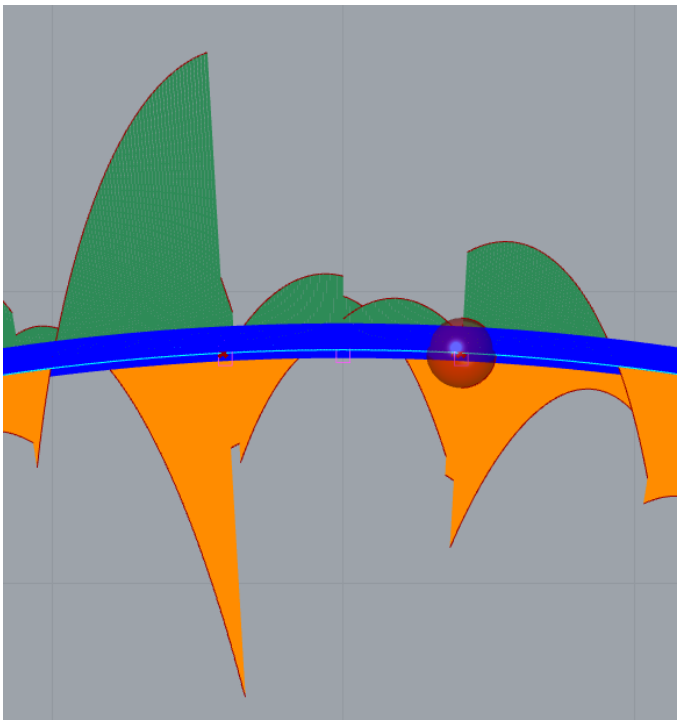

Figure B.69: 100 m span with three splices: Skew load. The figure shows the in-plane bending moment diagram at the top of the arches. The top beams are a pink color, and the most critical element is marked with a red sphere.

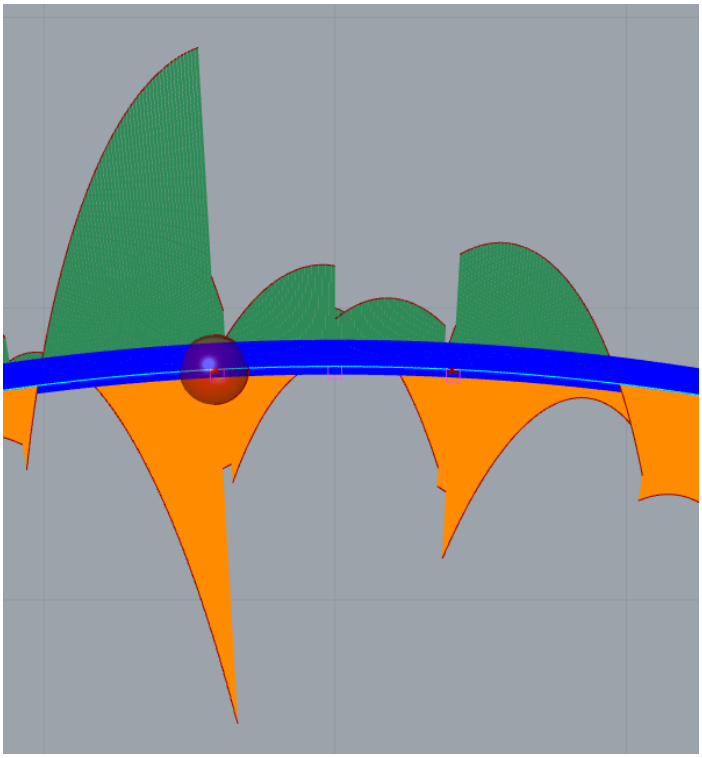

Figure B.70: 100 m span with four splices and 100 m span three splices configurations: Skew load. The figure shows the in-plane bending moment diagram at the top of the arches. The top beams are a pink color, and the most critical element is marked with a red sphere.

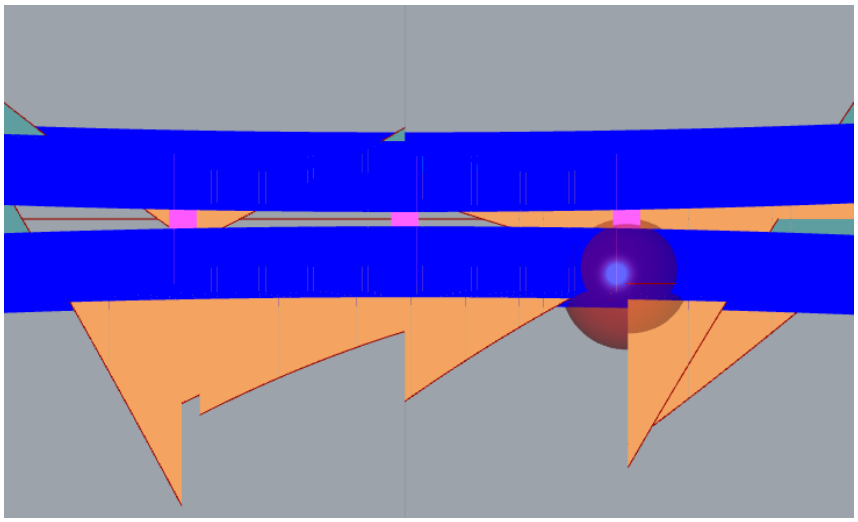

Figure B.71: 100 m span with three splices: Skew load. The figure shows the out-of-plane bending moment diagram at the top of the arches. The top beams are a pink color, and the most critical element is marked with a red sphere.

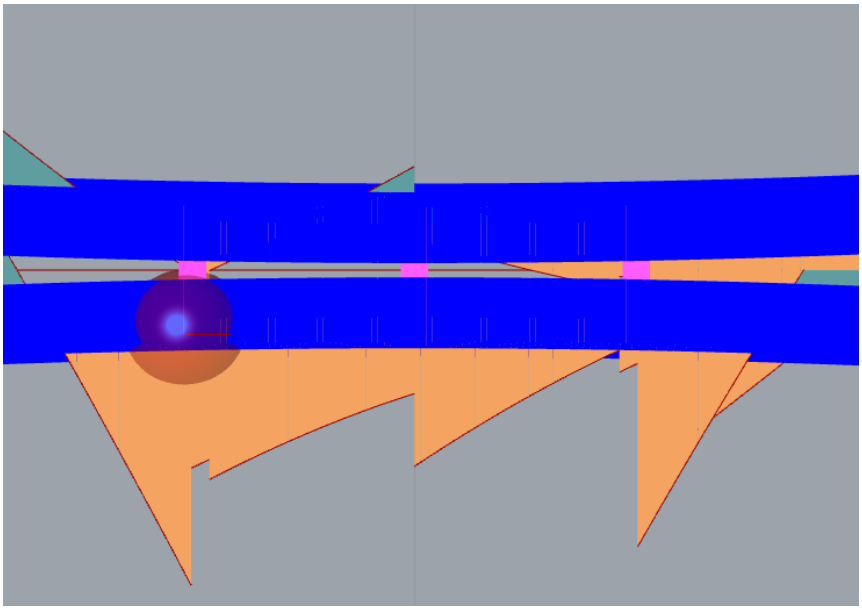

Figure B.72: 100 m span with four splices and 100 m span three splices configurations: Skew load. The figure shows the out-of-plane bending moment diagram at the top of the arches. The top beams are a pink color, and the most critical element is marked with a red sphere.

Table B.47: 100 m span with three splices configuration from Table 4.7 for no splices and the three-spliced and four-splices bridge. Element 1768 corresponds to the element in the arch connected to the outer top beam, closest to the unloaded part of the bridge. Element 1724 corresponds to the opposite top beam.

	Element 1768			Element 1724		
	0 splice	3 splices	4 splices	0 splices	3 splices	4 splices
$\sigma_{m,y}$ [MPa]	2.58	2.56	0.45	2.61	2.63	5.71
$\sigma_{m,z}$ [MPa]	1.07	1.31	0.51	0.37	0.49	1.84
$\sigma_{c,0,d}$ [MPa]	2.18	2.19	2.06	1.91	1.90	2.08

B.5 120 m span with four splices

Simulation 1

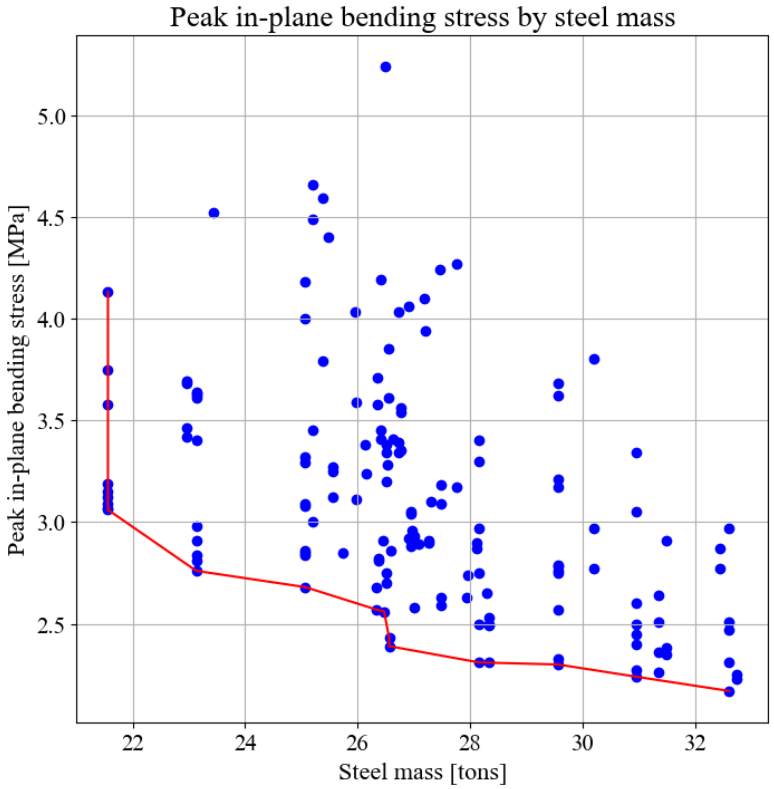

Figure B.73: 120 m span with four splices: Simulation 1, Full load

Table B.48: 120 m span with four splices: Simulation 1, Full load

Objective values		Parameter values	
Peak in-plane bending stress [MPa]	Steel mass [tons]	Number of crossbeams	Hanger angle [degrees]
2.17	32.6	25	35
2.31 - 2.5	28.2	21	35 - 38
2.56 - 2.57	26.3	18	35 - 40
3.06 - 3.12	21.6	10	38 - 40

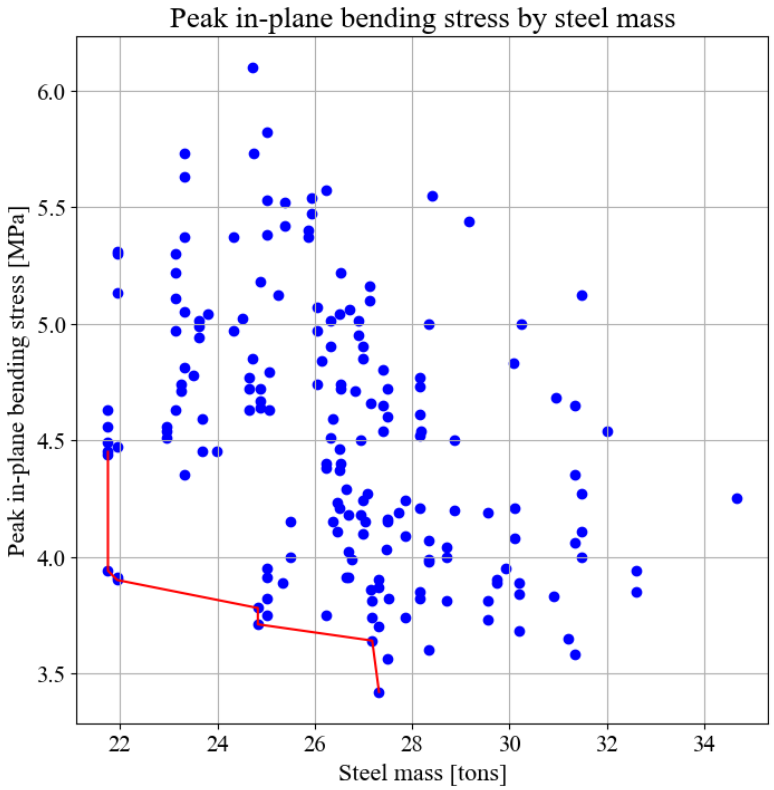

Figure B.74: 120 m span with four splices: Simulation 1, Skew load

Table B.49: 120 m span with four splices: Simulation 1, Skew load

Objective values		Parameter values	
Peak in-plane bending stress [MPa]	Steel mass [tons]	Number of crossbeams	Hanger angle [degrees]
3.42 - 3.64	27.3	19	49 - 48
3.75	26.2	14	50
3.78 - 3.91	25	13	48 - 46
3.94 - 4.45	21.8	10	49 - 46

Simulation 2

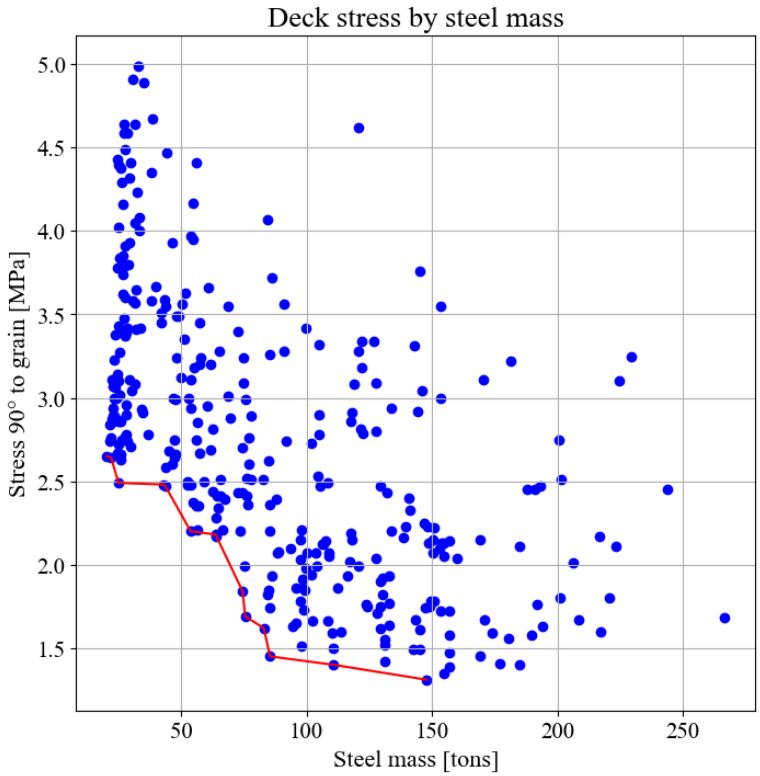

Figure B.75: 120 m span with four splices: Simulation 2, Full load

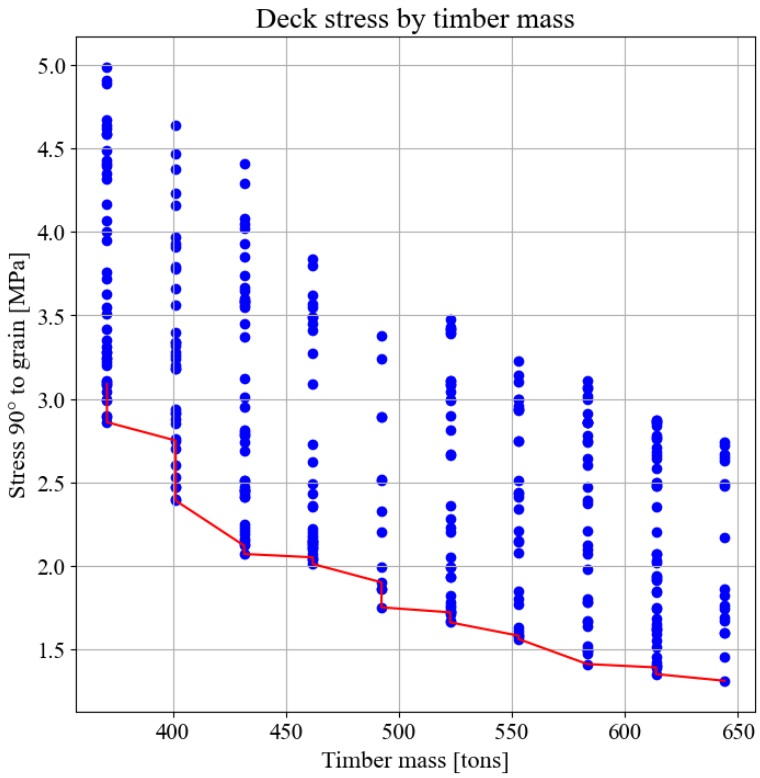

Figure B.76: 120 m span with four splices: Simulation 2, Full load

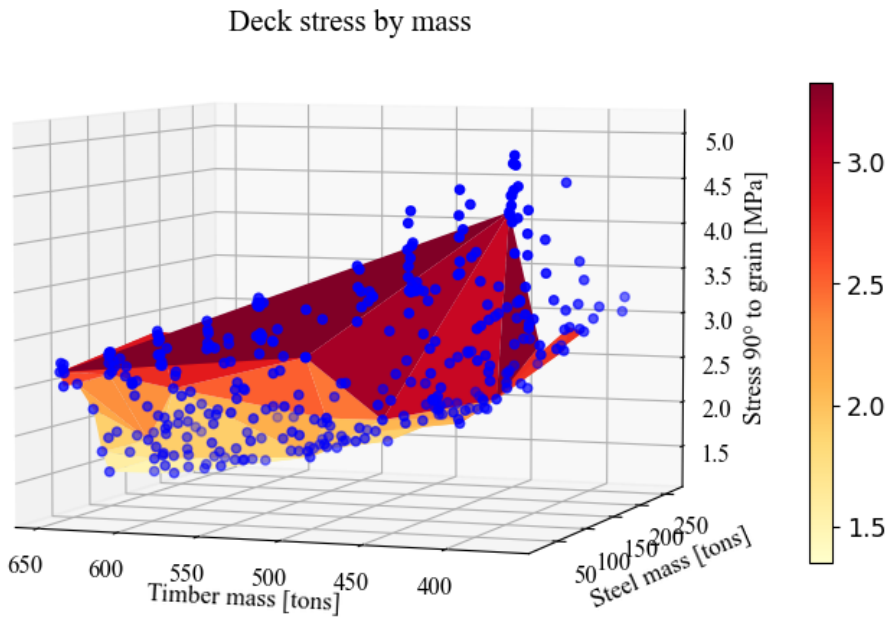

Figure B.77: 120 m span with four splices: Simulation 2, Full load

Table B.50: 120 m span with four splices: Simulation 2, Full load

Objective values			Parameter values	
Stress 90° to grain [MPa]	Steel mass [tons]	Timber mass [tons]	Number of crossbeams	Deck thickness [mm]
2.89	23.1	492	11	500
3.37	27.6	432	19	400
3.74	26.7	432	15	400
3.78 - 4.43	24.8	401 - 371	12	350 - 300

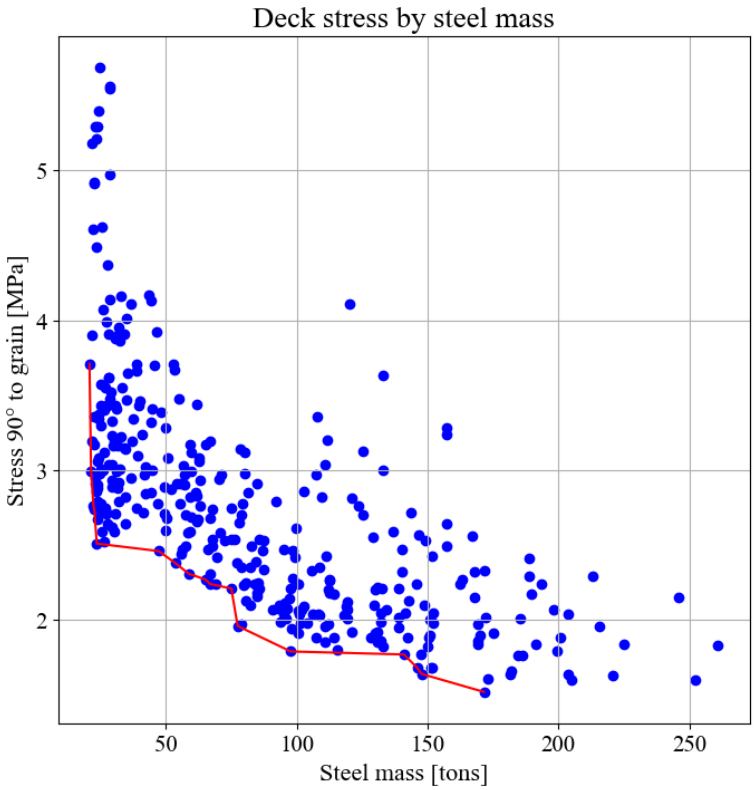

Figure B.78: 120 m span with four splices: Simulation 2, Skew load

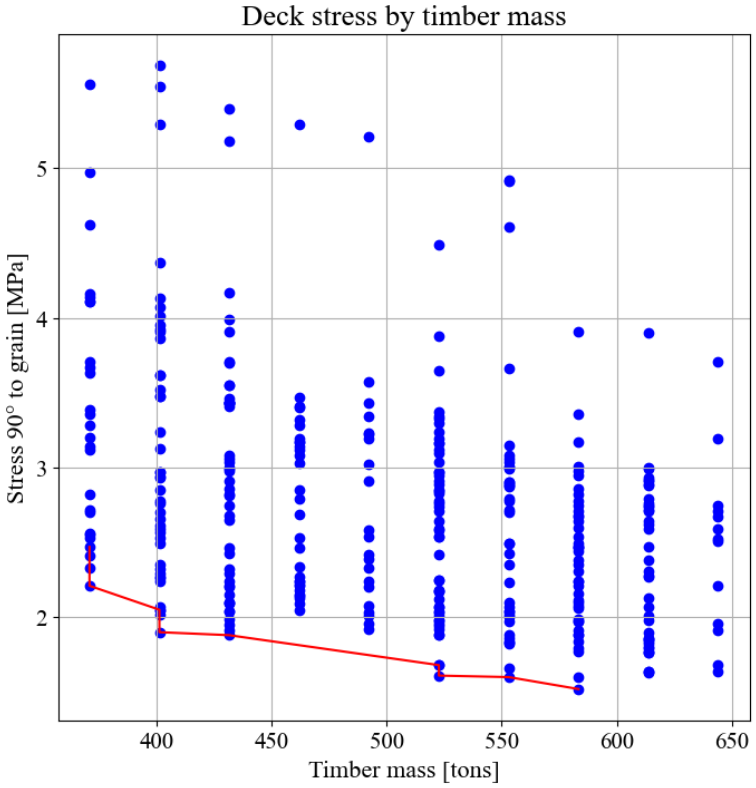

Figure B.79: 120 m span with four splices: Simulation 2, Skew load

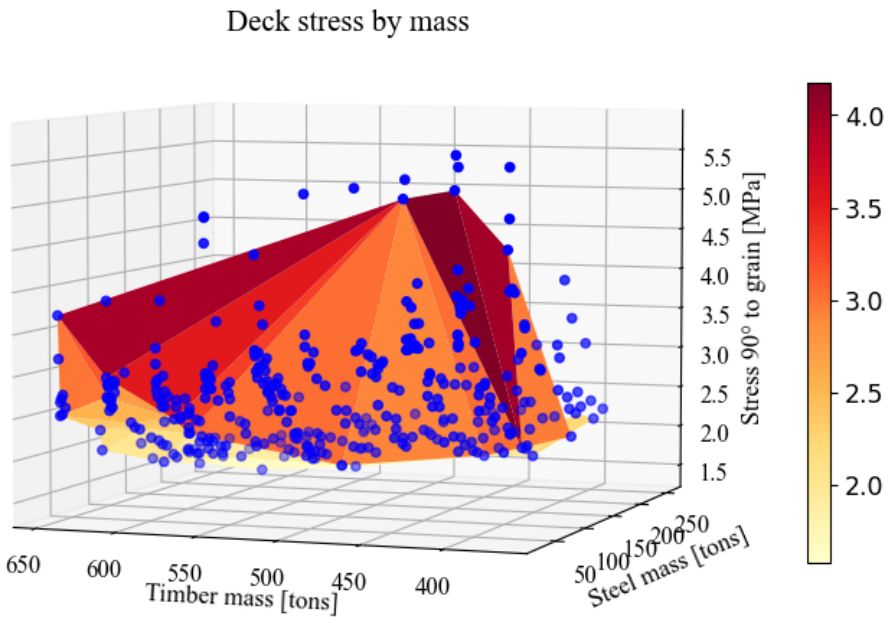

Figure B.80: 120 m span with four splices: Simulation 2, Skew load

Table B.51: 120 m span with four splices: Simulation 2, Skew load

Objective values			Parameter values	
Stress 90° to grain [MPa]	Steel mass [tons]	Timber mass [tons]	Number of crossbeams	Deck thickness [mm]
3.43 - 3.55	28.7 - 28.2	401	19 - 18	400
3.48 - 3.62	27 - 26.7	432	16 - 15	350
4.16	32.8	371	17	300
4.63	21.8	432	10	400

Simulation 3

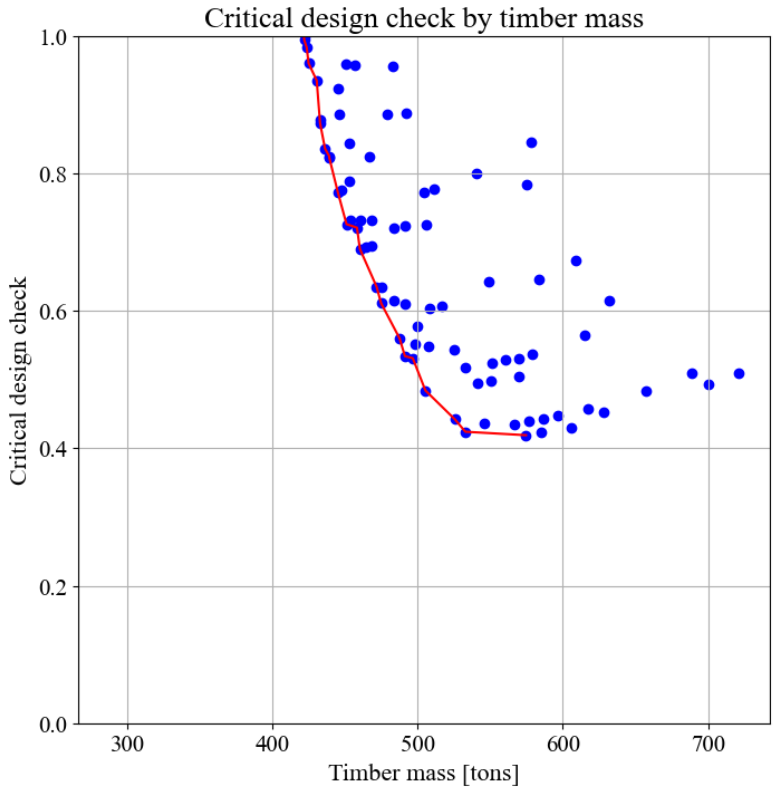

Figure B.81: 120 m span with four splices: Simulation 3, Full load

Table B.52: 120 m span with four splices: Simulation 3, Full load

Objective values		Parameter values	
Critical design check [0, 1]	Timber mass [tons]	Arch height [mm]	Arch width [mm]
0.836	436	800	1700
0.873	433	750	1750
0.878	433	850	1600
0.935	431	950	1450

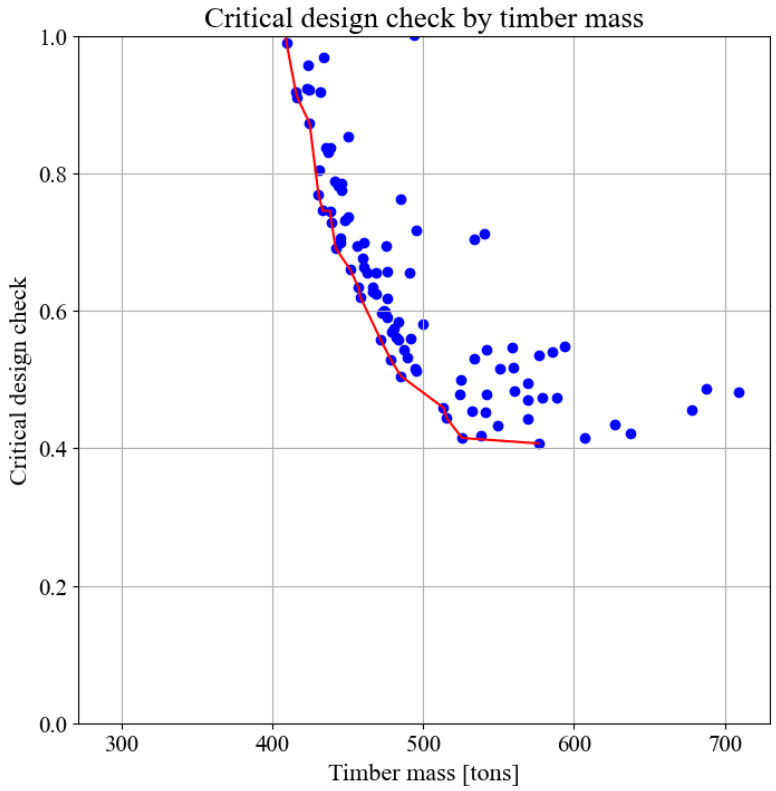

Figure B.82: 120 m span with four splices: Simulation 3, Skew load

Table B.53: 120 m span with four splices: Simulation 3, Skew load

Objective values		Parameter values	
Critical design check [0, 1]	Timber mass [tons]	Arch height [mm]	Arch width [mm]
0.838	436	900	1550
0.91	417	750	1600
0.918	432	1100	1300
0.919	416	850	1450

Simulation 4

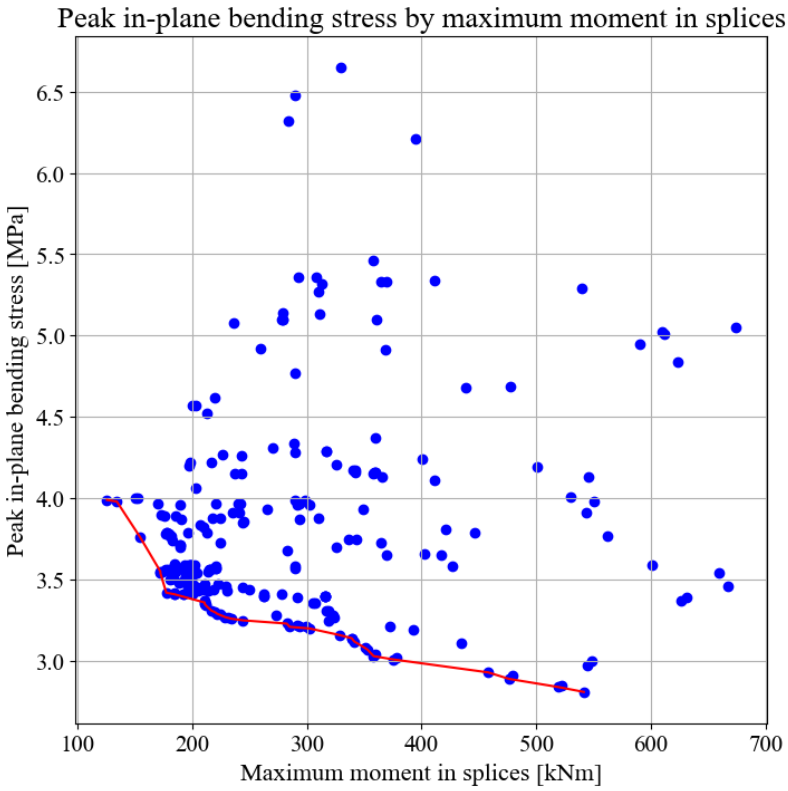

Figure B.83: 120 m span with four splices: Simulation 4, Full load

Table B.54: 120 m span with four splices: Simulation 4, Full load

Objective values		Parameter values		
Maximum moment in splices [kNm]	Peak in-plane bending stress [MPa]	Connection 1 placement [0, 1]	Connection 2 placement [0, 0.5]	Hanger angle [degrees]
126 - 134	3.99 - 3.98	0.4 - 0.6	0.3	40
155	3.76	0.2	0.3	41
172	3.54 - 3.55	0.8 - 0.9	0.2	36
375	3.01	0.4	0.5	38

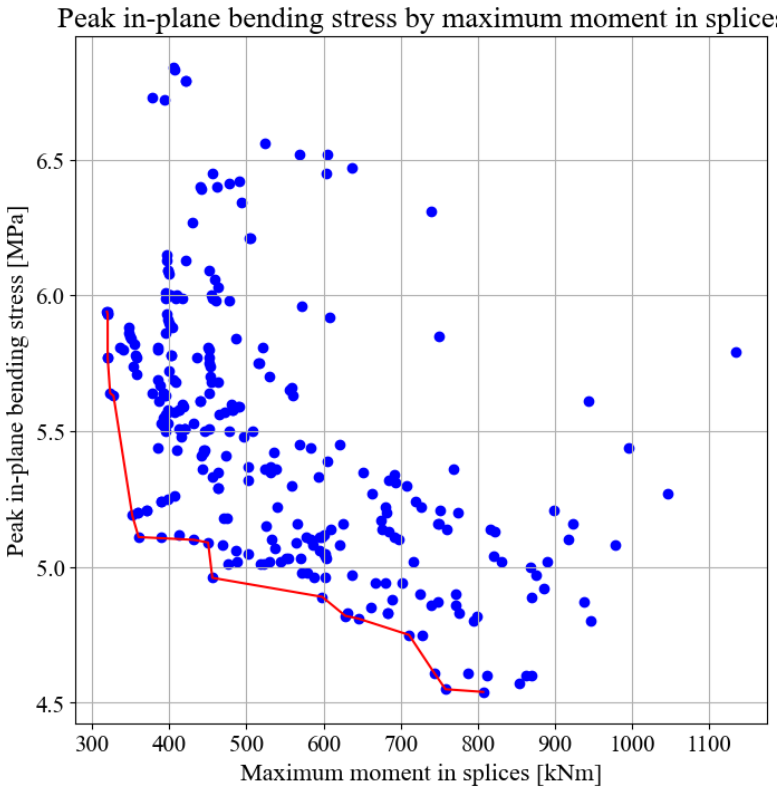

Figure B.84: 120 m span with four splices: Simulation 4, Skew load

Table B.55: 120 m span with four splices: Simulation 4, Skew load

Objective values			Parameter values		
Maximum moment in splices [kNm]	Peak in-plane bending stress [MPa]	Hangers in compression	Connection 1 placement [0, 1]	Connection 2 placement [0, 0.5]	Hanger angle [degrees]
320	5.93	8	0.3	0.2	44
323 - 328	5.64 - 5.63	7	0.1 - 0.3	0.3	45
360	5.11	5	0	0.3	49
456	4.96	3	0.3	0.2	57

Simulation 5

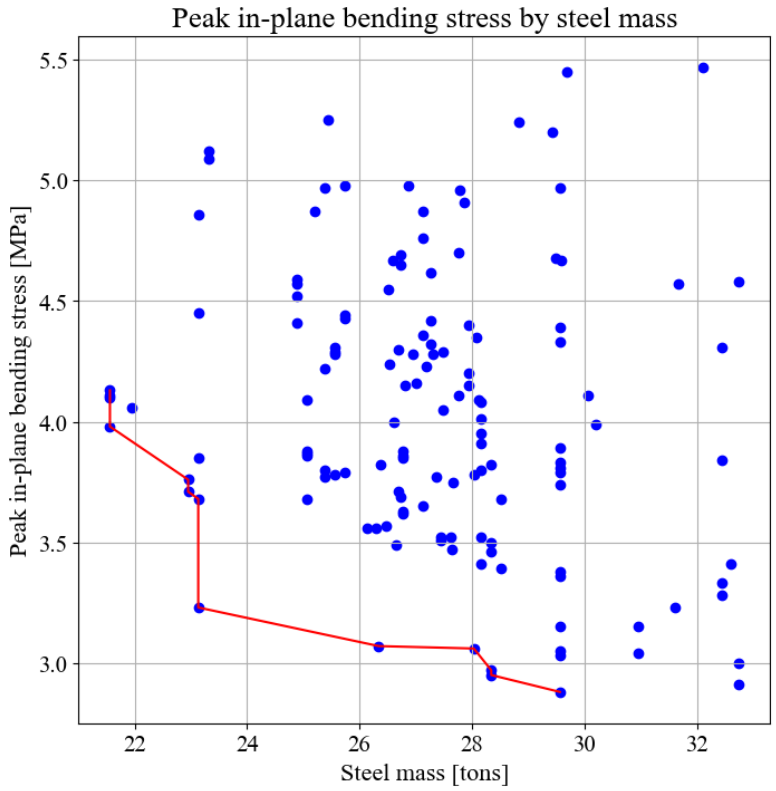

Figure B.85: 120 m span with four splices: Simulation 5, Full load

Table B.56: 120 m span with four splices: Simulation 5, Full load

Objective values		Parameter values	
Peak in-plane bending stress [MPa]	Steel mass [tons]	Number of crossbeams	Hanger angle [degrees]
2.88	29.6	22	36
2.95 - 2.97	28.3	21	35 - 36
3.07	26.3	17	35
4.06	21.9	10	39

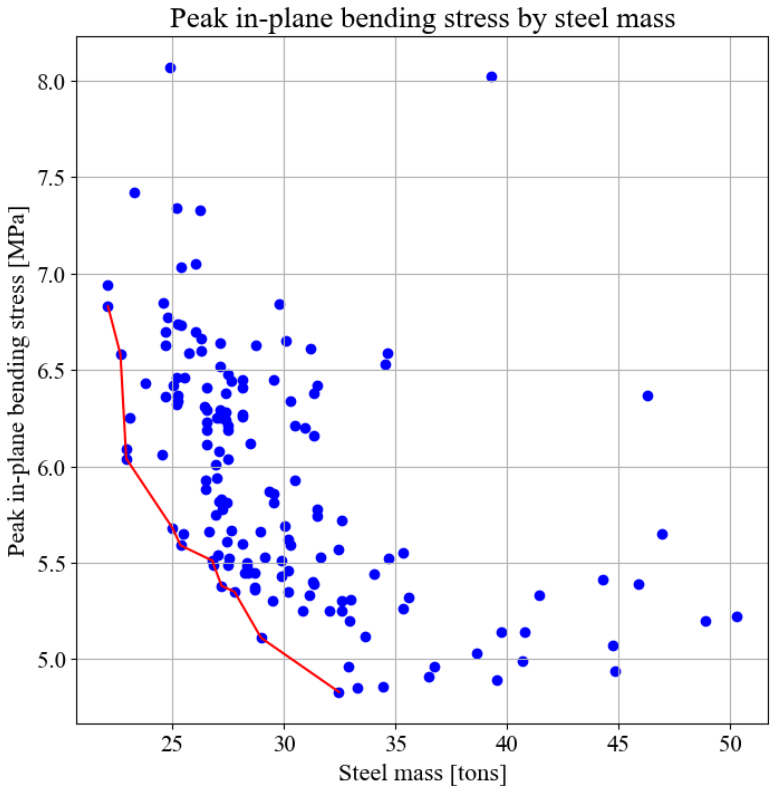

Figure B.86: 120 m span with four splices: Simulation 5, Skew load

Table B.57: 120 m span with four splices: Simulation 5, Skew load

Objective values		Parameter values	
Peak in-plane bending stress [MPa]	Steel mass [tons]	Number of crossbeams	Hanger angle [degrees]
4.83	32.5	24	52
5.45 - 5.66	28.3 - 26.6	19	48 - 45
5.49	27.5	20	47
5.59 - 5.68	25.4 - 25	13	46 - 45

Final results

Table B.58: 120 m span with four splices: Results with the final configuration from Table 4.7.

	Full load	Skew load	Governing load
Peak in-plane bending stress [MPa]	3.97	5.27	5.27
Critical design check Eq. (6.24)	0.931	0.798	0.931
Buckling load factor	2.32	2.53	2.32
Natural frequency [Hz]	0.571	0.518	0.518
Max stress 90°to grain [MPa]	3.47	3.11	3.47
% of deck exceeding Tsai-Wu criterion	7.2	2.4	7.2
Max moment in splices [kNm]	164	257	257
Number of relaxed hangers	0	6	6
Maximum displacement [mm]	283	319	319
Crossbeam utilization [%]	73.3	80.5	80.5
Hanger utilization [%]	21.6	25.3	25.5

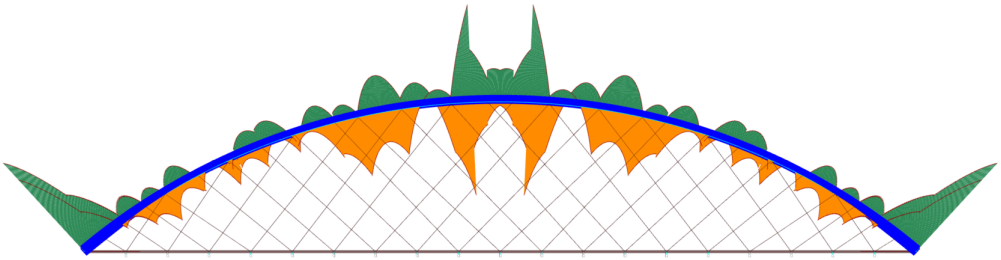

Figure B.87: 120 m span with four splices: Full load. Moment distribution in-plane with final configuration.

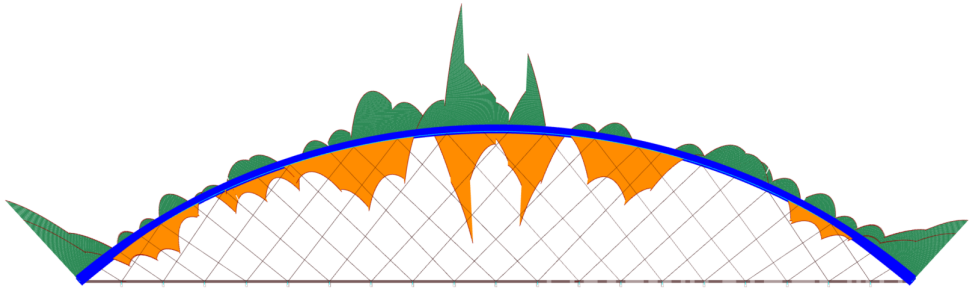

Figure B.88: 120 m span with four splices: Skew load. Moment distribution in-plane with final configuration.

B.6 100 m span with three splices and three sets of hangers

Simulation 1

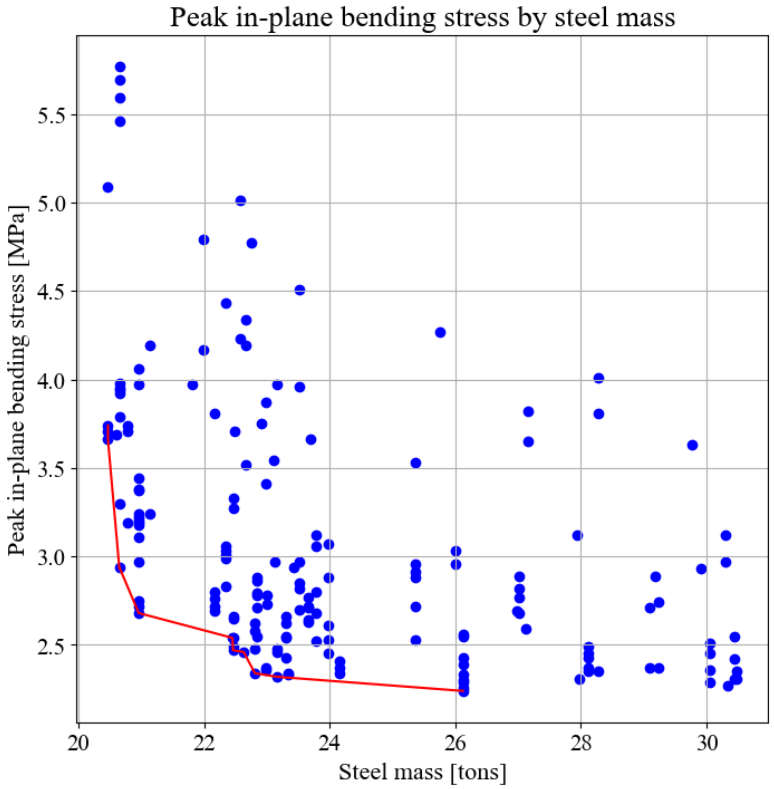

Figure B.89: 100 m span with three splices and three sets of hangers: Simulation 1, Full load

Table B.59: 100 m span with three splices and three sets of hangers: Simulation 1, Full load

Objective values		Parameter values	
Peak in-plane bending stress [MPa]	Steel mass [tons]	Number of crossbeams	Hanger angle [degrees]
2.32	23.1	14	44
2.46 - 2.58	22. 6 - 22.8	16	50 - 48
2.47 - 2.54	22.5	15	47 - 49
2.68 - 2.75	21	11	50 - 52

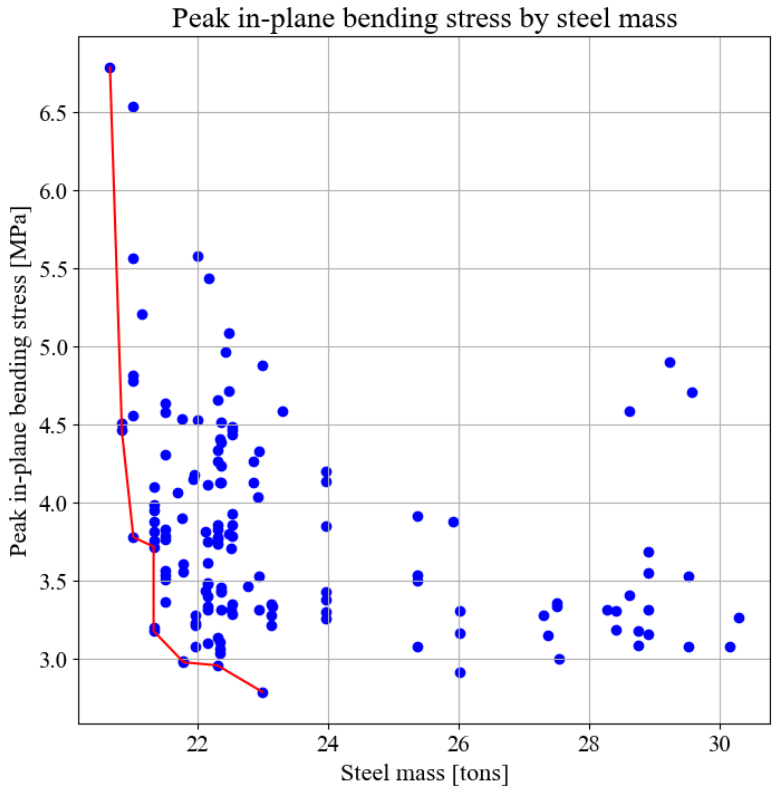

Figure B.90: 100 m span with three splices and three sets of hangers: Simulation 1, Skew load

Table B.60: 100 m span with three splices and three sets of hangers: Simulation 1, Skew load

Objective values		Parameter values	
Peak in-plane bending stress [MPa]	Steel mass [tons]	Number of crossbeams	Hanger angle [degrees]
2.79	21	16	50
2.98 - 3.08	21.8 - 22	15	51 - 52
3.78 - 4.51	21 - 20.8	10	53 - 52
6.54 - 6. 79	21 - 21.7	10	67 - 68

Simulation 2

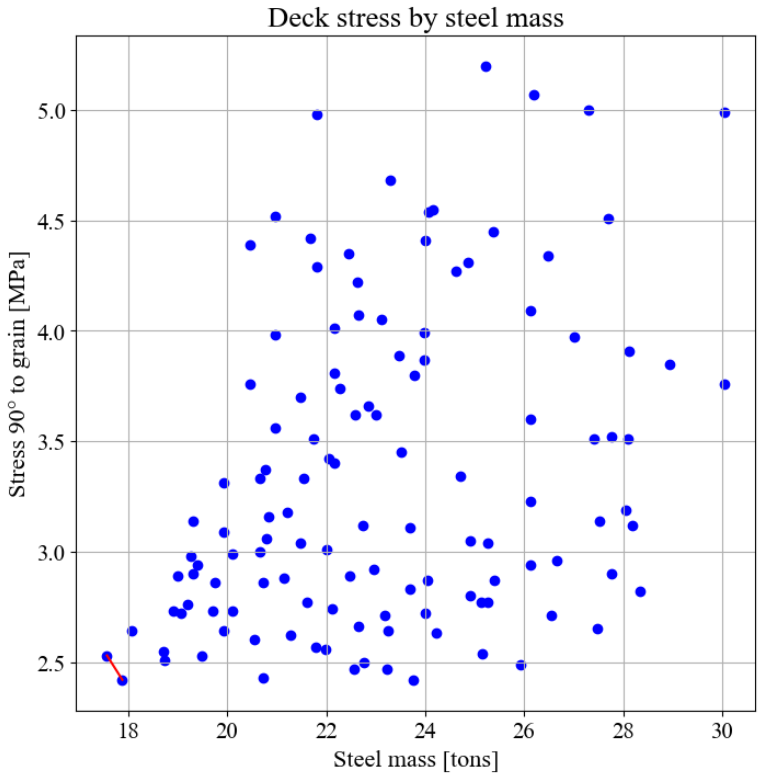

Figure B.91: 100 m span with three splices and three sets of hangers: Simulation 2, Full load

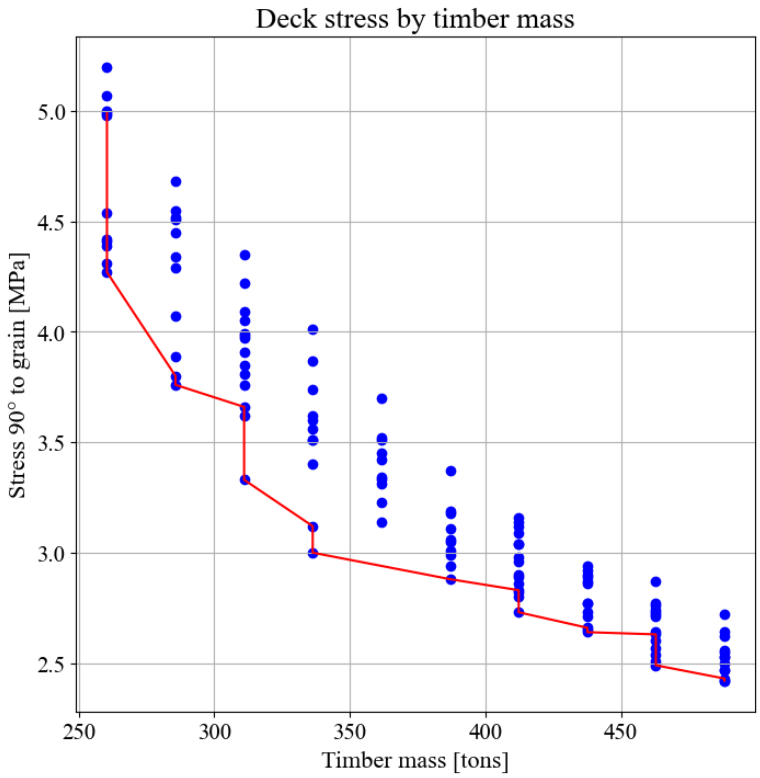

Figure B.92: 100 m span with three splices and three sets of hangers: Simulation 2, Full load

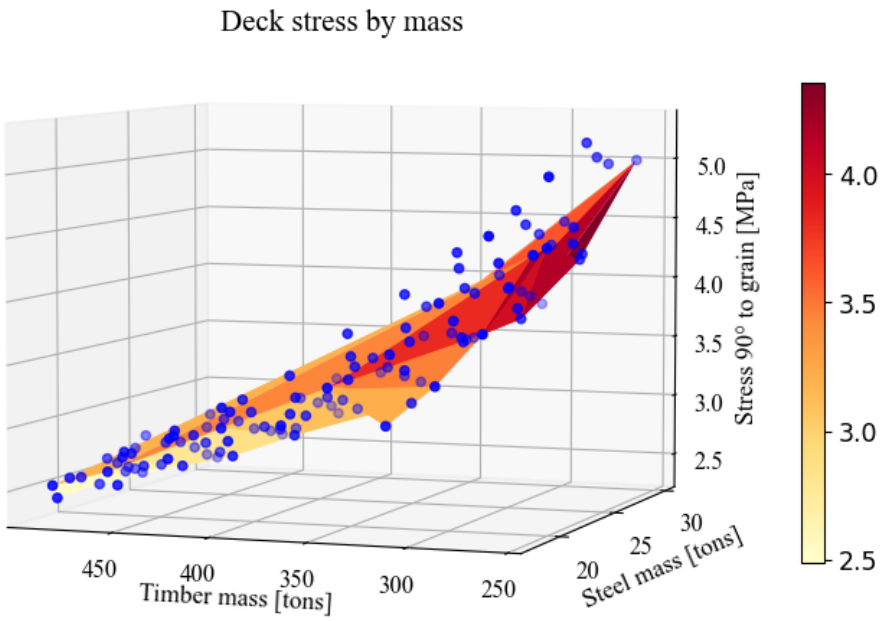

Figure B.93: 100 m span with three splices and three sets of hangers: Simulation 2, Full load

Table B.61: 100 m span with three splices and three sets of hangers: Simulation 2, Full load

Objective values			Parameter values	
Stress 90° to grain [MPa]	Steel mass [tons]	Timber mass [tons]	Number of crossbeams	Deck thickness [mm]
2.53 - 2.88	17.6 - 21.1	488 - 387	11	750 - 550
3.12	22.7	336	15	450
3.33 - 3.76	20.7 - 20.5	311 - 286	10	400 - 350
3.62	23	311	14	400

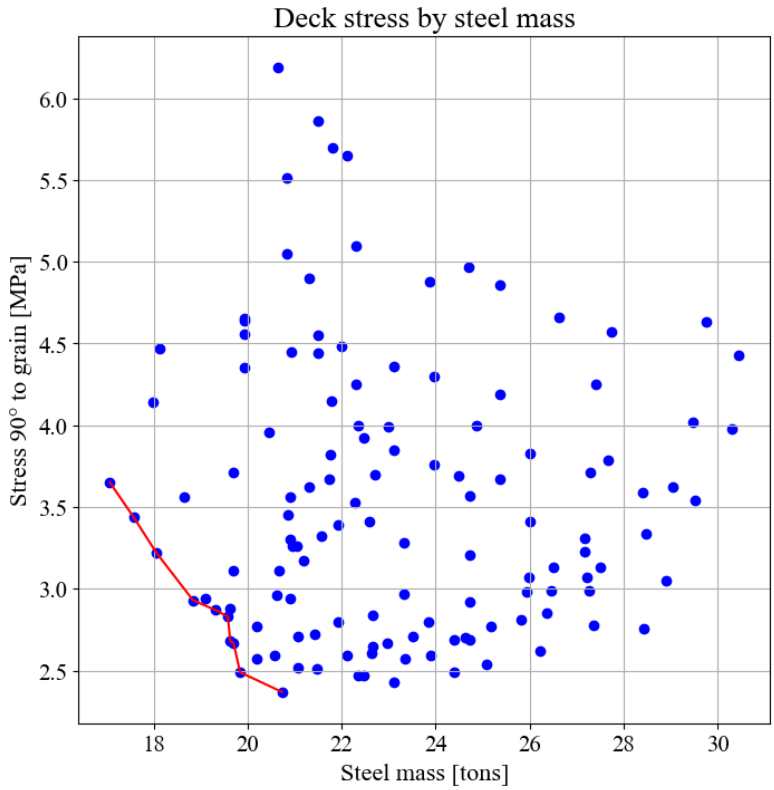

Figure B.94: 100 m span with three splices and three sets of hangers: Simulation 2, Skew load

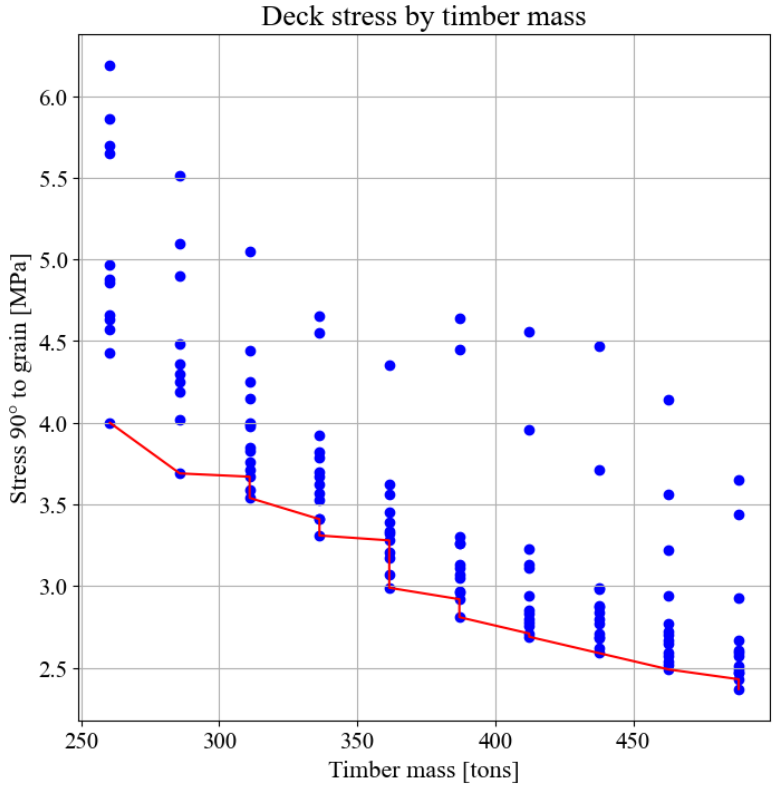

Figure B.95: 100 m span with three splices and three sets of hangers: Simulation 2, Skew load

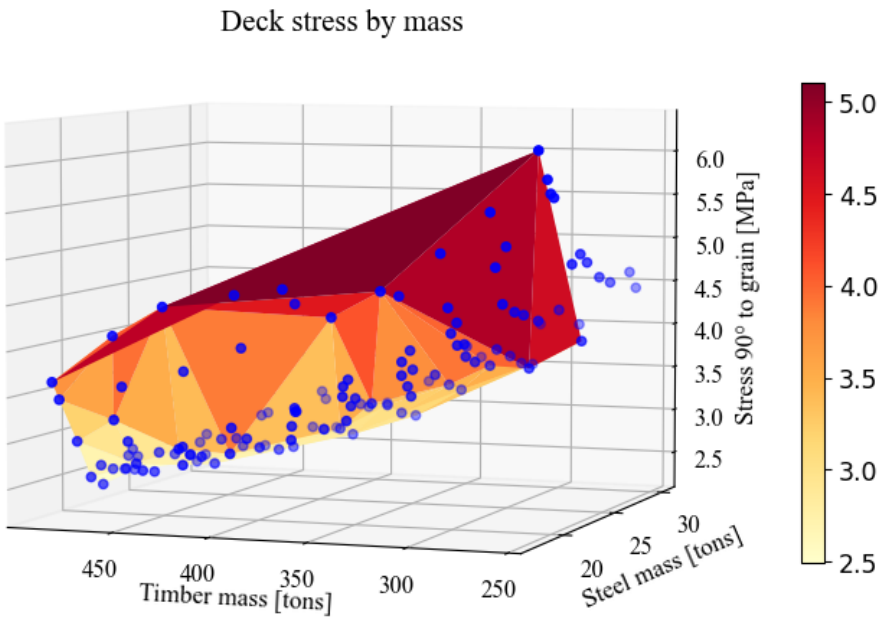

Figure B.96: 100 m span with three splices and three sets of hangers: Simulation 2, Skew load

Table B.62: 100 m span with three splices and three sets of hangers: Simulation 2, Skew load

Objective values			Parameter values	
Stress 90° to grain [MPa]	Steel mass [tons]	Timber mass [tons]	Number of crossbeams	Deck thickness [mm]
2.59 - 3.41	22.1 - 22.6	438 - 336	17	650 - 450
2.96	20.6	387	15	550
3.17 - 3.69	21.2 - 24.5	362 - 286	16	500 - 350
3.76	24	311	18	400

Simulation 3

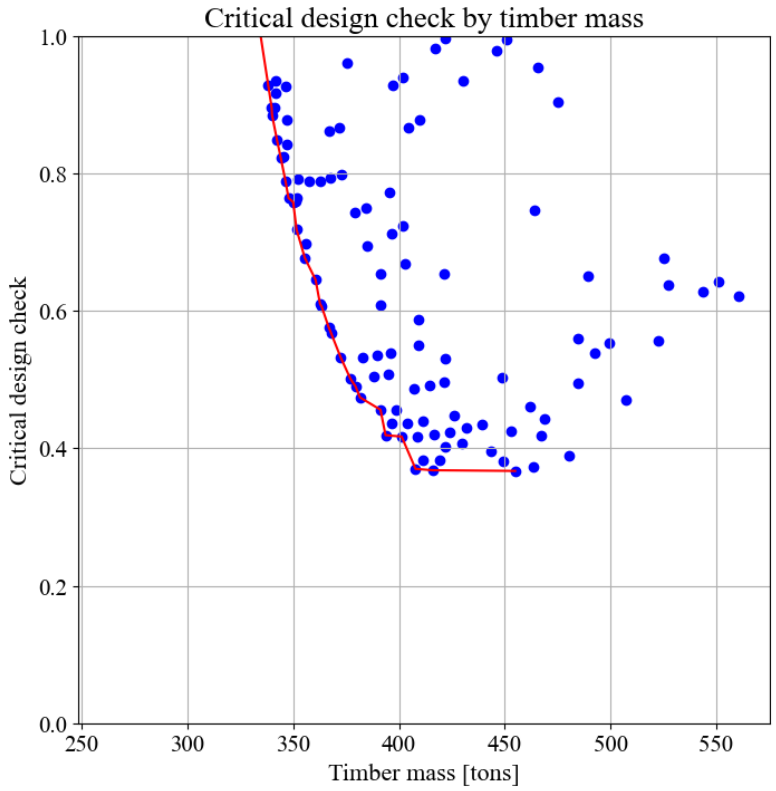

Figure B.97: 100 m span with three splices and three sets of hangers: Simulation 3, Full load

Table B.63: 100 m span with three splices and three sets of hangers: Simulation 3, Full load

Objective values		Parameter values	
Critical design check [0, 1]	Timber mass [tons]	Arch height [mm]	Arch width [mm]
0.849	342	700	1400
0.896	340	750	1300
0.927	347	1000	1100
0.934	342	900	1150

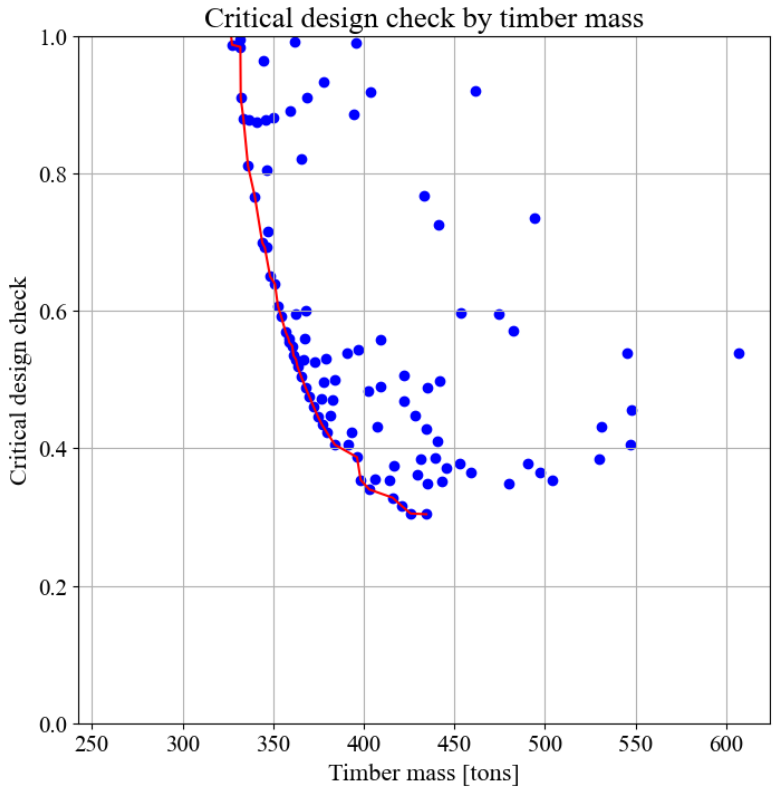

Figure B.98: 100 m span with three splices and three sets of hangers: Simulation 3, Skew load

Table B.64: 100 m span with three splices and three sets of hangers: Simulation 3, Skew load

Objective values		Parameter values	
Critical design check [0, 1]	Timber mass [tons]	Arch height [mm]	Arch width [mm]
0.699	344	750	1350
0.766	340	650	1450
0.804	347	1000	1100
0.995	331	950	1000

Simulation 4

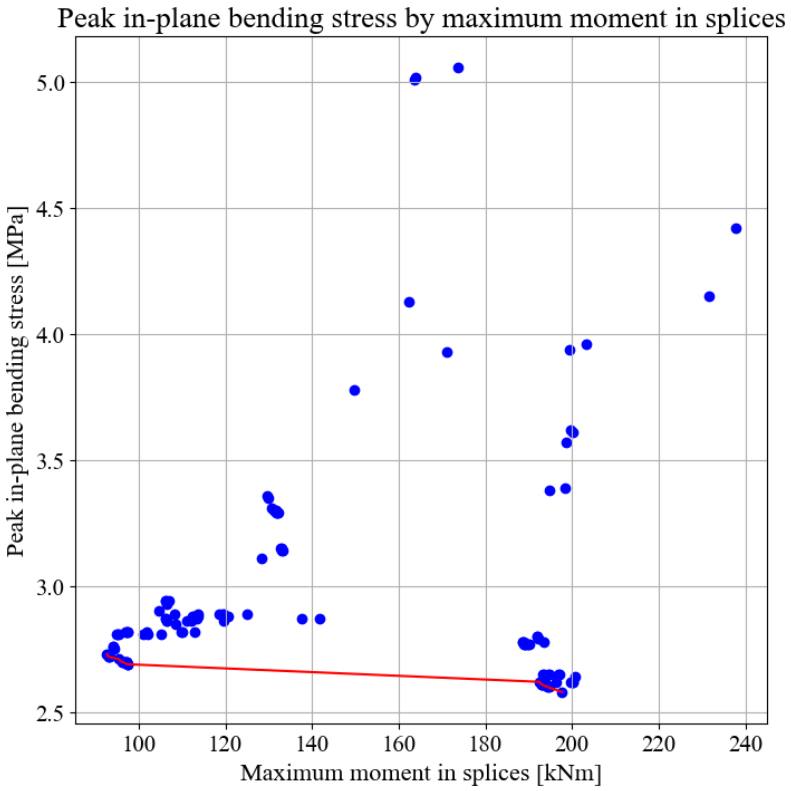

Figure B.99: 100 m span with three splices and three sets of hangers: Simulation 4, Full load

Table B.65: 100 m span with three splices and three sets of hangers: Simulation 4, Full load

Objective values			Parameter values	
Maximum moment in splices [kNm]	Peak in-plane bending stress [MPa]	Hangers in compression	Connection placement [0, 1]	Hanger angle [degrees]
92.7 - 94.4	2.73 - 2.75	6	0.5 - 0.6	40
95.2	2.81	6	0.2	42
96.4 - 97.4	2.7	6	0.8 - 0.2	41
193 - 194	2.6	8	0.7 - 0.8	48

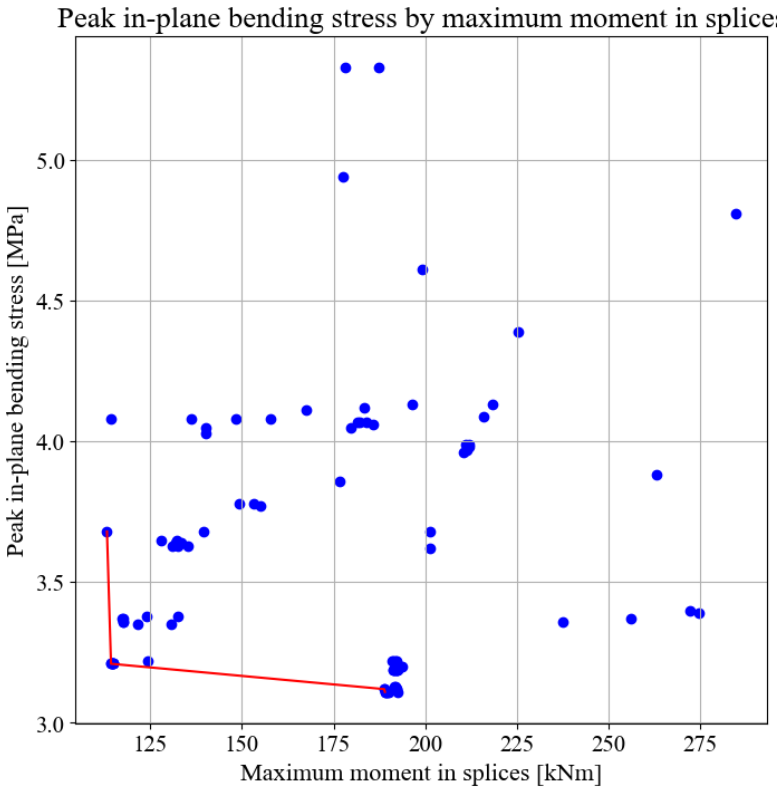

Figure B.100: 100 m span with three splices and three sets of hangers: Simulation 4, Skew load

Table B.66: 100 m span with three splices and three sets of hangers: Simulation 4, Skew load

Objective values			Parameter values	
Maximum moment in splices [kNm]	Peak in-plane bending stress [MPa]	Hangers in compression	Connection placement [0, 1]	Hanger angle [degrees]
113	3.68	21	0	45
114 - 124	3.2	16	0.7 - 0.8	52
189	3.12 - 3.11	15	0.8 - 0.5	50
192	3.12	16	0.8	51

Simulation 5

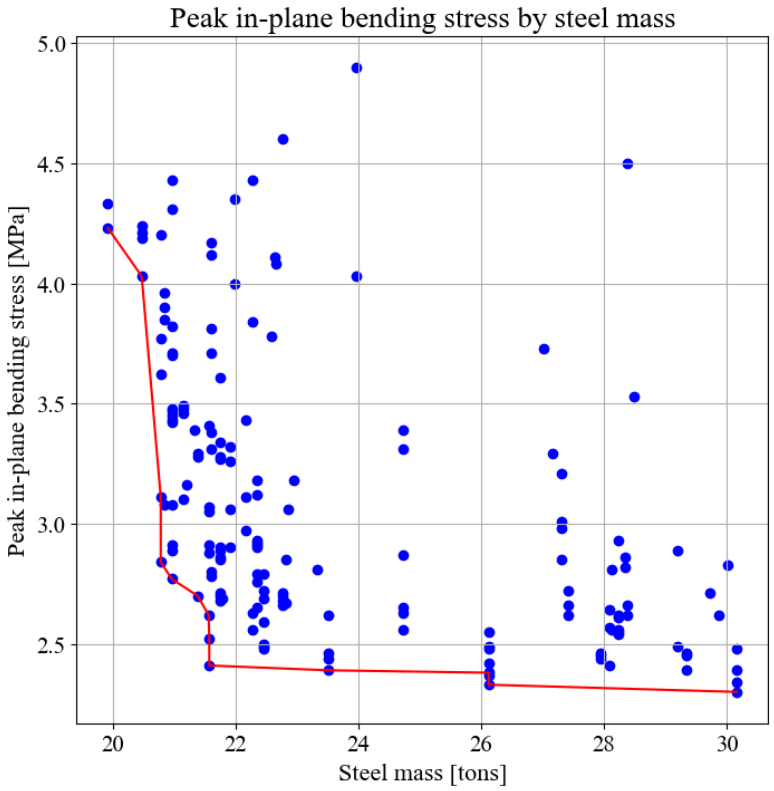

Figure B.101: 100 m span with three splices and three sets of hangers: Simulation 5, Full load

Table B.67: 100 m span with three splices and three sets of hangers: Simulation 5, Full load

Objective values		Parameter values	
Peak in-plane bending stress [MPa]	Steel mass [tons]	Number of crossbeams	Hanger angle [degrees]
2.33 - 2.42	26.1	20	43 - 44
2.39 - 2.44	23.5	18	41 - 42
2.62 - 2.7	21.6 - 21.4	15	41 - 47
4.03 - 4.23	20.5 - 20	10	54 - 56

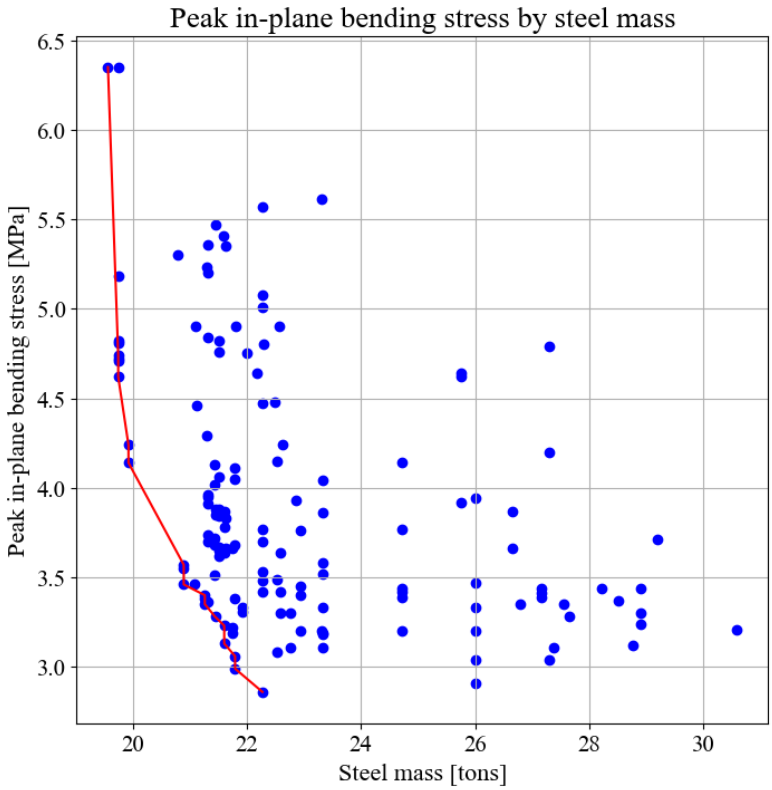

Figure B.102: 100 m span with three splices and three sets of hangers: Simulation 5, Skew load

Table B.68: 100 m span with three splices and three sets of hangers: Simulation 5, Skew load

Objective values		Parameter values	
Peak in-plane bending stress [MPa]	Steel mass [tons]	Number of crossbeams	Hanger angle [degrees]
2.86	22.3	16	50
3.13 - 3.23	21.6	15	51 - 52
3.28 - 3.4	21.4 - 21.3	13	51 - 54
4.14 - 4.62	19.9 - 19.7	10	43 - 40

Final results

Table B.69: 100 m span with three splices and three sets of hangers: Results with the final configuration from Table 4.7.

	Full load	Skew load	Governing load
Peak in-plane bending stress [MPa]	2.95	3.15	3.15
Critical design check Eq. (6.24)	0.877	0.739	0.877
Buckling load factor	2.55	2.88	2.55
Natural frequency [Hz]	0.781	0.795	0.781
Max stress 90°to grain [MPa]	2.79	3.27	3.27
% of deck exceeding Tsai-Wu criterion	1.7	0.37	1.7
Max moment in splices [kNm]	127	115	127
Number of relaxed hangers	6	15	15
Maximum displacement [mm]	241	241	241
Crossbeam utilization [%]	82.0	76.6	82.0
Hanger utilization [%]	28.8	27.1	28.8

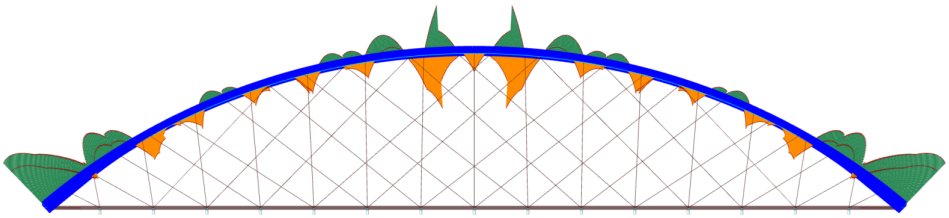

Figure B.103: 100 m span with three splices and three sets of hangers: Full load. Moment distribution in-plane with final configuration.

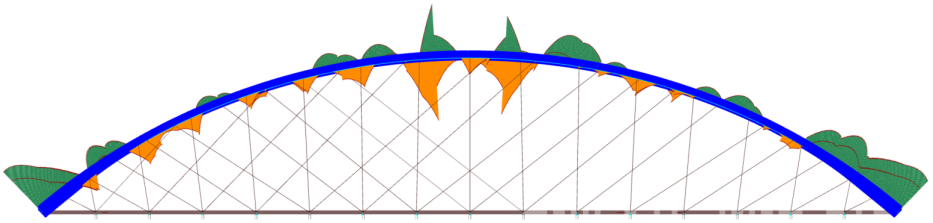

Figure B.104: 100 m span with three splices and three sets of hangers: Skew load. Moment distribution in-plane with final configuration.

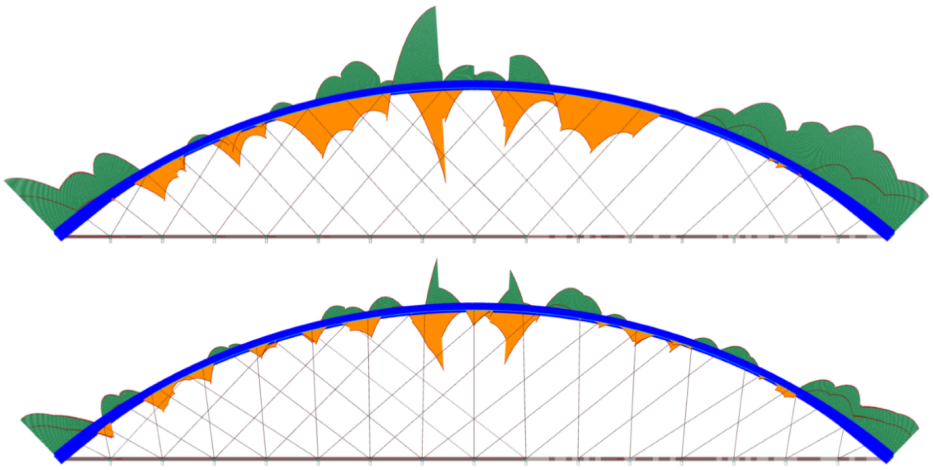

Figure B.105: 100 m span with three splices vs. 100 m span with three splices and three sets of hangers: Skew load. Moment distribution in-plane with final configurations.

Adjusting joint stiffness for top- and side beams

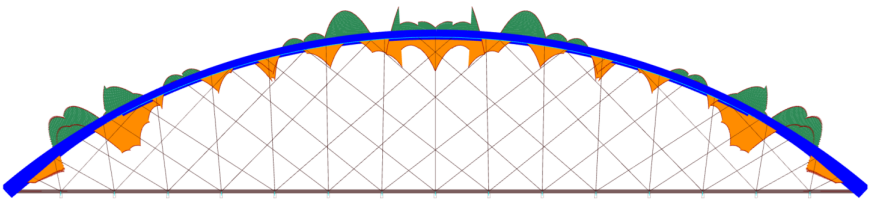

Figure B.106: 100 m span with three splices and three sets of hangers: Full load. Moment distribution in-plane with final configuration with rotational joint stiffness in top- and side-beams set to 280 kNm/rad and Max. arch height equal to 1500 mm.

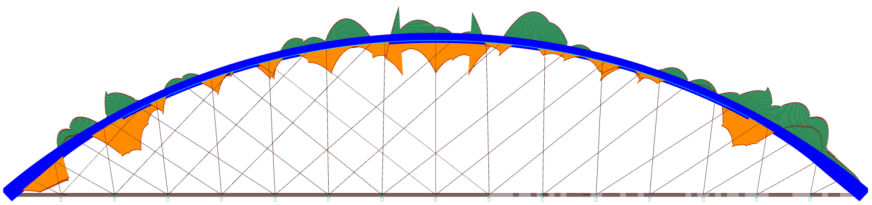

Figure B.107: 100 m span with three splices and three sets of hangers: Skew load. Moment distribution in-plane with final configuration with rotational joint stiffness in top- and side-beams set to 280 kNm/rad and Max. arch height equal to 1500 mm.

B.7 100 m span with three splices and triangular corners

Simulation 1

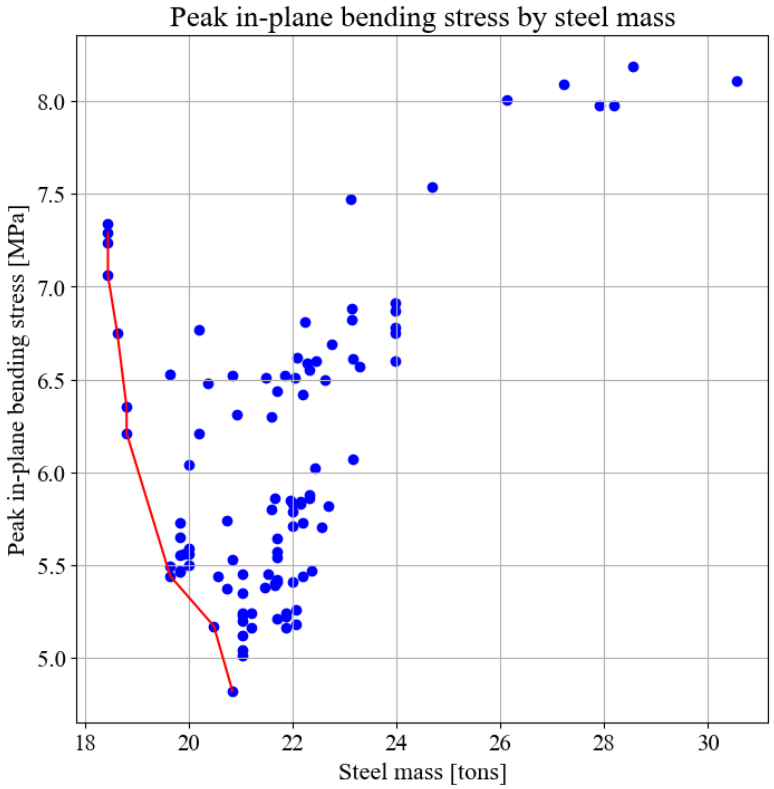

Figure B.108: 100 m span with three splices and triangular corners: Simulation 1, Full load

Table B.70: 100 m span with three splices and triangular corners: Simulation 1, Full load

Objective values		Parameter values	
Peak in-plane bending stress [MPa]	Steel mass [tons]	Number of crossbeams	Hanger angle [degrees]
4.8	20.8	12	54 - 55
5.17	20.5	12	47
5.37	20.2	11	57
5.44	19.6	11	43

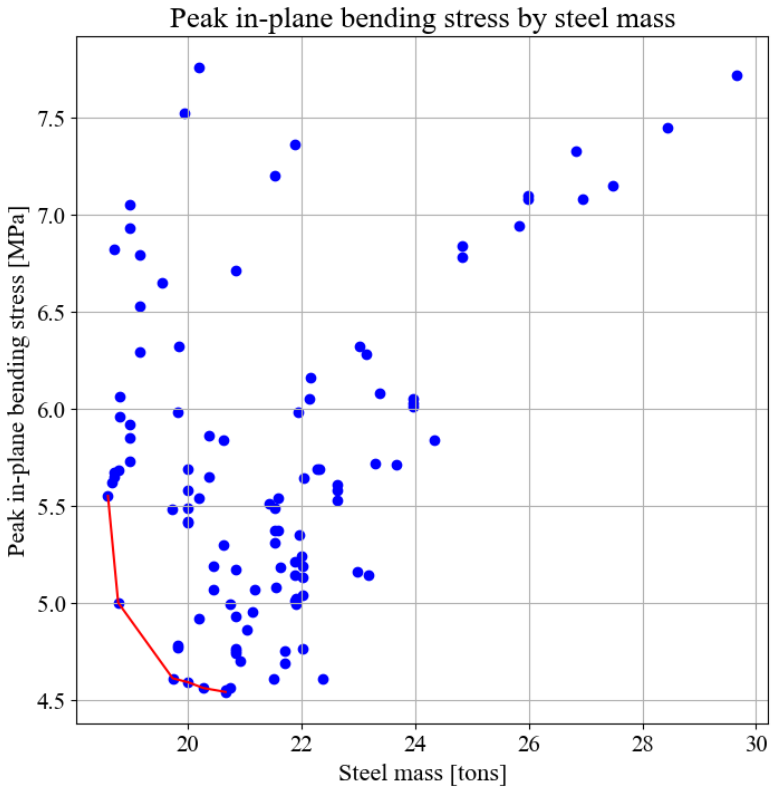

Figure B.109: 100 m span with three splices and triangular corners: Simulation 1, Skew load

Table B.71: 100 m span with three splices and triangular corners: Simulation 1, Skew load

Objective values		Parameter values	
Peak in-plane bending stress [MPa]	Steel mass [tons]	Number of crossbeams	Hanger angle [degrees]
4.54	20.7	12	46
4.56 - 4.61	20.3 - 19.7	12	55 - 54
4.59	20	11	55
5.17 - 5.62	18.9	10	57 - 58

Simulation 2

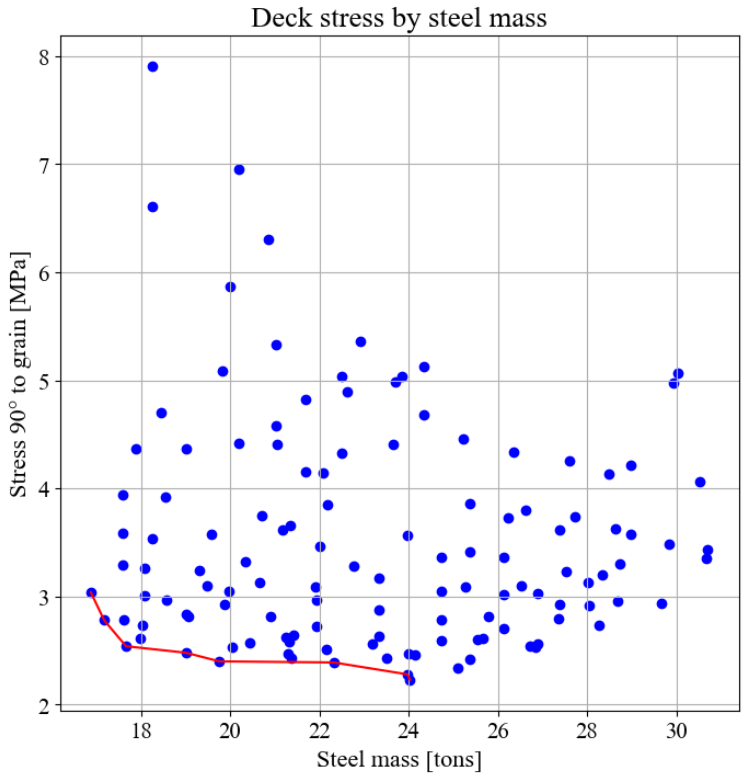

Figure B.110: 100 m span with three splices and triangular corners: Simulation 2, Full load

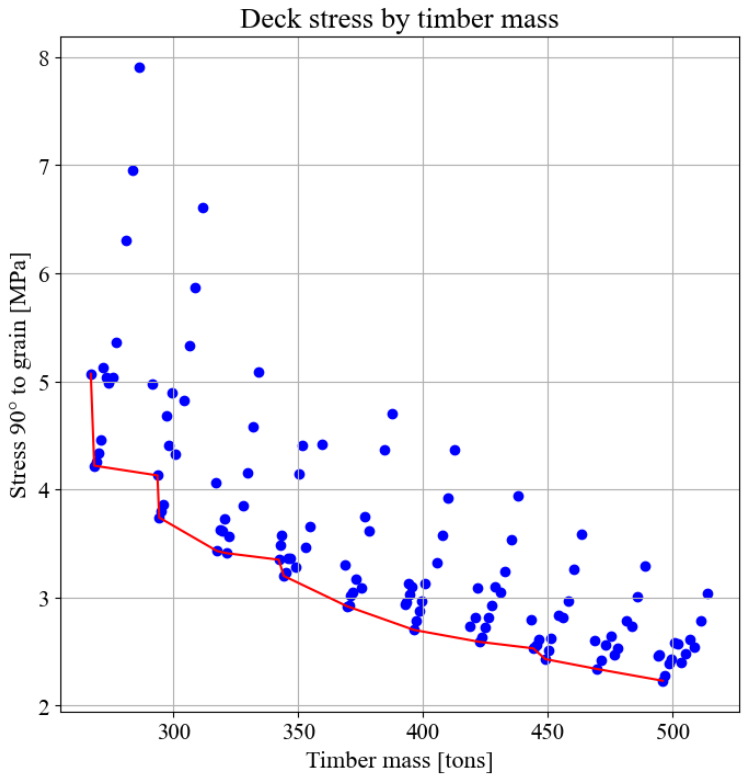

Figure B.111: 100 m span with three splices and triangular corners: Simulation 2, Full load

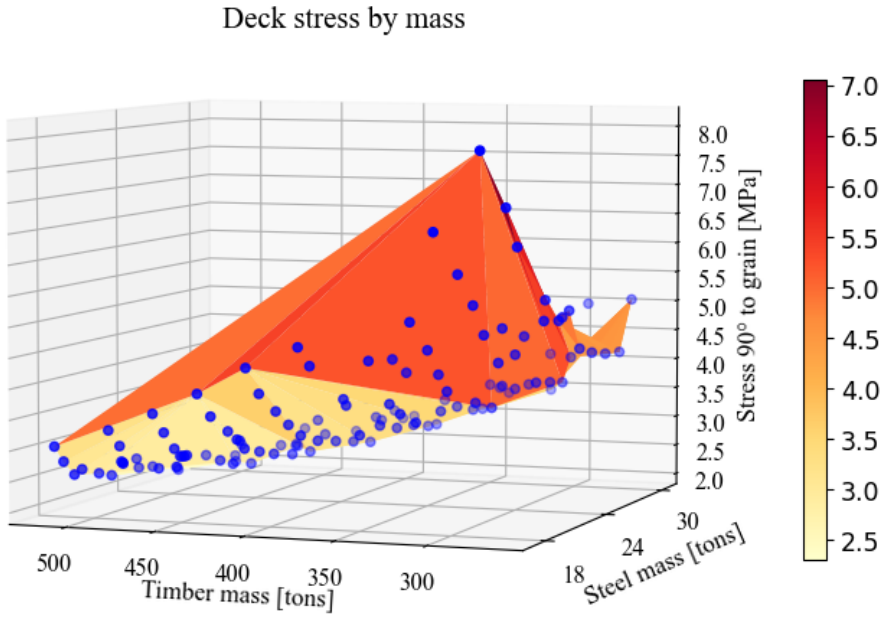

Figure B.112: 100 m span with three splices and triangular corners: Simulation 2, Full load

Table B.72: 100 m span with three splices and triangular corners: Simulation 2, Full load

Objective values			Parameter values	
Stress 90° to grain [MPa]	Steel mass [tons]	Timber mass [tons]	Number of crossbeams	Deck thickness [mm]
3.09	21.9	375	16	500
3.56 - 3.57 - 4.68	23.4 - 24 - 24.3	348 - 322 - 297	18	450 - 400 - 350
3.86	25.4	296	19	350
4.33 - 5.04	22.5	301 - 276	15	350 - 300

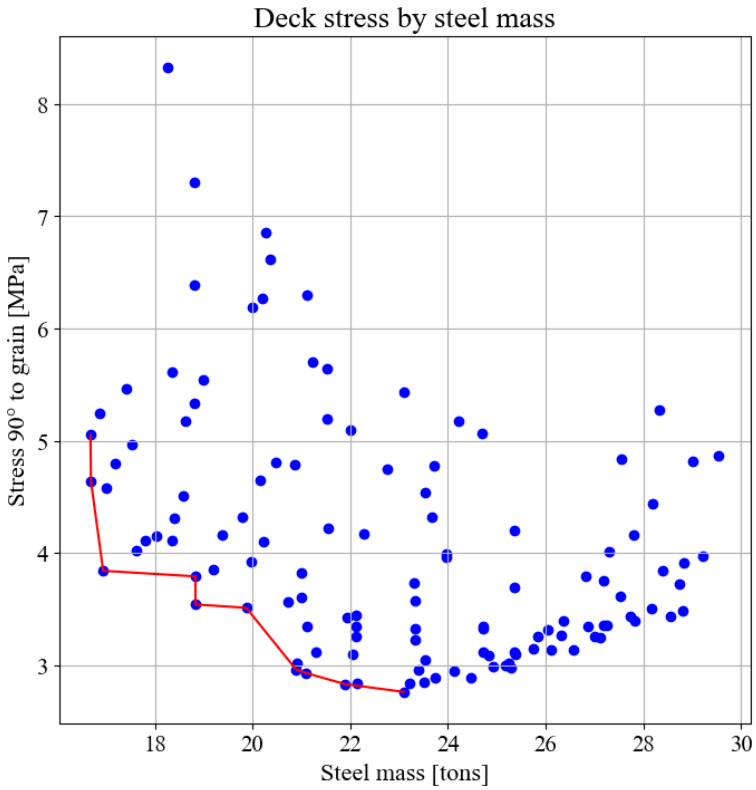

Figure B.113: 100 m span with three splices and triangular corners: Simulation 2, Skew load

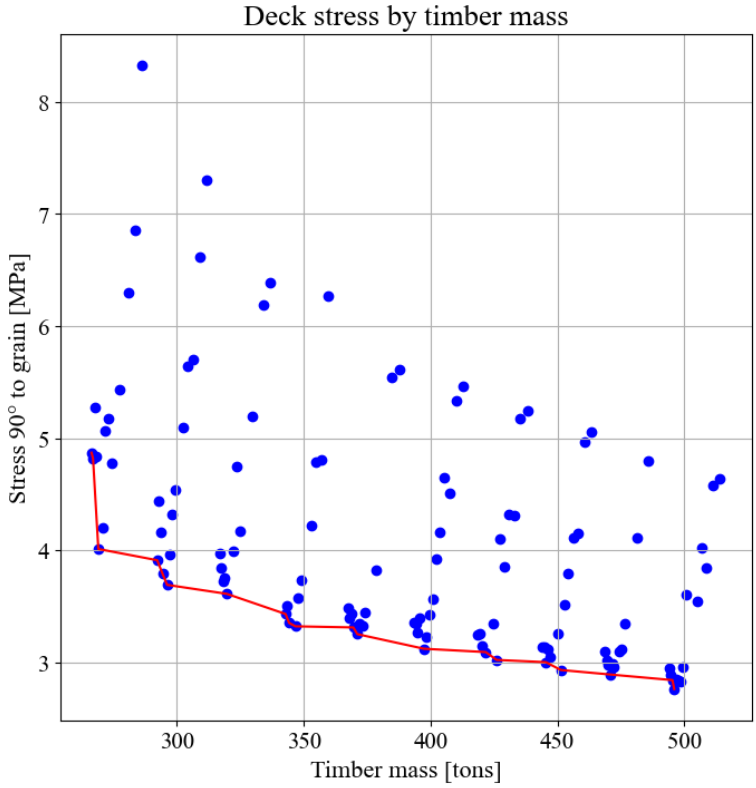

Figure B.114: 100 m span with three splices and triangular corners: Simulation 2, Skew load

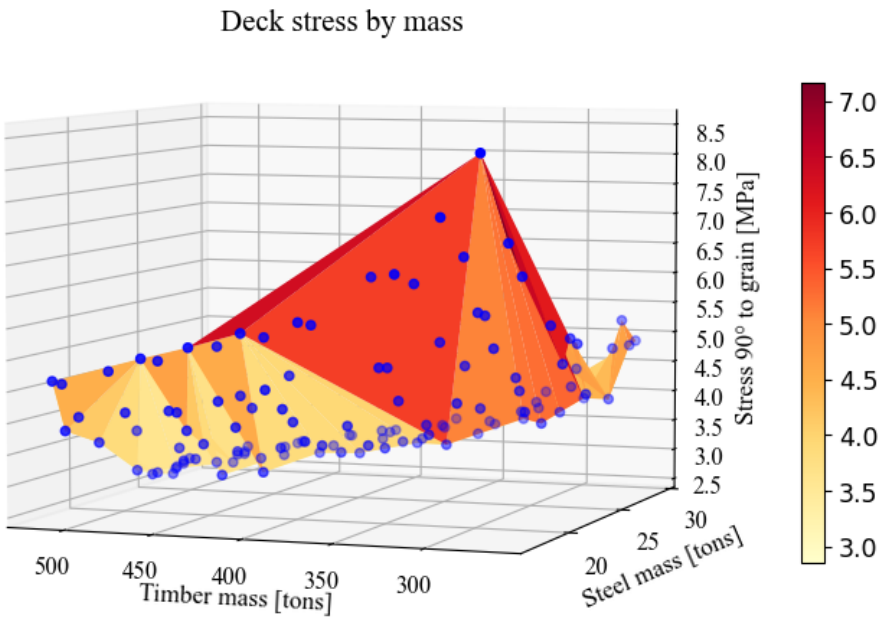

Figure B.115: 100 m span with three splices and triangular corners: Simulation 2, Skew load

Table B.73: 100 m span with three splices and triangular corners: Simulation 2, Skew load

Objective values			Parameter values	
Stress 90° to grain [MPa]	Steel mass [tons]	Timber mass [tons]	Number of crossbeams	Deck thickness [mm]
3.44	22.1	374	27	500
3.96 - 3.99	24	297 - 322	18	350 - 400
4.17	22.3	335	16	400
4.2	25.4	271	19	300

Simulation 3

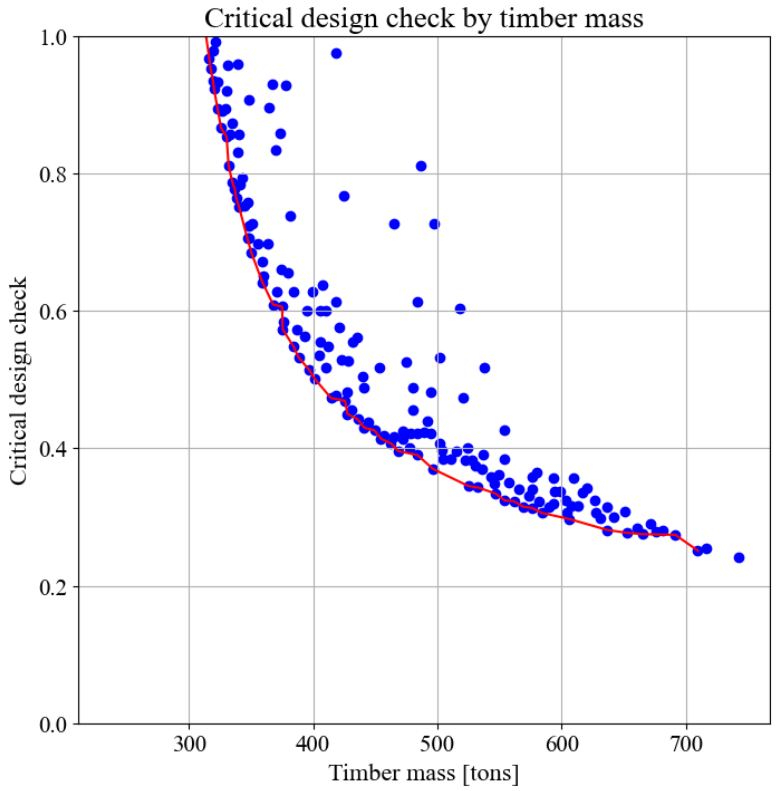

Figure B.116: 100 m span with three splices and triangular corners: Simulation 3, Full load

Table B.74: 100 m span with three splices and triangular corners: Simulation 3, Full load

Objective values		Parameter values	
Critical design check [0, 1]	Timber mass [tons]	Arch height [mm]	Arch width [mm]
0.866 - 0.894	326 - 323	550	2000 - 1950
0.924	320	550	1900
0.934	320	600	1700
0.967	316	600	1650

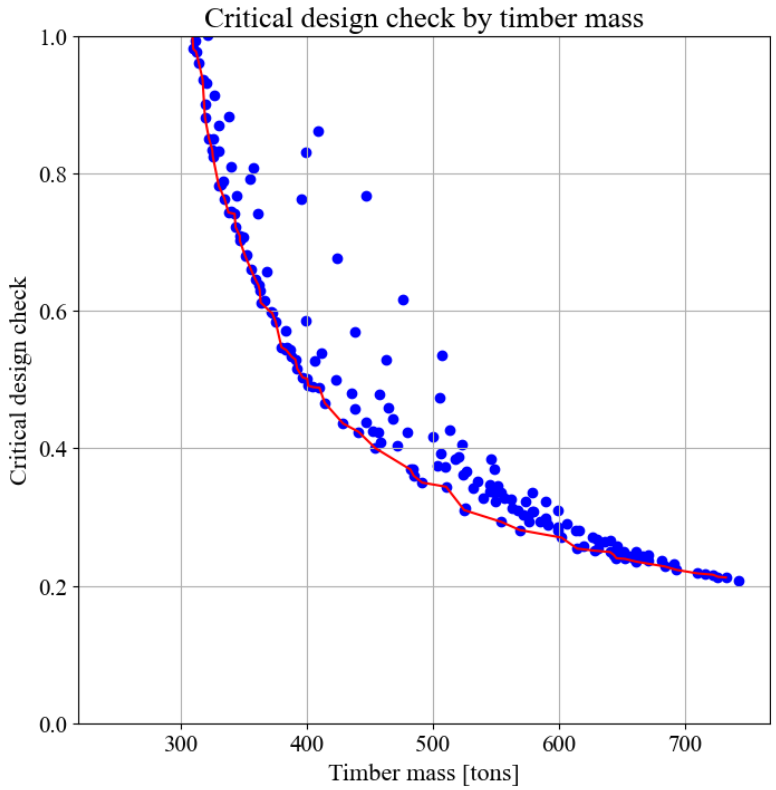

Figure B.117: 100 m span with three splices and triangular corners: Simulation 3, Skew load

Table B.75: 100 m span with three splices and triangular corners: Simulation 3, Skew load

Objective values		Parameter values	
Critical design check [0, 1]	Timber mass [tons]	Arch height [mm]	Arch width [mm]
0.851 - 0.881	323 - 320	600	1750 - 1700
0.932	320	650	1550
0.937	318	750	1250
0.981	310	600	1550

Simulation 4

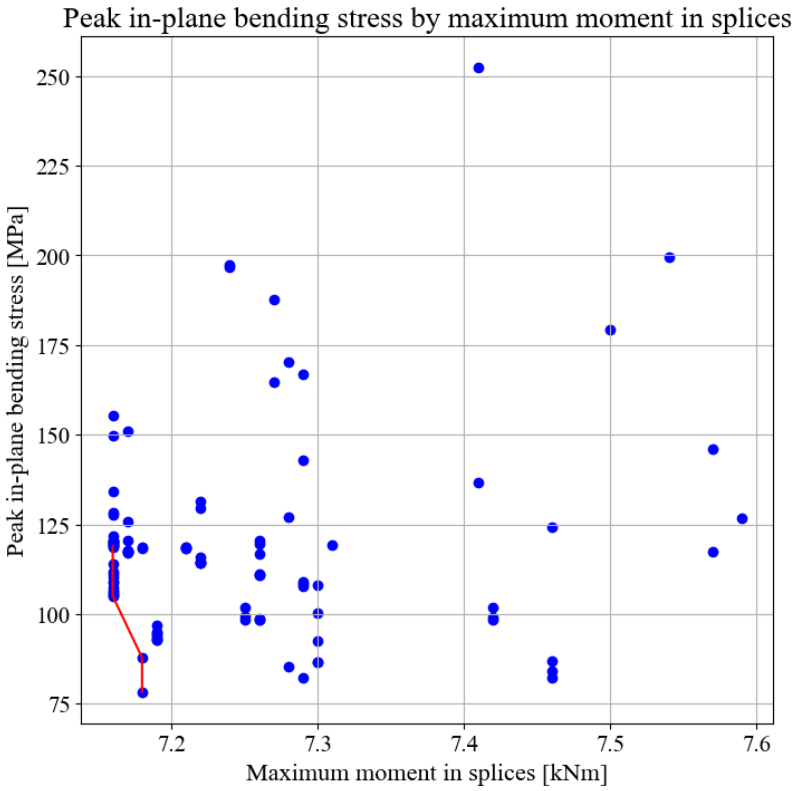

Figure B.118: 100 m span with three splices and triangular corners: Simulation 4, Full load

Table B.76: 100 m span with three splices and triangular corners: Simulation 4, Full load

Objective values			Parameter values	
Maximum moment in splices [kNm]	Peak in-plane bending stress [MPa]	Hangers in compression	Connection placement [0, 1]	Hanger angle [degrees]
78	7.18	2	0.9	44
82	7.29	0	0.3	51 - 53
93 - 97	7.19	0	0.3 - 0.9	46
105 - 112	7.16	2	0.2 - 1	41

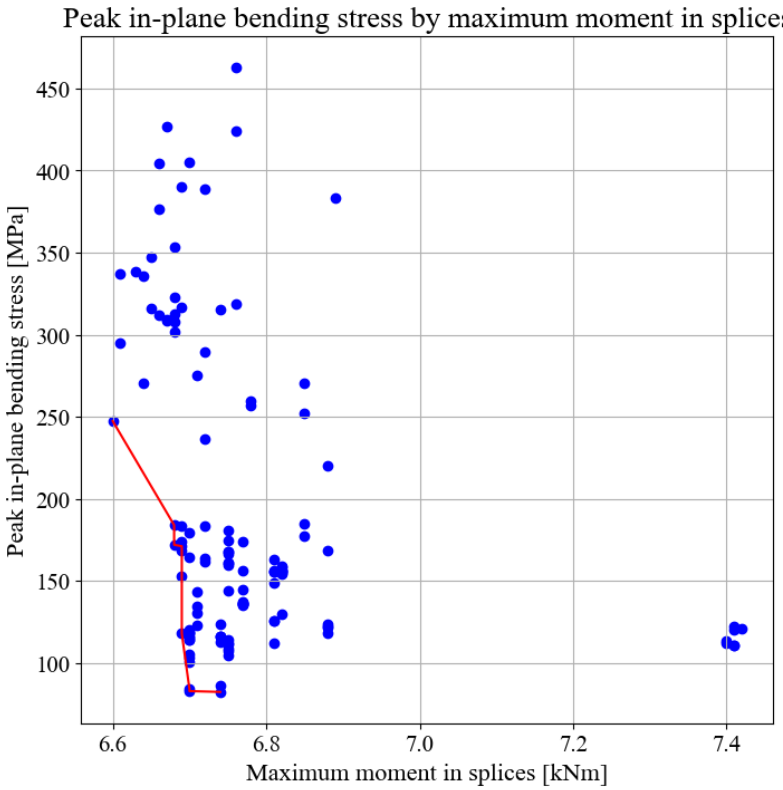

Figure B.119: 100 m span with three splices and triangular corners: Simulation 4, Skew load

Table B.77: 100 m span with three splices and triangular corners: Simulation 4, Skew load

Objective values			Parameter values	
Maximum moment in splices [kNm]	Peak in-plane bending stress [MPa]	Hangers in compression	Connection placement [0, 1]	Hanger angle [degrees]
82 - 86	6.74	10	0.9 - 0.8	44
84 - 101	6.7	9	0.9 - 0.6	45
118	6.69	6	0.4	49
247	6.6	4	0	56

Simulation 5

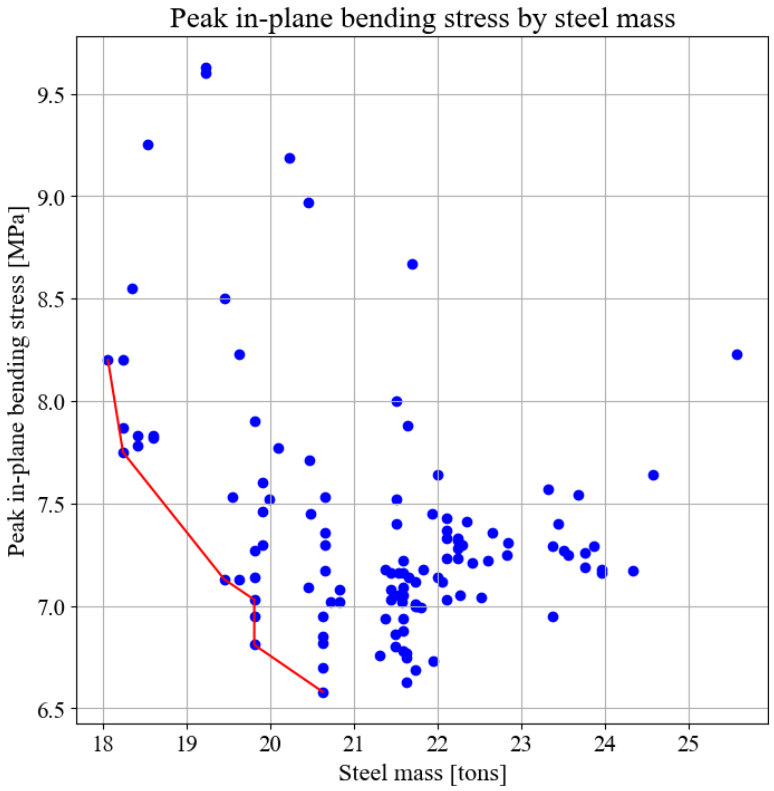

Figure B.120: 100 m span with three splices and triangular corners: Simulation 5, Full load

Table B.78: 100 m span with three splices and triangular corners: Simulation 5, Full load

Objective values		Parameter values	
Peak in-plane bending stress [MPa]	Steel mass [tons]	Number of crossbeams	Hanger angle [degrees]
6.58	20.6	12	53
6.81 - 7.27	19.8	11	53 - 46
7.18	24	18	44
7.75	18.2	10	46

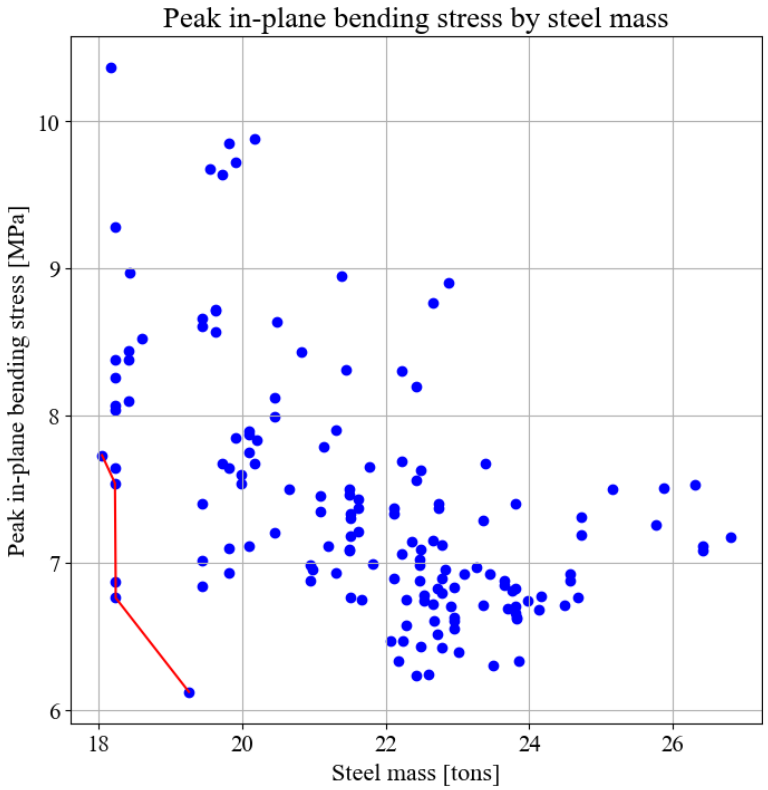

Figure B.121: 100 m span with three splices and triangular corners: Simulation 5, Skew load

Table B.79: 100 m span with three splices and triangular corners: Simulation 5, Skew load

Objective values		Parameter values	
Peak in-plane bending stress [MPa]	Steel mass [tons]	Number of crossbeams	Hanger angle [degrees]
6.12 - 6.84	19.3	11	54 - 55
6.72 - 6.87	18.2	10	51 - 50
6.74	24	18	44
6.88	21	13	43

Final results

Table B.80: 100 m span with three splices and triangular corners: Results with the final configuration from Table 4.7.

	Full load	Skew load	Governing load
Peak in-plane bending stress [MPa]	6.50	5.88	6.50
Critical design check Eq. (6.24)	0.943	0.837	0.943
Buckling load factor	3.30	3.58	3.30
Natural frequency [Hz]	0.925	0.816	0.816
Max stress 90°to grain [MPa]	4.80	5.21	5.21
% of deck exceeding Tsai-Wu criterion	7.4	3.3	7.4
Max moment in splices [kNm]	76	91	91
Number of relaxed hangers	2	7	7
Maximum displacement [mm]	203	230	230
Crossbeam utilization [%]	69.5	77.9	77.9
Hanger utilization [%]	28.6	34.4	34.4

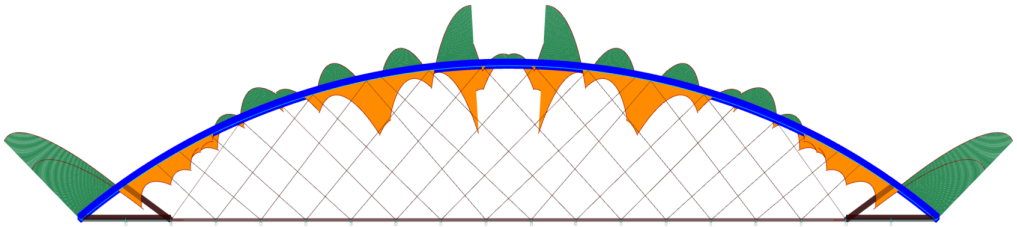

Figure B.122: 100 m span with three splices and triangular corners: Full load. Moment distribution in-plane with final configuration.

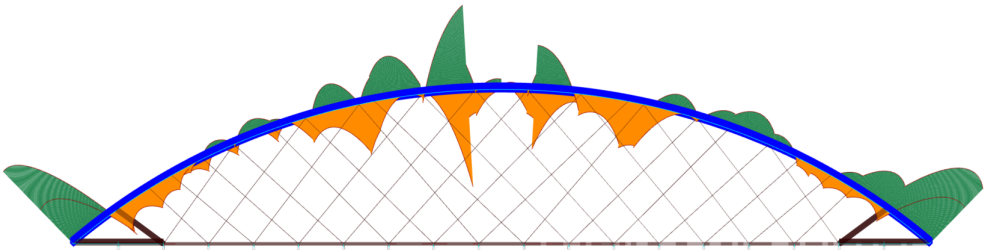

Figure B.123: 100 m span with three splices and triangular corners: Skew load. Moment distribution in-plane with final configuration.

B.8 100 m span with three splices and vertical arches

Simulation 1

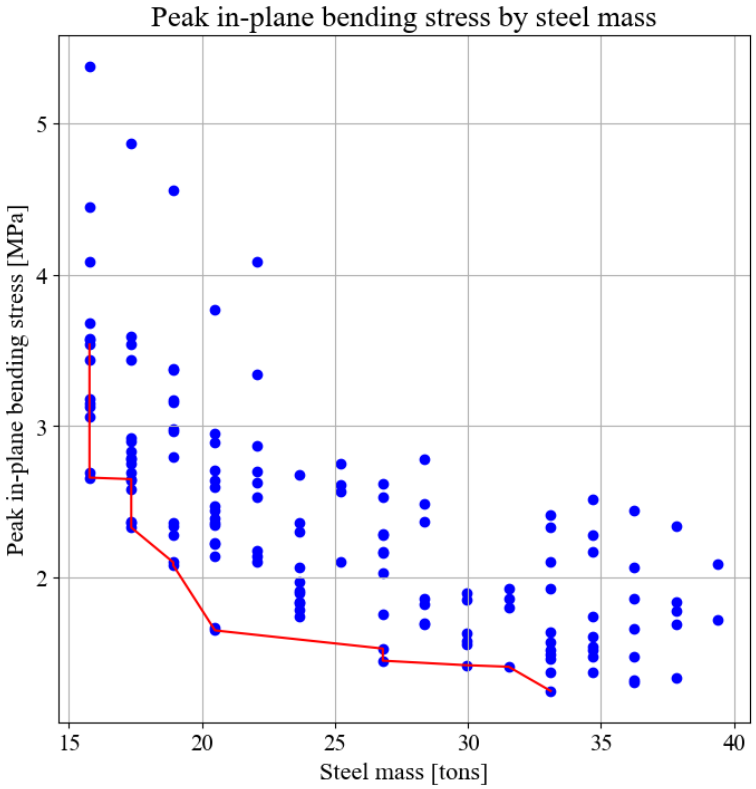

Figure B.124: 100 m span with three splices and vertical arches: Simulation 1, Full load

Table B.81: 100 m span with three splices and vertical arches: Simulation 1, Full load

Objective values		Parameter values	
Peak in-plane bending stress [MPa]	Steel mass [tons]	Number of crossbeams	Hanger angle [degrees]
1.25 - 1.37	33.1	21	35 - 37
1.74 - 1.79	23.7	15	38 - 39
2.1 - 2.18	22.1	14	36 - 39
2.1	25.2	16	42

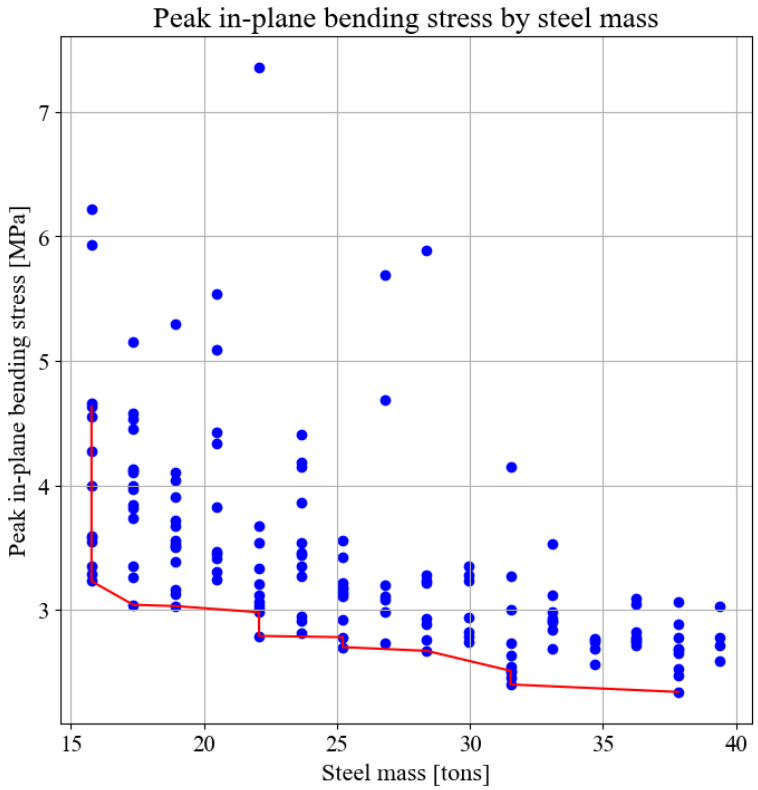

Figure B.125: 100 m span with three splices and vertical arches: Simulation 1, Skew load

Table B.82: 100 m span with three splices and vertical arches: Simulation 1, Skew load

Objective values		Parameter values	
Peak in-plane bending stress [MPa]	Steel mass [tons]	Number of crossbeams	Hanger angle [degrees]
2.7	25.2	16	50
2.79	22.07	14	48
2.81 - 2.95	23.7	15	51 - 50
3.23 - 3.35	15.8	10	52 - 50

Simulation 3

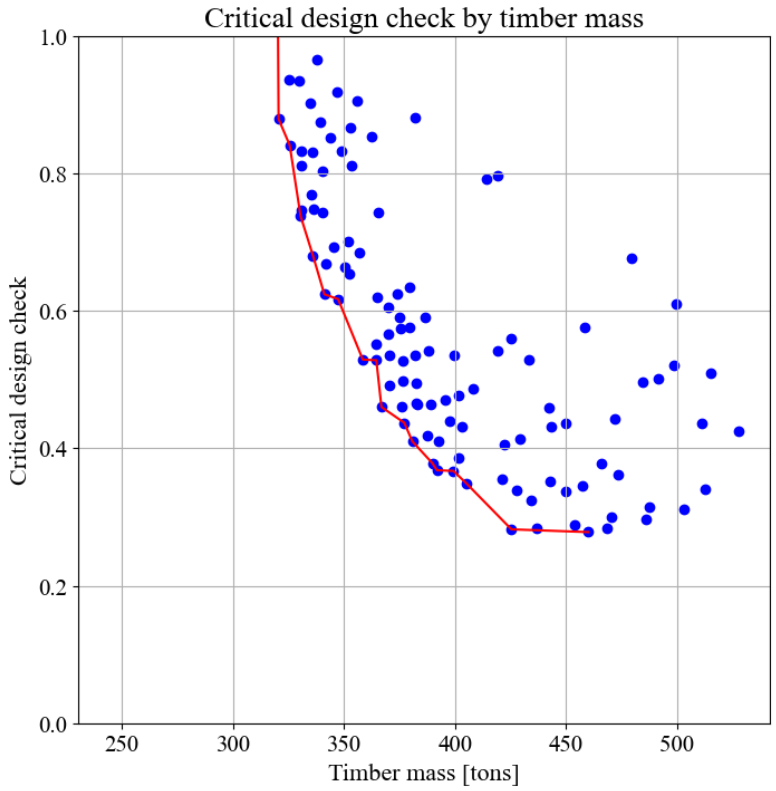

Figure B.126: 100 m span with three splices and vertical arches: Simulation 3, Full load

Table B.83: 100 m span with three splices and vertical arches: Simulation 3, Full load

Objective values		Parameter values	
Critical design check [0, 1]	Timber mass [tons]	Arch height [mm]	Arch width [mm]
0.738 - 0.879	331 - 321	850	1300 - 1200
0.812	331	950	1200
0.832 - 0.937	331 - 325	1000	1150 - 1100
0.902	335	1100	1100

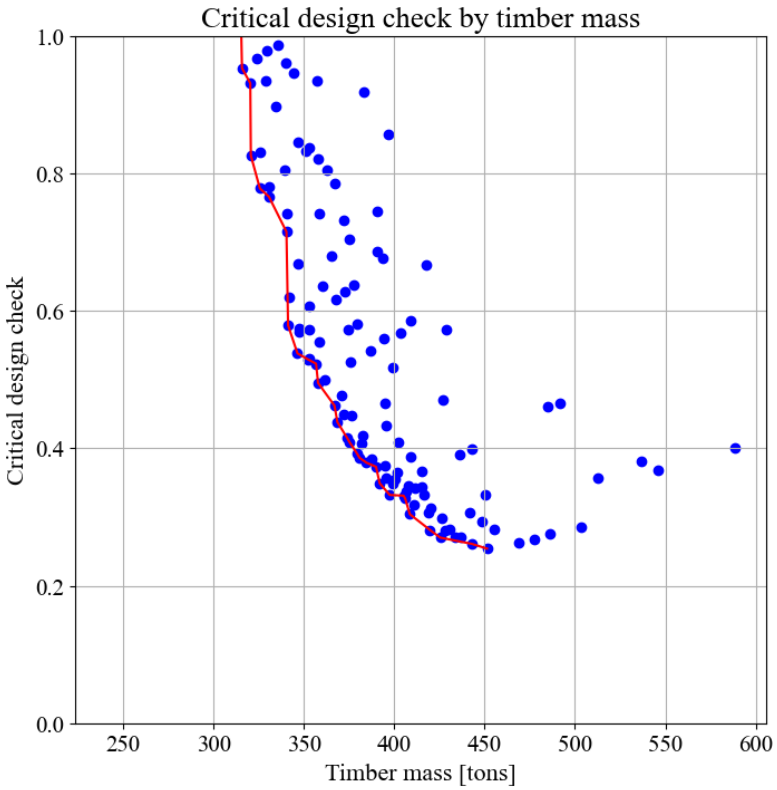

Figure B.127: 100 m span with three splices and vertical arches: Simulation 3, Skew load

Table B.84: 100 m span with three splices and vertical arches: Simulation 3, Skew load

Objective values		Parameter values	
Critical design check [0, 1]	Timber mass [tons]	Arch height [mm]	Arch width [mm]
0.778 - 0.953	326 - 316	850	1250 - 1150
0.826	321	850	1200
0.83 - 0.931	326 - 320	950	1150 - 1100
0.967	324	1050	1050

Final results

Table B.85: 100 m span with three splices and vertical arches: Results with the final configuration from Table 4.7.

	Full load	Skew load	Governing load
Peak in-plane bending stress [MPa]	2.08	2.59	2.59
Critical design check Eq. (6.24)	0.886	0.832	0.886
Buckling load factor	2.81	3.03	2.81
Natural frequency [Hz]	0.278	0.284	0.278
Max stress 90°to grain [MPa]	3.18	2.85	3.18
% of deck exceeding Tsai-Wu criterion	5.3	1.8	5.3
Max moment in splices [kNm]	192	246	246
Number of relaxed hangers	0	1	1
Maximum displacement [mm]	1301	1252	1301
Crossbeam utilization [%]	78.3	79.5	79.5
Hanger utilization [%]	30.8	34.7	34.7

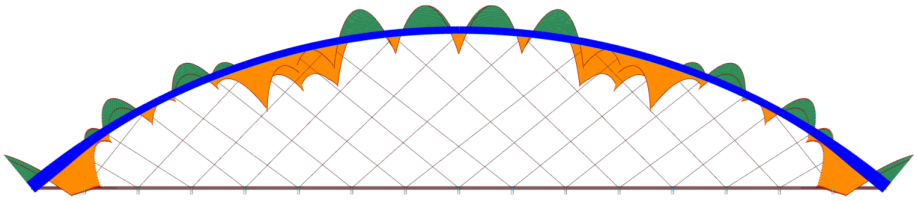

Figure B.128: 100 m span with three splices and vertical arches: Full load. Moment distribution in-plane with final configuration.

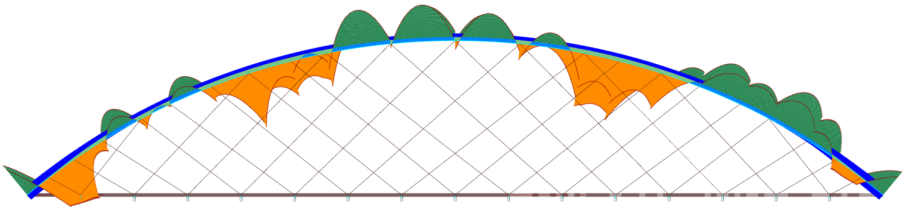

Figure B.129: 100 m span with three splices and vertical arches: Skew load. Moment distribution in-plane with final configuration.

B.9 100 m span with three splices and no side beams

Final results

Table B.86: 100 m span with three splices and no side beams: Results with the final configuration from Table 4.7.

	Full load	Skew load	Governing load
Peak in-plane bending stress [MPa]	4.64	5.32	5.32
Critical design check Eq. (6.24)	1.044	0.928	1.044
Buckling load factor	2.28	2.67	2.28
Natural frequency [Hz]	0.783	0.733	0.733
Max stress 90°to grain [MPa]	3.09	3.25	3.25
% of deck exceeding Tsai-Wu criterion	5.5	2.0	5.5
Max moment in splices [kNm]	230	268	268
Number of relaxed hangers	0	7	7
Maximum displacement [mm]	307	323	323
Crossbeam utilization [%]	79.9	89.6	89.6
Hanger utilization [%]	32.3	38.9	38.9

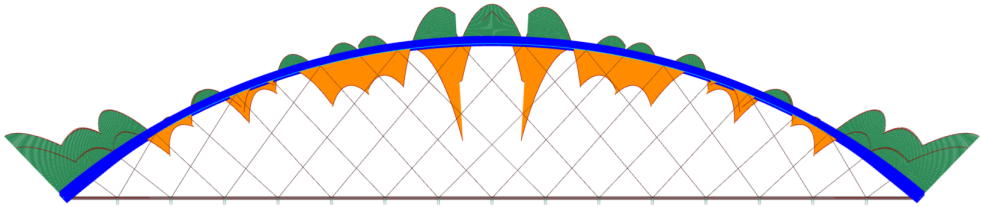

Figure B.130: 100 m span with three splices and no side beams: Full load. Moment distribution in-plane with final configuration.

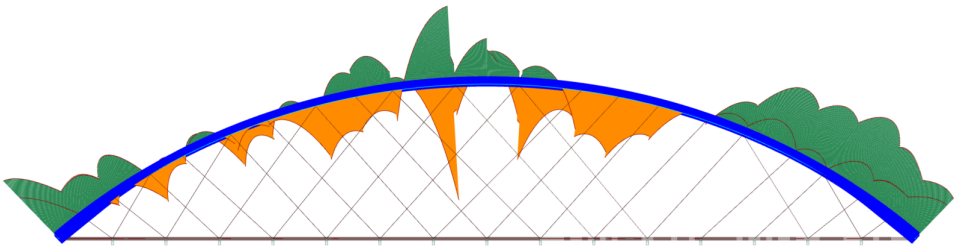

Figure B.131: 100 m span with three splices and no side beams: Skew load. Moment distribution in-plane with final configuration.

NTNU

Norwegian University of
Science and Technology